JOURNAL OF
CHEMICAL PHYSICS
Volume 20 Number 7
JULY, 1952

Phys
Fals

THEODORE H. BERLIN
B. P. DAILEY
A. W. LAWSON
HARALD H. NIELSEN
HARRISON SKULL
CHARLES P. SMYTH
FRANK H. WESTHEIMER

Tables may be typewritten on sheets separate from the accompanying text. Each table must have a caption which will make the data in the table intelligible without reference to the text. Avoid complicated column headings.

Wherever possible figures should be planned for the width of a column (3 in.). A convenient reduction ratio is usually 2:1 or 3:1. Lettering should be large enough on the original that when reduced it shall not be less than about 2 mm (~1/16 inch). Line drawings must be in *India ink* on white paper or tracing cloth. Coordinate paper is not acceptable but if used must be blue lined and the coordinate lines which are to show must be inked over. Photographs should have maximum black and white contrast. Identify each original drawing or photograph on the back with the author's name and the figure number. Figures should be numbered consecutively. Captions should be typed on a separate sheet of paper.

A limited number of alterations in proof are unavoidable, but the cost of making extensive alterations after the article has been set in type will be charged to the author.

Proof and all correspondence concerning papers in the process of publication should be addressed to the Publication Manager, American Institute of Physics, 57 East 55 Street, New York 22, New York.

Subscription Prices

	U. S. and Canada	Elsewhere
To members of the American Institute of Physics and Affiliated Societies	$12.00	$13.00
To all others	15.00	16.00

Back Number Prices

Single copies when complete year is available $17.00.
Single copies, $1.50 each.

Subscriptions, renewals, and orders for single copies should be addressed to the American Institute of Physics, 57 East 55 Street, New York 22, New York.

Changes of address should be sent to the American Institute of Physics.

Printed by Lancaster Press, Inc., Lancaster, Pennsylvania.

Entered as second class matter under the Act of August 24, 1912, authorized September 3, 1918.

Physics
Falxa

THE JOURNAL
OF
CHEMICAL PHYSICS

VOLUME 20, NUMBER 7 JULY, 1952

Interactions of Closed Shell Ions

GEORGE L. MONTET,* SEYMOUR P. KELLER AND JOSEPH E. MAYER
Department of Chemistry and Institute for Nuclear Studies, University of Chicago, Chicago, Illinois
(Received February 13, 1952)

Equations are written for the binding energy of a finite number of ions at fixed coordinate positions. Each ion is assumed to have a lowest nondegenerate (closed shell) configuration. In the Heitler-London approximation the state of the assembly is assumed to be: (a) a properly antisymmetrized sum of products of one-electron functions, and, (b) the constituent one-electron functions are assumed to be linear combinations of only the one-electron functions composing the ground states of the isolated ions. We use, for each ion a, its density matrix

$$\eta_a(\mathfrak{q}_i, \mathfrak{q}_j) = \Sigma \psi_{\nu a}(\mathfrak{q}_i)\psi_{\nu a}^*(\mathfrak{q}_j)$$

with $\mathfrak{q}_i$, $\mathfrak{q}_j$ the coordinates, including spin, of a single electron, and the sum including all filled one-electron functions, $\psi_{\nu a}$, of the ground state of ion a. The binding energy, consistent with the two assumptions (a) and (b) is then derived and found to be expressible in a reasonably compact exact form, using this density matrix. By making use of an approximate expression for the density matrix the integrations occurring in the energy expression are tractable.

I. INTRODUCTION

WE limit ourselves to the consideration of an assembly of a finite number of atoms or ions, $a, b, \cdots$, etc., at fixed coordinate positions of the nuclei, $\mathfrak{R}_a$, $\mathfrak{R}_b$, and assume that each ion has a closed shell configuration. The lowest electronic state for each isolated ion is then nondegenerate. The eigenfunction of this state is given to a reasonable approximation by an antisymmetrized sum of products of one-electron functions, which we designate $\psi_{\nu a}(\mathfrak{q}_i)$, with $\mathfrak{q}_i$ the vector coordinates, including spin, of one electron, and ν_a representing the appropriate quantum number, including spin, for a single electron state of ion a.

Now one may make two assumptions about the state of the assembly of ions: (a) the eigenfunction of the assembly is given (approximately) by an antisymmetrized sum of one single product of one-electron functions, $\varphi_\mu(\mathfrak{q}_i)$, which are normalized and mutually orthogonal, and (b) the one-electron functions, φ_μ, of the assembly are expressible as a linear combination of the functions, $\psi_{\nu a}$, of the isolated ions, in which case it is always possible to identify the quantum numbers μ of the functions φ_μ with those of the undisturbed ions, ν_a, ν_b, etc.

Although the one-electron functions φ_μ may be arbitrarily chosen, still, since their number is equal to the number of functions $\psi_{\nu a}$ from which they are formed, the antisymmetrized sum of products is unique, and the energy of the system is unique. This energy of the assembly minus the sum of the energies of the isolated ions is the binding energy. This approximation of (a) and (b) will be referred to as the Heitler-London approximation.

The equations for the computation of the binding energy have been derived previously for various cases, although most frequently with additional approximations. Recently Löwdin[1] has derived the general equations for an arbitrary assembly of closed shell ions with no essential approximation beyond (a) and (b). In this paper an equivalent, but formally different approach is made using the density matrix. Both general methods may be said to involve three difficulties.

(1) The first difficulty is purely formal. Since the eigenfunction of the assembly is antisymmetrized, and the Hamiltonian involves the interactions of all nuclei with all electrons, and each electron with every other, one cannot immediately write the Hamiltonian as a zero'th order term, giving the energy of the separated ions, plus a perturbation term, giving the binding

* Part of a dissertation submitted to the University of Chicago for the degree of Doctor of Philosophy.

[1] Per-Olov Löwdin, J. Chem. Phys. 18, 365 (1950).

energy. This difficulty is readily remedied in the usual approach using the eigenfunction, in which the energy is written as an integral, $E=\int\Phi^*H\Phi d\tau$. Since both Φ^* and Φ are sums of permutations of an unpermuted function Φ_u, one may multiply by the number, $N!$, of permutations and write $E=N!\int\Phi^*H\Phi_u d\tau$. For the definite permutation, Φ_u, each numbered electron is, so to speak, assigned to a definite nucleus, and the perturbation terms in the Hamiltonian, the interactions of the nuclei with the electrons on *other* nuclei, and the interactions of pairs of electrons on *different* nuclei, can now be singled out, so that the binding energy alone is directly computed. In the treatment of this paper this formal difficulty is somewhat greater, and the segregation of the energy of the isolated ions from the total energy of the system requires a little more manipulation.

(2) The second difficulty is that the functions $\psi_{\nu a}$ and $\psi_{\nu b}$ appropriate to two isolated ions a and b are no longer orthogonal when the two ions are close enough to interact. The one-electron functions, φ_u, of the assembly, if they are to be mutually orthogonal, are not then the functions, $\psi_{\nu a}$, of the isolated ions, but are linear combinations of them. One can, however, choose them so that to each $\varphi_{\nu a}$ there is one function $\psi_{\nu a}$ which plays a predominant role, thus identifying the quantum numbers, μ, with those, ν_a, ν_b, etc., of the isolated ions. This difficulty was first solved in general form by Löwdin.[1] Our solution is exactly his, although expressed by us in the density matrix form, and no more complication is encountered in the method used here than in the eigenfunction approach.

(3) The third difficulty with the usual approach is really the most formidable for numerical calculations. Even with only two ions, say K^+ and Cl^-, each ion has 18 electrons, and therefore, excluding spin, there are 9 different one-electron functions for each ion or 81 pair combinations between K^+ and Cl^-. Each such pair involves three integrals. Thus, if no neglects are made there are 243 integrations to perform, and indeed many more if higher than the lowest approximations are to be included. Although symmetry considerations slightly reduce the labor, the number is still extremely large. In our method only one function is written for each ion. The formidable array of summations is thus drastically reduced by a factor of order 80. Since it is to be expected that a reasonable approximation for the density matrix, $\eta_a(\mathfrak{q}_i, \mathfrak{q}_j)$, such as one which has been given by Dirac[2] would permit fairly accurate evaluations, one might hope that the computation chore could be reduced to reasonable limits. Even if this hope should prove illusory the compactness of our formulation may be regarded as sufficient excuse for its presentation.

Even if the computations are made exactly the assumptions (a) and (b) inherently limit the validity of a calculation to that of the Heitler-London approximation. This limitation is not serious for isotropic crystals. Löwdin's[1] computations for the alkali halide crystal lattice, KCl and NaCl, indicate that a remarkable agreement within the experimental error of about one or two percent in the binding energy can be obtained. To one accustomed to the "order of magnitude only" agreement obtained in the calculation of homopolar bond energies, for instance in H_2, this may seem remarkable. It is less remarkable when one remembers that although the energy per bond in the alkali halide crystal is about that of H_2, only about 10 percent of this energy is due to terms involving the electronic eigenfunctions, the 90 percent arising from the Madelung energy of the gross ionic charges. Using the rough rule that the percentage error of a perturbation calculation is proportional to the perturbation energy, one may well expect that the repulsive terms in the crystal energy should be calculable within 10 percent of their magnitude by a method which gives only an order of magnitube result for H_2. Since 10 percent of 10 percent is one percent, Löwdin's agreement is not unexpected.

However, it is easy to show that no such agreement could be obtained for the energy of an alkali halide gas molecule. The energy which Löwdin obtains for the crystals is rather closely given by the sum of the mutual energies of pairs of ions. One knows that the energy of the gas molecule is very significantly lower than that due to the Coulomb attraction plus the empirical repulsive term deduced from the crystal lattice energy expression. It is necessary to include in the gas molecule a term due to the polarization of the ions, and to take account of the changed[3] repulsion due to the distortion of the electron configuration of the ions. Translated into a quantum mechanical language this means that one must use a different electronic configuration for the ions than that of the ground state.

The equation which we give for the binding energy is then one which, if exactly computed, should probably yield excellent results for arrangements of ions in which the electric field around each is highly symmetric, as in an isotropic crystal. It will not be expected to be so good in cases in which a significant fraction of the ions would be expected to be polarized by the field of the others, as in a gas molecule. We suggest a procedure which might prove feasible for the treatment of the latter case.

II. THE DENSITY MATRIX

The mathematics of the method is formal, but reasonably short. In this section we derive an expression for the density matrix of the assembly in terms of those of the single ions, and display a few relations between some subsidiary functions.

A complete set of orthonormal functions, $\Theta_\nu(\mathfrak{q})$, may be said to form a unitary matrix, $\boldsymbol{\Theta}$, of elements,

[2] P. A. M. Dirac, Proc. Cambridge Phil. Soc. **26**, 376 (1930).

[3] Edmund S. Rittner, J. Chem. Phys. **19**, 1030 (1951).

$\Theta_{q,\nu}=\Theta_\nu(\mathfrak{q})$, of which the first index, $\mathfrak{q}$, is a continuous vector, and the second, ν, is discrete. The hermitian adjoint matrix, $\mathbf{\Theta}\dagger$, has elements $\Theta\dagger_{\nu,q}=[\Theta_{q,\nu}]^*=\Theta_\nu^*(\mathfrak{q})$. The product, $\mathbf{\Theta\Theta}\dagger=\mathbf{1}$, is the unit matrix, which is a delta function along the diagonal of the two continuous indices, $\mathfrak{q}_1$, $\mathfrak{q}_2$. The product $\mathbf{\Theta}\dagger\mathbf{\Theta}=\mathbf{1}$ is the unit matrix along the diagonal of the discrete indices, ν_1, ν_2.

The set of functions we have is not infinite and not complete. Let $\psi_{\nu a}(\mathfrak{q})$ be one of a set of N_a orthonormal functions which are one-electron functions of the coordinate plus spin, $\mathfrak{q}$, and which are the N_a lowest energy functions of the isolated ion a. The matrix, $\mathbf{\Psi}_a$, of elements $\psi_{q,\nu a}$ has N_a discrete columns. We have

$$\mathbf{\Psi}_a\dagger\mathbf{\Psi}_a=\mathbf{1}, \tag{1}$$

but

$$\mathbf{\Psi}_a\mathbf{\Psi}_a\dagger=\mathbf{n}_a \tag{2}$$

is the density matrix of ion a in its lowest energy configuration, having elements

$$\eta_a(\mathfrak{q}_1,\mathfrak{q}_2)=\sum_{\nu_a\geq 1}^{\nu_a=N_a}\psi_{\nu a}(\mathfrak{q}_1)\psi_{\nu a}^*(\mathfrak{q}_2), \tag{3}$$

and is *not* the unit matrix since the functions $\psi_{\nu a}$ are finite in number and do not form a complete set. However, if the number, N_a, of functions is not too small we may well expect $\mathbf{n}_a$ to be strongly concentrated along the diagonal. The diagonal element, $\eta_a(\mathfrak{q},\mathfrak{q})$, which is real and positive, is the probability density of electrons at $\mathfrak{q}$. Of course $\mathbf{n}_a$ is Hermitian; it does not, however, have an inverse $\mathbf{n}_a^{-1}$, since, when diagonalized, it has zero elements in the unfilled quantum states, the excited states of the ion.

If $N=\sum_a N_a$ is the total number of electrons of the assembly we interpret $\mathbf{\Psi}_a$ to be a matrix of N discrete columns, the elements of all columns ν with $N_a+1\leq\nu\leq N$ being zero. Let $\mathbf{\Psi}_b$ be a similarly constituted matrix for ion b having nonzero elements only in columns $N_a+1\leq\nu\leq N_a+N_b$, etc. Then define

$$\mathbf{\Psi}=\sum_a\mathbf{\Psi}_a, \tag{4}$$

for any finite number of ions at fixed coordinate positions, $\mathfrak{R}_a$. Define the matrix

$$\mathbf{S}=\mathbf{\Psi}\dagger\mathbf{\Psi}-\mathbf{1}, \tag{5}$$

with $\mathbf{1}$ the unit matrix. If all ions are far distant from each other then all functions ψ_a and ψ_b are orthogonal, and $\mathbf{S}$ will be zero. In general only the elements $s_{\nu a,\mu b}$, $a\neq b$, of $\mathbf{S}$ will be nonzero, and then only if ions a and b are spatially close enough to have "overlap" in the wave functions. The matrix

$$\mathbf{n}=\mathbf{\Psi\Psi}\dagger \tag{6}$$

will *not* be the density matrix for the system unless $\mathbf{S}\equiv 0$.

Form

$$\begin{aligned}\mathbf{\Phi}&=\mathbf{\Psi}(1+\mathbf{S})^{-\frac{1}{2}},\\ \mathbf{\Phi}\dagger&=(1+\mathbf{S})^{-\frac{1}{2}}\mathbf{\Psi}\dagger;\end{aligned} \tag{7}$$

then, from (5),

$$\begin{aligned}\mathbf{\Phi}\dagger\mathbf{\Phi}&=(1+\mathbf{S})^{-\frac{1}{2}}\mathbf{\Psi}\dagger\mathbf{\Psi}(1+\mathbf{S})^{-\frac{1}{2}}\\ &=(1+\mathbf{S})^{-\frac{1}{2}}(1+\mathbf{S})(1+\mathbf{S})^{-\frac{1}{2}}=\mathbf{1},\end{aligned} \tag{8}$$

and the elements $\varphi_{q,\nu}=\varphi_\nu(\mathfrak{q})$ are a set of orthonormal functions which are linear combinations of the functions of those of the isolated ions, the $\psi_{\nu a}(\mathfrak{q})$'s. These are Löwdin's functions. The matrix

$$\varrho=\mathbf{\Phi\Phi}\dagger \tag{9}$$

is the density matrix of the assembly of ions. From (7), using (6), one obtains

$$\begin{aligned}\varrho&=\mathbf{\Psi}[1+\mathbf{S}]^{-1}\mathbf{\Psi}\dagger=\sum_{n\geq 0}\mathbf{\Psi}(-\mathbf{S})^n\mathbf{\Psi}\dagger\\ &=\sum_{n\geq 0}\mathbf{\Psi}(-)^n[\mathbf{\Psi}\dagger\mathbf{\Psi}-1]^n\mathbf{\Psi}\dagger=\mathbf{n}\sum_{n\geq 0}(1-\mathbf{n})^n.\end{aligned} \tag{10}$$

From the way we have defined the matrices $\mathbf{\Psi}_a$ it follows that

$$\mathbf{\Psi}_a\mathbf{\Psi}_b\dagger=0,\quad b\neq a, \tag{11}$$

since $\mathbf{\Psi}_a$ has only zero elements in columns for which the corresponding row elements of $\mathbf{\Psi}_b$ are non-zero. From (2), (4), and (6), with (11), it follows that

$$\mathbf{n}=\sum_a\mathbf{n}_a. \tag{12}$$

From (2) and (1) we see that

$$\mathbf{n}_a\mathbf{n}_a=\mathbf{n}_a, \tag{13}$$

so that, with (12)

$$\left.\begin{aligned}\mathbf{n}^2-\mathbf{n}&=\sum_{a\neq b}\sum\mathbf{n}_a\mathbf{n}_b,\\ \mathbf{n}^3-2\mathbf{n}^2+\mathbf{n}&=\sum_{a\neq b}\sum_{b\neq c}\sum\mathbf{n}_a\mathbf{n}_b\mathbf{n}_c,\ \text{etc.}\end{aligned}\right\} \tag{14}$$

The product $\mathbf{n}_a\mathbf{n}_b$ for $a\neq b$ approaches zero rapidly if the ions a and b increase in distance apart. Using (12) and (14) in (10) one finds

$$\varrho=\sum_a\mathbf{n}_a-\sum_{a\neq b}\sum\mathbf{n}_a\mathbf{n}_b+\sum_{a\neq b}\sum_{b\neq c}\sum\mathbf{n}_a\mathbf{n}_b\mathbf{n}_c-\cdots. \tag{15}$$

We wish to introduce a few further matrices. Define

$$\begin{aligned}\varrho_a&=\mathbf{n}_a\sum_{n\geq 0}(1-\mathbf{n})^n\\ &=\mathbf{n}_a-\sum_{b\neq a}\mathbf{n}_a\mathbf{n}_b+\sum_{b\neq a}\sum_{c\neq b}\mathbf{n}_a\mathbf{n}_b\mathbf{n}_c-\cdots,\end{aligned} \tag{16}$$

so that

$$\varrho=\sum\varrho_a. \tag{17}$$

We also introduce

$$\boldsymbol{\sigma}_a=\boldsymbol{\varrho}_a-\mathbf{n}_a=\mathbf{n}_a\sum_{n\geq 1}(1-\mathbf{n})^n$$

$$=-\sum_{b\neq a}\mathbf{n}_a\mathbf{n}_b+\sum_{b\neq a}\sum_{c\neq b}\mathbf{n}_a\mathbf{n}_b\mathbf{n}_c-\cdots. \quad (18)$$

A number of relationships, some of which are important in obtaining physical interpretations later, for products of these matrices may be derived. From (8) and (9) one has

$$\boldsymbol{\varrho}\boldsymbol{\varrho}=\boldsymbol{\varrho}. \quad (19)$$

Since

$$\mathbf{n}_a=\boldsymbol{\Psi}_a\boldsymbol{\Psi}_a\dagger=\boldsymbol{\Psi}_a\boldsymbol{\Psi}\dagger,$$

we may also write, using (6) for $\mathbf{n}$, and (16),

$$\boldsymbol{\varrho}_a=\boldsymbol{\Psi}_a\boldsymbol{\Psi}\dagger\sum_{n\geq 0}(1-\boldsymbol{\Psi}\boldsymbol{\Psi}\dagger)^n$$

$$=\boldsymbol{\Psi}_a\sum_{n\geq 0}(-\mathbf{S})^n\boldsymbol{\Psi}\dagger=\boldsymbol{\Psi}_a(1+\mathbf{S})^{-1}\boldsymbol{\Psi}\dagger. \quad (20)$$

Use this with the first expression in (10) for $\boldsymbol{\varrho}$, and (5) for $\boldsymbol{\Psi}\dagger\boldsymbol{\Psi}=1+\mathbf{S}$, and one finds

$$\boldsymbol{\varrho}_a\boldsymbol{\varrho}=\boldsymbol{\varrho}_a. \quad (21)$$

Use (13) and (16) for $\boldsymbol{\varrho}_a$ and one obtains

$$\mathbf{n}_a\boldsymbol{\varrho}_a=\boldsymbol{\varrho}_a. \quad (22)$$

From (18), $\boldsymbol{\varrho}_a=\mathbf{n}_a+\boldsymbol{\sigma}_a$, and (13), $\mathbf{n}_a\mathbf{n}_a=\mathbf{n}_a$, one obtains from (22) that

$$\mathbf{n}_a\boldsymbol{\sigma}_a=\boldsymbol{\sigma}_a. \quad (23)$$

Use again $\mathbf{n}_a=\boldsymbol{\Psi}_a\boldsymbol{\Psi}\dagger$ and the first expression in (10) for $\boldsymbol{\varrho}$, and remember that $\boldsymbol{\Psi}\dagger\boldsymbol{\Psi}=1+\mathbf{S}$, Eq. (5), and one obtains

$$\mathbf{n}_a\boldsymbol{\varrho}=\mathbf{n}_a. \quad (24)$$

From this and (12), or from (6) and the second expression in (10) one finds

$$\mathbf{n}\boldsymbol{\varrho}=\boldsymbol{\varrho}\mathbf{n}=\mathbf{n}. \quad (25)$$

The trace of the density matrix is always the number of orthonormal functions which compose it, and therefore, also the number of electrons of the system. We have

$$[\mathbf{n}_a]_{tr}=\mathrm{N}_a=\int\eta_a(\mathfrak{q},\mathfrak{q})d\mathfrak{q}, \quad (26)$$

and

$$[\mathbf{n}]_{tr}=\sum_a[\mathbf{n}_a]_{tr}=\sum_a\mathrm{N}_a=\mathrm{N}. \quad (27)$$

Also, since there are N functions in $\boldsymbol{\varrho}$,

$$[\boldsymbol{\varrho}]_{tr}=\mathrm{N}. \quad (28)$$

We may write, using (20) and (5),

$$[\boldsymbol{\varrho}_a]_{tr}=[\boldsymbol{\Psi}_a(1+\mathbf{S})^{-1}\boldsymbol{\Psi}\dagger]_{tr}=[(1+\mathbf{S})^{-1}\boldsymbol{\Psi}\dagger\boldsymbol{\Psi}_a]_{tr}$$

$$=\sum_{\nu a}[(1+\mathbf{S})^{-1}(1+\mathbf{S})]_{\nu a,\,\nu a},$$

$$[\boldsymbol{\varrho}_a]_{tr}=\mathrm{N}_a. \quad (29)$$

From (26), (29), and (12) it follows that

$$[\boldsymbol{\sigma}_a]_{tr}=0. \quad (29')$$

We shall later need the trace of some products. The trace, $a\neq b$,

$$[\boldsymbol{\varrho}_a\boldsymbol{\varrho}_b]_{tr}=[\boldsymbol{\Psi}_a(1+\mathbf{S})^{-1}\boldsymbol{\Psi}\dagger\boldsymbol{\Psi}_b(1+\mathbf{S})^{-1}\boldsymbol{\Psi}\dagger]_{tr}$$

$$=[(1+\mathbf{S})^{-1}\boldsymbol{\Psi}\dagger\boldsymbol{\Psi}_b(1+\mathbf{S})^{-1}\boldsymbol{\Psi}\dagger\boldsymbol{\Psi}_a]_{tr}$$

$$=\sum_{\nu a}\sum_{\lambda b}[(1+\mathbf{S})^{-1}(1+\mathbf{S})]_{\nu a,\,\lambda b}[(1+\mathbf{S})^{-1}(1+\mathbf{S})]_{\lambda b,\,\nu a}$$

$$=0,$$

so

$$[\boldsymbol{\varrho}_a\boldsymbol{\varrho}_b]_{tr}=0 \quad \text{if} \quad a\neq b. \quad (30)$$

Similarly we use (18) for $\boldsymbol{\sigma}_a=\boldsymbol{\varrho}_a-\mathbf{n}_a$, with (20) for $\boldsymbol{\varrho}_a$ and (2) for $\mathbf{n}_a$ to write

$$[\boldsymbol{\sigma}_a\boldsymbol{\sigma}_a]_{tr}=\{\boldsymbol{\Psi}_a[(1+\mathbf{S})^{-1}-1]\boldsymbol{\Psi}\dagger\boldsymbol{\Psi}_a[(1+\mathbf{S})^{-1}-1]\boldsymbol{\Psi}\dagger\}_{tr}$$

$$=\{[(1+\mathbf{S})^{-1}-1]\boldsymbol{\Psi}\dagger\boldsymbol{\Psi}_a[(1+\mathbf{S})^{-1}-1]\boldsymbol{\Psi}\dagger\boldsymbol{\Psi}_a\}_{tr}$$

$$=\sum_{\mu a}\sum_{\mu a}\{[(1+\mathbf{S})^{-1}-1][1+\mathbf{S}]\}_{\nu a,\,\mu a}$$

$$\times\{[(1+\mathbf{S})^{-1}-1][1+\mathbf{S}]\}_{\mu a,\,\nu a}$$

$$=\sum_{\nu a}\sum_{\mu a}s_{\nu a,\,\mu a}s_{\mu a,\,\nu a}=0,$$

since $s_{\nu a,\,\mu a}=0$ because all functions of the same ion are orthogonal. One has

$$[\boldsymbol{\sigma}_a\boldsymbol{\sigma}_a]_{tr}=0. \quad (31)$$

Finally we wish to mention in this section that for the closed shell ions which we are considering there are two electrons, of different spin, in each orbital one-electron function, $\chi_{\mu a}(\mathfrak{r})$. Since the two spin functions are orthogonal the parts of the matrices with spin α and those with spin β never interact. If we define $\mathbf{n}_a'$ of elements

$$\eta_a'(\mathfrak{r}_1,\mathfrak{r}_2)=\sum_{\mu_a\geq 1}^{\mu_a=\mathrm{N}_a/2}\chi_{\mu a}(\mathfrak{r}_1)\chi_{\mu a}{}^*(\mathfrak{r}_2), \quad (32)$$

analogous to (3), then all the equations of this section become equally applicable to the "primed" matrices, for which the continuous and discrete indices have no spin coordinate or quantum number, except that the traces of the primed matrices will be half those of the unprimed.

If the nucleus of ion a of charge Z_a is located at $\mathfrak{R}_a$, then the function

$$q_a(\mathfrak{r})=Z_a\delta(\mathfrak{r}-\mathfrak{R}_a)-2\eta_a'(\mathfrak{r},\mathfrak{r}) \quad (33)$$

represents the classical density of electricity at $\mathfrak{r}$, measured in units of e, on the isolated ion a.

III. THE ENERGY

We now wish to write the expression for the energy of the assembly, and more specifically for the energy

of the assembly minus that of the isolated ions, using the density matrix.

To do this define three Hermitian operators, **H**, **fB**, **fA**. We use atomic units for which the electronic charge is unity, the unit of length is $a_0=0.529\times10^{-8}\,A$, and the unit of energy is 27 ev. Let **f** be any Hermitian matrix of the continuous indices $\mathfrak{q}_1$, $\mathfrak{q}_2$, having elements $f(\mathfrak{q}_1, \mathfrak{q}_2)$ and $\boldsymbol{\Theta}$ any matrix of elements $\Theta_{\mathfrak{q},\nu}$, the first of which, $\mathfrak{q}$, is continuous. The operator **H** is the usual Hamiltonian defined so that

$$[\mathbf{H}\boldsymbol{\Theta}]_{\mathfrak{q},\nu}=[-\tfrac{1}{2}\nabla^2+U(\mathfrak{q})]\Theta_{\mathfrak{q},\nu}, \tag{34}$$

with $U(\mathfrak{q})$ a potential energy. Operators **fB** and **fA** are defined by

$$[\mathbf{fB}\boldsymbol{\Theta}]_{\mathfrak{q}i,\nu}=\int f(\mathfrak{q}_k,\mathfrak{q}_k)(1/R_{ki})\Theta_{\mathfrak{q}i,\nu}d\mathfrak{q}_k, \tag{35}$$

$$[\mathbf{fA}\boldsymbol{\Theta}]_{\mathfrak{q}i,\nu}=\int f(\mathfrak{q}_i,\mathfrak{q}_k)(1/R_{ki})\Theta_{\mathfrak{q}k,\nu}d\mathfrak{q}_k. \tag{36}$$

If

$$\mathbf{g}=\boldsymbol{\Theta}\boldsymbol{\Theta}\dagger,$$

then

$$\begin{aligned}[\mathbf{H}\boldsymbol{\Theta}]\boldsymbol{\Theta}\dagger&=\mathbf{Hg},\\ [\mathbf{fB}\boldsymbol{\Theta}]\boldsymbol{\Theta}\dagger&=\mathbf{fBg},\\ [\mathbf{fA}\boldsymbol{\Theta}]\boldsymbol{\Theta}\dagger&=\mathbf{fAg},\end{aligned} \tag{37}$$

and

$$\begin{aligned}[\mathbf{fBg}]_{tr}&=[\mathbf{gBf}]_{tr},\\ [\mathbf{fAg}]_{tr}&=[\mathbf{gAf}]_{tr},\end{aligned} \tag{38}$$

in which $[\ ]_{tr}$ indicates the trace.

The energy of a system of electrons for which the density matrix is $\boldsymbol{\varrho}$ is given by

$$E_e=[\mathbf{H}\boldsymbol{\varrho}+\tfrac{1}{2}\boldsymbol{\varrho}(\mathbf{B}-\mathbf{A})\boldsymbol{\varrho}]_{tr}, \tag{39}$$

if U in **H** is the potential energy per electron due to any charges other than the electrons. The Fock equation for the determination of the eigenfunctions, $\varphi_\nu(\mathfrak{q})$, is

$$[\mathbf{H}+\boldsymbol{\varrho}(\mathbf{B}-\mathbf{A})]\boldsymbol{\Phi}=\boldsymbol{\Phi}\mathbf{E}, \tag{40}$$

where **E** is a diagonal matrix. From (9) relating $\boldsymbol{\Phi}$ and $\boldsymbol{\varrho}$, and (37), (39), and (40) one has

$$E_e=[\mathbf{E}-\tfrac{1}{2}\boldsymbol{\varrho}(\mathbf{B}-\mathbf{A})\boldsymbol{\varrho}]_{tr}. \tag{41}$$

For our assembly of ions we must use

$$U(\mathfrak{q}_i)=-\sum_a Z_a/R_{ai} \tag{42}$$

and add the interaction energy of the nuclei to obtain the total energy, E:

$$E=E_e+\tfrac{1}{2}\sum_{a\neq b}\sum Z_aZ_b/R_{ab}. \tag{43}$$

Thus (43), with (42) for U in **H**, and (39) for E_e, with (10) or (15) for $\boldsymbol{\varrho}$ gives the energy of the assembly of ions, at any positions, consistent with the Heitler-London approximations, (*a*) and (*b*). We wish, however, to subtract from this the energy of isolated ions, in order to obtain the binding energy.

To accomplish this subtraction we define $\mathbf{H}_a$ as Eq. (34) with $U=U_a=-Z_a/R_{ai}$, for any a, so that one may write

$$\mathbf{H}=\mathbf{H}_a-\sum_{b\neq a} Z_b/R_{bi}, \tag{44}$$

for any arbitrarily chosen ion a. In Eq. (39) we then use (17) and (18) that

$$\boldsymbol{\varrho}=\sum_a \boldsymbol{\varrho}_a=\sum_a (\mathbf{n}_a+\boldsymbol{\sigma}_a), \tag{45}$$

and for each a write **H** as the appropriate form of (44). We make use of (38) and find

$$\begin{aligned}E=\sum_a\{&[\mathbf{H}_a\mathbf{n}_a+\tfrac{1}{2}\mathbf{n}_a(\mathbf{B}-\mathbf{A})\mathbf{n}_a]_{tr}\\ &+[\mathbf{H}_a\boldsymbol{\sigma}_a+\mathbf{n}_a(\mathbf{B}-\mathbf{A})\boldsymbol{\sigma}_a]_{tr}+\tfrac{1}{2}[\boldsymbol{\sigma}_a(\mathbf{B}-\mathbf{A})\boldsymbol{\sigma}_a]_{tr}\}\\ &+\tfrac{1}{2}\sum_{a\neq b}\sum\left\{\frac{Z_aZ_b}{R_{ab}}+\left[-\frac{Z_b}{R_{bi}}\boldsymbol{\varrho}_a-\frac{Z_a}{R_{ai}}\boldsymbol{\varrho}_b\right.\right.\\ &\left.\left.+\boldsymbol{\varrho}_a(\mathbf{B}-\mathbf{A})\boldsymbol{\varrho}_b\right]_{tr}\right\}.\end{aligned} \tag{46}$$

The terms in the first bracket in the summation over a are just $E_a^{(0)}$, the energies of the isolated ions a. The second bracket, as we shall show, is zero. One finds for the binding energy,

$$\Delta E=E-\sum_a E_a^{(0)}, \tag{47}$$

$$\begin{aligned}\Delta E&=\tfrac{1}{2}\sum_a[\boldsymbol{\sigma}_a(\mathbf{B}-\mathbf{A})\boldsymbol{\sigma}_a]_{tr}+\tfrac{1}{2}\sum_{a\neq b}\sum\left\{\frac{Z_aZ_b}{R_{ab}}\right.\\ &\left.+\left[-\frac{Z_b}{R_{bi}}\boldsymbol{\varrho}_a-\frac{Z_a}{R_{ai}}\boldsymbol{\varrho}_b+\boldsymbol{\varrho}_a(\mathbf{B}-\mathbf{A})\boldsymbol{\varrho}_b\right]_{tr}\right\}\\ &=\tfrac{1}{2}\sum_{a\neq b}\sum\left\{\frac{Z_aZ_b}{R_{ab}}+\left[-\frac{Z_b}{R_{bi}}\mathbf{n}_a-\frac{Z_a}{R_{ai}}\mathbf{n}_b+\mathbf{n}_a\mathbf{B}\mathbf{n}_b\right]_{tr}\right\}\\ &+\tfrac{1}{2}\sum_{a\neq b}\sum\left\{\left[\left(-\frac{Z_b}{R_{bi}}+\mathbf{n}_b\mathbf{B}\right)\boldsymbol{\sigma}_a\right]_{tr}\right.\\ &+\left[\left(-\frac{Z_a}{R_{ai}}+\mathbf{n}_a\mathbf{B}\right)\boldsymbol{\sigma}_b\right]_{tr}-[\boldsymbol{\varrho}_a\mathbf{A}\boldsymbol{\varrho}_b]_{tr}\\ &\left.+[\boldsymbol{\sigma}_a\mathbf{B}\boldsymbol{\sigma}_b]_{tr}\right\}+\tfrac{1}{2}\sum_a[\boldsymbol{\sigma}_a(\mathbf{B}-\mathbf{A})\boldsymbol{\sigma}_a]_{tr}.\end{aligned} \tag{48}$$

We must now fill in the neglected proof that

$$\sum_a\{[\mathbf{H}_a+\mathbf{n}_a\mathbf{B}-\mathbf{n}_a\mathbf{A}]\boldsymbol{\sigma}_a\}_{tr}=I=0.$$

From (18), $\boldsymbol{\sigma}_a=\boldsymbol{\varrho}_a-\mathbf{n}_a$ with (20) for $\boldsymbol{\varrho}_a$ and (2) for $\mathbf{n}_a$

we have

$$I=\sum_a \{[\mathbf{H}_a+\mathbf{n}_a\mathbf{B}-\mathbf{n}_a\mathbf{A}]\Psi_a[(1+\mathbf{S})^{-1}-1]\Psi\dagger\}_{tr},$$

but Ψ_a obeys the Fock equation (40) with $\mathbf{H}=\mathbf{H}_a$, and $\mathbf{E}=\mathbf{E}_a$, a diagonal matrix with elements for va only. Therefore

$$I=\sum_a \{\Psi_a\mathbf{E}_a[(1+\mathbf{S})^{-1}-1]\Psi\dagger\}_{tr}$$
$$=\sum_a \{\mathbf{E}_a[(1+\mathbf{S})^{-1}-1]\Psi\dagger\Psi_a\}_{tr},$$

but since

$$\mathbf{E}=\sum_a \mathbf{E}_a,$$

$$\Psi=\sum_a \Psi_a,$$

then

$$I=\{\mathbf{E}[(1+\mathbf{S})^{-1}-1]\Psi\dagger\Psi\}_{tr}$$
$$=\{\mathbf{E}[(1+\mathbf{S})^{-1}-1][1+\mathbf{S}]\}_{tr}$$

from (5), or

$$I=-\{\mathbf{ES}\}_{tr}=0$$

since $\mathbf{S}$ has no diagonal elements and $\mathbf{E}$ has only diagonal elements.

In (48) we may simplify the form, and also aid in obtaining some physical insight into the terms by introducing the charge distribution, $q_a(\mathfrak{r})$, Eq. (33), for the isolated ion a. We define a potential,

$$U_a(\mathfrak{r}_i)=\int q_a(\mathfrak{r}_j)[1/R_{ij}]d\mathfrak{r}_j, \tag{49}$$

due to the classical charge distribution on ion a, and also the classical energy of interaction of the charges on ions a and b

$$Q_{ab}=\int U_a(\mathfrak{r})q_b(\mathfrak{r})d\mathfrak{r}=\int U_b(\mathfrak{r})q_a(\mathfrak{r})d\mathfrak{r}. \tag{50}$$

One may then write (48) as

$$\Delta E=\tfrac{1}{2}\sum_{a\neq b}\sum \{Q_{ab}-[U_a\boldsymbol{\sigma}_b+U_b\boldsymbol{\sigma}_a]_{tr}$$
$$-[\boldsymbol{\varrho}_a\mathbf{A}\boldsymbol{\varrho}_b]_{tr}+[\boldsymbol{\sigma}_a\mathbf{B}\boldsymbol{\sigma}_b]_{tr}\}$$
$$-\tfrac{1}{2}\sum_a[\boldsymbol{\sigma}_a(\mathbf{B}-\mathbf{A})\boldsymbol{\sigma}_a]_{tr}. \tag{51}$$

Introduce, now, for every pair of ions, a and b, the matrix, $\boldsymbol{\sigma}_{ab}$, which would be the $\boldsymbol{\sigma}_a$ if only this pair were present in the assembly

$$\boldsymbol{\sigma}_{ab}=\mathbf{n}_a\sum_{n\geq 1}(1-\mathbf{n}_a-\mathbf{n}_b)^n=-\mathbf{n}_a\mathbf{n}_b+\mathbf{n}_a\mathbf{n}_b\mathbf{n}_a-\cdots, \tag{52}$$

and then, for every c, the additional term which would have to be added to $\boldsymbol{\sigma}_{ab}+\boldsymbol{\sigma}_{ac}$ to give $\boldsymbol{\sigma}_a$ if only the three ions a, b, and c were present in the assembly

$$\boldsymbol{\sigma}_{abc}=\boldsymbol{\sigma}_{acb}=[\mathbf{n}_a\sum_{n\geq 1}(1-\mathbf{n}_a-\mathbf{n}_b-\mathbf{n}_c)^n]-\boldsymbol{\sigma}_{ab}-\boldsymbol{\sigma}_{ac}$$
$$=\mathbf{n}_a\mathbf{n}_b\mathbf{n}_c+\mathbf{n}_a\mathbf{n}_c\mathbf{n}_b-\cdots, \tag{53}$$

and so forth for higher numbers of ions. If the assembly contains only the two ions a and b, the binding energy, with $\boldsymbol{\sigma}_a=\boldsymbol{\sigma}_{ab}$ in (51), will become

$$\Delta E_{ab}=Q_{ab}-[\mathbf{n}_a\mathbf{A}\mathbf{n}_b]_{tr}$$
$$-[(U_a+\mathbf{n}_a\mathbf{A})\boldsymbol{\sigma}_{ba}-(U_b+\mathbf{n}_b\mathbf{A})\boldsymbol{\sigma}_{ab}]_{tr}$$
$$+\tfrac{1}{2}[(\boldsymbol{\sigma}_{ab}+\boldsymbol{\sigma}_{ba})(\mathbf{B}-\mathbf{A})(\boldsymbol{\sigma}_{ab}+\boldsymbol{\sigma}_{ba})]_{tr}. \tag{54}$$

The first three terms of this expression are the important ones, and those which are usually considered. The following term is of higher order in the overlap integrals.

If the assembly has three ions, a, b, c, only, the binding energy will include the terms for the three pairs, and, in addition a term:

$$\Delta E_{abc}=-[(U_a+\mathbf{n}_a\mathbf{A})(\boldsymbol{\sigma}_{bca}+\boldsymbol{\sigma}_{cab})$$
$$-(U_b+\mathbf{n}_b\mathbf{A})(\boldsymbol{\sigma}_{cab}+\boldsymbol{\sigma}_{abc})$$
$$-(U_c+\mathbf{n}_c\mathbf{A})(\sigma_{abc}+\boldsymbol{\sigma}_{bca})]_{tr}$$
$$+\tfrac{1}{2}[(\boldsymbol{\sigma}_{abc}+\boldsymbol{\sigma}_{bca}+\boldsymbol{\sigma}_{cab})$$
$$\times(\mathbf{B}-\mathbf{A})(\boldsymbol{\sigma}_{abc}+\boldsymbol{\sigma}_{bca}+\boldsymbol{\sigma}_{cab})]_{tr}. \tag{55}$$

In general, for any assembly one has

$$\Delta E=\tfrac{1}{2}\sum_{a\neq b}\sum\Delta E_{ab}+\tfrac{1}{6}\sum_{a\neq bc}\sum_{b\neq c}\sum\Delta E_{abc}+\cdots \tag{56}$$

in which the first terms are the pair energies, dependent on the properties and coordinates of the pair of ions, a, b, alone. The terms ΔE_{abc} depend specifically on all three ions but are terms of relatively high order only. As Löwdin[1] has shown these are responsible for the deviations from Cauchy's relations in the alkali halide crystals.

All the terms of (51) are interpretable as interactions between charges, or as interactions between an electric potential due to a charge and a charge distribution. The interpretation of Q_{ab}, Eq. (49), as the interaction of the charge distribution which the ions a and b would have as isolated ions is obvious and simple. The term $[U_a\boldsymbol{\sigma}_b]$ is the interaction of the charge of ion a with a charge of density $2\sigma_b'(\mathfrak{r},\mathfrak{r})$ at the position $\mathfrak{r}$, integrated over all values of $\mathfrak{r}$. Since $[\boldsymbol{\sigma}_b]_{tr}=0$, Eq. (29′), the charge distribution represented by $\sigma_b'(\mathfrak{r},\mathfrak{r})$ has a net magnitude zero, that is the positive and negative portions cancel. We might call such a charge distribution a quasi-dipole. The term $[\boldsymbol{\sigma}_a\mathbf{B}\boldsymbol{\sigma}_b]_{tr}$ may thus be said to represent the interaction of two quasi-dipoles.

The terms of type $[\mathbf{fAg}]_{tr}$ are

$$[\mathbf{fAg}]_{tr}=\int\int f(\mathfrak{r}_1,\mathfrak{r}_2)[1/R_{12}]g(\mathfrak{r}_2,\mathfrak{r}_1)d\mathfrak{r}_2d\mathfrak{r}_1. \tag{57}$$

If one interprets $f(\mathfrak{r}_1,\mathfrak{r}_2)\,g(\mathfrak{r}_2,\mathfrak{r}_1)$ as giving the product of the two charges, per unit volume, which can be simultaneously at $\mathfrak{r}_1$, $\mathfrak{r}_2$, then $[\mathbf{fAg}]_{tr}$ may be regarded

as the interaction of this double charge distribution. The charge distribution $\mathbf{fg}$ is thus not the product of two independent distributions, but the probability of finding charge at $\mathfrak{r}_1$ is influenced by the charge at $\mathfrak{r}_2$. The average value of the product of the two charges is $[\mathbf{fg}]_{tr}$. For the terms in (51) this average is zero from (30) that $[\varrho_a\varrho_b]_{tr}=0$ if $a\neq b$, and (31) that $[\boldsymbol{\sigma}_a\boldsymbol{\sigma}_a]_{tr}=0$.

IV. DISCUSSION

Equation (51) is the exact expression, correct to all orders, for the binding energy of an assembly of closed shell atoms or ions, within the limits of the two approximations, (a) that the eigenfunction of the system is an antisymmetrized sum of a single product of one-electron functions, and (b) that these functions are linear combinations of those of the lowest state of the isolated ions or atoms. It contains the classical interactions, Q_{ab}, between the electric charges of the undisturbed ions, without any normalization denominator. In addition it contains terms, $[U_a\boldsymbol{\sigma}_b]_{tr}$, which are interpretable as the interactions of the classical electrostatic potential, $U_a(\mathfrak{r})$, due to the undisturbed ion a and a charge distribution $\sigma_b(\mathfrak{r},\mathfrak{r})$ of net charge zero. All other terms are similarly interpretable as the electrostatic interactions of charge distributions of which the net charge is zero.

It is not the purpose of this paper to go further than to derive the Eqs. (51) to (56). However, it is to be emphasized that their use might facilitate computations. If the expression (3) for the elements, $\eta_a(\mathfrak{r}_1,\mathfrak{r}_2)$, of the density matrix of ion a is used, which gives these elements in terms of the one-electron functions, then the Eqs. (51) to (56) blow up into the usual long summations of integrals over products of single electron functions. However, various approximations for the elements, $\eta_a(\mathfrak{r}_1,\mathfrak{r}_2)$, may be used which would seem to offer hope of simplifying the computation.

One such approximation is to use

$$r=\tfrac{1}{2}|\mathfrak{r}_1+\mathfrak{r}_2|,\quad s=|\mathfrak{r}_1-\mathfrak{r}_2|, \tag{58}$$

and

$$\eta_a'(\mathfrak{r}_1,\mathfrak{r}_2)=f_a(r)g(x);\quad x=s[f_a(r)]^{\frac{1}{3}}; \tag{59}$$

where $g(0)\equiv 1$, and

$$\int_0^\infty 4\pi x^2 g^2 dx=1.$$

Then $f_a(r)$ is the electrical density of electrons of a single spin direction at the distance r from the nucleus. This form of Eq. (59) satisfies the requirement on the trace

$$[\mathbf{n}_a']_{tr}=[\mathbf{n}_a'\mathbf{n}_a']_{tr}.$$

The form $g(x)=(3/z^3)[\sin z-z\cos z]$, $z=(6\pi^2)^{\frac{1}{3}}x$, corresponds to the usual approximation that the kinetic energy at r is related to the density in the same way that it is for a free gas. Another approximation, $g(x)=\exp-\frac{1}{2}\pi x^2$, is almost equivalent to the Bessel function.

The work of Löwdin[1] has demonstrated that the lattice energy of the alkali halide crystals can be computed very accurately by equations essentially the same as (51). However, it is clear that the energy of the alkali halide gas molecules will not be given adequately by such equations. The failure is due primarily to the failure of the assumption which we have labeled (b), namely, that the one-electron functions of the assembly be made up of those of the isolated ions in their ground states.

To formally write the theory for the interaction energy including the perturbation effects of excitation to higher ionic states is quite feasible, but presumably a numerical computation using such a theory would be impracticable without recourse to some essential simplification. One simplifying procedure seems tempting. It is possible to write equations for the first-order perturbation, $\lambda\Delta\mathbf{n}_a$, to be added to the unperturbed matrix, $\mathbf{n}_a$, of an ion a in a perturbing potential, λV_a. Various approximate methods of doing this suggest themselves.

One might attempt then, to compute the perturbed density matrix for each ion, a, in the classical perturbing field V_a due to the other ions of the assembly, and use these in the density matrix of the assembly.

In general we would like to suggest that the great formal simplicity of writing reasonably exact equations with the use of the density matrix, coupled with the possibility of using relatively simple approximate forms for numerical evaluation, might be of considerable value in the study of atomic, ionic, and molecular interactions.

A Detailed Formulation of Kinetic Processes from the Point of View of the Activated Complex

SIDNEY W. BENSON
Professor of Chemistry, Chemistry Department, University of Southern California
(Received January 29, 1952)

By combining Slater's classical treatment for the adiabatic decomposition of an unstable molecule with the Lindemann mechanism for collisional activation it is possible to make a uniform and consistent treatment of kinetic processes of all orders. The high pressure rate constants may then be represented by

$$k_{obs}=\alpha\cdot\langle\bar{\nu}\rangle\cdot K^{\ddagger}\cdot\exp(-E^*/kT),$$

where $\langle\bar{\nu}\rangle$ is a root mean square average of the "n" normal modes of vibration of the activated complex, E^* is the minimum energy required for reaction, α is a "transmission coefficient" which is unity for unimolecular processes and between $\frac{1}{2}$ and 1 for higher order reactions, and $K^{\ddagger}$ can be interpreted in terms of an entropy of activation. A more complicated expression is obtained for lower pressures in the case of unimolecular reactions.

The theory is sufficiently detailed to allow predictions on the relation of molecular structure to the pressure region in which collisional activation becomes a limiting rate factor for unimolecular reactions. Similarly predictions may be made concerning the nature of recombination processes and their pressure and temperature dependence. It is shown that recombination processes will have a negative temperature coefficient and in addition the mean life of the activated complex will vary inversely with some power of the strength of the bond being formed. As a result of this, recombination will be more efficient in photochemical or, more generally, low temperature chain reactions than in pyrolytic reactions and consequently chain lengths will be longer in the latter.

A RECENT analysis by Slater[1] of the process of adiabatic decomposition of an unstable molecule has provided a sufficiently detailed description of the mechanism of this process to permit of an extended and uniform treatment of higher order processes as well as unimolecular processes.[2] It is the purpose of the present paper to extend the Slater theory and outline some of the quantitative predictions which it makes in regard to kinetic processes.

I. MATHEMATICAL FORMULATION IN TERMS OF THE ACTIVATED COMPLEX

The experimentally observable rate constant for a unimolecular decomposition may be formally written as[3]

$$k_{obs}=\int_0^\infty \bar{k}(\epsilon)P(\epsilon)d\epsilon, \tag{1}$$

in which $\bar{k}(\epsilon)$ is the mean probability per unit of time that a molecule having internal energy in the range ϵ, $\epsilon+d\epsilon$ decompose and $P(\epsilon)d\epsilon$ is the number of such molecules in the system. The process may be represented chemically as

$$(X)^*\xrightarrow[k_{obs}]{}\text{products}. \tag{2}$$

Most generally, even for an "isothermal" system, $\bar{k}(\epsilon)$ may be a function of time as well as energy, and $P(\epsilon)$ may be a function of pressure, temperature, and total composition, so that k_{obs} is not necessarily a constant.

A state of a polyatomic molecule X (N atoms) may be specified classically by a statement of the configuration of its internal coordinates $(x_1\cdots x_{3N-6})$ and components of momentum $(P_1\cdots P_{3N-6})$. The total energy E of the system is then given by the sum of potential and kinetic energies, usually of the form

$$E=U(x_1\cdots x_{3N-6})+\sum\frac{pi^2}{2m_i}, \tag{3}$$

and we can define an "activated complex" X^* as one having a total energy $\epsilon>\epsilon^*$, such that for molecules having energies $\epsilon\leqslant\epsilon^*$, $\bar{k}(\epsilon)=0$, while for all others $\bar{k}(\epsilon)>0$.

Equation (3) defines a $(6N-12)$ dimensional hypersurface over which the molecule is constrained to move. The chemical reaction can be defined by the statement that there is a bounded region on this hypersurface for which the potential energy function $U(x_i)$ has a maximum. Or, more generally, there is a set of configurations of the molecule, $L(x_i)$, such that $\partial U/\partial L=0$ and $\partial^2U/\partial^2L<0$. The family of configurations $L(x_i)$ can be described by a linear superposition of the internal coordinates

$$L(x_i)=\sum\alpha_i\cdot x_i, \tag{4}$$

and the intersection of the two surfaces[4] defined by Eqs.

[1] N. B. Slater, Proc. Roy. Soc. (London) **A194**, 112 (1948).
[2] S. W. Benson, J. Chem. Phys. **19**, 802 (1951).
[3] In this paper classical statistics will be used in place of quantum statistics. While a similar and parallel formulation can be made in terms of quantum statistics, it cannot be resolved analytically with the same facility, nor can $k(\epsilon)$ be calculated explicitly.

[4] $L(x_i)$ represents a $(3N-6)$ dimensional hyperplane, and ϵ^* is defined as the minimum value of ϵ for which $L(x_i)$ intersects (i.e., actually is tangent to) one of the energy surfaces. For surfaces of energy $\epsilon>\epsilon^*$, the intersection of $L(x_i)$ and $E(x_i, P_i)$ cuts $E(x_i, P_i)$ into two regions. The region for which $L(x_i)<L_0(x_i)$ (corresponding to the maximum in $E(x_i)$) will then represent reactants and the other region products. Any dynamical path of

(3) and (4) then defines the portion of the energy hypersurface corresponding to chemical reaction (i.e., mechanical instability).

Rigorously, we can now calculate $k(\epsilon)$, the rate of decomposition, as the inverse of the mean time needed for a molecule to diffuse from any given region of the hypersurface across the intersection. Such a complete solution has not been made. Slater,[1] however, has solved the idealized problem in which the dynamical motion over the hypersphere can be analyzed into a multiply periodic motion in terms of some set of normal coordinates, each of which is harmonic in character.

If we assume that there is equal density of occupation of all regions of the hypersurface ϵ, then Slater's solution for $\bar{k}(\epsilon)$ is given by[5]

$$\bar{k}(\epsilon)=\langle\bar{\nu}\rangle\cdot\left(1-\frac{\epsilon^*}{\epsilon}\right)^{n-1}, \tag{5}$$

where $\bar{k}(\epsilon)$ is the equally weighted average of $k(\epsilon)$ for all configurations,

$$\langle\bar{\nu}\rangle=\left[\frac{\sum\alpha_i^2\nu_i^2}{\sum\alpha_i^2}\right]^{\frac{1}{2}}, \tag{6}$$

and the ν_i are the normal frequencies of a subset of n, internal, "normal" coordinates which describe the decomposition.[6]

II. UNIMOLECULAR PROCESSES

The problem of computing a rate constant now becomes a problem of calculating a value for $P(\epsilon)$, the number of molecules having energy ϵ. For a unimolecular process we shall employ the Lindemann collision mechanism:

$$\begin{array}{l} A+A\underset{k_D}{\overset{k_A}{\rightleftarrows}}A^*+A \\ \qquad\qquad\quad \big\downarrow k_r \\ \qquad\qquad\quad \text{Products.} \end{array} \tag{7}$$

Employing the stationary state hypothesis we can write for the stationary concentration of $A^*(\epsilon)$

$$A_S^*(\epsilon)=\frac{k_A(\epsilon)\cdot A^2}{k_D(\epsilon)A+k_R(\epsilon)}, \tag{8}$$

and for the rate of reaction

$$R(\epsilon)=k_R(\epsilon)\cdot A_S^*(\epsilon)=\frac{k_A(\epsilon)\cdot k_R(\epsilon)\cdot A^2}{k_D(\epsilon)\cdot A+k_R(\epsilon)} \tag{9}$$

$$=K_{eq}(\epsilon)\cdot\mathcal{K}(\epsilon)\cdot k_R(\epsilon)\cdot A, \tag{10}$$

where $K_{eq}(\epsilon)=k_A(\epsilon)/k_D(\epsilon)$, the equilibrium constant for the equilibrium between normal molecules A and activated complexes $A^*(\epsilon)$ and

$$\mathcal{K}(\epsilon)=\left[1+\frac{k_R(\epsilon)}{k_D(\epsilon)\cdot A}\right]^{-1}<1.$$

The use of the stationary state hypothesis implies that $k_A(\epsilon)\ll[k_D(\epsilon)\cdot A+k_R(\epsilon)]$.[7]

If now we use the classical Boltzmann expression for $K(\epsilon)$,

$$K(\epsilon)=\frac{1}{(n-1)!}\left(\frac{\epsilon}{kT}\right)^{n-1}e^{-\epsilon/kT}. \tag{11}$$

We can write an integral for the rate (integrated over all energies), or for the rate constant k_{obs} defined as

$$k_{obs}=\frac{1}{A}\cdot\text{Rate}=\int_0^\infty K_{eq}(\epsilon)\cdot\mathcal{K}(\epsilon)\cdot k_R(\epsilon)d\epsilon$$

$$=\frac{\langle\bar{\nu}\rangle e^{-\epsilon^*/kT}}{(n-1)!}\int_0^\infty\frac{x^{n-1}e^{-x}dx}{1+(\langle\bar{\nu}\rangle/k_D\cdot A)(x/x+x^*)^{n-1}}, \tag{12}$$

where $x=(\epsilon-\epsilon^*)/kT$ and $x^*=\epsilon^*/kT$.[8]

If we now assume that $k_D(\epsilon)\cdot A\gg k_R(\epsilon)$ so that $\mathcal{K}(\epsilon)=1$, this last equation gives the familiar form for the high pressure rate constant

$$k_{obs}=\langle\bar{\nu}\rangle e^{-\epsilon^*/kT}. \tag{13}$$

This last condition implies that the detailed rate of deactivation is much faster than the rate of reaction; and since the maximum rate of deactivation, namely, the collision frequency, can be calculated from kinetic theory, this allows us to put a numerical limit on the permissible values of $k_R(\epsilon)$.[2] To do this in detail, let us examine Eq. (12). When $k_D(\epsilon)\cdot A\gg k_R(\epsilon)$ the integrand has a maximum at $x=n-1$ or $\epsilon_{max}=\epsilon^*+(n-1)kT$. As $k_D(\epsilon)\cdot A$ becomes smaller, this maximum recedes to smaller values. Furthermore, the curve will be fairly peaked about this maximum in terms of kT, so that

the molecule on $E(x_i, P_i)$ which crosses the intersection will react only if its internal coordinates satisfy the condition that $L(x_i)>L_0(x_i)$.

[5] Equation (5) can be given an interpretation in terms of an equilibrium model of the diffusion process. The frequency $\langle\bar{\nu}\rangle$ may be looked upon as a mean frequency of motion of the complex over the hypersurface. The fraction $[1-(\epsilon/\epsilon)^*]^{n-1}$ represents the ratio of that area of the hypersurface corresponding to reaction to the total surface. The product of these two quantities is then the mean rate at which an average complex will diffuse into a configuration corresponding to reaction. The analysis is thus formally identical with that of Kassel's [J. Phys. Chem. **32**, 225 (1928)] and that of Rice and Ramsperger [J. Am. Chem. Soc. **49**, 1617 (1927)]. The principal difference is that in the treatment of the latter authors the $\bar{\nu}$ was not explicitly calculated but introduced merely as a multiplicative constant.

[6] It should be noted that a truly harmonic system does not admit of a saddle point, i.e., there are no (x_i) satisfying $\partial U/\partial L=0$. This has been discussed in some detail by Slater (see reference 1) and by Kramers [Physica **7**, 284 (1940)]. Qualitatively it would make the true value of $\langle\bar{\nu}\rangle$ less than that calculated in Eq. (6). That is, the frequencies (ν_i) become somewhat smaller by the anharmonic distortion. Quantitatively, the effect is difficult to deal with.

[7] S. W. Benson, J. Chem. Phys. (to be published).

[8] This is formally identical with Kassel's expression, *Kinetics of Homogeneous Gas Reactions* (Reinhold Publishing Company, New York, 1932), Chapter V.

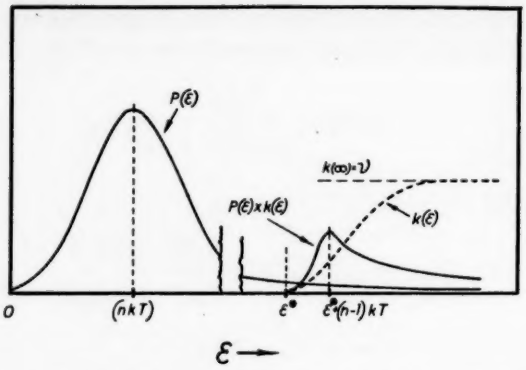

FIG. 1. Molecular distribution function ($P(\epsilon)$), detailed rate function ($k(\epsilon)$) and their product as a function of energy.

most of the contribution to the rate will come from molecules having energies ϵ_m, in the neighborhood of $\epsilon^*+(n-1)kT$. The integrand is shown in Fig. 1. The mean rate of decomposition of these molecules is given by

$$\bar{k}(\epsilon_m)=\langle\bar{\nu}\rangle\left(1-\frac{\epsilon^*}{\epsilon_m}\right)^{n-1}=\langle\bar{\nu}\rangle\left[\frac{(n-1)kT}{\epsilon^*+(n-1)kT}\right]^{n-1}$$

$$=\langle\bar{\nu}\rangle\left[1+\frac{\epsilon^*}{(n-1)kT}\right]^{1-n}. \quad (14)$$

Values of the ratio $\bar{k}(\epsilon_m)/\langle\bar{\nu}\rangle$ are given in Table I for different ϵ^*/kT and n.[9] The reciprocal of this quantity is shown plotted in Fig. 2.

In Table I, the first column gives the number of atoms in the molecule; column 2 gives n, the number of degrees of internal freedom and the last column gives $P_{eq}(35)$, the pressure (at 0°C) for which the collisional frequency would be equal to the rate of reaction when $\epsilon^*/kT=35$ and $\langle\bar{\nu}\rangle=1\times10^{13}$ sec^{-1}. This last column shows at once that the unimolecular decomposition constants for molecules containing more than 6 atoms will not be expected to show any pressure dependence until the total pressure has fallen to about 1 mm Hg. This is in agreement with the recent work of Swarc,[10] who has found that the rate constants for the unimolecular decomposition of substituted benzenes and other large molecules do not show any pressure dependence down to pressures of 10 mm Hg.[11] The frequency factors which he reports are also in the expected range, namely, 1×10^{-13} sec^{-1}. In fact it seems clear that if the Lindemann hypothesis is to be verified in available apparatus, then studies must be limited to polyatomic molecules having 3, 4, 5, or at most 6 atoms. Of these smaller molecules which have been studied, there is evidence available only for N_2O, thanks to the recent re-interpretation by Johnston.[12] The latter author has shown that the data from several laboratories do lend themselves to a consistent interpretation in terms of a formal equivalent of the Slater theory. In this case, $\langle\bar{\nu}\rangle\sim2\times10^{13}$ sec^{-1} and $n=4$, both of which are in accord with the linear structure of the molecule and its known frequencies. In the case of F_2O, a bent molecule with $n=3$, the data can be fitted to the Slater theory, but there are also indications that a chain reaction is important and the interpretation becomes ambiguous.[13] One point of considerable interest which arises from the present discussion is the effect of structure on rate of decomposition. Since a linear molecule will have one extra degree of freedom, its chances of decomposing unimolecularly are greater than that of a bent molecule having the same number of atoms.[14]

It is clear also from the present analysis why there are so many more first-order processes in solution than in the gas phase. In the solution, the solvent can form a loose complex with the reactant species in such a way that the effective number of coupled degrees of freedom becomes large even for a simple reactant, and the collision mechanism is masked by the slow internal energy transfer processes in the complex.[15]

TABLE I. Variation of mean reaction rate with number of degrees of freedom and activation energy.

		Values of $\bar{k}(\epsilon_m)/\langle\bar{\nu}\rangle$			
ϵ^*/kT		30	35	40	
No. of atoms	n				$P_{eq}(35)$[a]
2	1	1	1	1	1080 atmos
...	2	3.23×10^{-2}	2.78×10^{-2}	2.44×10^{-2}	30 atmos
3	3	3.91×10^{-3}	2.93×10^{-3}	2.27×10^{-3}	3.17 atmos
3	4	7.51×10^{-4}	4.92×10^{-4}	3.40×10^{-4}	0.53 atmos
...	5	1.92×10^{-4}	1.10×10^{-4}	6.83×10^{-5}	91 mm Hg
4	6	5.95×10^{-5}	3.05×10^{-5}	1.70×10^{-5}	25 mm Hg
4	7	2.14×10^{-5}	9.80×10^{-6}	4.90×10^{-6}	8.1 mm Hg
5	9	3.86×10^{-6}	1.42×10^{-6}	5.95×10^{-7}	1.2 mm Hg
6	12	5.08×10^{-7}	1.47×10^{-7}	4.65×10^{-8}	0.12 mm Hg
7	15	1.10×10^{-7}	2.42×10^{-8}	6.00×10^{-9}	0.020 mm Hg
8	18	3.10×10^{-8}	5.51×10^{-9}	1.18×10^{-9}	0.0045 mm Hg
...	∞	9.5×10^{-14}	6.6×10^{-16}	5.5×10^{-18}	5.4×10^{-10} mm Hg

[a] $P_{eq}(35)$ is calculated (0°C) for a molecule having collision cross section of 20 Ang^2 and a mass of 50, assuming that $\langle\bar{\nu}\rangle=1\times10^{13}$ sec^{-1} and $Z_{STP}=9.2\times10^9$ sec^{-1} (collision frequency).

[9] For bond breaking reactions, $\langle\bar{\nu}\rangle$ will generally be in the range 1×10^{13} to 3×10^{13} sec^{-1} depending on the bond strength and reduced mass. (It may be higher for the breaking of a C—H bond.) Since experimental observations are generally confined to reactions having half-lives of from 0.1 sec to 10^5 sec this will keep observable reactions [see Eq. (13)] to values of ϵ^*/kT in the range 30 to 40. For the known data there is a clustering about the mean value of 35.

[10] M. Swarc, Chem. Revs. **47**, 75 (1950).

[11] It is difficult to work effectively at pressures lower than 1 mm Hg since at these pressures, collisions with the wall become increasingly important in any normal size laboratory equipment. Thus in a flask of 5-cm radius, at 1 mm Hg pressure, there will be about 1 wall collision for every 1000 molecular collisions. If the activation energy is lower for a molecule on the wall by 4.5 kcal, then this difference will easily compensate for the lower collision rate at the wall.

[12] H. S. Johnston, J. Chem. Phys. **19**, 663 (1951).

[13] R. N. Pease, *Equilibrium and Kinetics in Gaseous Systems* (Princeton University Press, Princeton, New Jersey, 1942).

[14] In the case of a diatomic molecule (e.g., H_2, I_2, Br, etc.) $n=1$, $n-1=0$ and $k(\epsilon)=\langle\bar{\nu}\rangle$ where $\langle\bar{\nu}\rangle$ is now the "frequency" of vibration of the unstable molecule and the molecule will rupture within the time of a single vibration. Since these frequencies are of the order of 10^{13}–10^{14} sec^{-1}, it is clear that diatomic molecules will never decompose by a unimolecular process, but only by bimolecular processes.

[15] For such coupling to be effective, weak interaction of the order of van der Waal's forces are sufficient. The frequency of energy transfers will have an order of magnitude of the vibration

A special word must be added concerning intramolecular reactions such as internal cyclizations. In these cases the reaction between separated parts of the same molecule assume an almost bimolecular character, and it is undoubtedly very poor approximation to consider the interactions between these parts as given by a simple Hooke's Law expression. This difficulty can be resolved either by considering the reaction as "bimolecular" or else by introducing a statistical factor which counts as "reactant" molecules only those configurations in which the reactive groupings are in juxtaposition.*

III. BIMOLECULAR PROCESSES

It is possible to set up a series of equations for formation of a collision complex $(AB)^*$ comparable to the Lindemann system for the unimolecular process [Eq. (7)]. With the exception of reactions between two atoms or an atom and a diatomic molecule, it then turns out that the stationary concentration of complexes is practically independent of composition and pressure, so that we can write

$$A+B \overset{K(\epsilon)}{\rightleftarrows} (AB)^* \xrightarrow{k_R(\epsilon)} \text{Products} \tag{15}$$

and

$$(AB)_\epsilon^* = K \cdot A \cdot B \cdot \alpha, \tag{16}$$

where α is a fraction which may have a value generally close to unity but almost never less than $\frac{1}{2}$ and virtually independent of composition and total pressure.[16]

Under these conditions we can write for the detailed stationary rate of reaction

$$\frac{d(\text{Prod.})}{dt} = k_R(\epsilon)(AB)_\epsilon^* = K(\epsilon) \cdot k_R(\epsilon) \cdot \alpha \cdot A \cdot B, \tag{17}$$

and for the over-all experimental rate constant

$$k_{\text{obs}} = \frac{1}{A \cdot B} \cdot \frac{\langle d(\text{Prod.}) \rangle_{Av}}{dt} = \alpha \int_0^\infty K(\epsilon) \cdot k_R(\epsilon) d\epsilon. \tag{18}$$

If now we apply the Slater treatment, considering the internal modes of the complex $(AB)^*$ as classical and harmonic and using $k_R(\epsilon)$ from Eq. (5), we find for the integrated rate constant

$$k_{\text{obs}} = \alpha \cdot \langle \bar{\nu} \rangle \cdot K^\# \exp(-\epsilon/kT), \tag{19}$$

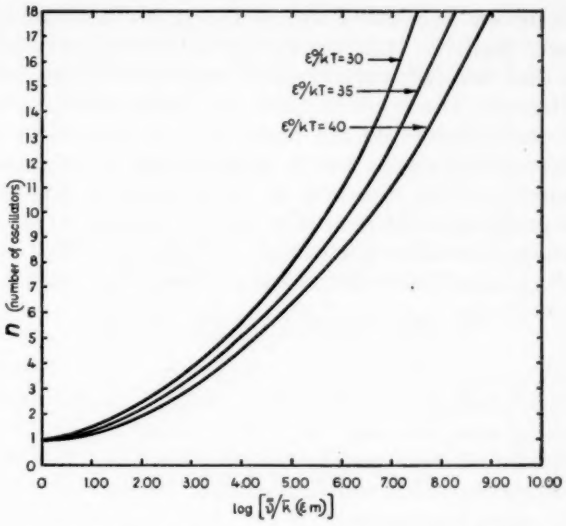

FIG. 2. Effect of molecular complexity and activation energy on the mean life of an activated complex.

where $\langle \bar{\nu} \rangle$ and ϵ^* are defined as before and $K^\#$ represents essentially an entropy of activation. $K^\#$ is the equilibrium constant for the equilibrium between $(AB)^*$ and normal A and B [Eq. (15)] from which the exponential energy term has been removed as well as the n internal vibrations describing the decomposition of the complex.[17]

The rate constant given in Eq. (19) bears a close resemblance to that derived by the Eyring treatment,[18] and given by the equation

$$k_{\text{obs}}(\text{Eyring}) = \mathfrak{K} \cdot \frac{kT}{h} \cdot K^\ddagger \exp(-\epsilon^*/kT). \tag{20}$$

The $K^\ddagger$ of the latter theory [Eq. (20)] is the equilibrium constant between A, B, and $(AB)^*$, with the exponential energy term and only one vibrational term removed. Since, however, the vibrational contributions to the equilibrium constant are generally negligible, it may be expected that $K^\ddagger$ and $K^\#$ will be nearly equal.

The α of Eq. (19) and the $\mathfrak{K}$ of Eq. (20) may both be looked upon as transmission coefficients, again having similar values (i.e., close to unity).[19] An essential difference lies in the two terms, $\langle \bar{\nu} \rangle$ on one hand and kT/h on the other. In the Slater theory, $\langle \bar{\nu} \rangle$ is a molecular constant, independent of temperature and lying in the range 1×10^{13}–1×10^{14} sec^{-1} (or even higher for reactions involving strong bonds). The factor kT/h has the value

frequencies of the uncoupled systems even for quite weak coupling. Infrared spectra are not too good a source of information in this regard since weak couplings between oscillators of different frequencies will not perturb the original frequencies greatly and can yet lead to very rapid energy transfer. Sound dispersion measurements in liquid mixtures, as a function of composition, would be much more informative.

* Such steric considerations are also of importance in higher order processes where certain configurations may completely inhibit reaction [see M. Magat and N. Ivanoff, J. Chim. Phys. **47**, 914 (1950); M. Magat, J. Chim. Phys. **47**, 922 (1950)].

[16] S. W. Benson, "The Role of Collision Processes in Reaction Kinetics" (to be published).

[17] For a reversible reaction (i.e., Products$\rightleftharpoons(AB)^*$) the product $\alpha^1\langle\bar{\nu}^1\rangle$ for the reverse reaction turns out to be equal to $\alpha\langle\bar{\nu}\rangle$ for the forward reaction.

[18] Glasstone, Laidler, and Eyring, *The Theory of Rate Processes* (McGraw-Hill Book Company, Inc., New York, 1941).

[19] In the case of simple systems (atom and diatomic molecule reactions) both α and $\mathfrak{K}$ should both be pressure dependent (see reference 16). In the case of reactions involving 5 or more atoms α is independent of pressure.

6×10^{12} sec^{-1} at 3000°K and is thus generally somewhat lower than $\langle\bar{\nu}\rangle$. It is, however, temperature dependent so that this difference becomes smaller at higher temperatures. The result of these similarities is such that the two theories do not easily lend themselves to an experimental distinction. It is the feeling of the author that the Slater theory is to be preferred as giving a more detailed and internally more consistent model of rate processes (see reference 2) and also one which permits of a unified treatment of processes of all orders.[20]

IV. RECOMBINATION PROCESSES

A special case of a bimolecular process which requires a more detailed consideration is that of recombination. In this case the reaction of the complex is not completed until the excess energy of its formation has been removed by collisional deactivation. We may represent the over-all sequence as

$$\begin{gathered} A+B\underset{k_2}{\overset{k_1}{\rightleftarrows}}(AB)^*;\quad K=k_1/k_2 \\ (AB)^*+M\underset{k_3}{\longrightarrow}(AB)+M^*, \end{gathered} \tag{21}$$

and for the steady state concentration of $(AB)^*$ we have

$$(AB)_s{}^*=\frac{k_1}{k_2}\cdot A\cdot B\left[\frac{k_2}{k_2+k_3M}\right], \tag{22}$$

and for the detailed rate of reaction

$$\text{Rate}=k_3(AB)^*\cdot M=K\cdot(A\cdot B)\cdot\left[\frac{k_2\cdot k_3\cdot M}{k_2+k_3\cdot M}\right], \tag{23}$$

or for the integrated rate constant defined as

$$k_{\text{obs}}=\frac{1}{A\cdot B}\overline{\text{Rate}}=\int_0^\infty\frac{K\cdot k_2\cdot k_3\cdot M}{k_2+k_3M}d\epsilon, \tag{24}$$

in which K, k_2, and k_3 are functions of ϵ.

If we assume that k_3 is independent of energy and replace k_2 by $k(\epsilon)$ [Eq. (5)], this becomes

$$k_{\text{obs}}=k_3M\cdot\int_0^\infty\frac{K(\epsilon)k(\epsilon)d\epsilon}{k(\epsilon)+k_3M}. \tag{25}$$

In the limiting case that the frequency of collisional deactivation is fast compared to fission of the complex ($k_3M\gg k(\epsilon)$) this integrates directly to give Eq. (19), and the pressure dependence of the rate disappears. In the other limit which is to be expected for the recombination of atoms ($k_3M\ll k(\epsilon)$) the expression is that for a third-order process

$$k_{\text{obs}}=k_3\cdot M\cdot K \tag{26}$$

or

$$k_{\text{obs}}{}'=\alpha'\cdot\langle\bar{\nu}\rangle'\cdot K^{\ddagger}(A,B,M)e^{-\epsilon^*/kT}, \tag{27}$$

where the primes refer to the three-body process

$$A+B+M\rightleftarrows(ABM)^*\rightarrow AB+M^*. \tag{28}$$

We can tell from Table I what systems will fall in either of the limiting categories or else be intermediate and show an involved pressure dependence given by Eq. (25). Recombinations of atoms will all fall into the first category [Eqs. (26), (27)], and these have been recognized for some time as three-body processes.[21] On the other hand, it is to be expected that the recombinations of complex radicals or molecules such as methyl radicals, triphenyl methyl radicals, cyclopentadiene, etc., will give rise to such long-lived complexes that they will show no pressure dependence except at pressures that are experimentally unfeasible. And this again seems to be in accord with the facts.[22]

On the other hand, we see from Table I that those recombination reactions in which the complex contains 3 or 4 atoms may be expected to show the intermediate pressure dependence of Eq. (25) in an experimentally accessible pressure range. Thus recombinations such as COCl+Cl, CO+Cl, HO+HO, NO+O, O_2+O, H+O_2, CO+O, etc., should fall into this category. In particular we observe again that the linear complexes will have a longer mean life than bent complexes and so show a lesser pressure dependence for recombination.†

There is one final point of interest in connection with these recombination processes. The average energy of the recombination complexes will be $\epsilon^*+(n-1)kT$, where ϵ^* is as great as the energy of the bond formed. The mean rate of decomposition of such complexes, $\bar{k}(\epsilon_m)$, is given by Eq. (14), namely,

$$\bar{k}(\epsilon_m)=\langle\bar{\nu}\rangle\left[1+\frac{\epsilon^*}{(n-1)kT}\right]^{-1n}. \tag{14}$$

Now in computing values of $\bar{k}(\epsilon_m)$ for Table I we made the assumption that $\epsilon^*/kT\approx35$. This is a valid

[20] The extension of the treatment to termolecular and higher order processes follows immediately from that given above for bimolecular processes and has precisely the same form. It should be observed, however, that in the case of higher order reactions whose rate may become diffusion controlled (i.e., polymerization in solution), the concentration dependence of α begins to become more important and may play a rather decisive role (see reference 16).

[21] The varying efficiencies of different third bodies M for atomic recombinations can be looked at in terms of the entropy term $K^{\ddagger}(A,B,M)$ and the activation energy ϵ^*. Since in general ϵ^* will be zero or at best of order of magnitude of kT, and the heat of association will be positive for the complex $(ABM)^*$, the net temperature coefficient for the reaction may be slightly negative. Thus we can expect most efficient recombinations to take place with those third bodies whose interactions with A and B will be greatest, and this has been recognized qualitatively for some time [see, for example, W. A. Noyes, Jr. and P. A. Leighton, *The Photochemistry of Gases* (Reinhold Publishing Company, New York, 1941)].

[22] The recent work on the recombination of methyl radicals though not complete or unambiguous, indicates that the rate is not pressure dependent [A. F. Trottman-Dickenson and E. W. R. Steacie, J. Chem. Phys. **18**, 1097 (1950)].

† Experiments are now being started in these laboratories to study some of these reactions in detail.

assumption for pyrolytic reactions. However, for sensitized reactions, photochemical reactions, or catalytically initiated chain reactions, the radicals are generally formed at temperatures far below the normal temperatures at which they would be formed in pyrolytic reactions. The result is that ϵ^*/kT for these "cold" radical reactions will have values much nearer 80–120 and we can write $\bar{k}(\epsilon_m)$ as

$$\bar{k}(\epsilon_m)\approx\langle\bar{\nu}\rangle\left[\frac{(n-1)kT}{\epsilon^*}\right]^{n-1}, \tag{29}$$

so that the complexes formed in the "cold" reaction will have much longer life times than those formed in the pyrolytic reactions. The difference in life times will usually be about a factor of 2^{n-1} to 4^{n-1}, that is, it could easily be a factor of several powers of 10 as, for example, in the recombination of methyl radicals at room temperature. It is further to be noted that since the activation energies for atom and radical recombinations are either zero or close to zero, that there will be a negative temperature coefficient for such reactions of the order of magnitude of $T^{(1-n)}$. This can be of considerable importance in the comparisons of radical recombinations in low temperature and in pyrolysis reactions.[23] There should also be a pronounced effect in reactions which reach explosion limits such as H_2+Cl_2 and H_2+O_2 where many of the chain-stopping reactions are recombination processes.

[23] That is, it may be quite misleading to simply carry over rate constants from one set of conditions to the other. Thus on the basis of the above we should expect recombinations to be more efficient in "cold" reactions (unless there is an activation energy involved) and so chain lengths should be shorter.

THE JOURNAL OF CHEMICAL PHYSICS VOLUME 20, NUMBER 7 JULY, 1952

Application of Eller's Optical Machine to the Determination of the Molecular Structure of Gases by Electron Diffraction

L. Bru, M. Pérez Rodriguez, and M. Cubero
Physics Laboratory, Seville University, Seville, Spain

(Received January 31, 1952)

We present in this paper a new application of the Eller's Optical Machine which allows one to reduce extraordinarily the time of calculations required in the trial and error method. We made the application to the chloride monoxide molecule.

In a recent work[1] presented to the Stockholm Congress, we studied the analogy existing between the diffraction of electrons by gaseous molecules and that of monochromatic light by a combination of slits picked for the purpose. The maxima and minima which appear in the diagrams obtained agree well, in position and intensity, with the corresponding ones of electron diffraction.

In the present work we present a variation on the former one in applying G. Eller's optical machine[2] which allows the experimental work to be simplified to an extraordinary extent.

As is known, Eller's machine allows one to add Fourier series very rapidly by photography, and generally speaking, any similar class of functions.

The intensity of the electron waves diffracted by gaseous molecules (rigid molecules) is given by the simplified expression

$$I(q)=\sum_{i,j}\frac{z_iz_j}{r_{ij}}\sin r_{ij}q, \tag{1}$$

r_{ij} being the distance which separates the atoms i and j and $q=4\pi(\sin\theta/2)/\lambda$.

Placing Eller's sinusoidal screen in a certain position, the illumination received on a photographic plate parallel to the screen along a direction perpendicular

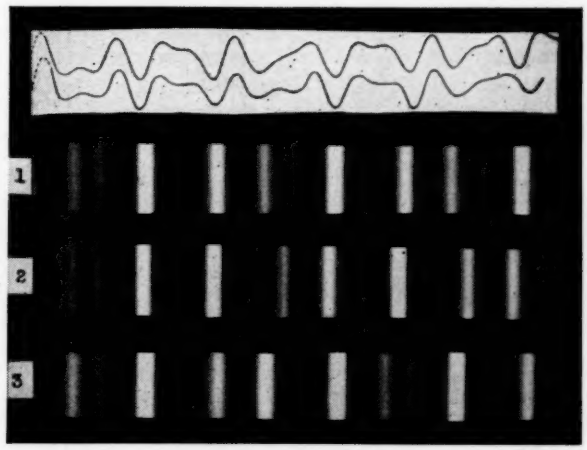

Fig. 1. Comparison of the intensities (visual) of the electron diffraction pattern and the intensities of the diagrams obtained with the Eller's optical machine. [(1) angle Cl—O—Cl 110.8°: (2) 114.4°; (3) 106.6°.]

[1] L. Bru and M. Perez Rodriguez, Proc. Phys. Soc. (London) B65, 249, 1952.
[2] G. Eller, Compt. rend. 232, 1122, 2333 (1951).

TABLE I.

Diagram	Distance Cl–O	Angle Cl–O–Cl
I	1.701A	110.8°
II	1.701A	114.4
III	1.701A	106.6

to the luminous slit is

$$E_R = F_R(1+\cos 2\pi Rx),$$

in which the factor F_R is proportional to the time of exposure and R measures the distance from the slit to the screen.

The same screen, properly dephased, brings to bear on the plate an illumination

$$E_R = F_R(1+\sin 2\pi rx)$$

in the same direction indicated. Let us write the latter expression in the following general form:

$$I(q) = K(1+\sin Rq).$$

With

$$K = z_i z_j / r_{ij} \quad \text{and} \quad R = r_{ij},$$

it follows that, by means of successive photographic impressions, one for each value of r_{ij}, we shall have added up on the photographic plate all the items of the sum

$$I(q) = \sum_{ij} \frac{z_i z_j}{r_{ij}} + \sum_{i,j} \frac{z_i z_j}{r_{ij}} \sin r_{ij} q,$$

TABLE II.

Max	Min	$\frac{q_{(ob)}\text{(Herberg)}}{q_{(exp.)}}$	$\frac{q_{(ob)}\text{(Dunitz)}}{q_{(exp.)}}$
	1	...	...
1		...	...
	2	...	118
2		118	117
	3	116	117
3		113	117
	4	119	117.5
4		117.5	116
	5	116	115.5
5		118	117
	6	117	117
6		118	120
	7	118	119.5
7		117	116.5
	8	117.5	118
8		116.5	116
	9	117.5	117.5
9		119	117
	10	119	118
10		117	117
	11	119	118
11		...	119
	12	...	119
12		...	117
	13	119	116
13		...	115
	14	...	116

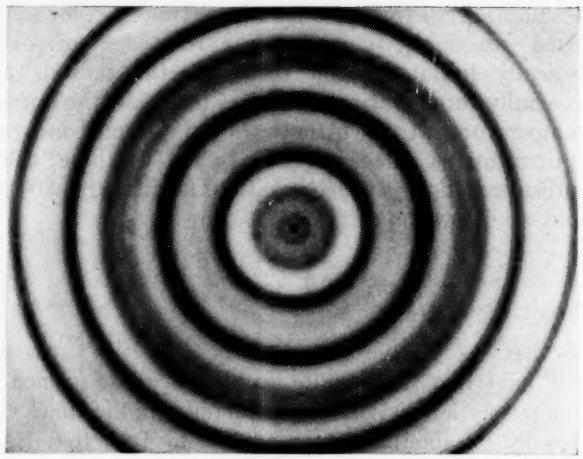

FIG. 2. Diagram obtained by rotating the original plate (1) during the printing of a diapositive.

which does not differ from Eq. (1) in more than a constant.

An application has been made to the case of chloride monoxide, the structure of which has been determined by J. D. Dunitz and K. Herberg.[3] In Fig. 1 we have reproduced the curves of intensities given by these authors, and also the corresponding diagrams we obtained with the data shown in Table I.

A simple observation of the figure tells us that the intensities and positions of the maxima and minima of the diagram I agree perfectly with those obtained by means of visual photomeasurement of the original diagram of electronic diffraction. The data shown in diagram I are exactly those accepted for the molecule of chlorine monoxide.

In order to judge the position of the maxima and minima, we reproduce in Table II the quotient between the observed values of q and those measured in a set of diagrams. As can be seen, they agree quite well.

In Fig. 2 we reproduce a diagram obtained by rotating one of the original plates during the printing of the positive.

Thus we see that with Eller's machine we can avoid the long and wearisome calculations necessary to determine the structure of gaseous molecules by the trial and error method, by using electronic diffraction. The time we employed in obtaining the photographs of Fig. 1 did not amount to half a minute. That is to say, that even in the case of a very complicated structure, containing a very large number of terms to be added up, it can always be done in less than an hour.

By means of the addition of a properly calculated screen to Eller's machine, the study of nonrigid molecules is also practicable. The method will be described in a next paper.

[3] J. Dunitz and K. Herberg, J. Chem. Soc. **72**, 3108 (1950).

Polarization in Electrolytic Solutions. Part I. Theory*

HUNG-CHI CHANG AND GEORGE JAFFÉ
Louisiana State University, Baton Rouge, Lousiana

(Received December 20, 1951)

The theory of "Conductance in Polarizable Media" developed by one of the authors is modified in such a way as to be applicable to electrolytic solutions. This is achieved by the introduction of a new set of boundary conditions. In their original form they expressed the fact that the polarizing ions could not carry any current through the boundary. Now it is assumed that the discharge at the electrodes is a rate process of the first order, characterized by a rate constant ξ. In Sec. II the case of an applied ac voltage is treated. The expressions for the equivalent parallel conductance and capacitance of the polarization layer $1/R_p$ and C_p are derived by the same method, and to the same extent, as in the older theory. If ξ tends to zero, the previous results are obtained ("completely blocked electrode"). If ξ increases, the "polarization capacitance" and the "excess resistance" both decrease until they vanish for $\xi=\infty$ ("open electrode"). The dependence on frequency remains similar for all finite values of ξ, and is represented in Figs. 1 and 2. Subsequently, in Sec. III, the older theory is improved by a determination of the thickness of the polarization layer. Reduced values of $1/R_p$ and C_p can be represented as universal functions of one reduced variable, which is proportional to the frequency. The two universal functions are tabulated to some extent in Table I. Finally the theory is extended to the case where several groups of ions of different mobilities are present in the electrolyte.

I. INTRODUCTION

MUCH experimental and theoretical work has been devoted to the phenomenon of polarization in electrolytic solutions.[1] It was recognized early that the effective resistance and capacitance of such solutions depend strongly on frequency. M. Wien, who studied this effect extensively,[2] correlated the phenomena by making use of the concept of "polarization capacitance," introduced previously by Kohlrausch, and of the concept of "excess resistance" which he introduced himself. He offered, however, no theory for either of these concepts.

The first attempt at a rational theory of polarization was made by Warburg.[3] He started from the differential equation for diffusion and made diffusion alone responsible for the emf of polarization. A little later Krüger[4] combined Warburg's diffusion theory with Helmholtz's concept of a double layer and thereby established that theory of polarization which seems to have been most widely accepted in electrochemistry.

None of the older theories, however, is theoretically quite acceptable because they neglect the possible influence of space charge and of the inhomogeneity of the electric field. It is evident that diffusion of charged particles will have these two consequences which should add strongly to the observable effects.

Now, a theory of conductance in polarizable media which takes account of diffusion, migration, and recombination of the ions and of the inhomogeneity of the field was developed by one of the authors many years ago.[5] At that time the investigation was undertaken mainly to explain the very strong polarization effects which are observed in crystals,[6] and the boundary conditions were chosen in such a way as to account for this extreme case.[7]

In order to include the possibility of a permanent current upon the application of a direct voltage, it was necessary to introduce two species of ions, those "of the first kind," or "polarization ions" as they may be called, and "ions of the second kind." The latter were supposed to carry the permanent current. Consequently, they were subjected to the boundary conditions in the usual form, i.e., vanishing of the ionic densities at the electrodes. On the other hand, it was assumed that the polarization ions could not carry a current through the boundary, be it by discharge to or by actual passage into the electrode.

The physical meaning of this boundary condition is that, in the case of dc, the ions will run up against the electrode and pile up there until the diffusion current in the direction away from the electrode just balances the current toward the electrode caused by the voltage. In the case of ac, polarization is effective only if the ions have time to accumulate near the electrode during one half-period; it will result in an increase of capacitance and a decrease in conductance. This accounts for the observed "polarization capacitance" and "excess resistance." As the frequency increases both effects die out until, at high frequencies, the normal conductance and the geometrical capacitance are reached. In recent

* This research was supported by the ONR.

[1] For the history of the subject and the older literature compare *Handbuch der Experimentalphysik* (Akademische Verlagsgesellschaft, Leipzig, 1933), Vol. XII. 2, Sec. VI, p. 161 ff.

[2] M. Wien, Wied. Ann. **58**, 37 (1896). See also C. W. Miller, Phys. Rev. **22**, 622 (1932).

[3] E. Warburg, Wied. Ann. **67**, 493 (1899); Drud. Ann. **6**, 125 (1901).

[4] F. Krüger, Z. phys. Chem. **45**, 1 (1903).

[5] G. Jaffé, Ann. Phys. **16**, 217, 249 (1933). We are going to refer to this paper in the text by I, and the page or the equation.

[6] It was pointed out, however, that the theory was applicable also to cases of conduction in liquids, liquid dielectrics in particular (see I, p. 265/6).

[7] The boundary conditions used in I are the same as those introduced by Warburg. It will be seen, however, that they are not adequate to describe the behavior of electrolytic solutions, being too stringent.

years this same theory has been applied to semiconductors.[8]

The boundary conditions as used in the interpretation of the behavior of crystals and semiconductors represent an ideal limiting case. It was pointed out already in I (see p. 219) that a more realistic model might be obtained if the discharge at the electrodes is not prohibited altogether but treated as a rate process. Evidently such a treatment will make the theory applicable to electrolytic solutions.

It is one of our two main objects in the present paper to generalize the older theory in this direction. This will be done in Sec. II, and the result can be expressed *approximately* by stating that a definite fraction of the ions, say qc_0, if c_0 is their concentration, behaves as if they were subjected to the older boundary conditions. The rest of them, $(1-q)c_0$, behave as if they were free to discharge at the electrodes. In a more rigorous representation the ratio q depends on frequency.

The second object of this paper is a more rigorous determination of the thickness of the polarization layer than had been achieved so far. It was stated in II [see Eq. (40)] that this thickness can be determined and that it is, for a given ionized medium, a function slowly varying with frequency and more rapidly changing with concentration. In the application to selenium this dependence was disregarded. This procedure appeared legitimate in the case of selenium since the changes in concentration were not considerable. In electrolytic solutions, however, it is desirable to take into consideration a wide range of concentrations.

Therefore, in Sec. III we shall do away with the assumption of constant thickness of the polarization layer. Thereby the theory becomes applicable to a wider range of frequencies and concentrations. The results will be represented in the form of Table I, which will serve as the basis for applications to be presented in the following paper.

II. THE AC CHARACTERISTIC FOR FINITE RATE OF DISCHARGE

We treat the linear case only and consider an electrolytic solution with two different species of ions, one positively charged, the other negatively. Let p, b, and D be, respectively, the concentration (number per cc), mobility, and diffusivity of the positive ions, and n, b', D' the same quantities for the negative ions. For the sake of simplicity we assume that the two species of ions have equal valence (charge ϵ) and that the electrolyte is completely dissociated for all concentrations considered. Furthermore, we restrict the investigation to the case that the applied voltage is of the simple form

$$V=V_0+V_1\exp(i\omega t). \tag{1}$$

We are going to assume, furthermore, that the alternating voltage V_1 is so small that all overtones may be neglected. Then the unknowns p, n, the field intensity E, and the current density j, can all be represented by equations of the form (1). We consider one cm² of cross section everywhere.

Under these circumstances the differential equations for the alternating component become (see II, Eqs. (9), (10) and (IVa))

$$i\omega p_1-D\frac{d^2p_1}{dx^2}=-b\frac{dF_1}{dx}, \tag{2}$$

$$i\omega n_1+D'\frac{d^2n_1}{dx^2}=b'\frac{dF_1'}{dx}, \tag{3}$$

$$(dE_1/dx)=(4\pi\epsilon/K)(p_1-n_1). \tag{4}$$

Here the abbreviations

$$F_1=E_0p_1+E_1p_0, \tag{5}$$

$$F_1'=E_0n_1+E_1n_0 \tag{6}$$

have been introduced.

Naturally, E_0 and E_1 have to be subjected to the conditions

$$\int_0^l E_0dx=V_0, \quad \int_0^l E_1dx=V_1, \tag{7}$$

where l is the thickness of the layer considered.

We have to introduce now the generalization of the boundary conditions indicated in the Introduction. In order to do this we make two assumptions of a physical nature:[9] (a) that, in the absence of an applied voltage, there exists a state of equilibrium for the electrolyte characterized by definite concentrations, $p=p^*$, $n=n^*$, at the electrodes; (b) that the rate of discharge of the ions is proportional to the difference between the instantaneous values at the electrodes, i.e., $p(0)$ and $n(0)$, or $p(l)$ and $n(l)$, and the equilibrium values p^* and n^*.

It is understood that the time-independent values p^* and n^* introduced in (a) need not necessarily be identical with the undisturbed concentration, say $p=n=c_0$, as it exists at large distances from the electrodes. The values p^* and n^* depend on the nature of the contact between the solution and the electrode. The assumption $p^*=n^*=0$ corresponds to the boundary conditions introduced by J. J. Thomson into the theory of gaseous conduction. As long as p^* and n^* are smaller than c_0, there will be a "depletion layer" at the electrodes. The assumption $p^*=n^*=c_0$ implies the existence of an electrode with no such depletion layer.

The physical assumption (b) can be formulated mathematically in the following way:

$$j^+=-\xi\epsilon(p(0)-p^*), \quad j^-=\xi'\epsilon(n(0)-n^*), \text{ for } x=0, \tag{8}$$

[8] Final report of the Signal Corps Project No. 152 B, pp. 14–74. G. Jaffé, Phys. Rev. **85**, 354 (1952). We are going to refer to this paper in the text with II.

[9] For the sake of simplicity we assume, furthermore, that the two electrodes are of identical nature.

and

$$j^+=\xi\epsilon(p(l)-p^*),\quad j^-=-\xi'\epsilon(n(l)-n^*),\quad \text{for}\quad x=l, \tag{9}$$

where j^+ and j^- are the parts of the current carried by the positive and negative ions, respectively, and where ξ and ξ' are positive "rate constants." The current densities j^+ and j^- are algebraic quantities. If they are positive, this means a flow of charge out of the solution; if they are negative, the solution receives charge from the electrode. The latter occurs whenever the instantaneous values of $p(0)$ or $n(0)$, etc., are below their equilibrium value p^* or n^*, respectively.

Our generalized boundary conditions include all cases previously treated. With $\xi=\xi'=0$ we obtain the conditions of the older theory (see I, p. 222 and II, Eqs. (3), (4)). In that case we shall call the electrodes "completely blocked." If ξ and ξ' increase indefinitely, the discharge becomes so quick that p and n have their equilibrium values p^* and n^* at all times at both electrodes. If, in addition, $p^*=n^*=c_0$, we shall call the electrodes "open."

The treatment of j^+ is entirely analogous to that of j^-. For the sake of brevity, we shall refer only to j^-, since a negative ionic component is treated also in II. As n^* is supposed to be time-independent, the Eqs. (8) and (9) imply different boundary conditions for the dc and ac component, respectively, namely

$$j_0^-=\xi'\epsilon(n_0(0)-n^*),\quad \text{for}\quad x=0, \tag{10}$$

$$j_0^-=-\xi'\epsilon(n_0(l)-n^*),\quad \text{for}\quad x=l, \tag{11}$$

$$j_1^-=\xi'\epsilon n_1(0),\quad \text{for}\quad x=0, \tag{12}$$

$$j_1^-=-\xi'\epsilon n_1(l),\quad \text{for}\quad x=l, \tag{13}$$

respectively.

We are interested in the ac behavior of the electrolyte and shall, therefore, treat only the differential equations (2), (3), and (4). The dc case can be treated by the same method. The mathematical procedure remains exactly the same as exposed in II (see Sec. IIa). The calculations become somewhat more lengthy but are quite straightforward. The final result for the complex current density, $(j_{tot})_1$, may be stated in the following form:

$$(j_{tot})_1=(i\omega K/4\pi)(V_1/l)+(\epsilon b/l)\int_0^l F_1dx+(\epsilon b'/l)\int_0^l F_1'dx+j_p^++j_p^-. \tag{14}$$

Here j_p^+ and j_p^- represent the changes in the current density brought about by the polarizing action of the positive and negative ions, respectively. The latter quantity is defined by

$$j_p^-=(\epsilon b'/l)[(G_1'(l)+\exp(\mu_1'l)\bar{G}_1'(l))/(\exp(\mu_1'l)+1)]\Phi_1'. \tag{15}$$

The variable μ_1', as well as the function $G_1'(x)$, etc., retain the values given in the previous paper [see II, Eqs. (15a), (15b), (16a), (16b)].

The complex admittance is obtained from (14) by division with V_1. The current [Eq. (14)] should be compared with the former result [II, Eq. (21)], from which it differs in two regards. First, there are *two* terms caused by polarization since we are dealing now with positive and negative ions. Second, there is the factor Φ_1', which is defined by

$$\Phi_1'=[1+(\xi'/\epsilon\mu'D')\tanh(\mu_1'l/2)]^{-1} \tag{16}$$

and a corresponding one in j^+. This factor Φ_1' expresses the influence of the finite rate of discharge of the negative ions. For $\xi'\to 0$, i.e., for "completely blocked surfaces," Φ_1' reduces to unity, and the result coincides with that of the older theory.

It remains to evaluate the quadratures involved in (14). In order to do this we have to assume a suitable zero solution. We assume the electrodes to be of such a nature that, in the absence of an external field, the undisturbed concentration $p=n=c_0$ extends up to the electrodes. This means setting $p^*=n^*=c_0$. With this assumption, and no bias applied ($V_0=0$), the set

$$E_0=0,\quad p_0=n_0=c_0,\quad j_0=0 \tag{17}$$

represents a solution for the dc component, including the boundary conditions (10) and (11).

As for the field E_1, we have carried the calculations with two different assumptions, namely for the hyperbolic field used in II [see II, Eqs. (24) to (26)], and for a homogeneous field

$$E_1=E_1^{(0)}=\text{const.} \tag{18}$$

Since we are assuming V_1 to be small, Eq. (18) represents a sufficient approximation [see II, after Eq. (25)]. Therefore, we are going to give the results only for the field (18). Furthermore, for the sake of simplicity, we shall assume $b=b'$, $D=D'$, and $\xi=\xi'$.

After substitution of (16), (17), and (18) into (14), division by V_1, and separation of the real and imaginary parts, the following results are obtained:

$$1/R_p=(1/R_\infty)[1-((g_1(\lambda)/\lambda)+(\rho/2)((g_1(\lambda)/\lambda)^2+(g_2(\lambda)/\lambda)^2))/(1+\rho(g_1(\lambda)/\lambda)+(\tfrac{1}{2})(\rho/\lambda)^2g_3(\lambda))], \tag{19}$$

$$C_p=(K/4\pi l)+C_0[(6/\lambda^3)g_2(\lambda)/(1+\rho(g_1(\lambda)/\lambda)+(\tfrac{1}{2})(\rho/\lambda)^2g_3(\lambda))]. \tag{20}$$

R_p and C_p represent the equivalent parallel resistance and capacitance of the layer l. They are "initial values" in the sense that they hold for $V_1\to 0$.

In Eqs. (19) and (20),

$$\lambda=l(\omega/2D)^{\frac{1}{2}} \tag{21}$$

is a dimensionless variable which is proportional to the

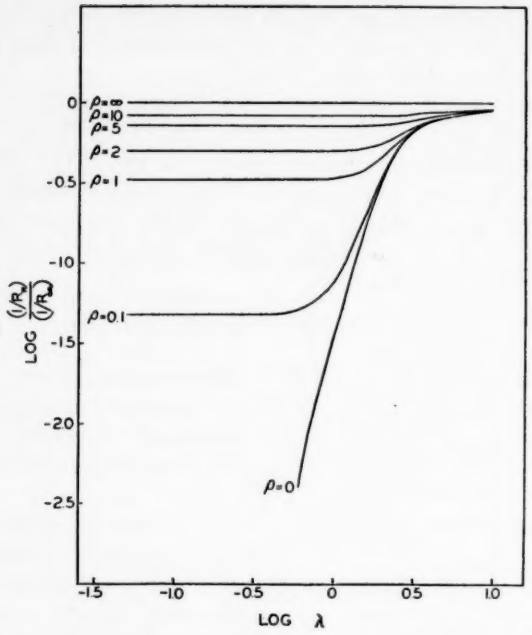

FIG. 1. Theoretical curves for the reduced conductance $(1/R_p)/(1/R_\infty)$ as function of the dimensionless variable $\lambda=l(\omega/2D)^{\frac{1}{2}}$ for selected values of the "reduced rate constant" ρ. The plot is doubly logarithmic.

square root of the frequency $f^{\frac{1}{2}}$, and

$$\rho=\xi l/D \tag{22}$$

is a dimensionless parameter characteristic of the rate of discharge.

The three functions g_1, g_2, and g_3 are defined as

$$g_1(\lambda)=(\sinh\lambda+\sin\lambda)/(\cosh\lambda+\cos\lambda), \tag{23}$$

$$g_2(\lambda)=(\sinh\lambda-\sin\lambda)/(\cosh\lambda+\cos\lambda), \tag{24}$$

and

$$g_3(\lambda)=(\cosh\lambda-\cos\lambda)/(\cosh\lambda+\cos\lambda). \tag{25}$$

Finally,

$$1/R_\infty=2\epsilon bc_0/l \tag{26}$$

is the normal conductance which is reached as $f\to\infty$, and

$$C_0=\epsilon bc_0 l/6D \tag{27}$$

is the maximum capacitance which is approached as $f\to 0$, and $\rho\to 0$.

In order to show the influence of an increasing rate constant ξ we have represented the reduced values $(1/R_p)/(1/R_\infty)$ and C_p/C_0 in Figs. 1 and 2 for selected values of ρ. The scale is doubly logarithmic. Owing to the reduced representation, Figs. 1 and 2 comprise all possible cases, and it is seen that the state of affairs depends only on the dimensionless variable λ and the parameter ρ, which might be called the "reduced rate constant."

Figure 1 shows that the conductance $1/R_p$ reaches its normal value $1/R_\infty$ under all circumstances, i.e., no matter what the value of ρ is. This result means physically that conditions at the electrodes become less and less important as the frequency increases. It confirms one of the rules established by Kohlrausch for the determination of the resistances, i.e., to operate at sufficiently high frequencies.

On the other hand, Fig. 2 shows that the capacitance for $\lambda\to 0$ depends very strongly on the value of the reduced rate constant. Our result that there is a constant capacitance as $\lambda\to 0$ (for any value of ρ) confirms Kohlrausch's concept of a "polarization capacitance." The existence of this polarization capacitance is thus traced back to the finite rate of discharge of the ions at the electrodes. For $\rho=0$ (no discharge at all) C_p reaches its maximum value C_0. The curves of Figs. 1 and 2 then represent the results of the older theory, provided the zero approximation of the field is treated as homogeneous. As ρ increases the effects of polarization become less marked. As a consequence of this the conductance (for small frequencies) becomes larger, and the capacitance smaller until, for $\rho\to\infty$, the effects of polarization become negligible. Then $1/R_p$ has its normal value, and C_p the geometrical value *for all frequencies*. The fact that, for low values of the frequencies, R_p is larger than the normal value, as long as ρ is finite, confirms Wien's concept of an "excess resistance."

The limiting values, as $\lambda\to 0$, are given by

$$1/R_p=(1/R_\infty)(\rho/(2+\rho)), \tag{28}$$

$$C_p=C_0/(1+\rho/2)^2, \tag{29}$$

and those for $\lambda\to\infty$ by

$$1/R_p=(1/R_\infty)[1-(1/\lambda)/(1+\rho/\lambda)], \tag{30}$$

$$C_p=(K/4\pi l)+C_0(6/\lambda^3)/(1+\rho/\lambda). \tag{31}$$

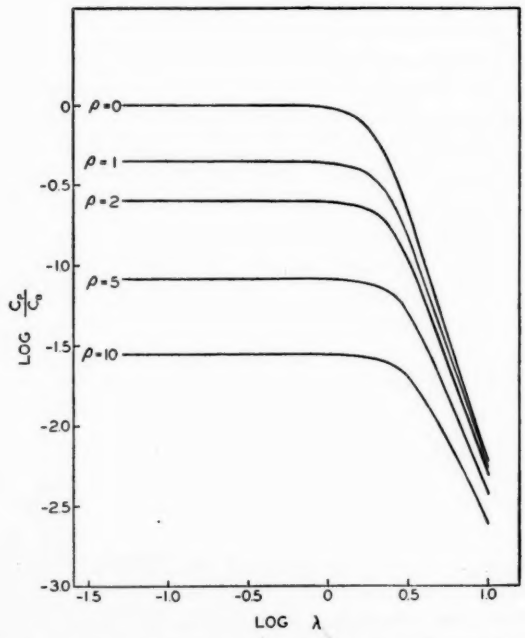

FIG. 2. Theoretical curves for the reduced capacitance C_p/C_0 as function of the dimensionless variable $\lambda=l(\omega/2D)^{\frac{1}{2}}$, for selected values of the "reduced rate constant," ρ. The plot is double logarithmic.

The transition from (28), (29) to (30), (31) occurs in the region where $\lambda \sim 2$, and sets in at slightly increasing values of λ as ρ increases.[10]

In a first rather rough approximation all curves of Fig. 2 can be made to coincide (except at large values of λ and ρ) by horizontal and vertical shifts. Since the representation is doubly logarithmic, this means that the dependence of the capacitance on frequency is approximately the same, for all values of the relevant parameters, if the scales of C_p and λ are suitably chosen. Evidently, the factor for the reduction of C_p, q, is given by (29). This approximately correct statement is useful in the applications.

III. THE AC CHARACTERISTIC CORRECTED FOR VARIABLE THICKNESS OF THE POLARIZATION LAYER

We now revert to the case of completely blocked electrodes, i.e., $\rho=0$, in order to correct the results for the variation of the thickness of the polarization layer with frequency. The determination of the thickness can be carried out only with an inhomogeneous field distribution. Therefore, we assume in what follows the hyperbolic field used in II [see II, Eqs. (24), (25), (26)].[11] The result becomes as given there [II, Eq. (38)], namely,

$$1/R_p=(1/R_\infty)\Gamma_2(\lambda,\beta), \quad C_p=C_0'\Gamma_1(\lambda,\beta). \quad (32)$$

Here Γ_1 and Γ_2 are the two functions defined by II [Eqs. (30) and (31)] and graphically represented in Fig. 1 of paper II. The dimensionless variable λ is the same as defined by Eq. (21) of this paper and the dimensionless parameter β, the "reduced plate distance," is defined by

$$\beta=\alpha l. \quad (33)$$

The maximum capacitance which is reached as $\omega\to 0$ now has the value[12]

$$C_0'=\epsilon b C_0/\alpha D, \quad (34)$$

whereas $1/R_\infty$ retains the value given in (26).

In II these formulas were obtained for a slab of thickness $l_1=l/2$ which contains only one polarization layer, at $x=0$, and they refer to one species of ions. Now we are dealing with a layer of thickness l and referring to two species of ions. The results are identical provided the two species have the same mobility, as we are going to assume again.

In order to determine the thickness l_1 of each of the polarization layers we assume the total distance of the electrodes to be $L \gg l$. Our solutions for the field and the densities are to hold from $x=0$ to $x=l_1$, and from $x=(L-l_1)$ to L, whereas from $x=l_1$ to $x=(L-l_1)$, a homogeneous field and the undisturbed densities are supposed to exist.

TABLE I. Table for the universal functions $\beta(\lambda)$, $\Gamma_1(\lambda)$, $\Gamma_2(\lambda)/\beta(\lambda)$ in their dependence on the dimensionless variable $\lambda=l(\omega/2D)^{\frac{1}{2}}$. $(\lambda/\beta)^2=f^*$, Γ_1, and Γ_2/β represent reduced values of the frequency, the capacitance, and the conductance, respectively.

λ	$\beta(\lambda)$	$\lambda/\beta(\lambda)=(f^*)^{\frac{1}{2}}$	$\Gamma_1(\lambda)$	$\Gamma_2(\lambda)/\beta(\lambda)$
0.050	25.0	0.0020	0.920	2.00×10^{-9}
0.260	17.0	0.0153	0.822	2.59×10^{-6}
0.415	14.5	0.0286	0.856	2.36×10^{-5}
0.606	12.0	0.0505	0.827	1.57×10^{-4}
0.768	11.0	0.0698	0.802	4.25×10^{-4}
0.902	10.0	0.0902	0.775	1.10×10^{-3}
1.280	8.0	0.160	0.680	5.63×10^{-3}
1.528	7.0	0.218	0.594	1.26×10^{-2}
1.80	6.0	0.300	0.479	2.66×10^{-2}
2.00	5.34	0.375	0.394	4.21×10^{-2}
2.30	4.73	0.486	0.294	6.81×10^{-2}
2.92	3.80	0.768	1.415×10^{-1}	1.30×10^{-1}
3.50	3.31	1.057	7.53×10^{-2}	1.82×10^{-1}
4.00	3.02	1.324	5.03×10^{-2}	2.23×10^{-1}
4.50	2.84	1.584	3.16×10^{-2}	2.54×10^{-1}
6.00	2.40	2.50	1.16×10^{-2}	3.38×10^{-1}
8.00	2.02	3.96	3.37×10^{-3}	4.33×10^{-1}
10.0	1.74	5.75	1.55×10^{-3}	5.17×10^{-1}

The boundary conditions at $x=l_1$ and $x=(L-l_1)$ require the continuity of the field and the current (which implies continuity of the densities). Owing to the complete symmetry of the solutions, the boundary conditions have to be set up only for one of the boundaries, say $x=l_1$.

Let the potential difference between $x=0$ and $x=l_1$ be V_{11}, that between $x=l_1$ and $x=(L-l_1)$ be V_{12}, and V_1^* the potential applied to the whole thickness L; then we must have

$$2V_{11}+V_{12}=V_1^*. \quad (35)$$

The continuity of the field requires

$$\alpha V_{11}/\sinh(\alpha l_1)=V_{12}/(L-2l_1), \quad (36)$$

and the continuity of the current[13] requires

$$[(\Gamma_2)^2+(\lambda^2\Gamma_1/2\alpha l_1)^2]^{\frac{1}{2}}(2V_{11}/R_\infty) = 2\epsilon b c_0 V_{12}/(L-2l_1). \quad (37)$$

These are three equations for the unknowns V_{11}, V_{12}, and l_1.

It is easy to derive from (36) and (37) the equation

$$[(\Gamma_2)^2+(\lambda^2\Gamma_1/\beta)^2]^{\frac{1}{2}}=\beta\exp(-\beta/2)/[1-\exp(-\beta)], \quad (38)$$

which determines β, and thereby l_1, as functions of λ.

For λ small, β becomes large and the approximations $\Gamma_1=(1-2/\beta)$ and $\Gamma_2=\lambda^4/6\beta$ may be used. This leads to the limiting solution

$$\lambda=\beta\exp(-\beta/4), \quad \lambda\ll 1. \quad (39)$$

For $\lambda\gg 1$, β tends toward zero and the approximations $\Gamma_1=\beta/\lambda^3$ and $\Gamma_2=(1-1/\lambda)$ are valid. Then the rela-

[10] This is seen better in a representation which is not logarithmic.

[11] It should be pointed out that in II, Eq. (26), V_1 should be replaced by $V_1/2$ in order to make II, Eq. (24) hold over the distance l.

[12] It might be mentioned that Eq. (34) becomes identical with the value (27) if $\beta=6$.

[13] The geometrical capacitance has been neglected as it is much smaller, in all cases, than the capacitance caused by polarization.

tion (38) becomes

$$\lambda=24/\beta^2, \quad \lambda\gg 1. \tag{40}$$

In the general case Eq. (38) has to be solved by graphical methods, which we have done. The relation between λ and β is given in the first two columns of Table I. From the definitions of λ and β, Eqs. (34) and (23), it follows that

$$\lambda/\beta=(f^*)^{\frac{1}{2}}=Qf^{\frac{1}{2}}, \quad Q=(\pi/\alpha^2 D)^{\frac{1}{2}}. \tag{41}$$

Hence, the ratio λ/β (third column of Table I) is proportional to the square root of the frequency. We shall call f^* the "reduced frequency."

If the first Eq. (32) is written in the form

$$1/R_p=P[\Gamma_2(\lambda)/\beta(\lambda)], \quad P=2\epsilon b c_0\alpha, \tag{42}$$

it is seen that $(1/R_p)/P$ is a universal function of λ, or λ/β. The same holds for C_p/C_0, as follows from the second Eq. (32). The universal functions $\Gamma_1(\lambda)$ and $\Gamma_2(\lambda)/\beta(\lambda)$ are tabulated in columns 4 and 5 of Table I.

The procedure in matching the experimental results with theory consists in plotting $\log\Gamma_1(\lambda)$ and $\log(\Gamma_2(\lambda)/\beta)$ *versus* $\log(\lambda/\beta)$, and comparing these curves with the experimental curves representing $\log C_p$, and $\log(1/R_p)$ *versus* $\log f^{\frac{1}{2}}$. If this matching is feasible the constants C_0, P, and Q can be determined from the vertical and horizontal shifts. The two horizontal shifts should, of course, be the same, as they determine the same combination of constants, namely, $\alpha^2 D$.

Consequently, there are two independent ways of determining the ionic constants, either from the experimental capacitance values or from the conductances. In both cases there are two constants, C_0 and Q or P and Q, which, together with the Townsend relation (i.e., $b/D=\epsilon/kT$) and the definition of α [II, Eq. (25)] determine the four unknowns b, D, c_0, and α.

So far our determinations are based on the assumption that there is only one group of ions, half of them positive and half of them negative, but all having the same mobility. The experimental results given in the following paper indicate that this assumption is not fulfilled. At least two groups of ions of very different mobilities have to be assumed. Therefore, our equations have to be generalized for this case [see II after Eq. (40)].

It is easy to obtain this generalization since parallel capacitances and conductances are additive. Let there be different groups of ions with mobilities b_i and diffusivities D_i. For the sake of simplicity we assume that there are in each group an equal number of positive and negative ions of equal mobility, equal valence, and equal concentration c_i. Then we obtain

$$1/R_p=\sum_i 2\epsilon b_i c_i\alpha[\Gamma_2(\lambda_i)/\beta(\lambda_i)], \tag{43}$$

and

$$C_p=\sum_i(\epsilon b_i c_i/\alpha D_i)\Gamma_1(\lambda_i), \tag{44}$$

where

$$\lambda_i=l(\omega/2D_i)^{\frac{1}{2}}. \tag{45}$$

It should be pointed out that α is the same constant throughout, as all ions move in the same field. It can be shown [see II, Eq. (41)] that now

$$\alpha^2=(8\pi\epsilon/K)(b/D)\sum_i c_i. \tag{46}$$

The thickness of the polarization layer should also be the same for all groups of ions. Equations for its determination, similar to (35), (36), (37), can be set up. The solution, however, becomes prohibitively complicated. We are, therefore, introducing the approximate assumption that the thickness may be determined for each species of ions independently of the presence of the others. Then Γ_1 and (Γ_2/β) in (43) and (44) are the universal functions defined above and tabulated in Table I.

From the comparison of the experimental curves with (43) and (44) all ionic constants c_i, b_i, D_i may be determined (see the following paper where the determinations are carried through for two different groups).

Finally, it should be pointed out that the generalizations and improvements of the theory introduced in Secs. II and III are not limited to electrolytes. They hold also, with very slight modifications, for other solutions, particularly with dielectric liquids as solvents, and also for semiconductors. It is only necessary to treat the various carriers (e.g., in semiconductors the electronic and ionic components) separately, and to apply the boundary conditions to each electrode separately.

The theory here proposed will be compared at some length with new experimental material in Part II of this paper. By far the most exact measurements reported in the literature are those of Jones and Christian,[14] and it is of some interest to compare their results with our formulas.

Since these authors have used comparatively high frequencies only (500 to 4000 cps), we have to use our asymptotic formulas (31a) and (31b). These have to be transformed into equivalent series values to make them comparable with the experimental results. If we do that, taking into account the definitions (23), (28), and (29) and restricting ourselves to the case $\rho=0$, we find for the excess (polarization) resistance ΔR_s,

$$\Delta R_s=R_\infty\gamma/\omega^{\frac{1}{2}}, \tag{47}$$

and for the series capacitance

$$C_s=(H/\omega^{\frac{1}{2}})(1-2\gamma/\omega^{\frac{1}{2}}), \tag{48}$$

where H has the two identical values

$$H=6\gamma C_0=K/(2D)^{\frac{1}{2}}, \tag{49}$$

and where γ is defined by

$$\gamma=(2D)^{\frac{1}{2}}/l. \tag{50}$$

Finally, the phase angle ψ is given by

$$\tan\psi=\Delta R_s C_s\omega=1-2\gamma/\omega^{\frac{1}{2}}. \tag{51}$$

[14] G. Jones and S. M. Christian, J. Am. Chem. Soc. **57**, 272 (1935).

It will be seen that for $\omega\to\infty$ these results reduce to Warburg's well-known conclusions, namely, $\Delta R_s\omega^{\frac{1}{2}}=\text{const.}$, $C_s\omega^{\frac{1}{2}}=\text{const.}$, and $\tan\psi=1$. This might have been expected, since Warburg disregards all space charge effects and uses the boundary conditions which correspond to $\rho=0$. Now, the space charge effects become unimportant as $\omega\to\infty$ (see above, Sec. II); consequently, our formulas should reduce to Warburg's for $\omega\to\infty$ and $\rho\to 0$. Beyond that, they establish the connection with R_∞ and C_0, and thereby determine the constants. Our results (47), (48), and (49) are independent of the plate distance, as might be expected, since they refer to the polarization layer only. They are, however, dependent on the thickness of the polarization layer $l_1=l/2$, as they depend on γ.

In the derivation of (47) to (49) we have neglected terms of the order $1/\omega$. They show that, within this approximation, $\Delta R_s\omega^{\frac{1}{2}}$ should be constant while $C_s\omega^{\frac{1}{2}}$ should increase slightly and $\tan\psi$ should approach 1 with increasing frequencies. All these consequences coincide with the results stated by Jones and Christian. If $C_s\omega^{\frac{1}{2}}$ is plotted *versus* $1/\omega^{\frac{1}{2}}$, a straight line with negative slope should be obtained. This is verified by most of the observations of the authors; as a rule, the agreement is better the smaller (numerically) the slope.

Jones and Christian's data clearly indicate that the solvent contributes considerably since an increase of the concentration from 0.01 to 0.1 normality only increases the capacitance (at 500 cps) from 10.0 to 13.3 microfarads. The measurements of Jones and Christian do not lend themselves to a quantitative analysis beyond what has been stated.[15] In order to separate the effect of the solvent from that of the solute either the water effect would have to be known, or a wider range of concentrations measured; furthermore, the frequencies should cover a much lower range. Therefore, we refer to Part II of this paper for a more quantitative comparison between experiment and theory.

[15] Measurements of the same nature, and in complete agreement with those of Jones and Christian, have been reported recently by S. Barnartt, J. Electrochem. Soc. **97**, 235 (1950).

THE JOURNAL OF CHEMICAL PHYSICS VOLUME 20, NUMBER 7 JULY, 1952

Polarization in Electrolytic Solutions. Part II. Measurements*

GEORGE JAFFÉ AND JOHN A. RIDER
Louisiana State University, Baton Rouge, Louisiana

(Received December 20, 1951)

The object of the present investigation was to supply material for testing the theory given in the preceding paper. Therefore, the "polarization capacitance" and the "excess resistance" of electrolytic solutions were measured over wide ranges of frequency and concentration, and for different plate distances. Also the material of the electrodes was modified, and some temperature coefficients were measured.

After the general introduction (Sec. I) the method used is described in Sec. II; it is essentially a Jones bridge method, with suitable modifications. In Sec. III the cell is described. Section IV deals with the general scope of the measurements and with the procedure in performing them. The range of frequencies was, as a rule, from 18 to 18,000 cps; the molar concentrations varied from 10^{-4} to 10^{-2} g-eq/liter. In addition to solutions of KCl and $MgSo_4$, conductance water was investigated. Electrodes of Al, Ni, Au, and Pt were used. In Sec. V a survey of the results, independent of any theory is given. Finally, in Sec. VI the results are compared with those of the theory, by analyzing completely several series of measurements referring to water and KCl solutions. A quantitative agreement can be realized, if (a) the effect of the solvent is taken into account, and if (b) it is admitted that there are, in "conductance water," ions of considerably (about 100 times) lower mobility than the ordinary electrolytic ions. With these assumptions the concentrations and the mobilities of the ions can be determined. Finally, the rate constants which are characteristic of the presented theory can be evaluated.

I. INTRODUCTION

THE influence of polarization on the passage of ac through electrolytes was noticed and discussed by Kohlrausch in his pioneer work on the determination of electrolytic resistances by the ac method.[1a] He showed how this influence could be eliminated by an increase of the surfaces of the electrodes. Somewhat later he introduced his concept of "polarization capacitance", showing that the observations could be correlated by the assumption that the electrolyte acts like a resistance and capacitance in series;[1b] he also made the first determination of a polarization capacitance, for platinum, finding it to be very high.

Following him numerous experimenters studied the behavior of the polarization capacitance under various aspects,[2] but it was not until more than twenty years later that Wien[2] recognized Kohlrausch's model to be incomplete. Wien showed that the resistance of an electrolyte measured by the ac method at sufficiently low frequencies (he went down to 64 cps) was always higher than corresponds to the normal value, and he called this increase the "excess resistance". Wien himself made a thorough experimental investigation of the

* This research was supported by the ONR.

[1] (a) F. Kohlrausch and W. A. Nippoldt, Pogg. Ann. **138**, 280, 370 (1869); (b) F. Kohlrausch, Pogg. Ann. **148**, 143 (1873).

[2] M. Wien, Pogg. Ann. **58**, 37 (1896). The older literature will be found in this paper.

dependence of polarization capacitance and excess resistance on frequency, voltage, and the nature of the electrodes, and his observations survey the experimental facts in a fairly complete way, except for the influence of concentration.

Other investigations of a similar kind were undertaken subsequently in order to test the theories of Warburg, Krüger,[3] and others.[4]

Very much later Jones and his collaborators[5] devoted a great amount of experimental work to the study of the factors which influence the measurements by the Kohlrausch method. Jones and Christian[6] developed a precision method for the determination of the excess resistance (which they call "polarization resistance"), and their measurements represent the most accurate determinations which have been made.

In spite of all these efforts of experimenters over a period of more than 70 years, our knowledge of the effects of polarization connected with the passage of ac through electrolytes is far from satisfactory. In the older measurements the range of frequencies and concentrations is usually somewhat limited. Wien[2] used frequencies from 68 to 535 cps and his concentrations were high and varied comparatively little. Even Jones and Christian extended their measurements[6] only from 500 to 4,000 cps, and thereby left out the low frequency range where the effects are most marked. Their concentrations varied from 10^{-2} to $10^{-1}N$ and they made no attempt to determine the influence of the solvent which, as will be seen, is very important.

With the modern vacuum tube generation and detection equipment available to cover the range of audio frequencies, it seems desirable to resume the problem and measure the effective values of resistance and capacitance over wide ranges of frequency and concentration.

This is all the more desirable, as a more complete theory which shows the connection between the resistance and capacitance effects has been developed (see *A*) and provides the means for correlating the experimental data.

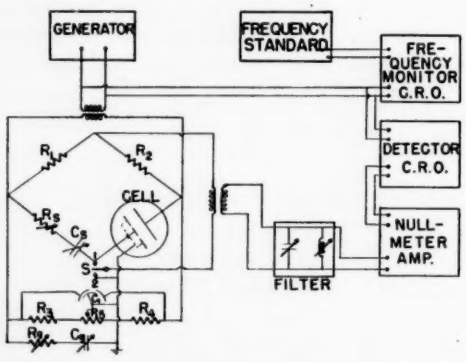

FIG. 1. Diagram of bridge assembly.

II. THE BRIDGE ASSEMBLY

Basically, the system used in these measurements consists of a Jones[7] bridge. Ordinarily, all possible provisions are made to minimize the effects of the capacitance and resistance due to polarization. Here, just the opposite techniques have been employed. As a result, it has been necessary to modify and supplement the Jones bridge in a number of ways:

1. The insertion of series capacitors in the standard arm of the bridge.
2. The employment of a conductance cell with a guard ring.
3. The addition of an auxiliary Wagner ground to balance large guard ring effects.

A schematic diagram of the apparatus is shown in Fig. 1. Discussion will be given of those features which are different from the usual equipment.

Since the polarization capacitance appears in series with the bulk resistance, the measurements were made with series values. This capacitance is by no means small. In this research, values as high as 35 microfarads have been measured, and values up to 250 microfarads had to be balanced in the guard ring system.

The capacitance range of the Jones bridge is much too small for balancing such large values. In addition, the capacitors are in parallel with the resistors. Consequently, these were removed and a set of standard capacitors were calibrated and inserted in the circuit as C_s in Fig. 1.

The original Wagner ground of the Jones bridge is shown in Fig. 1 as R_3, R_4, R_5, and C_1. It was necessary to add an auxiliary Wagner ground consisting of R_g and C_g. R_g is a General Radio decade resistance box having a range of from zero to 11,111.0 ohms. C_g is a locally assembled arrangement of Pyranol, Plasticon, and mica capacitors having a range of from 10^{-3} to 250 microfarads.

For balancing of the bridge with the present arrangement, stray effects due to the elements of the bridge and associated wiring are first balanced out by means of the bridge's original Wagner ground. This is done by balancing the bridge with C_g and R_g disconnected and a dummy impedance in place of the cell. From then on the bridge ground is left undisturbed, and subsequent measurements with the actual conductance cell are made as usual except that adjustments are made on R_g and C_g with the switch S is in position 2.

At balance, the central electrode and the guard ring are both at ground potential although there is no direct connection between them. The balance null is observed by means of a detector consisting of a General Radio amplifier Model 1231-B, and an Allen B. Dumont cathode-ray oscilloscope Model 208-B connected as

[3] H-C. Chang and G. Jaffé, J. Chem. Phys. **20**, 1071 (1952). We shall refer to this paper in the text with the letter A.
[4] C. W. Miller, Phys. Rev. **22**, 622 (1923).
[5] G. Jones and Associates, J. Am. Chem. Soc. (a) **50**, 1049 (1928); (b) **51**, 2407 (1929); (c) **53**, 411 (1931); (d) **53**, 1207 (1931); (e) **55**, 1780 (1933); (f) **57**, 272 (1935); (g) **57**, 280 (1935), (h) **59**, 731 (1937), (i) **62**, 2919 (1940).
[6] G. Jones and S. M. Christian, J. Am. Chem. Soc. **57**, 272 (1935).
[7] P. H. Dike, Rev. Sci. Instr. **2**, 379 (1931).

shown in Fig. 1. The wave filter is a locally assembled *LC* combination. The output of the amplifier is connected to the vertical deflection amplifier of the detector-scope, while the generator is connected to the horizontal amplifier terminals of the detector-scope. The final critical null is observed by causing the Lissajous ellipse on the screen of the detector-scope to degenerate into a horizontal line.

Two frequency standards have been used. Sixty cps line voltage furnishes a sufficient degree of accuracy at low frequencies, and a calibrated, electrically driven, 1000-cps tuning fork provides more accuracy than needed at medium and high audio frequencies. Frequency monitoring is done by simply maintaining the appropriate Lissajous figure on the monitoring oscilloscope screen.

III. THE CONDUCTANCE CELL

Previous investigators have been largely concerned with the determination of accurate values of conductance and consequently have sought to minimize the effects of polarization.[8,9] In our case, since the polarization effects were to be maximized rather than eliminated, the electrode separation had to be small compared to the diameter of the measuring electrode. Furthermore, it was desirable to perform measurements at variable plate distances. These considerations led to a cell of the form shown in Fig. 2.[10] From this drawing it will be seen that the electrode structure is that of a plane-parallel plate, guard ring condenser. The central electrode was supported in alignment by a polystyrene insert that was pressed into the annular space between it and the guard ring, and the opposite electrode was fastened to a micrometer driven dovetail.

It was found necessary to cover the rear of the electrodes and the rod supports with polystyrene coil dope in order to eliminate edge effects. The masonite top is machined to fit the top of a Pyrex beaker from which the rim is removed. The electrolyte is placed in the beaker and the cell immersed in a constant temperature bath.

The important dimensions of the electrodes are as follows:

Radius of central electrode	1.017 cm
Inner radius of the guard ring	1.056 cm
Outer radius of the guard ring	3.018 cm
Effective area of the central electrode	3.36 cm².

IV. THE MEASUREMENTS

Earlier observers[2,5] have reported on the difficulty, or rather on the impossibility of obtaining reproducible results in the determination of the polarization capacitance and the excess resistance. They have stated that the values obtainable change, not only from one sample of the liquid to another, or from one set of electrodes to another, but that they also change with time for the same set of electrodes and the same sample of liquid. This "aging process" makes it quite impossible to determine absolute values, and special precautions have to be taken, even to obtain relative values which are comparable.

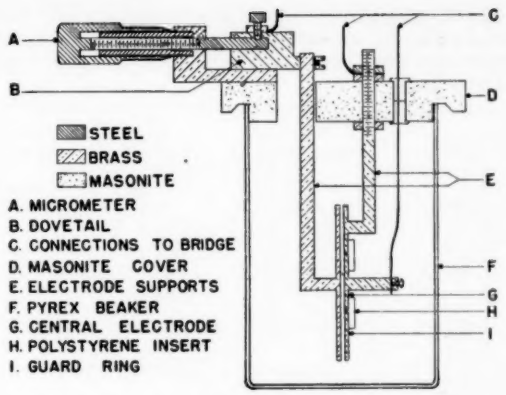

FIG. 2. Cross section through conductance cell.

Our observations, though based on much wider ranges of frequencies and concentrations, are in complete agreement with the older statements. It follows also from theory that the source of the variability may be found in varying surface conditions. The theory presented in A predicts that the anomalies due to polarization are largest for low frequencies. Now, Eqs. (28) and (29) in A show that conductance and capacitance, as frequency approaches zero, are strongly dependent on a rate constant for discharge, ρ, i.e., on the nature of the surface. The same fact is brought out by Figs. 1 and 2 of A which survey the complete range of frequencies.

No special efforts were made in our survey to obtain constant, or even reproducible surface conditions. It seems doubtful whether this would be feasible. Our measurements afford means of obtaining fairly good absolute values only in one regard, i.e., for the limiting resistance at high frequencies. Our cell was built in such a way that the cell constant could be calculated from its geometry. With standard solutions, such as KCl solutions, the well-known values for the conductivity should have been obtainable after the subtraction of the water value. Even that proved to be a fairly difficult task.

When the cell had been developed to its final form the conductance measurements taken with most care approached the accepted values to about 2 to 3 percent (see below, Table I). The method of measurement finally accepted will now be described briefly.

With the cell in place and the thermostat control set for regulation at the desired temperature, the equipment was left undisturbed for several hours in order to let the surfaces approach equilibrium (to "age") and

[8] F. Kohlrausch and L. Holborn, *Das Leitvermögen der Elektrolyte*. Second Edition, Leipzig, Teubner, 1916.

[9] G. Jones, and G. Bollinger, J. Am. Chem. Soc. **53**, 411 (1931).

[10] The cell herein described was originally constructed and used by *Norman M. Schaeffer*. It was also used for extensive measurements by *James R. Weston*. Full reports of their work may be found in Master's theses by them at this University.

TABLE I. Comparison of observed conductances with the accepted values for various concentrations of KCl solutions, conductances, κ, in ohm^{-1} cm$^{-1}\times10^{-6}$, concentration, m, in g-eq/liter. (Ni electrodes).

m	Observed	Accepted	Percent error
10^{-4}	15.9	15.44	+3.3
5×10^{-4}	80.0	77.63	+3.0
10^{-3}	150	152.3	−1.5
2×10^{-3}	304	302.1	+0.6
5×10^{-3}	731	744.0	−1.7
10^{-2}	1415	1464	−3.3

to permit the temperature to stabilize. After this the electronic circuits were turned on and allowed to warm up for about a half hour. A series of measurements was then commenced.

A single series of measurements consists of the determination of C_s, R_s, C_0, and R_0 at each of a selected set of frequencies usually extending from 18 to 18,000 cps. Each determination was made by balancing the bridge as described in Sec. II of this paper. The measurements were made beginning with the lowest frequency and proceeding in ascending order of frequency until the highest had been reached, whereupon the measurements were repeated in descending order of frequency. The corresponding ascending and descending values were averaged for each frequency, thereby eliminating the effects of variation that are linear with respect to time.

The water used was prepared in a Barnstead Still, Model *GL*-$\frac{1}{2}$. All solutions for each group of series were made from a single distillate in order to assure the same solvent. The data thus obtained furnished sets such as the one presented in Tables IV and V.

The voltage dependence of capacitance and resistance was investigated only to determine the extent to which variations of applied voltage would affect the validity of measurements. With a given electrolyte, no significant shift of bridge balance could be observed when the applied voltage was varied from 0.02 volt rms to 0.2 volt rms. All measurements were made with an applied voltage of 0.12±0.01 volt rms.

In discussing the accuracy of the measurements it is perhaps best to state the accuracy of the individual factors involved. By a careful examination of the prevailing circumstances we estimate the maximum errors as follows: frequency ±0.1 percent, temperature ±0.2°C (which amounts to about 0.5 percent in resistance or capacitance), standard capacitors ±1 percent, standard resistors ±.1 percent, incremental plate distance ±2 percent.[11]

According to these estimates, the over-all error should not exceed ±2 percent for a fixed plate distance. Now, it was observed that discrepancies between corresponding values taken with increasing and decreasing frequencies were much larger than this. They amounted to about 4 percent in the R-values and up to 8 percent in the capacitances. Consequently, these large errors must be ascribed to changes in the surface condition of the electrodes, and to changes in the solvent. This last statement agrees with the observation that the errors were largest with conductance water.

Summarizing, we estimate that the relative measurements have an accuracy of ±2 percent in the frequency interval between 300 and 5000 cps and are progressively less accurate as the ends of the range are approached.

V. RESULTS OF THE MEASUREMENTS

A large number of measurements were performed under varying conditions. Besides "conductance water" solutions of KCl and $MgSO_4$ were investigated. The latter salt was chosen because the theory presented in A refers to ions of equal valence. The results on the two salts were so similar (almost quantitatively), that is was not considered necessary to extend the measurements to other salts. Since the theory assumes complete dissociation, the concentrations had to be chosen low; the molar concentrations, m in g-equivalent per liter, extended from 10^{-4} to 10^{-2}.

The temperature was as a rule fixed at about 26°C, but a few measurements were taken over a range from 17 to 33°C.

The results are qualitatively so uniform that they may be described in a summary way.

(*a*) *Resistance.* At low frequencies and for all distances of the electrodes, the resistance is higher than the normal value. This "excess resistance" falls off with frequency and disappears at frequencies between about 100 and 1000 cps, according to the resistivity of the liquid. The larger the resistance of the solution, the

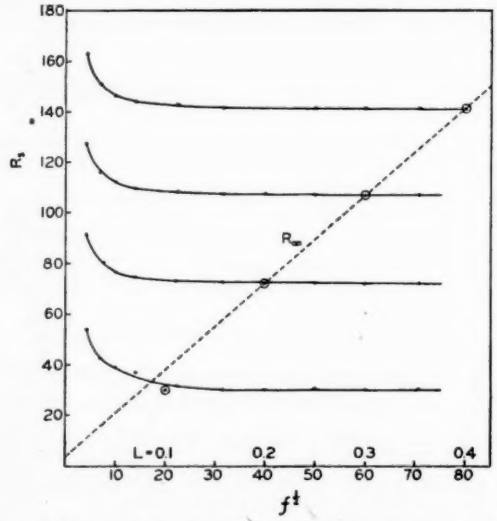

FIG. 3. Resistance of a $MgSO_4$ solution, $m=5\times10^{-4}$ g-eq/liter. Full lines: observed values of R_s as functions of $f^{\frac{1}{2}}$ for various values of plate distance L. The broken line represents the limiting values, R_∞, as function of L.

[11] The greatest error in distance determination was in establishing the zero reading. For this reason the smallest distance (L=0.1 cm) was eliminated in the determination of the specific conductances as given in Table I.

earlier the excess resistance ceases to be noticeable. At higher frequencies, over a wide interval the resistance remains approximately constant at its normal value and finally begins to drop below this normal value.

These features, except for the final drop, are shown in Fig. 3 which refers to $MgSO_4$ of $m=5\times10^{-4}$ (for $MgSO_4/2$) and represents R_s as function of $f^{\frac{1}{2}}$. Here, and in all which follows, we have chosen $f^{\frac{1}{2}}$ (or its logarithm) as abscissa because this is indicated by theory, where the dimensionless variables λ(A, Eq. (21)) and $(f^*)^{\frac{1}{2}}$(A, Eq. 41) both are proportional to $f^{\frac{1}{2}}$.[12]

The final drop (not shown in Fig. 3) sets in earlier and is stronger, the higher the resistance of the liquid. It is therefore most noticeable for pure water and the solutions of lowest concentrations. This is brought out in Figs. 5 and 7, and also by the numbers of Table V.

The excess resistance is independent of electrode distance[13] to a good approximation and decreases but slowly with concentration. These features are brought out by the figures of Table II.

The normal resistance, say observed between 1000 and 5000 cps, is always a linear function of electrode distance as it should be, but the straight line representing the resistance as function of distance (broken line of Fig. (3)) never passes accurately through the origin.

The middle part of the resistance curves which should represent the normal resistance freed of polarization effects was never accurately constant, but invariably showed a slow decrease with increasing frequencies (see the data of Table V.) This is a point of importance and will be discussed in Section VI.

(*b*) *Capacitance.* The observed values of C_s decrease monotonically over the entire range of frequencies. It is, therefore, not feasible to distinguish clearly the three parts which were recognizable in the R_s-curves. Only in the logarithmic plot the third part, corresponding to a rapid final drop in capacitance, is distinctly marked

TABLE II. Excess resistance, $(R_{18}-R_{5000})$ in ohms, of KCl and $MgSO_4$ solutions for various concentrations, m, and electrode distances, L. (Ni electrodes).

	$R_{18}-R_{5000}$			
m	$L=0.1$ cm	$L=0.2$ cm	$L=0.3$ cm	$L=0.4$ cm
		KCl		
10^{-4}	29.8	29.5	32.0	32.0
5×10^{-4}	28.8	28.3	27.7	30.8
10^{-3}	28.0	25.7	26.5	25.5
5×10^{-3}	24.3	22.2	21.0	19.0
		$\frac{1}{2}(MgSO_4)$		
10^{-4}	19.0	19.0	20.2	23.0
5×10^{-4}	18.8	19.3	20.3	22.0
10^{-3}	20.5	20.1	20.2	20.3
5×10^{-3}	20.4	19.5	16.7	17.3

[12] Figs. (3) and (4), and the figures of Table II, refer to an area of 26.85 cm²; they represent uncorrected observations.

[13] This fact is shown with much higher accuracy, but for a limited range of frequencies, by the measurements of Jones and Christian.[6]

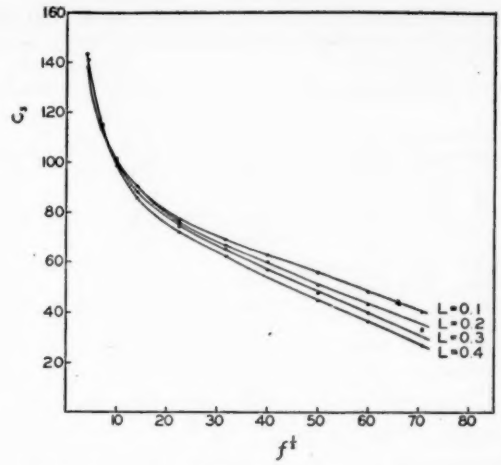

FIG. 4. Capacitance of a $MgSO_4$ solution, $m=5\times10^{-4}$ g-eq/liter. Observed values of C_s as functions of $f^{\frac{1}{2}}$ for various values of plate distance L.

for sufficiently high frequencies and resistances (see Figs. (6) and (8)). The first part, at lowest frequencies, should represent an approach to a constant value, C_0, as the frequency diminishes, but this stage is hardly indicated in our measurements.

As for the dependence on electrode distance, all final measurements show conclusively that the observed capacitances are independent of the distance for sufficiently low values of the frequency in agreement with the observations of Jones and Christian.[6] As the frequency rises, the capacitances for different plate distances begin to separate and arrange themselves in the order of the geometrical capacitance. The higher the resistance of a solution the lower the frequency at which the separation begins and the more marked it becomes.

These features are brought out by Fig. 4 which refers to the same solution as Fig. 3, and by Fig. 6 which refers to water. The degree of constancy which may be realized in the low frequency region is illustrated by Table III which refers to a KCl-solution of $m=10^{-3}$ at a temperature of 19°C.[14]

As a basis for detailed comparison with theory we give in Tables IV and V the complete results for one set of measurements. The data refer to KCl solutions from $m=10^{-4}$ to $m=10^{-2}$ and to the water used in their preparation. The plate distance, $L=0.127$, was kept constant throughout these measurements. The temperature was maintained at 26.8°C. The normal conductivities of these solutions were sufficiently near the accepted values and are those represented in Table I.

Three of the resistance series and three of the capacitance series, corresponding to $m=10^{-4}$, 10^{-3}, and 10^{-2}, are represented on a doubly logarithmic scale in Figs. 7 and 8 and will be discussed in detail in the following section.

[14] It proved to be difficult to maintain the temperature constant at the relatively low temperature of 19°C. This fact may account for some of the fluctuations.

TABLE III. Capacitance of a KCl solution, $m=10^{-3}$, at various frequencies for several plate distances, capacitances in microfarads. (Ni electrodes).

f cps	$L=0.1$ cm	$L=0.2$ cm	$L=0.3$ cm	$L=0.4$ cm
24	9.67	9.69	9.77	10.25
33	9.29	9.33	9.39	9.85
40	9.05	9.10	9.13	9.32
51	8.75	8.82	8.86	8.96
75	8.32	8.39	8.41	8.34
120	7.90	7.85	7.88	7.79
180	7.37	7.42	7.44	7.34
240	7.05	7.00	7.14	7.02
300	6.85	6.87	6.41	6.77
600	6.12	6.12	6.35	6.01
1000	5.61	5.58	5.67	5.26
1200	5.47	5.44	5.31	5.12
1800	5.01	4.95	4.94	4.54

(*c*) *Electrode material.* Complete sets of resistance and capacitance measurements were performed with Al, Ni, and Au electrodes (the latter two electroplated). Since the character of the frequency dependence did not change with the electrode material (see Fig. 9), it will be sufficient to show the influence of the electrode material for the highest observed capacitances, i.e., those at 18 cps. In Table VI the equivalent parallel values, C_p' per cm² area, are compared. They have been obtained from the directly observed series values by the method explained in Sec. VI.

Some series were also performed with platinized surfaces, but it proved to be particularly difficult to obtain reliable results with platinum black, in agreement with other observers.[15] A new feature which our observations revealed is the fact that the capacitances fall off more rapidly with increasing frequencies than they do for the other metals (see Fig. 9).

(*d*) *Temperature coefficient.* A few measurements were made between the temperatures of 17 and 33°C in order to serve as the basis for temperature corrections. They refer to a KCl solution of $m=10^{-3}$ and to an electrode distance of 0.1 cm.[16]

The temperature coefficients of conductance, $(1/\kappa)\times(d\kappa/dt)$, and of capacitance, $(1/C)(dC/dt)$, determined for five different frequencies, are united in Table VII. No great accuracy can be claimed for these data, but they show that the temperature coefficient for capacitance is positive and considerably smaller than that for the conductance. The values given here agree in order of magnitude with those determined by Jones and Christian[6] for the interval 0 to 25°C.

TABLE IV. Resistances of water and KCl solutions of several equivalent concentrations and for various frequencies; resistance in ohms, m in g-eq./liter, f in cps (Temperature=26.8° C; Ni electrodes).

$f\backslash m$	0(H_2O)	10^{-4}	5×10^{-4}	10^{-3}	2×10^{-3}	5×10^{-3}	10^{-2}
18	7255	2260	630	385	243	164	126
24	6850	2229	608	363	219	145	108
33	6700	2192	581	337.5	199	123.5	88.9
40	6404	2168	568.1	324.4	188.5	113.3	80.0
51	6385	2143	553.9	310.6	177.5	102.5	69.5
75	6365	2111	535.6	292.8	163.6	88.6	58.2
120	6565	2083	519.4	277.4	151.3	76.9	47.6
180	6740	2064	508.9	267.9	144.8	70.1	41.6
240	6705	2054	503.3	262.1	140.4	66.5	38.4
300	6745	2052	498.5	259.1	138.0	64.3	36.6
420	6740	2043	493.3	255.0	134.8	61.2	34.1
600	6805	2035	489.0	251.8	132.0	58.9	32.6
1800	6900	2019	481.1	245.4	126.9	54.6	27.2
3000	7015	2018	478.4	243.8	125.6	53.7	28.2
9000	6835	2009	475.8	242.0	124.2	52.4	27.4
18000	6310	1999	474.4	241.4	123.8	52.1	···

[15] See references (2) and (5g).

VI. COMPARISON BETWEEN EXPERIMENT AND THEORY

According to the theory proposed in A the effects of polarization are limited to very narrow layers adjacent to the electrodes. The thickness of the polarization layer varies slowly with frequency and concentration (A, Sec. III), and the computations made below show that

TABLE V. Capacitances in water and KCl solutions of several equivalent concentrations, and for various frequencies, capacitance in microfarads, m in g-eq/liter, f in cps. (Temperature=26.8°C; (Ni electrodes).

$f\backslash m$	0(H_2O)	10^{-4}	5×10^{-4}	10^{-3}	2×10^{-3}	5×10^{-3}	10^{-2}
18	11.9	10.5	13.8	13.5	14.1	14.5	14.8
24	11.2	9.9	13.21	12.66	13.6	14.0	14.4
33	10.0	9.16	12.54	12.13	13.09	13.44	13.87
40	9.5	8.77	12.16	11.74	12.78	13.12	13.63
51	9.3	8.32	11.66	11.30	12.40	12.68	13.25
75	8.4	7.64	10.86	10.62	11.75	11.98	12.62
120	6.82	6.87	10.04	9.80	11.07	11.29	11.94
180	5.55	6.19	9.04	9.16	10.45	10.72	11.43
240	4.74	5.64	8.44	8.70	9.97	10.29	10.98
300	3.92	5.18	8.12	8.36	9.62	9.95	10.66
420	3.05	4.67	7.55	7.88	9.00	9.46	10.21
600	2.16	4.06	6.95	7.34	8.51	8.97	9.72
1800	0.382	2.00	5.04	5.78	6.88	7.50	8.36
3000	0.140	1.18	3.98	5.03	6.10	6.81	7.71
9000	0.023	1.93	1.70	3.10	4.78	5.31	6.24
18000	0.005	0.050	0.64	1.46	2.76	3.90	···

they are of the order 10^{-5} cm. A necessary consequence is that the observed series values of the polarization capacitance and the excess resistance should be independent of the plate distance, L, for sufficiently low frequencies. We have shown in the previous section that the experimental results confirm this conclusion. Naturally, this would be true in any theory that localizes the effects near the electrodes.

As the frequency increases, the bulk of the liquid becomes more and more important and ultimately, according to our theory, the normal value of the resistance and the geometrical capacitance of the cell should be reached. Now we have seen that the resistance curves show distinctly three parts. Below frequencies of the order of 10^2 cps the polarization effects are marked and fall off rapidly. Then follows a range of

[16] The measurements were also taken at $L=0.2$, 0.3, and 0.4; they confirm the results on the influence of the plate distance stated above.

frequencies where the normal values are observed with fair approximation, and ultimately, say above frequencies of several thousands of cps, a final drop sets in. In the capacitance curves the third stage is particularly well marked in the case of high resistivities.

The third stage is easily explained by the geometry of our cells. Since the equivalent circuit is essentially a resistance and a capacitance in series, the observable equivalent series values should be given by

$$R_2' = R_2/(1+(\omega C_2 R_2)^2),$$
$$1/C_2' = (1/C_2)(\omega C_2 R_2)^2/(1+(\omega C_2 R_2)^2) \quad (1)$$

for sufficiently high values of the frequency, if R_2 represents the normal (undisturbed) resistance, and C_2 the geometrical capacitance of the cell.

In contradistinction from the usual type of cells the dimensions of our cell are such that the influence of its geometry begins to play a part at the upper end of our frequency range. As observed (see Sec. V) this influence sets in at the lower frequencies, the larger the specific resistance of the liquid, in agreement with (1). It will be seen below (compare Figs. 5 to 8) that the third part of the R_s- and C_s-curves is accounted for quantitatively by the geometry of the cell, provided its true geometrical capacitance, C_2, is augmented by a small apparent capacitance, C^*, which represents a parallel shunt inherent in the construction of the cell and the connections.

Thus, part three of our curves is of no particular interest in the present investigation. It remains to account for parts one and two. Irrespective of any theory, our material offers several reasons for the conclusion that the normal electrolytic ions, K^+ and Cl^- in the case of KCl solutions, are not the only ones which contribute to the observed effects of polarization. This fact is indicated by the considerable contribution of the solvent and by the relatively slow increase of the effects with concentration (see Tables V and VI).

From the point of view of our theory, it is easy to show more accurately that the normal ions are not the only ones contributing to the effects. Let us assume a KCl solution of $m=10^{-3}$; then all constants for the calculation of the reduced frequency, f^*, are known. From A, Eq. (41) we have

$$f^* = (\lambda/\beta)^2 = (\pi/\alpha^2 D)f, \quad (2)$$

where D is the (average) diffusivity of the positive and negative ions and where α is defined by II, Eq. (25). With $m=10^{-3}$ (i.e., $c_0=6.02\times10^{17}$), $D=1.98\times10^{-5}$cm^2/sec, $b/D=1.16\times10^4$ (b in electrostatic units), α becomes $\alpha=1.04\times10^6$ cm^{-1}, and $\pi/\alpha^2 D=1.46\times10^{-7}$. Now it follows from A, Table I that the initial value of the capacitance (represented by Γ_1) will have decreased to half its value for $(f^*)^{1/2}\sim0.3$, or $f\sim6\times10^5$ cps.

On the other hand, the experimental values drop off at much lower frequencies. Table V gives the highest capacitance, at $f=18$ cps, as 13.5 μF. From A, Table I it follows that the initial value should be about 14.5 μF.

TABLE VI. Parallel equivalent capacitances, microfarads per cm^2, for water and KCl solutions with different electrode surfaces, ($f=18$ cps).

Electrode surface	H_2O	KCl solutions of different concentrations m					
		10^{-4}	5×10^{-4}	10^{-3}	2×10^{-3}	5×10^{-3}	10^{-2}
Al	1.21	1.56	1.58	1.72	···	1.90	1.84
Ni	2.36	2.89	3.87	3.68	4.05	4.17	4.29
Au	1.78	4.17	4.52	5.50	···	···	7.16

Half of this value is reached for $f\sim600$ cps which is 10^3 times lower than the theoretical value. If we assume only one group of ions (half of them positive, half negative) their average diffusivity would have to be $(10^3)^{\frac{1}{2}}=32$ times *less* than the value given above to account for the rapid decrease. Hence, there must be other (slower) ions present in the liquid.

We are led to the same conclusion if we consider the dependence of the polarization capacitance on concentration. If the K^+ and Cl^- ions were alone (or predominantly) responsible for the effect, the capacitance should increase proportionally to the square root of the concentration (A, Eqs. (34), II, Eq. (25)). The values of C_{18}, collected in Table VI, however, increase much more slowly than $(c_0)^{\frac{1}{2}}$, even for gold electrodes where the increase is most marked. This leads to the conclusion that there is a contribution other than that due to the K^+ and Cl^- ions.

It is of interest to evaluate the thickness of the polarization layer which results from theory under the assumption that the normal ions alone are active. It follows from Eq. (2) that, for $m=10^{-3}$ and the constants given above, $(f^*)^{\frac{1}{2}}$ changes from 1.32×10^{-3} to 4.2×10^{-2} as f increases from 18 to 18,000 cps. Consequently, (from A, Table I) β will change from about 25.8 to 12.8. Now, from A, Eq. (33), we have $\beta=2l_1\alpha$; hence, l_1 decreases from 1.2×10^{-5} to 0.6×10^{-5} cm as f increases from 18 to 18,000 cps.

It is reasonable to assume and is brought out by the measurements (see Tables IV to VI) that the solvent contributes a very important part to the observed effects of polarization. Therefore, an analysis of the observations with "pure water" becomes necessary. In the course of the present investigation a considerable number (more that 10) samples of conductance water were measured over the entire range of frequencies. The specific conductances, for Ni electrodes, varied

TABLE VII. Temperature coefficients of conductance and capacitance at several frequencies. (KCl solution of $m=10^{-3}$; Ni electrodes).

f cps	Conductance $(1/\kappa)_{17}(\Delta\kappa/\Delta t)_{25}$	Capacitance $(1/C)_{17}(\Delta C/\Delta t)_{25}$
18	0.0146/°C	0.00718/°C
75	0.0174	0.00576
300	0.0215	0.00403
1000	0.0232	0.00481
1800	0.0238	(0.00781?)

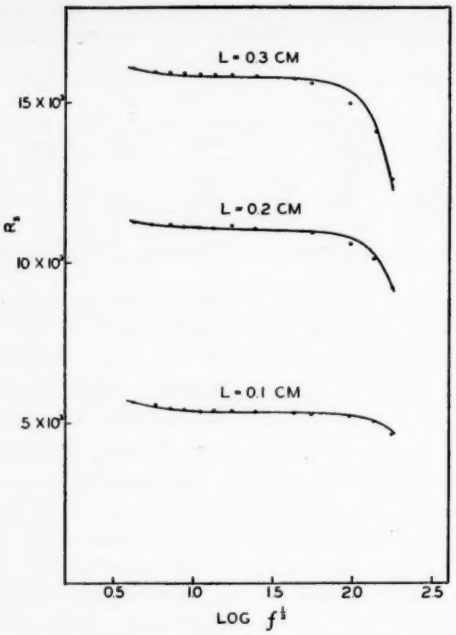

FIG. 5. Conductance water. Plot of resistance R_s, *versus* log $f^{\frac{1}{2}}$ for three plate distances, $L=0.1$, 0.2, 0.3 cm. Points observed, drawn-out curves calculated.

from 2.7 to 4.1×10^{-6} ohm^{-1} cm^{-1}, while the capacitance per cm^2 at 18 cps varied from 1.4 to 3.5 μF/cm^2. There was no correlation between the two series of values. This confirms the conclusion that the ions which carry the current are not necessarily the same which cause the capacitance. The influence of the material of the electrodes is shown by the first column of Table VI. Our general remarks regarding the lack of reproducibility should be remembered (see Sec. IV).

The falling off of the C_s values always occurs at lower frequencies and is much more marked for water than for solutions (see Table V). This, however, is due to the geometrical effect which sets in at lower frequencies for higher resistivities. The excess resistance is hardly ever observable in pure water on account of its smallness relative to the large error of observation for water samples.

We are now going to analyze completely one set of three series, referring to gold-plated electrodes and extending over the range $f=18$ to $f=30{,}000$ cps, with plate distances $L=0.1$, 0.2, and 0.3 cm. The observed values are marked by points in Figs. (5) and (6). The coordinates are R_s and log C_s *versus* log $f^{\frac{1}{2}}$, respectively. The resistances and capacitances are the directly observed values, i.e., they refer to the effective area of the central electrode, $A=3.36$ cm^2. The specific conductance of this sample was rather high, namely, $\kappa=5.7\times10^{-6}$. The drawn-out curves of Figs. 5 and 6 are theoretical curves which were calculated in a way to be described presently.

For a comparison between experiment and theory it must be borne in mind that the observations represent equivalent series values, whereas A, Eqs. (32) give parallel values. In order to reduce the experimental values to the parallel values of the polarization layers alone, first the bulk values, as given by Eq. (1) have to be subtracted. Suitable values of the true resistance R_2, had to be chosen (near the end of part two of the resistance curves), and the geometrical capacitances C_2 had to be augmented by a shunt impedance. A fairly satisfactory fit of the high frequency end of the curves could be realized by choosing for the shunt impedance a pure capacitance of amount $C^*=100$ $\mu\mu F$. The agreement, for resistances and capacitances, is good enough to prove that we are dealing here with an effect caused mainly by the geometry of the cell. The values of R_2, C_2, and C^* used in the computations are listed in Table VIII.

After subtraction of the "bulk values" (R_2' and $1/C_2'$) from the directly observed values R_s and $1/C_s$, there remain the effective series values of the two polarization layers, namely,

$$R_s'=R_s-R_2', \quad 1/C_s'=1/C_s-1/C_2'. \tag{3}$$

These have to be transformed into the parallel values of conductance $1/R_p'$ and capacitance C_p' in the usual manner. The values obtained in this way should be independent of plate distance, as they refer to the polarization layers alone. This conclusion was verified with good approximation. Finally $1/R_p'$ and C_p' may be compared with the theoretical formulas A, Eqs. (32), or eventually A, Eqs. (43), (44), if the necessity arises of admitting more than one group of ions.[17]

If it is possible to represent the behavior of water by one group of ions, and with the value $\rho=0$, the doubly logarithmic experimental plots can be made to coincide with the theoretical ones by horizontal and vertical shifts. The horizontal shift, furthermore, has to be the same for the conductance and the capacitance curves since it only depends on α^2D (see Eq. (2)).

It was impossible to meet these exigencies with sufficient accuracy in any of the numerous cases tested (either for water or for solutions), and this we consider as the final proof that there are several groups of ions present in the liquids. As will be seen, a very satisfactory agreement between experiment and theory can be obtained if, besides the ions of normal mobility, *one* further group of considerably lower mobility is assumed.

With two groups of ions the general equations A, (43) to (46) can be written in the form

$$1/R_p'=2\epsilon b_2c_2\alpha[\Gamma_2(f_2^{*\frac{1}{2}})/\beta(f_2^{*\frac{1}{2}}) + (b_1c_1/b_2c_2)\Gamma_2(f_1^{*\frac{1}{2}})/\beta(f_1^{*\frac{1}{2}})], \tag{4}$$

$$C_p'=(\epsilon b_2c_2/\alpha D_2)[\Gamma_1(f_2^{*\frac{1}{2}})+(c_1/c_2)\Gamma_1(f_1^{*\frac{1}{2}})], \tag{5}$$

if the two reduced frequencies

$$f_i^*=(\pi/\alpha^2D_i)f, \quad i=1, 2 \tag{6}$$

[17] Following A we speak of one "group" of ions if there are positive and negative ions of equal valence and number and approximately the same mobility. Different "groups" refer to ions of widely different mobilities.

TABLE VIII. Constants referring to water and used in the calculation of the theoretical curves of Figs. 5 and 6.

L(cm)	R_2(ohms)	C_2 ($\mu\mu F$)	C^* ($\mu\mu F$)
0.1	5240	233	100
0.2	10900	116	100
0.3	15680	77.5	100

$\alpha = 4.75 \times 10^3$

$c_1 = 1.37 \times 10^{15}$ cm^{-3} $\quad b_1 = 2.27 \times 10^{-3}$ cm^2/volt sec
$c_2 = 6.83 \times 10^{15}$ cm^{-3} $\quad b_2 = 2.27 \times 10^{-5}$ cm^2/volt sec

are introduced. We refer the index 1 to the normal (faster) group of ions.

The laborious task of fitting these theoretical formulas to the experimental data is greatly facilitated by the construction of a set of templates (on a doubly logarithmic scale) for various values of c_1/c_2 and b_1/b_2.[18]

It was found that the six curves for water could be matched by choosing $c_1/c_2 = 0.2$ and $b_1/b_2 = 10^2$. These determinations are by no means exact, since the templates change but slowly with the value of the two ratios. We estimate that the error may be as high as 20 or 30 percent. The absolute values of b_i are uncertain to at least the same degree. We have assumed that the swifter group of ions corresponds to the normal electrolytic ions, and that they are essentially those of hydrogen and CO_2. This assumption makes $b_1 = 2.27 \times 10^{-3}$ cm^2/volt sec, $D_1 = 5.87 \times 10^{-5}$ cm^2/sec, and b_2, D_2 100 times smaller, respectively. With D_2 known, α can be determined from the horizontal shift, which was chosen the same for the conductance and capacitance curves. Finally c_2, and thereby c_1 also, is found from the vertical shifts. The vertical shifts for the conductance and capacitance curves should yield identical values. This was never the case, the difference in some cases being as large as 30 percent. This we attribute to the uncertainty in the absolute values of the capacitances due to varying surface conditions. We have, therefore, used the conductance curves only in determining the c's. The values finally accepted are summarized in Table VIII.

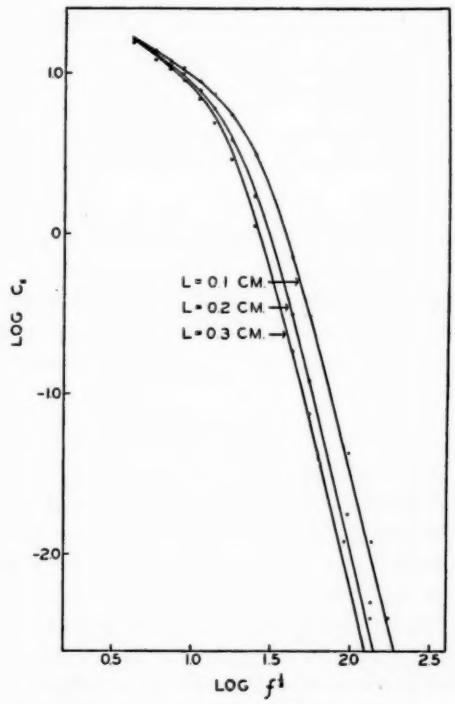

FIG. 6. Conductance water (same as Fig. 5), Plot of log C_s *versus* log $f^{\frac{1}{2}}$, for three plate distances, $L = 0.1$, 0.2, 0.3 cm. Points observed, drawn-out curves calculated.

[18] Such templates were prepared for the work of the Signal Corps Project No. 152 *B*. We are indebted to Dr. L. W. Morris for letting us use them.

With the ionic constants determined as described, it becomes possible to calculate the observed series values. The procedure is exactly the reverse of that used in the analysis of the data. First $1/R_p'$ and C_p' are determined from (4) and (5) by the use of A, Table I. Then the parallel values are converted into series values, $1/R'$ and C_s', and finally the bulk values (1) are added. The results of these calculations are the drawn-out curves of Figs. (5) and (6). It will be seen that the theoretical curves represent the observations sufficiently well for all three plate distances L, and over the parts 1 and 2 of the curves (the parts 3 have been discussed above[19]). It should be mentioned that the maximum value of the capacitance for $f \to 0$, as extrapolated by theory, is 79 μF. This high value is mainly due to the slow group; the normal group contributes only 20 percent. On the other hand, the slow ions carry only 5 percent of the current as $f \to \infty$. This verifies quantitatively the conclusion previously arrived at that the polarization effects are mainly due to ions other than the normal ones.

We have represented the observations using the theoretical curves for $\rho = 0$. The agreement would not be affected by using a constant small value of ρ, since the curves for variable ρ are similar to each other to a good approximation, as long as ρ is small (see A, p. 1075). All that can be claimed, therefore, is that the ions which cause the polarization in water discharge sufficiently slowly to make $\rho = 0$ an acceptable approximation. It will be seen that this is not true for the ions K^+ and Cl^-.

With the behavior of water sufficiently clarified we can approach the analysis of the data on KCl solutions. We shall confine ourselves to the set of measurements given in Tables IV and V and shall treat in detail the concentrations $m = 10^{-2}$, 10^{-3}, and 10^{-4} only, as otherwise the diagrams become too confused. The observations in question are represented in Figs. 7 and 8 by the points; the curves are calculated from theory with the constants collected in Table IX.

The analysis proceeds in exactly the same way as described above, with one characteristic difference. After subtraction of the bulk values and transformation to parallel values there remain the $1/R_p'$ and C_p' values which refer to the polarization layers only. If these

[19] One observational point (R_s for $f = 1{,}800$ and $L = 0.2$) has been omitted because it was evidently affected by some large error.

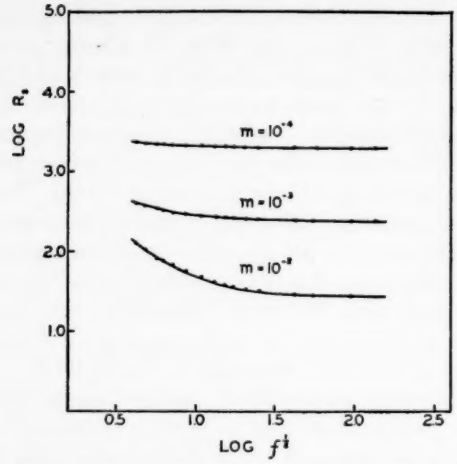

FIG. 7. KCl solutions. Plot of log R_s *versus* log $f^{\frac{1}{2}}$, for three concentrations $m = 10^{-4}, 10^{-3}, 10^{-2}$. Points observed, drawn-out curves calculated.

values are plotted *versus* $f^{\frac{1}{2}}$, or log $f^{\frac{1}{2}}$, the conductance values coincide, as they should, since the contribution of the K^+ and Cl^- ions has been subtracted. The C_p' values, however, arrange themselves in curves which are different for the various concentrations *but which are mutually parallel* with good approximation. This is exactly what might be expected if the K^+ and Cl^- ions contribute to the capacity effect. This contribution would be independent of frequency in our range of frequencies, as the decrease for normal ions does not set in before the frequency becomes of the order 10^4 to 10^5 cps (see p. 1082). Hence, the contribution of the salt can be found from the vertical distances $\Delta C_p'$ of the C_p' curves. They are given in Table IX.

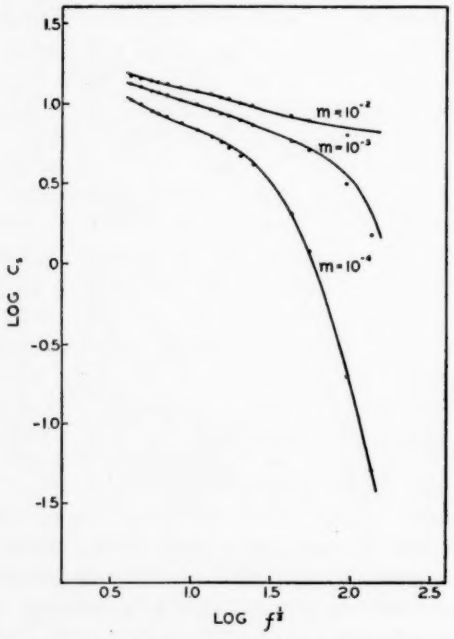

FIG. 8. KCl solutions (same as Fig. 7) plot of log C_s *versus* log $f^{\frac{1}{2}}$ for three concentrations $m = 10^{-4}, 10^{-3}, 10^{-2}$. Points observed, drawn-out curves calculated.

After subtraction of the $\Delta C_p'$ values all points naturally fall on one curve. This curve, together with the corresponding one for $1/R_p'$, gives the contribution of the solvent and may now be treated in the same way as the directly observed water values. The ratio c_1/c_2 had to be chosen as 0.4, but the same ratio $b_1/b_2 = 10^2$ could be maintained. The results of this analysis are summarized in Table IX. Finally, by the inverted procedure, the theoretical curves of Figs. 6 and 7 were obtained.

All essential features of the observations are represented adequately by the theoretical curves. Whereas the observations on water exhibited mainly parts 2 and 3 of the curves, the solutions show more distinctly parts 1 and 2. It now becomes clear why the stage 2 never is quite horizontal for the R_s-curves. The reason for this observation lies in the fact that there are two species of ions present with mobilities as different as 1 to 100. The superposition of two curves, with different scales for the abscissae, invariably makes the R_p and C_p values fall off more slowly than for a unique group. In particular, when the resistivity is relatively low, and consequently the excess resistance very marked (see the $m = 10^{-2}$ curve of Fig. 7), the decrease continues over the whole range of frequencies and may still be noted when the trivial effect of geometry sets in. This is one reason why it proves to be difficult to determine the true normal values with high accuracy using a condensor like ours built to accentuate the polarization effects.

TABLE IX. Constants referring to KCl solutions and used in the calculation of the theoretical curves of Figs. 7 and 8.

m (g-eq per liter)	R_2 (ohms)	C_p (μF)	c_1 (number cm^{-3})	c_2 (number cm^{-3})
10^{-2}	27.9	6.76	1.26×10^{15}	3.14×10^{15}
10^{-3}	241.7	4.55	1.51×10^{15}	3.77×10^{15}
10^{-4}	2020	1.36	1.62×10^{15}	4.07×10^{15}

$C_2 + C^* = 374\ \mu\mu F$ $\qquad \alpha = 1.42\times10^4$
$b_1 = 2.27\times10^{-3}$ cm²/volt sec $\qquad b_2 = 2.27\times10^{-5}$/volt sec

The ionic data, i.e., the values of c_i and b_i, as determined for water and compiled in Tables VIII and IX agree sufficiently well, if it is taken into account that they refer to different samples of water and that the values of Table IX are obtained in an indirect way from KCl solutions. The ionic concentrations in Table IX change for the three plate distances. They were taken in the indicated order, and the figures might very well reflect real changes in the nature of the water, since the vessel was in connection with the atmosphere.

If we summarize, we do not believe that the ionic data as given in Tables VIII and IX give much more than the order of magnitude. Nor do we claim that the existence of a group of slow ions of well-defined mobility has been proved. The identity of the slow ions would have to be ascertained before such a claim could be

made. In our opinion the most probable assumption is that they are hydrated ions, i.e., ordinary ions surrounded by an atmosphere of H_2O molecules. Now, if these "big ions" are in dynamic equilibrium with the solvent, it might be expected that they are of variable sizes and, therefore, might represent a whole "spectrum" of mobilities.

Finally we are able to form an estimate of the rate at which the K^+ and Cl^- ions are discharged at the electrodes. In Table X we have compared the observed values of $\Delta C_p'$ with those maximum values C_0' which would hold if ρ were zero (see A, Eq. (34)). From the ratio of these two values the reduced discharge constant ρ can be obtained by the use of A, Eq. (29). The values so obtained are given in the third row. It will be seen that they are of the order of 2, and this represents strongly reduced polarization effects, as is evident from A, Figs. 1 and 2. From ρ the discharge constant ξ itself may be obtained from the definition of ρ (A, Eq. (22)) if l_1 is known. Assuming for l_1 the average value 10^{-5} cm, the values of ξ given in the fourth row are obtained. As

TABLE X. Determination of rate constants. C_0' = maximum capacitance per cm² area, deduced from theory for $\rho=0$ for various concentrations of KCl solutions; $\Delta C_p'$ = capacitance per cm² area, deduced from the analysis of experimental data; ξ = rate constant, dimension: cm/sec; ρ = reduced rate constant.

m	10^{-4}	5×10^{-4}	10^{-3}	2×10^{-3}	5×10^{-3}	10^{-2}
C_0' ($\mu F/cm^2$)	1.13	2.51	3.56	5.05	7.96	11.2
$\Delta C_p'/A$ ($\mu F/cm^2$)	0.40	1.00?	1.35	1.71	1.85	2.01
ρ_{Ni}	1.4	1.2	1.2	1.4	2.2	2.8
ξ_{Ni}	4.3	3.7	3.7	4.3	6.8	8.6
ρ_{Al}	3.0	···	2.8	···	···	4.8
ρ_{Au}	0.4	···	0.3	···	···	1.3

far as we are aware these are the first rate constants for the discharge of ions which have been determined.

According to our theory the difference in behavior of various electrode materials is caused by the difference in the rate of discharge at those electrodes. An inspection of the figures of Table VI shows that Al should have a more rapid discharge than Ni, and Au a slower rate of discharge than Ni.

Without going into an elaborate analysis as performed for the Ni series, we can form an estimate of the constant ρ for Al and Au electrodes by the following procedure. First the values in Table VI pertaining to KCl solutions have to be corrected for the solvent. This correction is not performed by simple subtraction of the water values, but has to be based on Eq. (5) (with the assumption that $\Gamma_1=1$ is a sufficient approximation for as low a frequency as 18 cps). It is found that the values for Al, Ni, and Au, so corrected, are proportional to each other with a fair accuracy. The

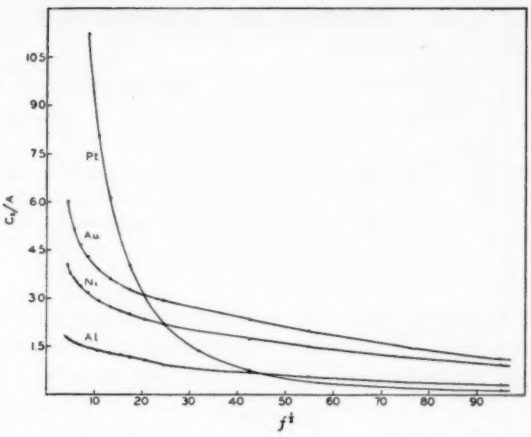

FIG. 9. KCl solution of $m=10^{-3}$ g-eq/liter capacitance per cm² C_s/A, as function of $f^{\frac{1}{2}}$ for electrodes of Al, Ni, Au, Pt surfaces.

corrected values are as 0.47:1.00:2.01 for Al, Ni, and Au, respectively (the average error for Al being 13 percent, and that for Au 6 percent).

From these ratios and A, Eq. (29) the constant ρ for the various concentrations can be deduced. They are given in the last two rows of Table X and verify the expected behavior.

All our computations refer to Al, Ni, and Au electrodes, i.e., to electrodes which are not attacked by the solutions. For these the agreement between experiment and theory is satisfactory. The question remains open how reversible electrodes (of the first or the second kind) behave with regard to polarization with ac. It is well known[2] that polarization capacitances of extremely high values, up to $.02F/cm^2$ are observed with reversible electrodes, and it remains doubtful whether our theory in its present form can explain them. The behavior of platinum black approaches that of reversible electrodes in giving very high polarization capacitances, and our Fig. 9 shows qualitatively how different platinized electrodes behave from either Al, Ni, or Au electrodes. It might very well be that in all the cases of extremely high polarization capacitances the formation of a very thin insulating layer takes place besides the effects of ion diffusion and space charge considered here. Experiments to clarify this point are being carried out in this laboratory at present.

ACKNOWLEDGMENT

The authors wish to express their indebtedness to the Office of Naval Research for supporting this research and to Dean A. R. Choppin for lending them the Jones bridge. They are also obliged to Mr. N. M. Schaefer and Mr. J. R. Weston for allowing them to publish here some of their experimental results. Table II and Figs. 3 and 4 are taken from Mr. Schaefer's thesis, and Tables I, III, IV, V, and VII from Mr. Weston's thesis.[10]

Temperature Dependence of the Viscosity of Associated Liquids

THEODORE A. LITOVITZ
Physics Department, Catholic University of America, Washington, D. C.
(Received March 13, 1952)

By assuming that the activation energy for flow in associated liquids is proportional to the inverse square of the absolute temperature, an empirical expression for the viscosity is obtained, which fits the data well. An empirical expression for the activation energy of mixtures of associated liquids is also proposed.

IT has long been observed[1] that temperature dependence of associated liquids did not follow the simple expression derived by Andrade,[2] where

$$\eta = Ae^{E/RT}, \tag{1}$$

where E is a constant, R is gas constant, and A is a constant. The same type of equation has been derived by Eyring[3] using a reaction rate theory in which E has been assumed to be an activation energy for shear flow.

Tammann and Hesse[4] have proposed an empirical expression which fits the observed viscosity data in associated liquids. Their equation is

$$\eta = A \exp[B/(T-T_\infty)], \tag{2}$$

where B and T_∞ are constants dependent on the liquid involved.

An explanation of the unusual temperature dependence of associated liquids is that the activation energy changes with temperature. This activation energy is assumed to be a function of the average hydrogen bonding in the liquids which will decrease with increasing temperature due to the thermal motion of the molecules.

If one assumes that

$$E = a/T^2, \tag{3}$$

where "a" is the activation energy constant dependent on the liquid and T is the absolute temperature, then the viscosity expression becomes

$$\eta = A \exp(a/RT^3). \tag{4}$$

Table I and Figs. 1 and 2 show the fit of this expression with the viscosity data of water and glycerol. Also in Fig. 1 is a semilog plot of viscosity *vs* the reciprocal of the absolute temperature to show the deviation from Eq. (1). Figure 3 shows the semilog plot of the viscosity of glycerol (0.5 percent water content) *vs* temperature from −4°C to −41°C, showing that Eq. (4) holds also for the liquids in the supercooled state.

In Table II the constant "a" is tabulated for several liquids and one can note that "a" is roughly proportional to the number of OH groups per molecule. This is to be expected if the hydrogen bonding is the cause of the relatively high viscosities found in associated liquids.

TABLE I. Comparison of experimental and calculated values of the viscosity in millipoise of water.

T°C	η_{exp}[a]	η_{calc}[b]	Percent difference
0	17.96	18.01	0.3
10	13.0	13.22	1.7
20	10.05	10.12	0.7
30	7.99	7.99	0
40	6.55	6.71	−0.6
50	5.49	5.43	−1.1
60	4.73	4.63	−2.1
70	4.07	4.02	−1.2
80	3.56	3.58	0.6
90	3.13	3.18	1.6

[a] η_{exp} from reference 5.
[b] η_{calc} from Eq. (4) where $a = 12.3 \times 10^7$.

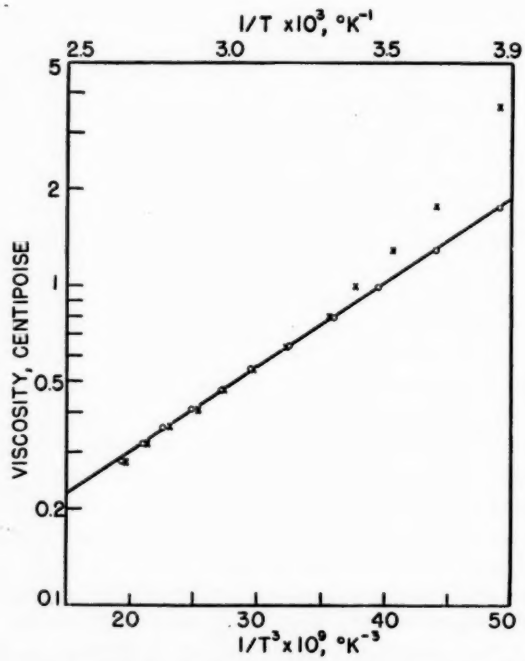

FIG. 1. Semilog plot of the viscosity of waver *vs* the reciprocal of the absolute temperature cubed. X marks are a semilog plot of viscosity *vs* the reciprocal of absolute temperature. Data taken from reference 5.

[1] S. Glasstone, *Physical Chemistry*, (D. Van Nostrand Company, Inc., New York), p. 502.
[2] E. N. da Andrade, Phil. Mag. **17**, 497, 698 (1934).
[3] H. Eyring, J. Chem. Phys. **4**, 283 (1936).
[4] Tamman and Hesse, Z. anorg. u. allgem. Chem. **156**, 245 (1926).
[5] E. C. Gingham and G. F. White, Z. physik Chem. **83**, 641 (1913).

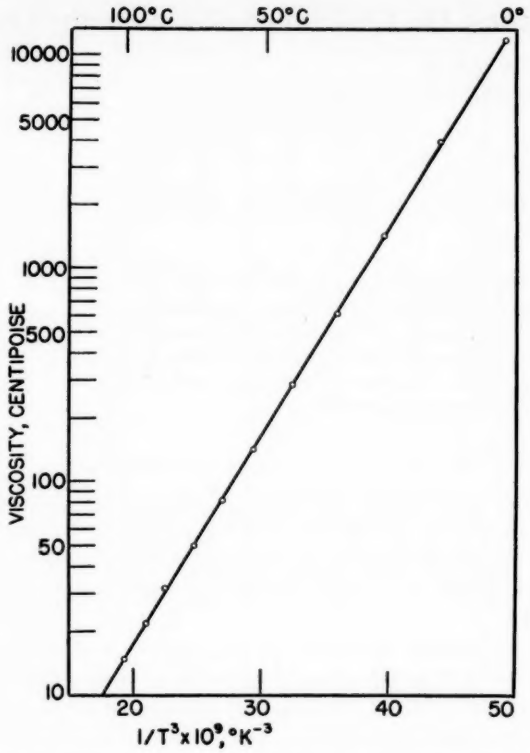

FIG. 2. Semilog plot of the viscosity of pure glycerol *vs* the reciprocal of the absolute temperature cubed. Data from reference 4.

It is interesting to consider the effect on "a" when two associated liquids are mixed. In Fig. 4 the "a"[6] constant for glycerol-water mixtures is plotted as a function of the composition in mole-fractions. A linear relationship appears to exist except for concentrations of water in glycerol less than 0.2 mole fractions. The intercept of the curve on the 100 percent glycerol axis gives a value for "a" of 47.4×10^8 as compared with the experimental value of 45.6×10^8.

Thus, it would appear that the following relation exists to within 5 percent:

$$a_{\text{mixture}}=X_1a_1+X_2a_2, \tag{5}$$

where X_1 and X_2 are the mole fractions of liquids 1 and 2, respectively; a_1 and a_2 are the activation energy constants of liquids 1 and 2.

It is difficult to find the theoretical significance of the above empirical expressions, but Eq. (5) should serve as a useful extrapolation formula for the viscosity of associated liquids.

TABLE II. Activation energy constant "a"[a] for various liquids.

Liquid	"a" $\times10^{-7}$
Water	12.3
Methyl alcohol	7.5
Ethyl alcohol	11.4
Prophyl alcohol	13.2
Butyl alcohol	14.5
Glycol	22.2
Glycerol	45.6

[a] Units of "a" are cal $\times$°K³.

[6] J. B. S. Segur and Helen B. Oberstar, Ind. Eng. Chem. **43**, 2117 (1951).

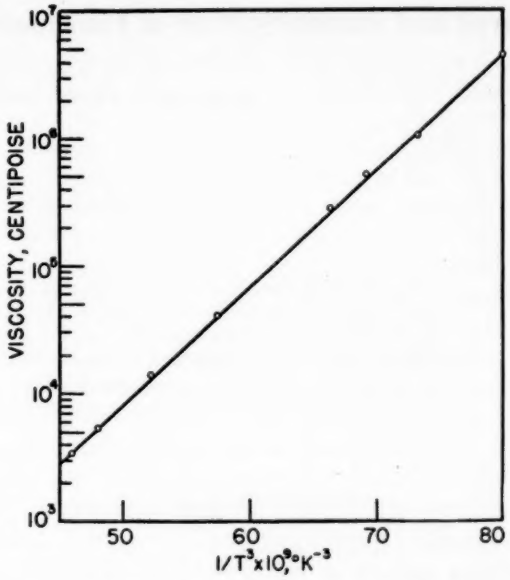

FIG. 3. Semilog plot of the viscosity of supercooled glycerol *vs* reciprocal of temperature cubed. Data from reference 4.

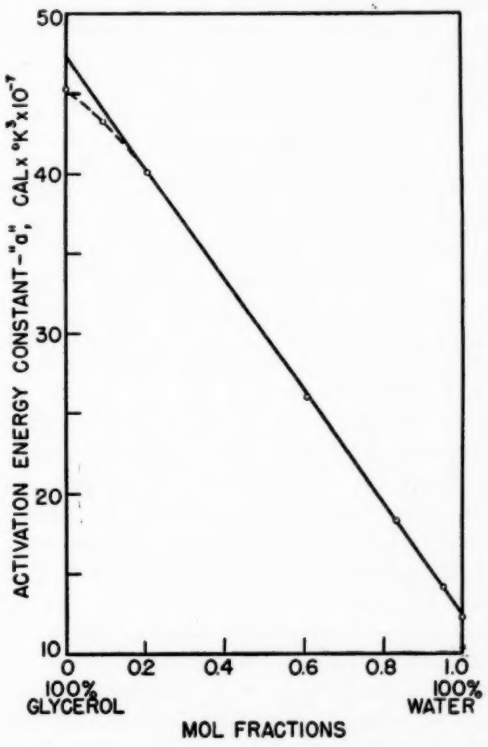

FIG. 4. Plot of activation energy constant "a" as a function of the mole fraction composition of glycerol water mixtures. Viscosity data used in calculating "a" are taken from reference 6.

Infrared and Raman Spectra of Fluorinated Ethylenes. IV. 1,1-Difluoro-2-chloroethylene*

J. Rud Nielsen and C. Y. Liang
Department of Physics, University of Oklahoma, Norman, Oklahoma

and

D. C. Smith†
Naval Research Laboratory, Washington, D. C.

(Received January 28, 1952)

The infrared absorption spectra of gaseous and liquid CF_2:CHCl have been obtained in the regions 2–22μ and 2–38μ, respectively, with the aid of LiF, NaCl, KBr, and KRS-5 prisms. The Raman spectrum of the liquid phase has been photographed with a three-prism glass spectrograph of linear dispersion 15 A/mm at 4358A. Relative intensities and depolarization ratios have been measured for the stronger Raman bands. A complete assignment of fundamental vibration frequencies is given, the spectra are interpreted in detail, and thermodynamic functions are calculated for the temperature range 253–600°K.

INTRODUCTION

In previous papers[1,2] of this series the infrared and Raman spectra of CF_2:CH_2 and CF_2:CCl_2 have been reported. In the present paper spectral data will be given for the intermediate compound CF_2:CHCl. Assignments of fundamentals, detailed interpretations of the spectra, and calculated thermodynamic functions will be presented. No previous spectral studies seem to have been made of this compound.

EXPERIMENTAL

Two samples of CF_2:CHCl were kindly supplied by the Laurel Hill Laboratory of General Chemical Division, Allied Chemicals & Dye Corporation. No information was available about their purity. However, the second sample (Ser. No. 493) was believed to be of higher purity than the first (Ser. No. 478). The infrared absorption spectrum of the first sample in the gaseous state was measured from 2 to 22μ in the manner previously described[1] and in the range from 22 to 38μ by means of a 26° KRS-5 prism mounted in a Perkin-Elmer Model 12C spectrometer. Stray light was reduced to a very low level by replacing the plane source mirror with a LiF plate and using a LiF shutter. Under normal operating conditions the amplifier gave 0.1 microvolt full scale deflection with about one percent noise but with 2–5 percent uncertainty due to zero and amplification drift. The wavelength drive of the instrument was modified so as to maintain spectrometer and recorder chart in synchronism while driving either forwards or backwards with a wide range of speeds. The instrument was calibrated in the manner described by Plyler,[3] but the calibration was improved by the use of Raman frequencies of a number of sharp bands of certain fluorinated aromatics. Because of the poor optical quality of the soft KRS-5 prism the measured positions of absorption bands are probably not accurate to more than ± 2 cm^{-1}, except for sharp symmetrical bands.

The infrared spectrum of the second sample (Ser. No. 493) in the liquid state (at −30°C) was studied in the range 2–22μ by means of a variable-thickness low temperature cell similar to that recently described by Holden, Taylor, and Johnston.[4] KBr was used for the Dewar windows, and the AgCl cell windows were seated against Teflon gaskets to form a closed system that can be filled by evacuation and admission of condensable gases. A blank was run for each spectrum with the cell closed (but with some absorption by the liquid film), and the thickness of subsequent films was reckoned from this setting of the cell.

The Raman spectra were obtained of both samples in the liquid state at room temperature, and quantitative polarization measurements were made in the manner previously described.[2] No significant differences were found between the Raman spectra of the two samples.

RESULTS

The infrared absorption of gaseous and liquid CF_2:CHCl between 2 and 22μ is shown in Fig. 1. The wave numbers of the observed absorption maxima are listed in Table I. The relative intensities, and in some cases the sharpness, of the bands are indicated by means of the previously used abbreviations. The observed Raman shifts for liquid CF_2:CHCl are given in the first column of Table II. The relative intensities and depolarization ratios of the Raman bands are listed in the second and third columns, and the exciting mercury lines are given in the fourth column in the Kohlrausch notation.[5]

* This work has been supported in part by the AEC under contract No. AT-(40-1)-1074.

† Present address: Phillips Petroleum Company, Bartlesville, Oklahoma.

[1] Smith, Nielsen, and Claassen, J. Chem. Phys. **18**, 326 (1950).

[2] Nielsen, Claassen, and Smith, J. Chem. Phys. **18**, 485 (1950).

[3] E. K. Plyler, J. Chem. Phys. **15**, 885 (1947); J. Opt. Soc. Am. **38**, 664 (1948).

[4] Holden, Taylor, and Johnston, J. Opt. Soc. Am. **40**, 757 (1950).

[5] K. W. F. Kohlrausch, *Der Smekal-Raman-Effekt* (Julius Springer, Berlin, 1931).

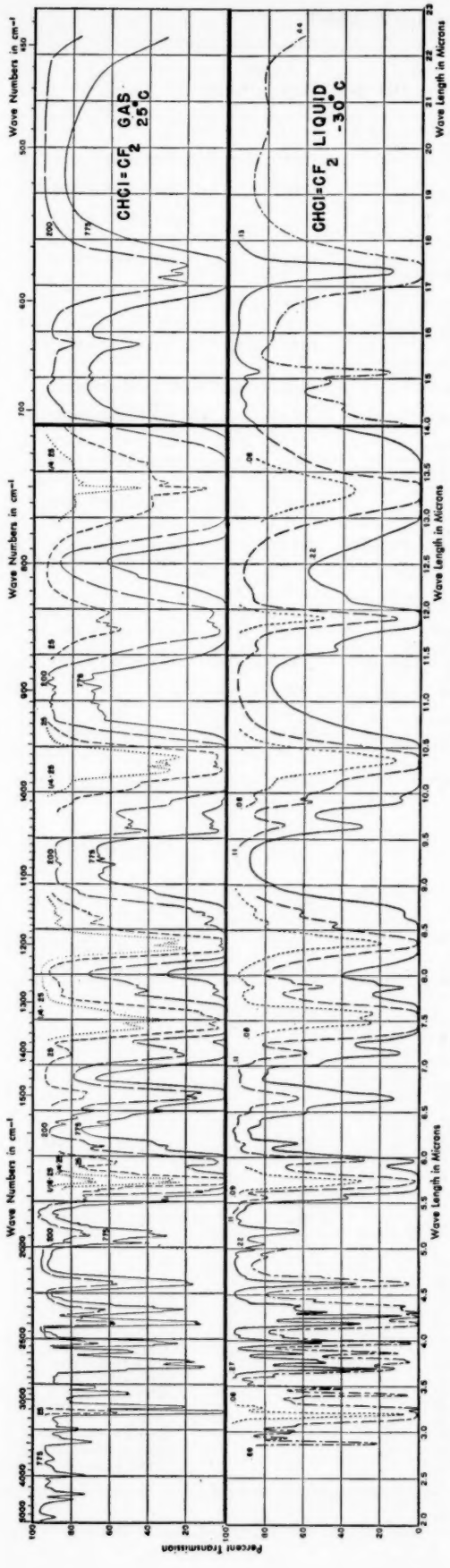

FIG. 1. Infrared spectra of gaseous and liquid CF_2:CHCl (KRS-5 region not included).

INTERPRETATION

The CF_2:CHCl molecule undoubtedly has a planar configuration. Nine of its fundamentals belong to species A', and three fundamentals to species A''. The former give rise to polarized and the latter to depolarized Raman bands. When Badger and Zumwalt's parameters[6] are calculated from the moments of inertia of the CF_2:CHCl molecule given below, values are obtained that lie outside the range of the tables given by these authors. However, since the two largest moments of inertia are equal to within 20 percent, it is possible to make a rough prediction of the contours of the infrared bands by means of Gerhard and Dennison's theory for symmetrical top molecules.[7] It is found in this way that parallel bands should have a Q branch of intensity about 15 percent of that of the entire band and P and R maxima lying 6.4 cm^{-1} from the Q branch. Perpendicular bands should not show PQR structure but should have only a single, fairly broad peak. The A'' fundamentals should give perpendicular infrared bands, whereas the A' fundamentals should give bands with contours intermediate between those of parallel and perpendicular bands.

Fortunately, the nine A' fundamentals are readily assigned on the basis of their intensities in the two spectra and their depolarization ratios. The highest A' fundamental, at 3130 cm^{-1}, is associated with C—H stretching; the next, at 1745 cm^{-1}, with C=C stretching. The A' fundamentals at 1333 and 1199 cm^{-1} are both very strong in the infrared and rather weak in the Raman effect, indicating that they involve largely C—F stretching. The next two A' fundamentals, at 968 and 845 cm^{-1}, must correspond to C—Cl stretching and C—H bending motions, and that at 579 cm^{-1} largely to CF_2 deformation. The two lowest A' fundamentals, at 432 and 201 cm^{-1}, represent rocking modes.

Four of the A' fundamentals have fairly well-defined contours in the infrared spectrum of the gas, namely, P and R maxima 6 to 7 cm^{-1} from a rather weak Q branch. The band at 1333 cm^{-1} appears to have an abnormal contour, and the spectrum of the liquid shows that this is caused by overlapping with another band. The remaining A' fundamentals are observed with so low resolution in the infrared that their contours are ill-defined, or lie outside the wavelength range covered.

The depolarized Raman band at 243 cm^{-1} must represent an A'' fundamental corresponding to twisting or a mixture of twisting and wagging of the ends of the molecule. The intense infrared band at 715 cm^{-1} which has a contour that marks it as a perpendicular band, and the corresponding Raman band which is almost certainly depolarized, must represent another A'' fundamental. Since it lies less than 100 cm^{-1} from the out-of-plane C—H bending frequencies in olefines of structure

[6] R. M. Badger and L. R. Zumwalt, J. Chem. Phys. **6**, 711 (1938).
[7] S. L. Gerhard and D. M. Dennison, Phys. Rev. **43**, 197 (1933).

TABLE I. Infrared absorption spectrum of CF_2:CHCl.

Gas Wave number	Gas Description	Liquid Wave number	Liquid Description	Interpretation
~ 424	*s*			*A'* fundamental $\{Cl^{37}$
~ 433	*s*			$Cl^{35}\}$
		490	*vw*	$2\times243=486$ *A'*
~ 573				*A''* fundamental
579	*s, sh*	577	*m*	*A'* fundamental
~ 585				
~ 635	*w*	625	*w*	$201+432=633$ *A'*
~ 637				$845-201=644$ *A'*
662	*vw*	661	*vw*	$243+428=671$ *A''*
668	*vw*	671	*w*	$243+432=675$ *A''*
~ 695	*vw*	694	*w*	
736				$970-243=727$ *A''*?
747				
751	*vs, sh*	752	*s*	*A''* fundamental
~ 753				
~ 761				$970-201=769$ *A'*?
		775	*vw*?	$201+576=777$ *A'*
809	*vw*	821	*w*	$243+576=819$ *A''*
~ 835				
838				
845	*s, sh*	840	*m*	*A'* fundamental
~ 849				
		864	*w*	$2\times432=864$ *A'*
890	*vw*			Impurity[a]
897	*vw*			Impurity
902	*vw*			Impurity
~ 907				Impurity
912	*vw*			Impurity
~ 919				Impurity
923	*vw*			Impurity
~ 962				
969	*vs, sh*			
971	*vs, sh*	964	*s*	970 fundamental (*A'*)
976				
~ 993	*w*	993	*w*	$243+751=994$ *A'*
		1005	*w*	$428+579=1007$ *A'*, ($CF_2=CCl_2$ impurity)
~1012	*w*	1008	*w*	$432+579=1011$ *A'*
1033				
1038	*m*			$CF_2=CCl_2$ impurity?
1044		1037	*w*	$201+845=1046$ *A'*
1074				
1079	*vw, sh*			$243+845=1088$ *A''*
1086				
~1096				$1333-243=1090$ *A''*
~1121	*vw*			$1333-201=1132$ *A'*, or impurity
~1145				
1152	*m, sh*	1147	*w*	$2\times579=1158$ *A'*
1160				
~1171	*w*	1166	*w*	$201+970=1171$ *A'*
1193				
1199	*vs, sh*	1195	*s*	*A'* fundamental
1206				
~1263		1265	*w*	
1271	*w, sh*	1271	*m*	$428+845=1273$ *A'*
1279				$432+845=1277$ *A'*
~1319		1320	*s*	$572+754=1326$ *A'*
1333	*vs*	1337	*s*	*A'* fundamental
1350				
1395	*s*	1397	*m*	$201+1199=1400$ *A'*; $432+970=1402$ *A'*
1406	*s*	1418	*w*	$579+845=1424$ *A'*
		1443	*w*	$243+1199=1442$ *A''*
1493	*s, sh*			
~1497		1504	*m*	$2\times751=1502$ *A'*
1506				
1538	*vw*	1543	*w*	$201+1333=1534$ *A'*
1558	*vw*?			$579+970=1549$ *A'*
1575	*vw*	1573	*w*	$243+1333=1576$ *A''*
		1600	*w*	$754+841=1595$ *A''*, $752+845=1597$ *A''*
~1621				
1637	*w, sh*	1626	*w*	$432+1199=1631$ *A'*
~1675				
1684	*s*	1673	*w*	$2\times845=1690$ *A'*
~1689				
~1706				
~1721		1710	*w*	$751+970=1721$ *A''*

Gas Wave number	Gas Description	Liquid Wave number	Liquid Description	Interpretation
~1730				
1739	*vs*			
~1748		1739	*vs*	1745 fundamental (*A'*)
1751	*vs*			
~1773		1773		$432+1333=1765$ *A'*?
1779				
1783	*m, sh*			$579+1199=1778$ *A'*
1805				
1815	*w, sh*	1804	*w*	$845+970=815$ *A'*
1818				
~1842	*vvw*	1833	*vvw*	
1869	*vvw*			
~1898				
1901	*vw, sh*	1892	*vw*	$579+1333=1912$ *A'*
~1908				
1931		1928	*w*	$2\times970=1940$ *A'*
1942				$201+1745=1946$ *A'*
1949	*w, sh*			$751+1199=1950$ *A''*
~1961				
1980	*w, sh*	1982	*w*	$243+1745=1988$ *A''*
~1992				
~2041	*vw*	2035	*vw*	$845+1199=2044$ *A'*
		2131	*vw*	
2160				
2169	*w, sh*	2157	*m*	$970+1199=2169$ *A'*
2174				$845+1333=2178$ *A'*
2227	*vw*	2255	*w*	
~2247				
~2288		2281	*w*	$970+1333=2303$ *A'*
2299				
2315	*w, sh*	2317	*w*	$579+1745=2324$ *A'*
2326				
2364	*vw*?	2342	*m*	
2389				
2395	*w, sh*	2387	*m*	$2\times1199=2398$ *A'*
2401				
~2463	*vw*	2462	*w*	$751+1745=2496$ *A''*?
~2475	*vw*			
~2519				
~2528				
2532	*w, sh*	2510	*m*	$1199+1333=2532$ *A'*
2538				
~2584				
2597	*w*	2586	*w*	$845+1745=2590$ *A'*
		2637	*w*	
2660				
2667	*w, sh*	2650	*m*	$2\times1333=2666$ *A'*
2685				
2703	*w, sh*	2702	*m*	$970+1745=2715$ *A'*
2717				
		2730	*w*	
~2770		2763	*vw*	
~2778	*vw*			
~2817	*vw*	2816	*vw*	
2874	*w*	2872	*w*	
2886	*w*			
2933	*w*			
2946	*w*	2933	*m*	$1199+1745=2944$ *A'*
2976	*vw*	2963	*w*	
3021	*vw*	2994	*w*	
		3049	*w*	
3067	*w*	3066	*m*	$1333+1745=3078$ *A'*
3077	*W*			
~3125				
3130	*s*	3125	*s*	*A'* fundamental
3268	*vw*	3265	*vw*	
3322	*vw*	3321	*vw*	$201+3130=3331$ *A'*
3333	*vw*	3335	*vw*	
~3413	*vw*	3412	*vw*	
3484	*vw*	3470	*w*	$2\times1745=3490$ *A'*
3731	*vw*			$579+3130=3709$ *A'*
~3846	*vw*			$751+3130=3781$ *A''*?
3984	*vw*			$845+3130=3975$ *A'*
4098	*vw*			$970+3130=4100$ *A'*
~4255	*vw*			
4329	*vw*			$1199+3130=4329$ *A'*
4444	*vw*			$1333+3130=4463$ *A'*
4878	*vw*			$1745+3130=4875$ *A'*

[a] Infrared spectrum of the liquid was obtained for a different sample of higher purity.

TABLE II. Raman spectrum of CF_2:CHCl (liquid).

Wave number	Relative intensity	Depolarization	Exciting Hg lines	Interpretation
201 cm^{-1}	30	0.50	$\pm e$	A' fundamental
243	6	0.86	e	A'' fundamental
428, 432	65	0.12	k, $\pm efk$	A' fundamental $\{Cl^{37}, Cl^{35}\}$
484	1	p	ek	$2\times243=486$ A'
572, 576	70	0.66	k, $\pm efi$	A'' fundamental, A' fundamental
754	8	~0.8	efk	A'' fundamental
819	2	···	e	$243+576=819$ A''
841.0	95	0.03	$\pm efikl$	A' fundamental
865	2	···	e	$2\times432=864$ A'
967	35	0.25	ek	A' fundamental
1074	*vvw*	···	e	$243+841=1084$ A''
1148	4	0.1	ek	$2\times576=1152$ A', $2\times572=1144$ A'
1198	5	0.65	e	A' fundamental
1322	2		ek	$572+754=1326$ A'
1337	3	0.65	e	A' fundamental
1500	*vw*	···	e	$2\times754=1508$ A'
1600	*vvw*	···	e	$754+841=1595$ A''
1676	2	p	e	$2\times841=1682$ A'
1704	*vw*	···	e	$754+967=1721$ A''
1742	100	0.04	eil	A' fundamental
1804	1	···	e	$841+967=1808$ A'
2931	*w*	···	ek	$1198+1742=2940$ A'
3063	*w*	···	ek	$1337+1742=3079$ A'
3127	80	0.20	$eikg$	A' fundamental

RR′C:CHR″,[8] it is undoubtedly associated with a similar C−H wagging in CF_2:CHCl and must be the highest A'' fundamental.

The assignment of the last A'' fundamental presents some difficulty. The weak Raman band at 484 cm^{-1} appears to be polarized and must undoubtedly be interpreted as the overtone of 243 cm^{-1}. The few very weak infrared bands that lie in the proper spectral region are either extremely faint or can readily be interpreted as binary combination bands. Thus, it appears that the A'' fundamental in question must overlap another fundamental. With 4047A excitation the highly polarized Raman band at 432 cm^{-1} is observed to have a much weaker companion at 428 cm^{-1}. However, this band is very sharp and undoubtedly of species A'. It is interpreted as caused by molecules containing the Cl^{37} isotope. On the other hand, the weakly polarized Raman band at 576 cm^{-1}, which is asymmetrical and abnormally wide when excited by the 4358A mercury line, appears with 4047A excitation to overlap with another band with maximum near 572 cm^{-1}. In the infrared spectrum of liquid CF_2:CHCl a slight shoulder indicates the presence of this companion. On the basis of these facts, the value 572 cm^{-1} has been tentatively assigned to the third A'' fundamental. It must involve largely CF_2 wagging. This assignment is supported by the presence of a strong band at 1321 cm^{-1} in the spectra of liquid CF_2:CHCl. The interpretation of this band as $576+754=1330A''$ is not very plausible because of its high intensity. On the other hand, its interpretation as $572+754=1326A'$, enhanced by its proximity to the A' fundamental at 1337 cm^{-1}, is entirely satisfactory.

The infrared and Raman frequencies interpreted as fundamentals are listed in Table III. They are represented graphically in Fig. 2 together with the previously assigned fundamentals for CF_2:CH_2 and CF_2:CCl_2. Infrared frequencies are indicated by solid vertical lines, Raman frequencies by broken vertical lines. When frequencies coincide, these lines are separated somewhat so as to make both visible. The height of each line roughly indicates the band intensity. Corresponding frequencies of the different compounds are joined by slanting lines, totally symmetrical fundamentals by solid and others by broken lines. The fact that no solid (broken) lines cross, and the regularity of the correlation diagram strongly support the assignments made.

On the basis of the fundamental frequencies listed

TABLE III. Fundamental vibration frequencies for CF_2:CHCl.

Symmetry species	Infrared (gas) Wave number	Description	Infrared (liquid) Wave number	Description	Raman (liquid) Wave number	Relative intensity	Depolarization
A'					201 cm^{-1}	30	0.50
A''					243	6	0.86
A'	433 cm^{-1}	*s*			432	65	0.12
A''					572		
A'	579	*s, sh*	577 cm^{-1}	*m*	576	70	0.66
A''	751	*vs, sh*	752	*s*	754	8	~0.8
A'	845	*s, sh*	840	*m*	841.0	95	0.03
A'	970	*vs, sh*	964	*s*	967	35	0.25
A'	1199	*vs, sh*	1195	*s*	1198	5	0.65
A'	1333	*vs*	1337	*s*	1337	3	0.65
A'	1745	*vs*	1739	*vs*	1742	100	0.04
A'	3130	*s*	3125	*s*	3127	80	0.20

[8] See, for example, Cross, Richards, and Wallis, Disc. Faraday Soc. 9, 235 (1950).

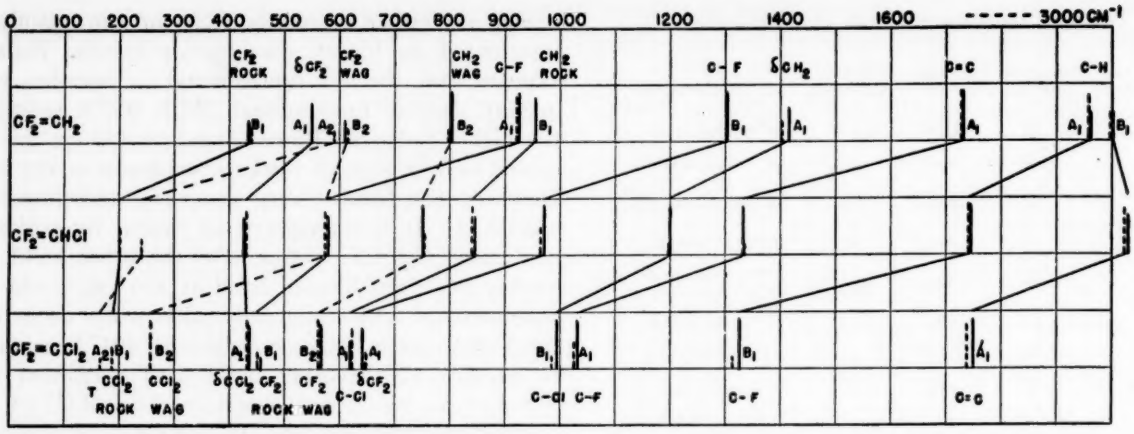

FIG. 2. Fundamental vibration frequencies for CF_2:CH_2, CF_2:CHCl, and CF_2:CCl_2.

in Table III all of the observed Raman bands and all but a few of the infrared bands have been interpreted. The interpretations are given in the last column of Tables I and II. All binary sum bands that lie in the wavelength range covered and are not masked by fundamentals have been observed in the infrared. A few bands have been interpreted as binary difference bands. The bands for which no interpretation is given are all very weak and could undoubtedly be accounted for as ternary combinations, e.g., 695 cm^{-1} could be interpreted as $201+2\times243=687A'$. However, since some of the uninterpreted bands undoubtedly are caused by impurities, it does not seem worthwhile to list such interpretations.

TABLE IV. Calculated thermodynamic functions for CF_2:CHCl at one atmosphere (in cal/deg-mole).

T		$(H^0-H_0^0)/T$	C_p^0	S^0	$-(F^0-H_0^0)/T$
253.46°K (bp)	Trans+Rot	7.949	7.949	64.640	56.691
	Vibr	3.230	7.791	4.961	1.731
	Total	11.18	15.74	69.60	58.42
298.16	Trans+Rot	7.949	7.949	65.932	57.983
	Vibr	4.027	9.259	6.346	2.319
	Total	11.98	17.21	72.28	60.30
400	Trans+Rot	7.949	7.949	68.267	60.318
	Vibr	5.744	12.134	9.491	3.747
	Total	13.69	20.08	77.76	64.07
600	Trans+Rot	7.949	7.949	71.490	63.545
	Vibr	8.558	15.896	15.190	6.632
	Total	16.51	23.85	86.68	70.18

CALCULATED THERMODYNAMIC FUNCTIONS

No electron diffraction data are available for CF_2:CHCl. However, from the work of I. L. Karle and J. Karle[9] on CF_2:CH_2 and C_2F_4, the C−C and C−F distances may be assumed to be 1.31 and 1.32A, respectively, and the FCF angle 112°. Taking $d_{CH}=1.08$A, $d_{CCl}=1.69$A, and HCCl, CCCl, and CCH angles all equal to 120°,[10] we obtain the following principal moments of inertia for the CF_2:CHCl molecule:

$$I_A=78.1,\quad I_B=353.0,\quad I_C=431.1\times10^{-40}\text{ g cm}^2.$$

The axis of smallest moment makes an angle of 32°44′ with the C=C bond. From these moments of inertia and the fundamental vibration frequencies listed in Table III the thermodynamic functions given in Table IV have been calculated. Except for the three fundamentals observed only in the Raman effect the infrared frequencies for the gaseous phase have been used. The gas was assumed to be ideal, and the harmonic oscillator approximation was made. No calorimetric data appear to be available for comparison.

ACKNOWLEDGMENT

The writers wish to acknowledge their indebtedness to General Chemical Division, Allied Chemicals and Dye Corporation, for the gift of the samples.

[9] I. L. Karle and J. Karle, J. Chem. Phys. **18**, 963 (1950).
[10] L. Pauling, *The Nature of the Chemical Bond* (Cornell University Press, Ithaca, New York, 1940).

Transition Probabilities III. Dipole Velocity Computations for C_2 and N_2^+. The Question of Degree of Hybridization*

HARRISON SHULL
Department of Chemistry and Institute for Atomic Research, Iowa State College, Ames, Iowa
(Received September 6, 1951)

Previous computations of transition probabilities for hydrogen using the dipole velocity operator are here extended to the diatomic molecules C_2 and N_2^+ with particular reference to the former. Whereas previous calculations have shown the dipole length method to be relatively insensitive to the effective nuclear charge, the present computations show great sensitivity of the dipole velocity method to the ratio of the effective Z of the bonding orbital to that of the antibonding orbital. The results are less sensitive to the absolute magnitude of the Z's. The results are discussed with respect to reasonable assignments for the degree of s and $p\sigma$-hybridization of the respective orbitals and with respect to reasonable choices for the effective Z values. It is concluded that the degree of hybridization is most probably considerably higher than previously estimated. The dipole velocity method is a promising one for further development.

I. INTRODUCTION

RECENTLY the author of this paper has explored the possibility of using the dipole velocity form of the transition moment operator for dipole radiation for the computation of transition probabilities in the hydrogen molecule.[1] These computations paralleled the calculations on hydrogen of Mulliken and Rieke[2] who used the dipole length form of the operator. In that case very good agreement was found between the two methods both with LCAO molecular orbital (MO) and atomic orbital (AO) approximations. Agreement was moderately good with experiment, being somewhat better using the MO approximation. The present calculations extend in a similar manner the dipole length calculations made by the author on C_2 and N_2^+.[3] In addition to the problem of effective nuclear charge which was encountered in the hydrogen problem, the computations for C_2 and N_2^+ involve the question of the degree of hybridization of the orbitals involved in the transition. Both these points are considered in some detail in this paper.

II. THE METHOD OF COMPUTATION

This paper compares two formally equivalent methods for the calculation of transition probabilities. If one were to use exact wave functions, the two methods would yield identical results. On the other hand, since only very approximate wave functions are used, it is not to be expected *a priori* that the dipole velocity and dipole length computations agree. The formulas summarized by Mulliken and Rieke[2] for the dipole length method lead to

$$f=1.085\times10^{11}\nu G\sum_i \mathbf{Q}_i^2, \tag{1}$$

with ν in cm^{-1} and $\mathbf{Q}_i=\mathbf{Q}_x$, $\mathbf{Q}_y$, or $\mathbf{Q}_z$ in cm. G is an integer which must be introduced to take care of the cases in which transitions may take place to more than one equivalent final level from a given initial state. In the calculations carried through here G is always unity, and the z component of Q is the only nonzero one.

$$\mathbf{Q}_z=\int\psi_a(\textstyle\sum_j \mathbf{z}_j)\psi_b d\tau. \tag{2}$$

Here a refers to the lower and b the upper state. The summation is over the z coordinates of each electron j. In order to obtain the dipole velocity form of the equation, one substitutes for Q_z the equivalent expression

$$\mathbf{Q}_{vz}=(h/4\pi^2 m\nu c)\int\psi_a\left(\sum_i\frac{\partial}{\partial z_i}\right)\psi_b d\tau. \tag{3}$$

If one performs this substitution, changing the Q's to atomic units and canceling one of the ν's which arise from Q_{vz}^2 with the one in Eq. (1), one arrives at the convenient dipole velocity Eq. (4)

$$f=1.463\times10^5 G\mathbf{Q}_v^2/\nu, \tag{4}$$

in which

$$\mathbf{Q}_v=\int\psi_a\left(\sum_i\frac{\partial}{\partial z_i}\right)\psi_b d\tau.$$

The transitions under consideration here are the Swan band system of C_2, $^3\Pi_g-{}^3\Pi_u$, the Deslandres-D'Azambuja system of C_2, $^1\Pi_g-{}^1\Pi_u$, and the first negative band system of N_2^+, $^2\Sigma_u^+-{}^2\Sigma_g^+$. For C_2 we may write the electron configurations

$$C_2:\quad (K)(K)(z\sigma_g)^2(y\sigma_u)^2(w\pi_u)^3(x\sigma_g),\quad {}^{3,1}\Pi_u$$

for the ground state, and

$$C_2:\quad (K)(K)(z\sigma_g)^2(y\sigma_u)(w\pi_u)^3(x\sigma_g)^2,\quad {}^{3,1}\Pi_g$$

for the appropriate excited state. Similar configurations may be written for N_2^+, yielding, respectively, $^2\Sigma_g^+$

* Contribution number 191 from the Institute for Atomic Research and Department of Chemistry, Iowa State College. This work was supported in part by the Ames Laboratory of the AEC. This paper was presented before the XIII International Congress of Chemistry, New York City, September 10–13, 1951.

[1] H. Shull, J. Chem. Phys. **20**, 18 (1952).

[2] R. S. Mulliken and C. A. Rieke, Repts. Progress Phys. **8**, 231 (1941).

[3] H. Shull, Astrophys. J. **112**, 352 (1950). This is paper I of the current series.

and $^2\Sigma_u^+$ states, the only difference being the presence of four instead of three electrons in the $w\pi_u$ orbitals. Similar transitions are well known in CN, CO^+, BO and between two excited states in N_2. Because of the presence of an additional variable, the polarity, in the first three of these cases and the doubtful utility of such calculations for transitions not involving the ground state (in the last case), the calculations have not been extended to include these molecules.

We assume that the orbitals not directly involved in the transition are unaffected by the resulting change in electron distribution. This is most certainly not completely valid since one can expect a fair amount of reorganization of the remaining electrons as a result of the changing field involved in the transition of one electron from the lower to a higher orbital. This assumption, however, probably introduces smaller errors than the actual use of the LCAO MO method itself. The transition then involves that electron in a $y\sigma_u$ orbital whose spin is the same as that of the empty position in the $x\sigma_g$ orbital. Furthermore, the electron in the $y\sigma_u$ orbital moves in the same field (neglecting reorganization, that of $(y\sigma_u)(x\sigma_g)$) before the transition as the electron in the $x\sigma_g$ orbital after the transition. It thus seems reasonable to consider just a one-electron problem.

As in the previous work on C_2 and N_2^+, the molecular orbitals are taken as linear combinations of atomic orbitals on each carbon (nitrogen) atom, namely,

$$\psi\sigma_g=[(-\beta_1 2s_a+\alpha_1 2p\sigma_a)+(-\beta_1 2s_b+\alpha_1 2p\sigma_b)]/[2(1-S_g)]^{\frac{1}{2}}, \quad (5)$$

$$\psi\sigma_u=[(\alpha_2 2s_a-\beta_2 2p\sigma_a)-(\alpha_2 2s_b-\beta_2 2p\sigma_b)]/[2(1-S_u)]^{\frac{1}{2}}. \quad (6)$$

The α's and β's (taken to be positive) are chosen to satisfy the normalization conditions: $\alpha_1^2+\beta_1^2=1$ and $\alpha_2^2+\beta_2^2=1$. For the reasons discussed in the previous work the ranges of the coefficients used in these computations were

$$0\leq\beta_1^2\leq 0.5 \quad 1.0\geq\alpha_1^2\geq 0.5 \quad 0\leq\beta_2^2\leq 0.5 \quad 1.0\geq\alpha_2^2\geq 0.5.$$

The terms S_g and S_u are normalization factors arising from the nonorthogonality of the AO's on atoms a and b.

$$S_g=\alpha_1^2\int 2p\sigma_a 2p\sigma_b d\tau+\beta_1^2\int 2s_a 2s_b d\tau-2\alpha_1\beta_1\int 2s_a 2p\sigma_b d\tau,$$

$$S_u=\alpha_2^2\int 2s_a 2s_b d\tau+\beta_2^2\int 2p\sigma_a 2p\sigma_b d\tau-2\alpha_2\beta_2\int 2s_a 2p\sigma_b d\tau.$$

In all the above formulas and elsewhere in this paper, by $2s$ is meant a normalized atomic $2s$ wave function. Similar meaning applies to other symbols of this kind. The $2p\sigma$ AO's on each atom are taken with the positive lobe pointing towards the other atom.

The substitution of these wave functions into the formula for Q_v is carried forward in straightforward manner. There result a series of integrals of general form similar to

$$\int 2s_a\frac{\partial}{\partial z}2p\sigma_a d\tau,$$

with appropriate choice of the AO's. These are readily evaluated in closed form if one uses Slater AO's. It was found convenient to perform the indicated differentiation in Cartesian coordinates and the integration in prolate spheroidal coordinates in which the variables separate. The resulting integrals have exactly the same form as the well-known overlap integrals and indeed may be expressed as linear combinations of such overlap integrals in all cases if one includes overlap with "$1p$" orbitals (i.e., the usual p angular factor, but r dependence only in the exponential). It was found easier, however, to evaluate the integrals directly from A and B integrals[4] computed for the desired parameter by well-known recursion formulas. Appendix I lists detailed formulas for integrals necessary for the present computations, and Appendix II summarizes in tabular form the values of these integrals for the parameters of interest for C_2 and N_2^+.

In addition to the use of Slater AO's, the computations were carried through for one case using Slater $2p$ AO's together with orthogonalized Slater $2s$ AO's (see reference 4), and for one case using self-consistent-field functions as tabulated by Jucys[5] and fitted by analytic functions of the Slater form. The normalized

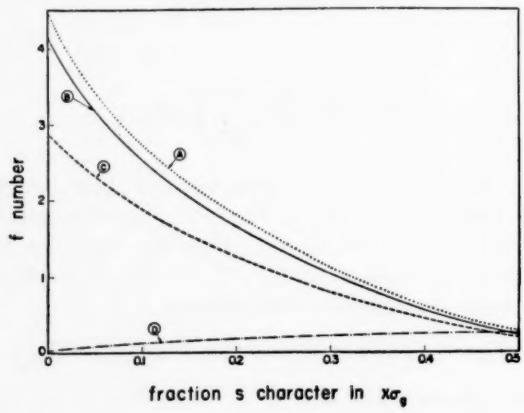

FIG. 1. f numbers as a function of hybridization. The curves are for equal hybridization of $x\sigma_g$ and $y\sigma_u$ orbitals. All curves use Slater AO's. Curve A: N_2^+, dipole velocity, $Z=Z'=3.90$. Curve B: C_2, dipole velocity, $Z=Z'=3.25$. Curve C: C_2, dipole velocity, $Z=Z'=2.60$. Curve D: C_2, dipole length, $Z=Z'=3.25$.

[4] Mulliken, Rieke, Orloff, and Orloff; J. Chem. Phys. **17**, 1248 (1949).

[5] A. Jucys, Proc. Roy. Soc. (London) **A173**, 59 (1939).

functions used were

$$\psi_{2s}{}^{SCF}=-0.2260\chi_{1s}(5.7)+1.0252\chi_{2s}(1.625),$$
$$\psi_{2p\sigma}{}^{SCF}=0.5142\chi_{2p\sigma}(2.00)+0.5560\chi_{2p\sigma}(1.00),$$

in which by $\chi_{1s}(5.7)$ is meant a normalized Slater $1s$ AO with $\mu=Z_{\text{eff}}/n$ of 5.7 and similarly for the remaining symbols. Z_{eff} is the effective nuclear charge and n is the effective principal quantum number.

III. DISCUSSION OF RESULTS

In considering the results of these computations, the writer adopts the philosophy that agreement within a factor of two or three is good agreement. This philosophy is supported on the one hand by the great difficulty of experimental determinations of transition probabilities in systems of this kind (seldom reliable to better than a factor of two) and on the other hand by the very rough approximate methods used in these computations. In this connection, for example, Mulliken[2] found an empirical factor of three necessary to obtain agreement between experimental and calculated values of transition probabilities.

As in the dipole length calculations[3] the results for N_2^+ parallel those for C_2 so closely that the calculations for the former were carried out in detail in two cases only. Figure 1 shows the f numbers for the dipole velocity operator as a function of hybridization for N_2^+ using $Z=Z'=3.90$ (A) and for C_2 with $Z=Z'=3.25$ (B) and also $Z=Z'=2.60$ (C).

Also plotted is the dipole length result for C_2 for $Z=Z'=3.25$ (D) taken from reference 3. The points graphed in Fig. 1 refer to equal hybridization in the $x\sigma_g$ and $y\sigma_u$ orbitals; i.e., there is as much s character in $x\sigma_g$ as there is p character in $y\sigma_u$. The square of the coefficient is used for the abscissa. The fact that N_2^+ gives results closely similar to those for C_2 is itself promising, for in the previous dipole length calculations it was found that the higher frequency of the transition in the former case just compensated for the lower dipole strength of the transition. In the present calculations, however, because of the cancellation of energies made earlier, the frequency occurs in the denominator. That the resulting f numbers agree with each other is some indication that this cancellation is not unwarranted.

The second feature to notice in Fig. 1 is that the f number for the dipole velocity method is somewhat, but not strongly (the variation is less than 50 percent at all hybridizations), affected by simultaneous variation in the Z value of both the excited and ground-state orbitals. This was also found to be true for dipole length calculations. Finally, one notices as very striking features the completely different dependence upon hybridization shown by the two alternative methods and the entirely unreasonable f numbers resulting from the dipole velocity computations except for very large amounts of hybridization. For the case of like Z the

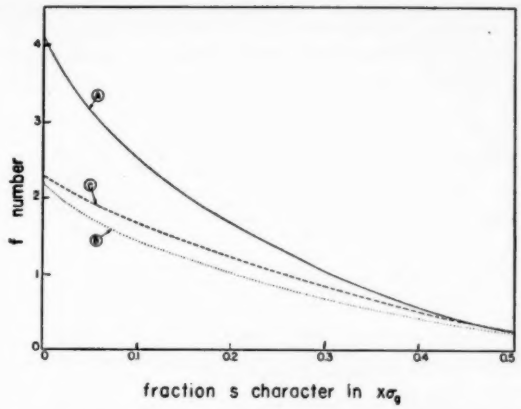

FIG. 2. Dipole velocity f numbers for C_2 as a function of hybridization and form of AO's used. Curve A: Slater AO's with $Z=Z'=3.25$. Curve B, orthogonalized Slater $2s$ with Slater $2p\sigma$. $Z_{1s}=5.7$, $Z_{2s}=Z_{2p\sigma}=3.25$. Curve C, SCF, $2s$ and $2p\sigma$-functions using two-term analytic fits (see text). All curves have equal hybridization in the $x\sigma_g$ and $y\sigma_u$ orbitals.

dipole length and dipole velocity calculations agree only at the very highest hybridizations, closely approaching digonal', $(2s-2p\sigma)/2^{\frac{1}{2}}$. (The notation digonal' follows Mulliken[6] and refers to opposite signs for the $2s$ and $2p\sigma$ AO.) Large amounts of hybridization might be expected in these orbitals in view of the relatively small changes in internuclear distance observed in the ionization of the $y\sigma_u$ (slightly antibonding) and $x\sigma_g$ (slightly bonding) orbitals in going from N_2 to N_2^+, but on the other hand, it would be surprising to find hybridization close to digonal' in view of the large promotional energy this would require.

The effect of variation of the basic AO form for the dipole velocity operator is graphed in Fig. 2. In this case the use of the usual Slater AO with $Z=3.25$ (A) is compared with the use of the orthogonalized Slater $2s$ AO ($Z_{1s}=5.7$; $Z_{2s}=3.25$) together with the usual Slater $2p\sigma$ AO (B) and also compared with the use of SCF AO (C) computed through the use of the analytic functions mentioned above. The change in AO has a moderate effect upon the f number but relatively little in the region of high hybridization—the only region in which the f numbers are not grossly high. The effect introduced by using the orthogonalized Slater $2s$ orbital is partially compensated in going over to the SCF $2p\sigma$-function by the relative diffuseness of the latter as compared to the Slater $2p\sigma$. The drop in f number in introducing the orthogonalized Slater $2s$ function indicates the greater sensitivity of the dipole velocity form to portions of the wave function near the respective atom centers. Such a change has very little effect upon either dipole length calculations of f numbers or upon calculation of overlap integrals at ordinary internuclear distances.

In Fig. 3 are presented curves for four dipole velocity computations using different Z values for the $y\sigma_u$ and

[6] R. S. Mulliken, J. Chem. Phys. **19**, 900 (1951).

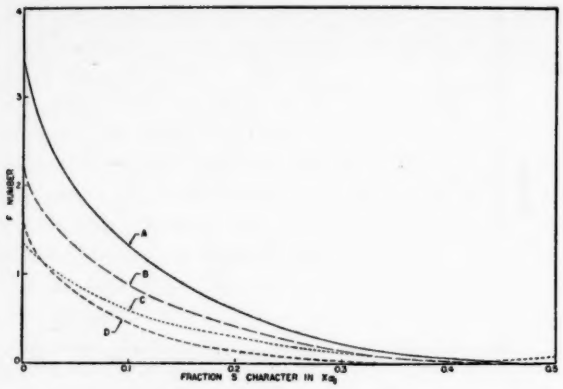

FIG. 3. Dipole velocity f numbers for C_2 as a function of hybridization and effective Z values with equal hybridization in the $x\sigma_g$ and $y\sigma_u$ orbitals. Curve A: $Zx\sigma_g=3.90$, $Zy\sigma_u=3.25$. Curve B: $Zx\sigma_g=3.25$, $Zy\sigma_u=2.60$. Curve C: $Zx\sigma_g=2.60$, $Zy\sigma_u=2.08$. Curve D: $Zx\sigma_g=3.90$, $Zy\sigma_u=2.60$.

$x\sigma_g$ MO but equal hybridization in these two MO. From the curves one can see that alteration of the relative Z values of the two orbitals has a marked effect upon the computed f number as a function of hybridization. In particular, it is to be noted that the three cases involving the pairs 3.90, 3.25 (A); (the first number referring to $Zx\sigma_g$, the second to $Zy\sigma_u$); 3.25, 2.60 (B); and 2.60, 2.08 (C) give closely agreeing results for higher hybridizations and somewhat different (but absurdly high) values for low hybridizations. In each of these three cases, the ratio of Z bonding to Z antibonding is 1.25 to 1.2. In the variation treatment of hydrogen with similar kinds of approximate wave functions, the ratio of the best possible Z for the bonding MO to the Slater Z is found to be 1.198.[7] Increase of the ratio in the case of C_2 to 1.5 for the pair 3.90, 2.60 (D) once again causes a marked effect on the computed f number. In this case the f number falls very quickly with increasing hybridization, actually going to zero at about 40 percent p character in $y\sigma_u$ (and 40 percent s character in $x\sigma_g$) and then rising quite appreciably by the time the digonal' form is reached.

Figure 4 indicates the effect of variation of relative amounts of hybridization in the $x\sigma_g$ and $y\sigma_u$ orbitals. The three curves shown correspond, A, to 10 percent more p character in $y\sigma_u$ than s character in $x\sigma_g$; B, to equal hybridizations in the two; and C, to 10 percent more s character in $x\sigma_g$ than p character in $y\sigma_u$ for the dipole velocity operator. $Zx\sigma_g$ is 3.90, while $Zy\sigma_u$ is taken as 2.60. It is evident that the computed f numbers are relatively insensitive to the amounts of hybridization in one orbital as compared to the amounts in the other provided, at least, that they are approximately equal. (That is to say, a change in 10 percent relative hybridization changes the f number by not more than a factor of two or three—at least in the range where the computed f numbers are not absurdly high.) This was also found to be true in the previous calculations by the dipole length method.

Within the framework of the assumptions involved in the LCAO MO method itself and in the approximate AO used, a knowledge of the correct Z values taken with the expected equality of the dipole length and dipole velocity computations will lead to a knowledge of approximate hybridizations in the orbitals concerned. Table I lists the pertinent f numbers and hybridizations for those intersections obtained from the computed functions. It was pointed out in paper I of this series[3] that Professor Mulliken had estimated a reasonable hybridization for these orbitals in N_2 as 17 percent p character in $y\sigma_u$ with 8 percent s character in $x\sigma_g$. These values were obtained by minimizing the energy in a semiempirical manner. The "best" f number for the Swan band system (triplet system) in C_2 was at that time suggested as 0.13 with a probable error of perhaps 25 percent.

Since the f numbers reported in Table I are relatively insensitive to the absolute magnitude of Z, we need not concern ourselves too closely with the problem of the best choice of Z for molecular problems. It seems likely, however, that the Slater Z values are themselves reasonably good values to use and, if anything, may be too low. (See, however, Mueller and Eyring[8] for another viewpoint.) Furthermore, it would seem unlikely that such slightly bonding and antibonding oribtals as are involved here, judging from the previously mentioned small changes in internuclear distance upon the ionization of N_2 (N_2, 1.096 A goes to N_2^+, 1.117 A upon ionization of an $x\sigma_g$ electron; to N_2^+, 1.07 A upon ionization of a $y\sigma_u$ electron), would approach the united atom approximation for the bonding orbital any closer than is reflected in the ratio of Z bonding to Z antibonding of 1.5. If anything, it seems reasonable that this is an upper limit to the expected variation of Z in

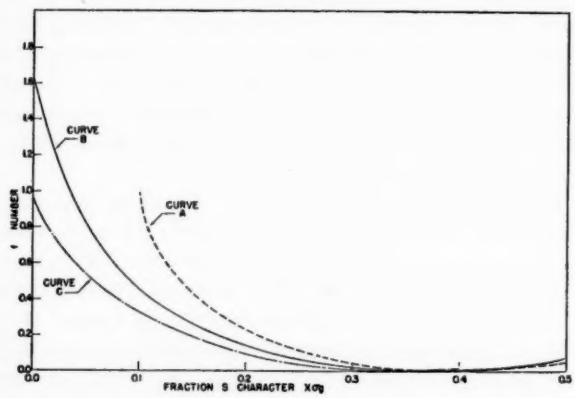

FIG. 4. Dipole velocity f numbers for C_2 as a function of relative hybridization. $Zx\sigma_g=3.90$; $Zy\sigma_u=2.60$. Curve A: 10 percent more $2p\sigma$ in $y\sigma_u$ than $2s$ in $x\sigma_g$. Curve B: Equal hybridization. Curve C: 10 percent more $2s$ in $x\sigma_g$ than $2p\sigma$ in $y\sigma_u$.

[7] C. A. Coulson, Trans. Faraday Soc. **33**, 1484 (1937).

[8] C. R. Mueller and H. Eyring, J. Chem. Phys. **19**, 193 (1951).

this polyelectron molecule as compared to the two-electron case in hydrogen.

We conclude from this discussion that the respective intersections of dipole velocity and dipole length curves for the pairs 3.90, 3.25 and 3.90, 2.60 represent probable limits upon the situation actually obtaining. Thus, it seems probable from the present analysis that hybridization in both orbitals is considerably higher than previously estimated. Something on the order of 25 percent hybridization is more likely to be correct. The corresponding new "best" f number can be taken to be 0.18 with about the same uncertainty as given for the previous value. The intersection criterion, it may be noted, makes the f number almost independent of relative hybridization of the two orbitals, far less dependent than either of the methods alone.

In connection with the estimate of 25 percent hybridization arrived at in the above analysis, it is interesting to note that Professor Mulliken has very recently improved his "magic formula" for empirical calculations of molecular energies.[6] In a note added in proof at the end of this paper he reports a total of 22 percent hybridization for the bonding σ-orbitals. It is very encouraging that these figures from such dissimilar methods should agree so closely.

The dipole velocity method for computing transition probabilities thus appears to be a very promising tool of theoretical investigation, not only for confirmation of semiempirical transition probability computations by the dipole length method, but also for evaluation of approximate wave function forms. Indeed, it may well be that the latter use will outweigh the former in importance, for the computed f values from the examples considered thus far, namely, hydrogen and C_2 and related molecules, are more sensitive by far to the wave function forms than is the energy criterion of the usual variation method. Further work along this line is in progress. Of course, one disadvantage of the criterion is that it depends both upon a ground state and an excited state wave function and seems to be more sensitive to the differences between these than to either alone.

The computations in this paper have been, with two exceptions, for the $^3\Pi_u - {}^3\Pi_g$ system of C_2 (Swan bands). The computed results may be carried over directly to the corresponding singlet system of C_2 by multiplying the dipole length f numbers and dividing the dipole velocity f numbers by 1.34, the ratio of the frequencies of the two transitions. The internuclear distances are close enough in the two cases that an inappreciable error is introduced in this transfer. It should be noted that if one uses the criterion of intersection for the choice of the "best" f number, then the different functional dependence of the two methods on the frequency makes the f number and hybridization a more complicated function of this frequency factor. Thus, the equal hybridization curves of the singlet system for (3.90; 3.25) intersect at an f number of 0.26 and 26 percent hybridization. Those for (3.90; 2.60) intersect at 15 percent hybridization and 0.20 f number. One might therefore choose 0.23 as a best f number for the singlet system. The average of these hybridizations ($\sim$20 percent) is seen to be somewhat lower in the singlet than in the triplet system. This is an effect that should be studied in more detail.

Because of the close similarity of the results for the triplet system of C_2 and the 1st negative system of N_2^+, the results reported here for the Swan bands of C_2 are approximately correct for N_2^+, certainly within the likely experimental error were one to attempt the measurement directly. All calculations, of course, refer to vertical excitation, i.e., to the excited state in a high vibrational level in which the internuclear distance is the same as in the ground state.

TABLE I. Data for intersections of dipole length and dipole velocity computed curves for C_2 (triplet system).

Relative hybridization[a]	Z_{σ_g}	Z_{σ_u}	f	% s in $x\sigma_g$	Average f	Average s in $x\sigma_g$	Average p in $y\sigma_u$
A	3.90	2.60	0.15	16	0.18	21	31
A	3.90	3.25	0.20	26			
B	3.90	2.60	0.16	20	0.18	25	25
B	3.90	3.25	0.20	30			
C	3.90	2.60	0.16	23	0.18	29	19
C	3.90	3.25	0.20	34			
A	3.25	2.60	0.23	24			
B	3.25	2.60	0.23	27			
C	3.25	2.60	0.23	29			
B	3.25	3.25	0.27	48			

[a] *A* refers to 10 percent more p character in $y\sigma_u$ than s character in $x\sigma_g$; *B* refers to equal hybridization in the two MO; *C* refers to 10 percent more s in $x\sigma_g$ than p in $y\sigma_u$.

APPENDIX I. FORMULAS FOR DIPOLE VELOCITY INTEGRALS

(For other formulas see paper II of this series (reference 1).)†

For orbitals with equal μ:

$$\int 2s_a\frac{\partial}{\partial z}2s_a d\tau=0$$

$$\int 2p\sigma_a\frac{\partial}{\partial z}2p\sigma_a d\tau=0$$

$$\int 2s_a\frac{\partial}{\partial z}2p\sigma_a d\tau=\mu/2\sqrt{3}$$

$$\int 2s_a\frac{\partial}{\partial z}2s_b d\tau=\mu e^{-\mu R}[(\mu R)^3+(\mu R)^2+5(\mu R)+5]/45$$

$$\int 2s_a\frac{\partial}{\partial z}2p\sigma_b d\tau=\mu e^{-\mu R}[2(\mu R)^4-(\mu R)^3-6(\mu R)^2-15(\mu R)-15]/30\sqrt{3}$$

$$\int 2p\sigma_a\frac{\partial}{\partial z}2p\sigma_b d\tau=\mu e^{-\mu R}[(\mu R)^4-2(\mu R)^3-9(\mu R)^2-9(\mu R)]/15.$$

For orbitals with different μ (μ *and* μ'):

$$\int 1s_a\frac{\partial}{\partial z}2s_a' d\tau=0$$

$$\int 2s_b'\frac{\partial}{\partial z}1s_a d\tau=(\mu\mu')^{5/2}R^4[2A_1B_1+2A_2B_2-A_2B_0-A_0B_2-A_3B_1-A_1B_3]/8\sqrt{3}$$

$$\int 2s_a\frac{\partial}{\partial z}2s_a' d\tau=0$$

$$\int 2s_a\frac{\partial}{\partial z}2s_b' d\tau=(\mu\mu')^{5/2}R^4\{[A_3B_1+A_1B_3-A_2B_0-A_0B_2+2A_2B_2-2A_1B_1]$$
$$+R\mu'[A_1B_4-A_4B_1+A_3B_0-A_0B_3+A_2B_1-A_1B_2+A_2B_3-A_3B_2]/2\}/24.$$

$$\int 2s_a\frac{\partial}{\partial z}2p\sigma_a' d\tau=8(\mu\mu')^{5/2}(3\mu-\mu')/(\mu+\mu')5\sqrt{3}$$

$$\int 2s_a\frac{\partial}{\partial z}2p\sigma_b' d\tau=(\mu\mu')^{5/2}R^4\{[A_0B_3-A_3B_0+A_1B_2-A_2B_1]$$
$$+R\mu'[A_2B_0+A_0B_2+2A_1B_1-4A_2B_2+2A_3B_3-2A_3B_1-2A_1B_3+A_4B_2+A_2B_4]/2\}/8\sqrt{3}.$$

$$\int 2p\sigma_a\frac{\partial}{\partial z}2p\sigma_a' d\tau=0$$

$$\int 2p\sigma_a\frac{\partial}{\partial z}2p\sigma_b' d\tau=(\mu'\mu)^{5/2}R^4\{[A_0B_2-A_2B_0+A_1B_3-A_3B_1]$$
$$+R\mu'[A_1B_0+A_0B_1+A_4B_3+A_3B_4-A_2B_1-A_1B_2-A_3B_2-A_2B_3]/2\}/8.$$

† Notes to Appendixes I and II.

R = internuclear distance in atomic units
$\mu = Z/n$
Z = effective nuclear charge
n = principal quantum number

$$A_m(\gamma)=\int_1^\infty \xi^m e^{-\gamma\xi}d\xi$$

$$B_m(\lambda)=\int_{-1}^{+1}\nu^m e^{-\lambda\nu}d\nu$$

The argument γ of the A integrals is $R(\mu+\mu')/2$.
The argument λ of the B integrals is $R(\mu-\mu')/2$.

Related integrals may be easily derived by interchanging the subscripts a and b (referring to the two nuclei), resulting in a change in sign of the dipole velocity integrals and no change in sign for the overlap integrals. Interchanging the orbitals in the dipole velocity integrals likewise changes the sign since these are not Hermitian as written here. In using the general formulas for integrals transformed in this manner, it should be remembered that $B_{2m}(\lambda)=B_{2m}(-\lambda)$, but $B_{2m+1}(\lambda)=-B_{2m+1}(-\lambda)$.

APPENDIX II. NUMERICAL VALUES OF INTEGRALS‡

μ	1.95	1.56	2.00	1.625	1.95	1.625
μ'	1.95	1.56	2.00	2.00	1.625	1.625
R	2.11	2.11	2.48	2.48	2.48	2.48
$\int 2s_a \frac{\partial}{\partial z} 2p\sigma_a' d\tau$	+0.5629	+0.4503	···	+0.4040	+0.5973	+0.4691
$\int 2s_a' \frac{\partial}{\partial z} 2p\sigma_a d\tau$	+0.5629	+0.4503	···	···	+0.4135	+0.4691
$\int 2s_a \frac{\partial}{\partial z} 2s_b' d\tau$	+0.0793	+0.0876	···	···	+0.2738	+0.0685
$\int 2s_a \frac{\partial}{\partial z} 2p\sigma_b' d\tau$	+0.1995	+0.0779	···	+0.1642	+0.2207	+0.1609
$\int 2s_a' \frac{\partial}{\partial z} 2p\sigma_b d\tau$	+0.1995	+0.0779	···	···	+0.1648	+0.1609
$\int 2p\sigma_a \frac{\partial}{\partial z} 2p\sigma_b' d\tau$	−0.0890	−0.3134	+0.0895	···	−0.0011	−0.0947
$\int 2s_a 2s_b' d\tau$	+0.4366	+0.5831	···	···	···	+0.4506
$\int 2s_a 2p\sigma_b' d\tau$	+0.4325	+0.4984	···	+0.3405	···	+0.4409
$\int 2p\sigma_a 2p\sigma_b' d\tau$	+0.3250	+0.2278	+0.3206	···	···	+0.3207

μ	1.95	2.00	1.625	1.625	1.30	1.30	1.00
μ'	1.30	1.00	1.30	1.00	1.30	1.04	1.00
R	2.48	2.48	2.48	2.48	2.48	2.48	2.48
$\int 2s_a \frac{\partial}{\partial z} 2p\sigma_a' d\tau$	+0.5930	···	+0.5002	+0.4834	+0.3753	+0.4002	···
$\int 2s_a' \frac{\partial}{\partial z} 2p\sigma_a d\tau$	+0.2542	···	+0.3183	···	+0.3753	+0.2546	···
$\int 2s_a' \frac{\partial}{\partial z} 2s_b' d\tau$	+0.2461	···	+0.2535	···	+0.0748	+0.2071	···
$\int 2s_a \frac{\partial}{\partial z} 2p\sigma_b' d\tau$	+0.1876	···	+0.1314	+0.0727	+0.0563	+0.0190	···
$\int 2s_a' \frac{\partial}{\partial z} 2p\sigma_b d\tau$	+0.0851	···	+0.0791	···	+0.0563	−0.0064	···
$\int 2p\sigma_a \frac{\partial}{\partial z} 2p\sigma_b' d\tau$	−0.1058	−0.1637	−0.1906	···	−0.2818	−0.3341	−0.3923

‡ See preceding page for Notes to Appendixes.

$\int 2s_a 2s_b' d\tau$	...	...	...	...	+0.5960	...	...
$\int 2s_a 2p\sigma_b' d\tau$	...	...	...	+0.6021	+0.5017	...	...
$\int 2p\sigma_a 2p\sigma_b' d\tau$	...	+0.1789	...	...	+0.2132	...	−0.0122
μ		5.70		5.70	5.70		5.70
μ'		5.70		2.00	1.625		1.00
R		2.48		2.48	2.48		2.48
$\int 1s_a \frac{\partial}{\partial z} 2p\sigma_a' d\tau$		...		+0.9986	+0.7256		+0.3080
$\int 1s_a \frac{\partial}{\partial z} 2s_b' d\tau$		...		...	+0.0598		...
$\int 1s_a \frac{\partial}{\partial z} 2p\sigma_b' d\tau$		...		+0.0901	+0.0998		+0.0657
$\int 1s_a \frac{\partial}{\partial z} 1s_b' d\tau$		+0.0003		...	...		...
$\int 1s_a 1s_b' d\tau$		+0.00006		...	...		...
$\int 1s_a 2s_a' d\tau$		...		...	+0.2205		...
$\int 1s_a 2s_b' d\tau$		...		...	+0.0511		...
$\int 1s_a 2p\sigma_b' d\tau$		...		+0.0597	+0.0865		+0.1175

High Concentration Limit of Unimolecular Reaction Kinetics*

HAROLD S. JOHNSTON
Department of Chemistry, Stanford University, Stanford, California
(Received July 6, 1950)

A general sum-over-states form of the Lindemann theory of unimolecular reactions is analyzed with respect to properties in the high concentration region, and results are compared with similar deductions found in the low concentration region. In a general form the theory can set a limit on the low concentration rate constant from data taken in the high concentration region alone, and it can set a limit on the high concentration rate constant from data taken in the low concentration region alone. If there are data at both the low and high concentration regions, one can compute two dimensionless parameters which are useful in interpreting kinetic data. In particular, these parameters may be used to select the number of oscillators and their frequency in the Rice-Ramsperger-Kassel form of the theory. These methods are applied to nitrogen pentoxide and nitrous oxide.

ASSUMED COLLISIONAL MECHANISM

A GENERAL form of the Lindemann[1] mechanism for unimolecular reactions is

$$\begin{aligned} A_j+M_k &\xrightarrow{a_{jkil}} A_i^*+M_l \\ A_i^*+M_l &\xrightarrow{b_{iljk}} A_j+M_k \\ A_i^* &\xrightarrow{c_i} \text{products}. \end{aligned} \tag{1}$$

The over-all reaction is $A\rightarrow$products; M is an inert gas present in great excess, or the pure reactant A for the initial reaction. The subscript j represents completely a quantum state of A and goes from ground energy to infinity; the subscript k or l represents completely a quantum state of M and goes from ground energy to infinity; and the subscript i represents the states of A from the critical energy[2] to infinity. Above the critical energy the subscripts j and i represent the same thing, and at present the case $j=i$ is not excluded, that is, a collision of an activated molecule with no change of quantum states. The first step of the mechanism represents the completely general case of a collision between A and M such that A is left in the quantum state i; the subscript l allows for the degeneracy of M. The second step is the exact reverse of the first step; microscopic reversibility guarantees that if the first step includes all such processes and if the second step includes the reverse of each, no detailed processes are omitted. In the third step the rate constants c_i have been implicitly summed over all allowed states of the products. Since the sum of a set of constants is a constant, one may abbreviate $\sum_l a_{jkil}=a_{jki}$ and $\sum_j\sum_k b_{iljk}=b_{il}$. The asterisk represents activated molecules, that is, reactant molecules with energy above the critical energy.

According to this general mechanism the rate of formation of excited molecules in a specified state i is

$$\frac{d[A_i^*]}{dt}=\sum_j\sum_k a_{jki}[A_j][M_k] - \sum_l b_{il}[A_i^*][M_l]-c_i[A_i^*]. \tag{2}$$

Brackets refer to concentration. This relation can be expressed in terms of observable macroscopic concentrations, $[A]$ and $[M]$, by use of the following definitions of probability:

$$\begin{aligned} P_j^A&=[A_j]/[A], \\ P_l^M&=[M_l]/[M], \end{aligned} \tag{3}$$

and the general definition of an average when one has a normalized probability function, P_r and a variable X_r

$$\langle X\rangle_{Av}=\sum_r X_r P_r. \tag{4}$$

Combining Eqs. (2), (3), and (4), one gets

$$\begin{aligned} \frac{[dA_i^*]}{dt}&=[A][M]\sum_j\sum_k a_{jki}P_j^A P_k^M - [M][A_i^*]\sum_l b_{il}P_l^M-c_i[A_i^*] \\ &=[A][M]\langle a_i\rangle_{Av}^{A \text{ and } M} - [A_i^*][M]\langle b_i\rangle_{Av}^M-c_i[A_i^*]. \end{aligned} \tag{5}$$

Now there is added an assumption which is equivalent to assuming that a bimolecular second-order rate constant is a constant. It is assumed that (for purposes of analyzing kinetic data) the averages of a_i and b_i are constant. This assumption is not as severe as assuming the probability functions to be constant. It is certain that the i portion of the j distribution is a function of $[M]$, but it is assumed that this does not upset much the constancy of the bimolecular rate constants of activation and deactivation to the state i. With this assumption one uses the following abbreviations: $\langle a_i\rangle_{Av}^{A \text{ and } M}=a_i$ and $\langle b_i\rangle_{Av}^M=b_i$. Now the steady state assumption is made for activated molecules, that is, Eq. (5) is set equal to zero. With these assumptions the

* This study was supported in part by the ONR Contract N6 onr 25131, Project NR 058 246.
[1] F. A. Lindemann, Trans. Faraday Soc. **17**, 598 (1922).
[2] L. S. Kassel, *Kinetics of Homogeneous Gas Reactions* (Chemical Catalog Company, Inc., New York, 1932), p. 98.

TABLE I. Values of four observable quantities from high and low pressure extapolations.

Reaction	N_2O_5 (in presence of NO)	N_2O
Temp °K	300	888
k_∞ sec^{-1}	0.277	7.5×10^{-4}
m mole cc^{-1} sec^{-1}	1.333×10^{-6}	13×10^{-8}
k_0' cc mole^{-1} sec^{-1}	1.80×10^{5}	14.5
n cc^2 mole^{-2} sec^{-1}	1.33×10^{12}	72×10^{4}
F	3.1	3.3
G	11.4	2.6

general mechanism Eq. (1) gives

$$k=\frac{\text{Rate}}{[A]}=\sum_i\frac{a_ic_i[M]}{b_i[M]+c_i}. \tag{6}$$

It is of extremely great interest to interpret experimental data by means of Eq. (6). An independent continuous macroscopic variable $[M]$ occurs *inside* the sum over the activated states of the molecule, unlike the corresponding expression for bimolecular reactions. Thus from experimental data it is hoped that some information can be obtained about the detailed rate constant functions, a_i, b_i, and c_i.

The high concentration region is that where $b_i[M]>c_i$ for all i from the critical energy to infinity. Here one must note that "practical infinity" is meant, that is, an energy region so high that the product a_ic_i has effectively converged to zero. If the condition $b_i[M]>c_i$ for all i is met, then expansion of Eq. (6) gives for the high concentration region

$$k_H=\sum_ia_ic_i/b_i-\sum_ia_i(c_i/b_i)^2(1/[M])\cdot +\sum_ia_i(c_i/b_i)^3(1/[M])^2-\cdots. \tag{7}$$

For the high concentration limit $b_i[M]\gg c_i$ for all i, and only the first term in Eq. (7) is retained. From Eq. (7) it can be seen that the appropriate way to extrapolate to the high concentration limit is to plot the observed first-order rate constant k against $1/[M]$. If the curve is nonlinear everywhere, the high concentration region has not been attained. If near the origin of $1/[M]$ the points lie on a straight line, the extrapolation of this line to zero $1/[M]$ gives the high concentration limit k_∞. The slope of this straight line, $-\mathbf{m}$, is easily observed from kinetic data; the coefficients of $(1/[M])^2$ and higher terms of Eq. (7) are usually lost in experimental error. However, the slope and intercept are readily available, observable quantities, and in terms of the mechanism these are

$$k_\infty=\sum_ia_ic_i/b_i \tag{8}$$

$$\mathbf{m}=\sum_ia_i(c_i/b_i)^2. \tag{9}$$

In the low concentration region where $b_i[M]<c_i$ for all i expansion of Eq. (6) gives

$$(k/[M])_l=\sum_ia_i-\sum_ia_i(b_i/c_i)[M] +\sum_ia_i(b_i/c_i)^2[M]^2-\cdots. \tag{10}$$

A plot of observed $k/[M]$ against $[M]$ gives, near the origin of $[M]$, a straight line of slope $-\mathbf{n}$ and intercept k_0', a second-order rate constant. In terms of the mechanism these observables are

$$k_0'=\sum_ia_i \tag{11}$$

$$\mathbf{n}=\sum_ia_ib_i/c_i. \tag{12}$$

There can be proved two relations between these four observables. Define f_i as $a_i^{\frac{1}{2}}(c_i/b_i)$ and g_i as $a_i^{\frac{1}{2}}$. Then $\sum_if_i^2=\mathbf{m}$, $\sum_ig_i^2=k_0'$, and $\sum_if_ig_i=k_\infty$. But it can be shown[3] for any such functions f_i and g_i

$$(\sum_if_i^2)(\sum_ig_i^2)\geq(\sum_if_ig_i)^2. \tag{13}$$

Thus, it is seen that

$$k_0'\geq(k_\infty)^2/\mathbf{m}, \tag{14}$$

or this inequality may be written as

$$k_0'=\mathbf{F}(k_\infty)^2/\mathbf{m}, \tag{15}$$

where **F** is a dimensionless number necessarily greater than one. In exactly the same fashion f_i may be defined as $(a_ib_i/c_i)^{\frac{1}{2}}$ and g_i as $(a_ic_i/b_i)^{\frac{1}{2}}$. Equation (13) now gives

$$k_\infty\geq(k_0')^2/\mathbf{n}, \tag{16}$$

$$k_\infty=\mathbf{G}(k_0')^2/\mathbf{n}. \tag{17}$$

With Eq. (14) one can predict a lower limit on the zero-concentration second-order rate constant from data observed only in the high concentration region, and from Eq. (16) one can set a lower limit on the infinite-concentration first-order rate constant from data obtained in the low concentration region alone. These predictions may be of some practical importance in planning experiments designed to cover the entire range from low to high limits. If one has data at both high and low pressure regions, one can evaluate and study the properties of the dimensionless factors **F** and **G**.

For nitrogen pentoxide there are data which extend from the low limit to the high limit. Recent measurements[4] in this laboratory have established the relative efficiencies of N_2O_5, NO, N_2, and CO_2, so that studies with various M gases on the decomposition of nitrogen pentoxide in the presence of nitric oxide[5,6] can be expressed in terms of a single variable $[\mathbf{M}]$, the equivalent concentration of nitrogen pentoxide. By fitting all points[5] above one atmosphere by the method of least squares to the relation $k=k_\infty-\mathbf{m}/[\mathbf{M}]$, one finds the values of these two observables, and they are listed in Table I. The lowest 35 points of the study[6] of this reaction in a 22-liter bulb at 27° were fitted by least

[3] H. Margenau and G. M. Murphy, *Mathematics of Physics and Chemistry* (D. Van Nostrand Company, Inc., New York, 1943), p. 131.

[4] (To be published in J. Am. Chem. Soc.)

[5] R. L. Mills and H. S. Johnston, J. Am. Chem. Soc. **73**, 938 (1951).

[6] H. S. Johnston and R. L. Perrine, J. Am. Chem. Soc. **73**, 4752 (1951).

squares to the relation $k/[\mathbf{M}]=k_0'-\mathbf{n}[\mathbf{M}]$; the values of the slope and intercept are listed in Table I. Thus, for nitrogen pentoxide the four observables are based directly on kinetic data.

Nitrous oxide is the only other molecule for which both high and low limits are more or less well known.[7] The data do not go to the high concentration limit, but the set of c_i values which fit the rest of the curve do permit calculation of k_∞ at 888°K. The slope $\mathbf{m}$ is found by connecting the value of k_∞ to the cluster of points observed at about 40 atmos. The low concentration parameters are interpolated to 888°K from observed, corrected[7] values at other temperatures. Thus for nitrous oxide the four observables are based on measured rates which, however, have been corrected, interpolated, and extrapolated.

The values of the dimensionless parameters **F** and **G** are of order of magnitude one to ten. For both nitrogen pentoxide and nitrous oxide the value of **F** is about 3 and **G** is, respectively, 11 and 3. Thus, for these molecules the predictions based on Eq. (14) and (16) would have been better than an order of magnitude estimate.

Without additional assumptions the two dimensionless parameters can only be regarded as empirical quantities which may or may not turn out to have a correlation with molecular properties. By adding the assumptions that go into the Rice-Ramsperger-Kassel theory of unimolecular reactions, one gets a less general and more questionable theory than at this level, but on the other hand, the four observables and the two dimensionless parameters take on very definite interpretations. These assumptions will be added one by one, and the interpretations made at each stage. The object of the rest of this article is not to evaluate the assumptions, but only to notice what interpretations they lead to.

ASSUMPTION OF MICROSCOPIC REVERSIBILITY

At equilibrium every detailed process and its exact reverse occur at the same average rate, and thus in the hypothetical absence of reaction[8] $a_i=b_iP_i$ where P_i is the Maxwell-Boltzmann probability of the state i. The relation $a_i=b_iP_i$ is derived at equilibrium, but it is true whether or not the system is at equilibrium. Thus, it is *not* implicitly assumed that the actual distribution is the equilibrium one when reaction occurs, even though P_i is to be interpreted as the equilibrium probability of the state i. The averages deduced below are not averages over actual distributions, but are the formal averages over the equilibrium distribution. With the substitution of $a_i=b_iP_i$ in Eqs. (7) and (10), one gets for the four observables

$$k_\infty=P\langle c\rangle_{Av}{}^*=\langle c\rangle_{Av}{}^A, \tag{18}$$

$$\mathbf{m}=P\langle c^2/b\rangle_{Av}{}^*, \tag{19}$$

$$k_0'=P\langle b\rangle_{Av}{}^*, \tag{20}$$

$$\mathbf{n}=P\langle b^2/c\rangle_{Av}{}^*, \tag{21}$$

where $P=\sum_i P_i$ is the normalizing constant for the distribution function P_i. The asterisk denotes averaging over activated molecules only, and the superscript A on Eq. (18) denotes averaging over all states of A.

ASSUMED FORM FOR THE FUNCTION b_i

There are clear-cut arguments against this assumption, and the arguments for it are to the effect that deviations may be small compared to the accuracy of kinetic data. It leads to a number of definite interpretations which by their definiteness may eventually be used to evaluate the theories up to this point. Physically the assumption is that every collision of an activated molecule results in its deactivation, and the physical picture of collisions is an encounter of hard spheres. Mathematically the assumption is that b_i is a constant, the kinetic collision constant,[9]

$$b=(8\pi\mathbf{k}T/\mu)^{\frac{1}{2}}\sigma^2N. \tag{22}$$

With this assumption the four observables have the same form as Eqs. (18–21), except that the constant b is taken outside the average. By computation of b from Eq. (22) one gets the following quantitative interpretations

$$P=k_0'/b, \tag{23}$$

$$\langle 1/c\rangle_{Av}{}^*=\mathbf{n}/bk_0', \tag{24}$$

$$\langle c\rangle_{Av}{}^*=bk_\infty/k_0', \tag{25}$$

$$\langle c^2\rangle_{Av}{}^*=b^2\mathbf{m}/k_0', \tag{26}$$

$$\mathbf{F}=\langle c^2\rangle_{Av}{}^*/\langle c\rangle_{Av}{}^{*2}=1+V, \tag{27}$$

$$\mathbf{G}=\langle c\rangle_{Av}{}^*\langle 1/c\rangle_{Av}{}^*. \tag{28}$$

P is the equilibrium fraction of molecules above the critical energy, 0.693 $\langle 1/c\rangle_{Av}{}^*$ is the average half-life of activated molecules with respect to decomposition, $\langle c\rangle_{Av}{}^*$ and $\langle c^2\rangle_{Av}{}^*$ are the first and second moments of the function c_i, and V is the variance of the function c_i in units of $\langle c\rangle_{Av}{}^{*2}$. The quantity $\mathbf{F}-1$ may be interpreted as a measure of the spread of the function c_i. This quantity is zero if all values of c_i are constant, that is, Hinshelwood's original theory.[10] By anticipating forms for P_i and c_i one can get an interpretation of the quantity **G**. One expects c_i to increase rapidly with energy above the critical amount and P_i to decrease exponentially with energy. Thus, the product P_i/c_i should decrease very rapidly with energy, so that $\langle 1/c\rangle_{Av}{}^*$ is close to the reciprocal of the minimum value of c_i (numerical computations with nitrous oxide data[7] tend to confirm this as a fair approximation). Thus, the

[7] H. S. Johnston, J. Chem. Phys. **19**, 663 (1951).
[8] R. C. Tolman, *Statistical Mechanics with Applications to Physics and Chemistry* (Chemical Catalog Company, Inc., New York, 1927), p. 262.
[9] Reference 8, p. 69.
[10] Reference 2, p. 100.

TABLE II. Computed values of **F** and **G** for various assumed numbers of oscillators and frequencies (critical energy = 35 kT).

s	m	x	**F**	**G**
15	11	3.2	5.3	1.61
15	22	1.6	200	15
10	11	3.2	2.9	1.33
10	22	1.6	26	5.2
5	11	3.2	1.43	1.12
5	22	1.6	3.9	2.0
5	44	0.8	9.8	5.9
4	11	3.2	1.24	1.08
4	22	1.6	2.5	1.63
4	30	1.174	3.4	2.2
4	35	1.0	4.0	2.6
4	44	0.8	4.9	3.4
4	88	0.4	7.8	10.0
4	...	0	23	∞
3	11	3.2	1.12	1.04
3	22	1.6	1.64	1.31
3	44	0.8	2.6	2.0
3	75	0.47	3.3	3.4
3	88	0.4	3.5	3.8
2	11	3.2	1.03	1.00
2	22	1.6	1.17	1.11
2	44	0.8	1.39	1.31
2	88	0.4	1.62	1.60
N_2O (obs)			3.3	2.6
N_2O_5 (obs)			3.1	11.4

quantity **G** gives a rough measure of the ratio of the average value of c_i to its minimum value. Furthermore, the minimum value of c_i is a mechanical property of the molecule and independent of distribution or temperature. Thus $\langle 1/c\rangle_{Av}$* is expected to be temperature independent, as has been observed.[6,7]

RICE-RAMSPERGER-KASSEL THEORIES

These theories when referred to observable kinetic data involve all of the preceding assumptions plus two more, assumed forms for the functions c_i and P_i. Kassel's[11] form of the theories gives

$$P_i=\frac{(m+i+s-1)!(1-e^{-x})^s e^{-mx}e^{-ix}}{(m+i)!(s-1)!}, \tag{29}$$

$$c_i=D\frac{(m+i)!(i+s-1)!}{i!(m+i+s-1)!}, \tag{30}$$

where $mh\nu$ is the critical energy, x is $h\nu/\mathbf{k}T$, ν is the frequency of each of the idealized quantum oscillators, s is the number of these oscillators, i goes from zero to infinity, and D is an unknown constant. From the four observables from kinetic data all parameters of Kassel's theory can be found with no outside assumption about their magnitude. Kassel[2] showed that $mh\nu$ is the energy of activation at the high concentration limit, and D is the pre-exponential factor there. The remaining parameters may be regarded as s, x, and b; these can be evaluated from **F**, **G**, and k_0'. The two dimensionless quantities according to Kassel's theory are

$$\mathbf{F}=\left[\frac{(1-e^{-x})^s}{(s-1)!}\right]^2\left[\sum_i\frac{(m+i+s-1)!e^{-ix}}{(m+i)!}\right]\times\left[\sum_i\frac{(m+i)!}{(m+i+s-1)!}\left\{\frac{(i+s-1)!}{i!}\right\}^2 e^{-ix}\right], \tag{31}$$

$$\mathbf{G}=\frac{(s-1)!\sum_i\frac{i!}{(i+s-1)!}\left[\frac{(m+i+s-1)!}{(m+i)!}\right]^2 e^{-ix}}{(1-e^{-x})^s\left[\sum_i\frac{(m+i+s-1)!}{(m+i)!}e^{-ix}\right]^2}. \tag{32}$$

These expressions are functions of m, s, and x, with, however, a connection between x and m: $mx=\epsilon_c/\mathbf{k}T$. Thus by computing **F** and **G** for a variety of values of s and x, one can select the values of s and x which give calculated **F** and **G** in agreement with experimental values. In Table II there are listed a series of values of **F** and **G** calculated from Eq. (31) and (32) where $\epsilon_c/\mathbf{k}T$ is 35. By coincidence it happens that the critical energy divided by $\mathbf{k}T$ is the same within experimental uncertainty for the reaction $N_2O_5\rightarrow NO_2+NO_3$ at 300°K and for the decomposition of nitrous oxide at 888°K. Thus the values in Table II apply equally well to nitrous oxide or nitrogen pentoxide. From the structure of these molecules it is assumed that nitrogen pentoxide has a maximum of 15 and nitrous oxide a maximum of 4 oscillators. The summations in Eqs. (31) and (32) converge rapidly, so that not more than 32 terms needed to be retained for any summation. The value of **F** for $x=0$ represents the classical limit of the *RRK* theory, and it was obtained by graphical integration.

In Table II there is no choice of s and x which will fit both **F** and **G** for nitrogen pentoxide. Graphical interpolation of the computed quantities indicate that for 15 oscillators or less no choice of s and x can be found which gives calculated values of the dimensionless parameters in agreement with the observed ones. Thus Kassel theory fails for nitrogen pentoxide, and this failure is very large compared to experimental error. It is not obvious which of the many assumptions in the theory is most to blame. It is felt that the assumptions about b_i, c_i, and P_i are of about the same degree of idealization. These three uncertain assumptions should not be made all at once, but only one at a time. The data on nitrogen pentoxide should be interpreted with only one of these assumptions, and expressions kept general with respect to the other two. In this way it may eventually be possible to use experimental data to improve on one or more of these three assumptions.

The uncertainties in the data for nitrous oxide are much larger than those for nitrogen pentoxide. Within experimental error there is one choice of s and x which gives satisfactory values of **F** and **G**. For $s=4$ and $x=1.174$, **F** is 3.3 obs and 3.4 calc; **G** is 2.6 obs and 2.2

[11] Reference 2, pp. 96–97.

calc. No other choice of s and x is as satisfactory as this one. Thus from kinetic data alone s, x, and m are fixed; P can be calculated directly from these parameters; and b can be calculated from k_0'.

$$P\approx\frac{(m+s-1)!}{m!(s-1)!}\frac{(1-e^{-x})^s e^{-mx}}{\left(1-\frac{m+s}{m+1}e^{-x}\right)}=0.98\times10^{-12}. \quad (33)$$

From the observed value of $k_0'=bP$, one finds b is 1.5×10^{13} cc mole^{-1} sec^{-1}. With this value and Eq. (22) one gets 1.9×10^{-8} cm for the collisional diameter of nitrous oxide (the value from gas viscosity is 3.3×10^{-8} cm). The frequency deduced from **F** and **G** is 730 cm^{-1} (the fundamental frequencies of the normal modes are 1289, 588, 588, 2238 cm^{-1}). With all parameters of Kassel's theory determined, the theory predicts the form of k *vs* [**M**] curve at all intermediate concentrations of M. The values of k at intermediate concentrations were calculated and compared with observed[7] values at intermediate pressures. Unfortunately, the agreement at intermediate pressures was very poor. Thus there remains a conflict between Kassel's theory and these data at the intermediate pressures. At the present time it is not clear whether this conflict is due to poor data or to the theory.

THE JOURNAL OF CHEMICAL PHYSICS VOLUME 20, NUMBER 7 JULY, 1952

Dielectric Dispersion in Materials Having a Distribution of Relaxation Times

J. Ross Macdonald
Armour Research Foundation of Illinois Institute of Technology, Chicago, Illinois
(Received March 10, 1952)

On the basis of considerable experimental evidence, a particular form for the dielectric loss factor, ϵ'', is assumed to hold for many materials exhibiting a distribution of relaxation times. The dielectric constant, ϵ', corresponding to the assumed form of ϵ'' is then computed by means of the Kronig-Kramers relations and tabulated as a function of log frequency and of the distribution function half-width parameter, α. Using these results, experimental ϵ' and ϵ'' curves can be easily tested for mutual consistency and can be fitted individually. In conclusion, a brief discussion of other methods of dealing with the many-relaxation-time dispersion problem is given.

INTRODUCTION

THIS paper is concerned with an extension of a much-used treatment of Fuoss and Kirkwood[1] of dielectric dispersion in materials exhibiting a distribution of relaxation times. For such materials, the simple Debye equations based on a single relaxation time do not correctly describe experimental results for the frequency dependence of the real dielectric constant, ϵ', and the dielectric loss factor, ϵ'', where the complex dielectric constant is given by $\epsilon^*=\epsilon'-i\epsilon''$. Instead, experimental curves are broader than Debye curves and can often be analyzed in terms of a parameter $\alpha(0\leqslant\alpha\leqslant1)$ which determines the half-width of the relaxation-time distribution function. When $\alpha=1$, there is only a single relaxation time, while the distribution function and the dispersion curves become broader and broader as α decreases.

Fuoss and Kirkwood give a sensitive test for the applicability of their method to experimental dispersion data, and, when it is applicable, precise values can be obtained for α and for f_m, the frequency at which ϵ'' reaches its maximum value, ϵ_m''. These two quantities, together with the scale factor, ϵ_m'', obtained directly from measurement, are then sufficient to determine the ϵ' and ϵ'' curves as functions of frequency within the dispersion region. Therefore, the variation of these derived quantities with temperature, impurity content, etc., is of considerable usefulness in interpreting dielectric data.

One of the main purposes of the paper of Fuoss and Kirkwood was to derive a general expression connecting the imaginary part of the reduced polarization, accounting for losses in the material, with the corresponding relaxation-time distribution function. In addition, they were also concerned with relating the reduced polarization to the complex dielectric constant and with obtaining the real part of the dielectric constant corresponding to a given specific form for the imaginary part which had been found to fit considerable experimental data. The Fuoss-Kirkwood treatment of these latter subjects is somewhat limited, however, by the use of the not-always applicable modified[2] Onsager[3] relation between dielectric constant and polarization. The use of this relation leads them to useful results for the functional dependence of ϵ' and ϵ'' on frequency applicable only when $|\epsilon^*|\gg1$ and $\epsilon'^2\gg\epsilon''^2$. Finally, they only compute analytic forms of ϵ' for two specific fractional values of α, whereas for complete comparison

[1] R. M. Fuoss and J. G. Kirkwood, J. Am. Chem. Soc. **63**, 385 (1941).

[2] J. G. Kirkwood, J. Chem. Phys. **7**, 911 (1939).

[3] L. Onsager, J. Am. Chem. Soc. **58**, 1486 (1936).

with experiment it would be useful to be able to determine the dependence of ϵ' on frequency for any α-value in the range from zero to unity.

In the present work, the starting point of the Fuoss-Kirkwood treatment is retained, but it is found unnecessary to introduce the Onsager formula and the results obtained hold without restriction. In addition, a family of curves and a table are presented through whose use ϵ' curves for comparison with experiment may be obtained for any α-value in the above range.

THE FORM OF THE DIELECTRIC LOSS FACTOR

One of the principal results of the Fuoss-Kirkwood paper is that the half-width parameter α may be determined from the slope of the function $\cosh^{-1}[\{\epsilon_m''(2+1/\epsilon_m'^2)\}/\{\epsilon''(2+1/\epsilon'^2)\}]$ plotted against the natural logarithm of the frequency, provided that such a test plot yields a straight line. Here ϵ_m' is the value of ϵ' at $f=f_m$. In data considered so far, ϵ_m' has always been fairly large compared to unity, and therefore the simpler function $\cosh^{-1}(\epsilon_m''/\epsilon'')$ could be used in place of the above form and a straight line still obtained. When this approximation is valid, Fuoss and Kirkwood found the empirical result $\epsilon''=\epsilon_m''\,\mathrm{sech}\alpha x$, where $x=\ln(f_m/f)$. This is the form which will be used in the present analysis. It must be emphasized that this expression for ϵ'' is thus obtained heuristically as that which best fits a large amount of dispersion data; it is not derived from a theoretical consideration of possible dispersion mechanisms.

When ϵ'' is well represented by such a function, $\cosh^{-1}(\epsilon_m''/\epsilon'')=\alpha x$. Therefore, α is given by the slope of the line $\cosh^{-1}(\epsilon_m''/\epsilon'')$ *versus* $\ln f$, and f_m is accurately determined from the intersection of this line with the $\cosh^{-1}(\epsilon_m''/\epsilon'')=0$ axis.

DIELECTRIC CONSTANT FREQUENCY DEPENDENCE

Since the above simple expression for ϵ'' has been found to be capable of fitting a large amount of experimental ϵ'' dispersion data with $\alpha<1$, it seemed worthwhile to attempt to obtain the corresponding expression for ϵ' as a function of α and x by using the Kronig-Kramers integrals.[4,5] This approach differs considerably from that of Fuoss and Kirkwood, who assumed the $\mathrm{sech}\alpha x$ form for the imaginary part of the reduced polarization and by means of the Onsager relation and contour integration involving the relaxation-time distribution function itself arrived at approximate expressions for the dependence of ϵ' and ϵ'' on α and x.

The Kronig-Kramers integral relations connecting ϵ' and ϵ'' may be written in the form

$$\epsilon'(f)-\epsilon_\infty'=\frac{2}{\pi}\int_0^\infty \epsilon''(\mu)\frac{\mu}{\mu^2-f^2}d\mu,$$
$$\epsilon''(f)=\frac{-2f}{\pi}\int_0^\infty \frac{[\epsilon'(\mu)-\epsilon_\infty']d\mu}{\mu^2-f^2}, \tag{1}$$

where both integrals are principal values and ϵ_∞' is the value of ϵ' at very high (optical) frequencies. The above integrals are here assumed to cover two separate dispersion regions: that at medium or low frequencies which is postulated to involve a distribution of relaxation times, and that at infrared frequencies which occurs when the dipoles or ions of the material can no longer follow the applied alternating field.

We are particularly concerned with the former dispersion region and wish to use the first of the above integrals to obtain the analytical dependence of ϵ' on α and x when $\epsilon''(x)$ is given by $\epsilon_m''\,\mathrm{sech}\alpha x$, $x=\ln(f_m/f)$, and f_m is a much lower frequency than that at which the final dispersion region occurs. Since the two dispersion regions are assumed to be widely separated, their contributions to ϵ' are essentially independent, and we may write

$$\epsilon'(f)-\epsilon_1'=\frac{2\epsilon_m''}{\pi}\int_0^\infty \frac{\mu\,\mathrm{sech}(\alpha\ln f_m/\mu)d\mu}{\mu^2-f^2}, \tag{2}$$

where ϵ_1' is the dielectric constant for frequencies much higher than f_m (beyond the first dispersion region) yet much lower than the frequency of the infrared or very high frequency dispersion region. If only one dispersion region is present, ϵ_1' is identical with ϵ_∞'. The upper limit of integration in Eq. (2) can justifiably be extended to infinity because of the excellent exponential convergence produced by the hyperbolic term, which ensures that there will be negligible contribution from this integral for frequencies near the final dispersion region.

The integral (2) may be reduced to manageable form by the substitutions $\mu=f_m e^{\nu/\alpha}$ and $x=\ln f_m/f$. One then obtains

$$\epsilon'(x)-\epsilon_1'=\frac{2\epsilon_m''}{\pi\alpha}\int_{-\infty}^\infty \frac{d\nu}{\cosh\nu(1-e^{-2x-2\nu/\alpha})}. \tag{3}$$

For future convenience, let us define the function $J(\alpha, x)$ by

$$J(\alpha,x)=\frac{\alpha}{2\epsilon_m''}[\epsilon'(x)-\epsilon_1']$$
$$=\frac{1}{\pi}\int_{-\infty}^\infty \frac{d\nu}{\cosh\nu(1-e^{-2x-2\nu/\alpha})}. \tag{4}$$

It has been found that this integral may be evaluated by contour integration for any α-value of the form $(2n+1)/m$ where m and n are positive integers and $m>0$. Zeros of $\cosh z$ occur for $z=\pm i\pi(l+\frac{1}{2})$, while zeros of $(1-e^{-2x-2z/\alpha})$ occur when $z=\alpha(-x\pm i\pi k)$, and $l, k=0, 1, 2\cdots$. The contour employed for the integration is rectangular and is defined by the points $z=\pm A$ and $z=\pm A+i\pi(2n+1)$. There is no contribution to the integral from the short sides of the rectangle at $z=\pm A$ when A approaches infinity. In order to carry out the integration, it is necessary that the integrand

[4] R. Kronig, J. Opt. Soc. Am. **12**, 547 (1926).
[5] H. Kramers, Atti Congz. dei Fisici, Como, 545 (1927).

along the real axis be the negative of that along the $y=\pi(2n+1)$ axis. This will only be the case provided that $(2n+1)=m\alpha$; this equation determines those values of α for which the integral can be evaluated.

The contour is drawn so as to include within it the pole on the real axis at $z=-\alpha x(k=0)$ and to exclude the corresponding pole at $z=-\alpha x+i\pi(2n+1)(k=m=(2n+1)/\alpha)$. It can be shown, however, that the residue of the pole on the real axis at $z=-\alpha x$ contributes nothing to the principal value of the integral. Thus, the residues at the following poles inside the contour must be evaluated: $z=i\pi(l+\frac{1}{2})$, $0\leqslant l\leqslant 2n$; $z=\alpha(-x+i\pi k)$, $1\leqslant k\leqslant m-1$. The residues are found to be

$$R_l=\frac{-\left[e^{-2x}\sin\frac{\pi}{\alpha}(2l+1)+i\left\{1-e^{-2x}\cos\frac{\pi}{\alpha}(2l+1)\right\}\right]}{\pi\sin\pi(l+\frac{1}{2})\left[\left\{e^{-2x}\sin\frac{\pi}{\alpha}(2l+1)\right\}^2+\left\{1-e^{-2x}\cos\frac{\pi}{\alpha}(2l+1)\right\}^2\right]},$$

$$R_k=\frac{\alpha}{2\pi}\frac{\cos\alpha k\pi\cosh\alpha x+i\sin\alpha k\pi\sinh\alpha x}{(\cos\alpha k\pi\cosh\alpha x)^2+(\sin\alpha k\pi\sinh\alpha x)^2}. \tag{5}$$

The function $J(\alpha, x)$ can easily be shown to equal $i\pi(\sum_l R_l+\sum_k R_k)$ where the values of l and k are as above. The real part of the sum of the residues is identically zero.

On evaluating $J(\alpha, x)$ for several values of α, it was found to be identical with a similar function used by Fuoss and Kirkwood and defined by them in terms of another equivalent but more complicated definite integral. It appears that the equivalence of the two definite integral expressions for $J(\alpha, x)$, both involving ϵ'' in their integrands, may impose an interesting restriction on the analytic forms of ϵ'' suitable for representing the loss factor of a many-relaxation-time material and yet consistent, together with its pair ϵ', with the Kronig-Kramers relations. In Fuoss and Kirkwood's analysis, $J(\alpha, x)$ is the real part of the reduced polarization, Q, and is related to ϵ' by means of the modified Onsager relation. The result there obtained is

$$J(\alpha, x)\cong\frac{\alpha}{4\epsilon_m''}\left[2\epsilon'(x)-1-1/\epsilon'(x)-\frac{(n^2-1)(2n^2+1)}{n^2}\right], \tag{6}$$

where $n^2=\epsilon_\infty'$ and is the square of the index of refraction of the material. For comparison, the present treatment gives

$$J(\alpha, x)=\frac{\alpha}{2\epsilon_m''}[\epsilon'(x)-\epsilon_1']. \tag{7}$$

Since $J(\alpha, \infty)=1$, we may also write

$$\epsilon'(x)-\epsilon_1'=(\epsilon_0'-\epsilon_1')J(\alpha, x), \tag{8}$$

where ϵ_0' is the static dielectric constant.

The fact that the real part of the reduced polarization of Fuoss and Kirkwood is found to be directly related to the real part of the dielectric constant for the specific case of the hyperbolic form for ϵ'' is not surprising. In fact, it can be shown[6] that the following relation connects the complex dielectric constant, ϵ^*, and the reduced polarization, Q, of Fuoss and Kirkwood

$$\epsilon^*-\epsilon_1'=(\epsilon_0'-\epsilon_1')Q,$$

provided only that the principle of superposition applies (implying the independence of different relaxation mechanisms).

Because of the complexity of their integral for $J(\alpha, x)$, Fuoss and Kirkwood evaluated it explicitly only for $\alpha=\frac{1}{3}$ and $\alpha=\frac{1}{2}$. If, in addition, the results of the present work are used, the following expressions for $J(\alpha, x)$ may be given:

$$J(1, x)=(1+e^{-2x})^{-1}, \tag{9}$$

$$J(\tfrac{3}{4}, x)=\frac{3}{8\sinh(3x/4)}-\frac{1}{1-e^{-2x}}+\frac{2(1+\frac{1}{2}e^{-2x})}{(1+\frac{1}{2}e^{-2x})+\frac{3}{4}e^{-4x}}-\frac{3\sqrt{2}\sinh(3x/4)}{4\cosh(3x/2)}, \tag{10}$$

$$J(\tfrac{1}{2}, x)=(1-e^{-2x})^{-1}-(4\sinh(x/2))^{-1}, \tag{11}$$

$$J(\tfrac{1}{3}, x)=\frac{1}{1+e^{-2x}}-\frac{2\sinh(x/3)}{\sqrt{3}(2\cosh(2x/3)-1)}, \tag{12}$$

$$J(\tfrac{1}{5}, x)=\frac{1}{1+e^{-2x}}-\frac{\sinh(x/5)}{5}\times\sum_{j=1}^{2}\frac{\sin(j\pi/5)}{\cosh^2(x/5)-\sin^2(j\pi/5)}, \tag{13}$$

[6] H. Fröhlich, *Theory of Dielectrics* (Clarendon Press, Oxford, England, 1949), p. 91.

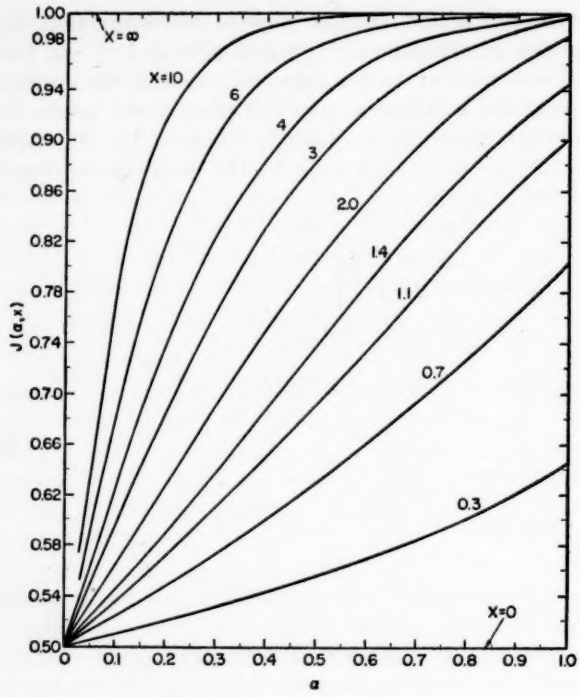

FIG. 1. The function $J(\alpha, x)$.

$$J(\tfrac{1}{10}, x)=\frac{1}{1-e^{-2x}}-\frac{1}{20\sinh(x/10)}$$

$$-\frac{\sinh(x/10)}{10}\sum_{j=1}^{4}\frac{\sin(j\pi/10)}{\cosh^2(x/10)-\sin^2(j\pi/10)}, \quad (14)$$

$$J(0, x)=\tfrac{1}{2} \quad J(\alpha, 0)=\tfrac{1}{2}, \quad (15)$$

$$J(\alpha, x)+J(\alpha, -x)=1. \quad (16)$$

Expressions for $J(\alpha, x)$ for other fractional α-values may easily be calculated from the residues given in Eqs. (5). The above formulas for $J(\alpha, x)$ are sufficient, however, for the computation of the family of parametric curves presented in Fig. 1. Using curves of this nature, the values of $J(\alpha, x)$ as a function of x may be read off directly for any experimental values of α. Thus, when α has been determined from the straight-line plot of $\cosh^{-1}(\epsilon_m''/\epsilon'')$ *versus* $\ln f$, Fig. 1 and Eq. (7) may be used to compute $\epsilon'(x)-\epsilon_1'$. If ϵ_1' is determined experimentally or is independently known, $\epsilon'(x)$ derived in the above fashion may then be compared directly with the experimental $\epsilon'(x)$ curve. For greater accuracy, the data used in plotting the curves of Fig. 1 are presented in Table I, so that the curves may be replotted on graph paper.

An example of curve fitting using the above method is presented in Fig. 2 for dispersion data obtained by Fuoss[7] on polyvinyl chloride-diphenyl. The $\cosh^{-1}$ plot yielded a good straight line from which the values of α and f_m shown on the figure were obtained. Then the $\epsilon'(x)-\epsilon_1'$ curve was computed with the aid of Fig. 1 and the applicable α-value. Since ϵ_1' was not measured by Fuoss, it was necessary to select a value of this constant which gave best agreement with the experimental ϵ' points. The calculated curves are symmetric and antisymmetric about $x=0$, and it will be seen that although this is the case for the experimental ϵ'' points, there is a progressive deviation of the experimental ϵ' points from the calculated curve at high frequencies. This deviation is a real effect and is discussed to some extent by Fuoss.[7] It indicates either that the hyperbolic form for ϵ'' is not a sufficiently good approximation for this material or that there is another dispersion region sufficiently near that considered here that the separation procedure used in this paper is not completely valid. The latter is probably the correct explanation since ϵ_∞' is known not to exceed 2.5 for this material whereas the best value of ϵ_1' is found to be 2.9.

CONCLUSION

In conclusion, it is worth while to discuss briefly the relation of this method of treating many-relaxation-time data with others which have been developed. The first such method is due to Maxwell[8] and Wagner[9] and assumes that the relaxation times are distributed according to a normal law around a most probable relaxation time. Comparison of the results of this assumption with experimental data is difficult, although such comparison has been somewhat simplified by a graphical method developed by Yager.[10] In the remaining methods to be considered, the forms of the distribution function are determined essentially from the experimental data. Rather than assuming *ab initio* the form of the relaxation-time distribution function, in these latter methods, an assumed, relatively general, form for the experimental dispersion data (such as the present hyperbolic form for ϵ'') is used from which to derive the applicable distribution function. The latter is the preferable approach since it makes more direct use of the results of dispersion measurements.

TABLE I. Calculated values of the function $J(\alpha, x)$.

x \ α	1	3/4	1/2	1/3	1/5	1/10	0
0	½	½	½	½	½	½	½
0.30	0.646	0.593	0.558	0.535	0.520	0.511	½
0.70	0.803	0.711	0.629	0.581	0.547	0.523	½
1.1	0.900	0.801	0.691	0.623	0.571	0.532	½
1.4	0.943	0.856	0.736	0.655	0.588	0.540	½
2.0	0.982	0.914	0.806	0.710	0.628	0.562	½
3.0	0.998	0.965	0.885	0.789	0.686	0.595	½
4.0	1	0.984	0.931	0.847	0.736	0.625	½
6.0	1	0.996	0.975	0.923	0.819	0.682	½
10	1	1	0.997	0.979	0.917	0.777	½
∞	1	1	1	1	1	1	—

[7] R. M. Fuoss, J. Am. Chem. Soc. **63**, 378 (1941).

[8] J. C. Maxwell, *Electricity and Magnetism* (Oxford University Press, London, England, 1889), Vol. 1.

[9] K. W. Wagner, Ann. Physik **40**, 817 (1913).

[10] W. A. Yager, Physics **7**, 434 (1936).

Cole and Cole[11] observed that when experimental values of ϵ' and ϵ'' are plotted *versus* one another on the complex plane, a good circular arc whose center lies on or below the ϵ' axis is often obtained. When this is the case, it is then possible to compute the analytic dependence of ϵ' and ϵ'' on frequency required by such a curve. Further, the intersections of the circular arc with the ϵ'-axis give ϵ_0' and ϵ_∞' (or ϵ_1' if the measured dispersion region is not the one of highest frequency). From the displacement of the circle center below the ϵ'-axis, the distribution function half-width parameter may be obtained. The expressions derived for ϵ', ϵ'', and the corresponding distribution function are quite similar to those arising from the Fuoss-Kirkwood treatment. This approach of Cole and Cole has the advantage of supplying an easy test for the applicability of their method and for the mutual consistency of ϵ' and ϵ'' data. However, it is not as easy to compare the precise agreement of experimental ϵ' and ϵ'' values individually with the corresponding analytic forms for these quantities as it is using the Fuoss-Kirkwood approach together with the results of the present work.

When the algebraic forms given herein for ϵ' and ϵ'' as functions of frequency are plotted on the complex ϵ', ϵ'' plane according to the method of Cole and Cole, a good circular arc is obtained for values of α near unity. As α decreases, however, it is found that if a circular arc is drawn through the $(\epsilon_m', \epsilon_m'')$ and $(\epsilon_0', 0)$, $(\epsilon_1', 0)$ points, intermediate points fall progressively farther inside the arc and the calculated points tend to approach the ϵ'-axis along straight lines rather than along the arc. Here ϵ_m' is the value of ϵ' for the frequency at which ϵ'' is a maximum and is equal to $\epsilon_1'+\epsilon_m''/\alpha=\epsilon_1'+(\epsilon_0'-\epsilon_1')/2$. Although the Cole-Cole formulas give this same value for ϵ_m', they lead to an expression for ϵ_m'' different from that following from the present treatment. Because they both lead to the Debye equations for $\alpha=1$, it is difficult to determine whether the Cole-Cole or the Fuoss-Kirkwood assumption most nearly describes the experimental results for α-values near unity, but distinction becomes progressively more certain as α decreases.

Recently, Davidson and Cole[12] have proposed a new analytic form for ϵ^* applying to many-relaxation-time materials. This formula yields a circular arc when plotted on the ϵ', ϵ'' plane, except that the approach to the ϵ'-axis at high frequencies may be along a straight line rather than along the arc. In the present treatment, the approach to the ϵ'-axis is along straight lines

[11] K. S. Cole and R. H. Cole, J. Chem. Phys. **9**, 341 (1941).
[12] D. W. Davidson and R. H. Cole, J. Chem. Phys. **19**, 1484 (1951).

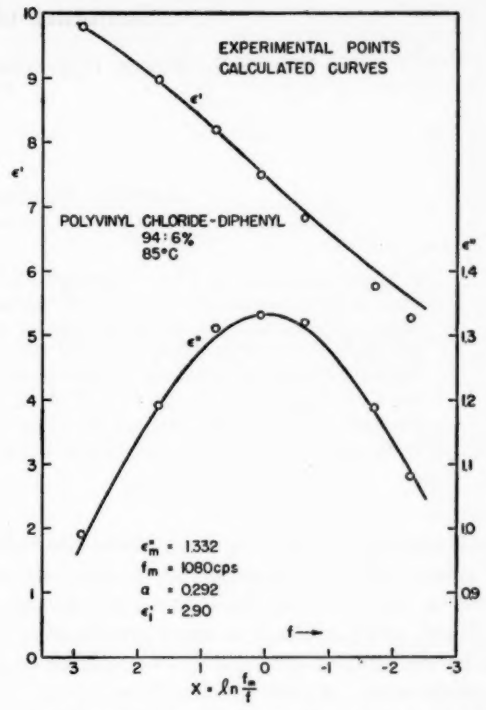

FIG. 2. Real and imaginary dielectric constants of polyvinyl chloride-diphenyl, 94:6, at 85°C (after Fuoss, reference 7).

(for small α) for both high and low frequencies. Considerable experimental data have been well fitted by Davidson and Cole, but their method does not seem to allow the data of Fuoss presented in Fig. 2 of this paper to be fitted as closely as does the present analysis.

It is not possible to say at this point that any one of the above approaches is more nearly correct, to the exclusion of the other methods, for all dispersion data involving a distribution of relaxation times. Considerable published data have been fitted with the use of either the Cole-Cole, the Fuoss-Kirkwood, or the Davidson-Cole methods, however, and it is likely that each has its own exclusive sphere of applicability. In specific cases, it may be important to determine which approach allows experimental data to be fitted most accurately in order to aid in the development of a detailed theory of the relaxation processes occurring in the material. Some possible mechanisms leading to deviations from the simple Debye dispersion curves are discussed by Cole and Cole.[10]

ACKNOWLEDGMENT

The author is much indebted to Dr. J. K. Tyson for several discussions and to Professor R. M. Fuoss for helpful correspondence.

Structure of the Methyl Halides*

S. L. MILLER, L. C. AAMODT, G. DOUSMANIS, AND C. H. TOWNES
Physics Department

AND

J. KRAITCHMAN
Chemistry Department, Columbia University, New York

(Received March 3, 1952)

Microwave spectroscopic measurements on the partially deuterated forms of CH_3Cl, CH_3Br, and CH_3I allow a determination of the structural parameters which is less subject to zero-point vibration errors than other methods. In addition, examination of all measured isotopic species reveals that the C−D distance is shorter than C−H by 0.009A, and the D−C−D angle greater than that for H−C−H by about 12 minutes. Best values of structural parameters for the species containing the light isotope of hydrogen only are C−Cl distance 1.781, C−Br 1.939, C−I 2.139, C−H 1.11 (same for all halides), H−C−H angle 110°31′ for CH_3Cl, 111°14′ for CH_3Br, and 111°25′ for CH_3I. Deuteration not only gives a change in the C−H bond but also a well-correlated change in the quadrupole coupling constant of the halogen.

THE structure of the methyl halides has been the subject of many measurements and discussions.[1] It might be expected that the accurate measurements of moments of inertia of three isotopic species of a methyl halide by microwave spectroscopy could give complete and satisfactory answers for the three structural parameters involved. However, because of zero-point vibrations a wide variety of values for the structural parameters may be obtained, depending on which isotopic combinations are used, and several sets of values have been published.[1] The positions and bond angles of the hydrogen are particularly uncertain because these parameters are relatively insensitive to the measurements. Both the H−C−H angle and the H−C bond length can be increased in such a ratio that the rotation constants B for various isotopic species are not very much changed. Various combinations of three different isotopic species of CH_3Cl may be seen from Table I to yield a wide variety of values for the three molecular parameters if, as usual, zero-point vibrations are neglected. These variations are almost entirely due to the presence of zero-point vibrations, since the experimental measurements are very accurate.

TABLE I. Molecular parameters for CH_3Cl computed from moments of inertia of various combinations of three isotopic species. Variations are primarily due to zero-point vibrations, which are neglected in the calculation. Experimental data used are listed in Table IV.

Isotopic species	C−Cl distance (angstroms)	C−H distance (angstroms)	H−C−H angle
$C^{12}H_3Cl^{35}$, $C^{12}H_3Cl^{37}$, $C^{13}H_3Cl^{37}$	1.7813	1.1227	110°57′
$C^{12}H_3Cl^{35}$, $C^{13}H_3Cl^{35}$, $C^{13}H_3Cl^{37}$	1.7813	1.0906	109°45′
$C^{12}H_3Cl^{35}$, $C^{12}H_3Cl^{37}$, $C^{12}D_3Cl^{37}$	1.7872	1.1281	112°31′
$C^{12}H_3Cl^{37}$, $C^{13}H_3Cl^{37}$, $C^{12}D_3Cl^{37}$	1.7850	0.9489	104°09′
$C^{12}H_3Cl^{37}$, $C^{12}D_3Cl^{37}$, $C^{12}D_3Cl^{35}$	1.7880	1.1635	113°40′

The difficulties in determining the methyl halide structures can be partially circumvented by use of singly or doubly deuterated methyl halides.[2] These are slightly asymmetric tops, with transitions $1_1 \rightarrow 2_0$ at a frequency $3B+C$ and $1_0 \rightarrow 2_{-1}$ at $3C+B$. The separation between these two lines, $2(B-C)$, gives a rather sensitive indication of the distance between the hydrogen nuclei and the molecular axis, and hence allows a better separation of the effects of changes in H−C−H angle and H−C distance on experimental observations.

Table II gives observed microwave absorption frequencies of asymmetric methyl halides and the values of $2(B-C)$. $2(B-C)$ is obtained by measuring the distance between corresponding quadrupole hyperfine structure components in the patterns for the transitions $1_0 \rightarrow 2_{-1}$ and $1_1 \rightarrow 2_0$. Because of the asymmetry, there is a small variation in the contributions of the quadrupole coupling to the frequencies of the two different transi-

TABLE II. Observed rotational frequencies and values of $2(B-C)$ for asymmetric methyl halides. The separation $2(B-C)$ between transitions was measured to an accuracy of about 0.05 Mc/sec, although individual lines may have considerably larger errors.

Molecule	Rotational transition	Hyperfine transition	Frequency (megacycles/sec)	$2(B-C)$ (megacycles/sec)
$C^{12}HD_2Cl^{35}$	$1_0\ 2_{-1}$	$F=5/2\rightarrow 7/2$	45789	617.90
	$1_1\ 2_0$	$F=5/2\rightarrow 7/2$	46407	
$C^{12}HD_2Br^{79}$	$1_0\ 2_{-1}$	$F=5/2\rightarrow 7/2$	32739.4	317.70
	$1_1\ 2_0$	$F=5/2\rightarrow 7/2$	33057.1	
$C^{12}HD_2Br^{81}$	$1_0\ 2_{-1}$	$F=5/2\rightarrow 7/2$	32610.6	314.44
	$1_1\ 2_0$	$F=5/2\rightarrow 7/2$	32925.1	
$C^{12}HD_2I^{127}$	$1_0\ 2_{-1}$	$F=7/2\rightarrow 9/2$	25826.9	195.44
	$1_1\ 2_0$	$F=7/2\rightarrow 9/2$	26022.2	

* Work supported jointly by the ONR and Signal Corps.

[1] Gordy, Simmons, and Smith, Phys. Rev. **74**, 243 (1948); J. W. Simmons, Phys. Rev. **76**, 686 (1949); J. W. Simmons and W. O. Swan, Phys. Rev. **80**, 289 (1950); Matlack, Glockler, Bianco, and Roberts, J. Chem. Phys. **18**, 332 (1950); H. A. Skinner, J. Chem. Phys. **16**, 553 (1948).

[2] Miller, Kraitchman, Dailey, and Townes, Phys. Rev. **82**, 993 (1951).

TABLE III. Structural parameters for methyl halides obtained from the values of B for $C^{12}H_3X$ and $C^{13}H_3X$ and of $B-C$ for $C^{12}HD_2X$, which minimizes the errors due to zero-point vibrations.

Molecules	C−H distance (angstroms)	C−X distance (angstroms)	H−C−H angle
CH_3Cl	1.101	1.7815	110°13′
CH_3Br	1.100	1.9393	111°0′
CH_3I	1.102	2.1389	111°2′

tions. This effect is largest in the methyl iodide case and gives an error in the value $2(B-C)$ when no variation is assumed of only 0.07 Mc/sec which is too small to affect the present results.

The three molecular parameters for CH_3Cl, CH_3Br, and CH_3I shown in Table III are obtained from the values of $2(B-C)$ of Table II and values of B for the symmetric isotopic species $C^{12}H_3X$ and $C^{13}H_3X$ of each compound. These parameters are thought to be considerably more reliable than those obtained from

TABLE IV. Rotational constants of isotopic species of methyl halides.

Molecule	B (megacycles/sec)	Reference
$C^{12}H_3Cl^{35}$	13292.89	a
$C^{13}H_3Cl^{35}$	12796.2	a
$C^{12}H_3Cl^{37}$	13088.19	a
$C^{13}H_3Cl^{37}$	12590.0	a
$C^{12}D_3Cl^{35}$	10841.93	b
$C^{12}D_3Cl^{37}$	10658.48	b
$C^{12}H_3Br^{79}$	9568.40	a
$C^{12}H_3Br^{81}$	9532.00	a
$CC^{13}H_3Br^{79}$	9119.51	c
$C^{13}H_3Br^{81}$	9082.86	c
$C^{12}D_3Br^{79}$	7714.57	b
$C^{12}H_3I^{127}$	7501.25	a
$C^{13}H_3I^{127}$	7119.04	a
$C^{12}D_3I^{127}$	6040.29	b

[a] P. Kisliuk and C. Townes, J. Research Natl. Bur. Standards **44**, 611 (1950).
[b] J. W. Simmons and J. H. Goldstein, J. Chem. Phys. **20**, 122 (1952).
[c] J. W. Simmons and W. O. Swan, Phys. Rev. **80**, 289 (1950).

other isotopic combinations previously used. An estimate of the effect of zero-point vibrations on the rotational constants indicates that errors in the CH_3Cl parameters given in Table III are approximately 0.01A for the C−H distance and 30′ for the H−C−H angle. These are less than one-half the estimated errors of the most favorable isotopic combination used in Table I, which happens to be the first one listed in this table. It may be seen, too, that these two sets of parameters (first in Table I and Table III) which are estimated to be most accurate are in fair agreement with one another. Since the system used for evaluating parameters of CH_3Br and CH_3I in Table III is similar to that for CH_3Cl, the increase in angle from CH_3Cl to CH_3Br or CH_3I given in this table is very probably real.

The errors associated with zero-point vibrations come from the variation of average internuclear distances and angles with isotopic substitution. These variations were estimated from the observed values of rotation-vibration interactions in diatomic molecules. It was

TABLE V. Best structural parameters for methyl halides allowing change in C−H bond with deuteration.

Molecule	C−X distance (angstroms)	C−H or C−D distance (angstroms)	H−C−H or C−C−H angle
CH_3Cl	1.7810	1.113	110°31′
CD_3Cl	1.7810	1.104	110°43′
CH_3Br	1.9391	1.113	111°14′
CD_3Br	1.9391	1.104	111°26′
CH_3I	2.1392	1.113	111°25′
CD_3I	2.1392	1.104	111°37′

assumed that a change in Cl mass affects only the C−Cl distance, a change in H mass only the C−H distance and H−C−H angle, and a change in C mass affects all the molecular parameters. The error in molecular parameters for a given set of three isotopic species could then be calculated for each bond variation due to isotopic substitution. The net error for a given set of isotopic molecules was taken as the square root of the sum of squares of all separate errors due to bond variations.

These estimates indicate plainly that by far the largest errors come from the change in C−H distance and H−C−H angles with isotopic substitution of D for H. Since rotational constants for a large number of isotopic species of CH_3Cl have been measured, it is possible to allow a difference between C−H and C−D bonds and solve for the five parameters, C−Cl, C−H, and C−D distances and H−C−H, D−C−D angles. The values of B for six different isotopic species of CH_3Cl and of B−C for one asymmetric species are available as shown in Tables IV and II. It was found that these could all be fitted to an accuracy better than 0.2 Mc/sec by allowing the D−C bond to be 0.009A shorter than the C−H bond, and the angle between the C−D bond and the molecular axis to be 12′ greater than the corresponding angle for C−H.

Without such changes in structure with isotopic substitution, discrepancies in the rotational constants cannot be made much less than 10 Mc/sec. Furthermore, the values of these changes are approximately what had been estimated as due to the decrease in amplitude of zero-point vibrations in substituting deuterium for hydrogen. Any changes in the length of the C−Cl bond are expected to be considerably smaller and to produce only very small discrepancies in the values of B; hence this distance can reasonably be assumed constant. The resulting molecular parameters for the two types of molecules CH_3Cl and CD_3Cl are given in Table V.

It may be expected that the change in H−C−H bond length and angle with deuteration is essentially the same in CH_3Br and CH_3I as in CH_3Cl, since the halide should affect the C−H vibrations only in a secondary way. The seven rotational constants for CH_3Br may in fact be accurately fitted with three parameters (C−H distance, H−C−H angle, and C−Br distance) with this assumption. The change in

C—H bonds and angles with deuteration was taken to be exactly the same in CH_3Br as for CH_3Cl. The rms error in fitting the data of Tables IV and II is less than 0.1 Mc/sec, whereas very much larger errors are obtained if the C—H and C—D bonds are assumed to be the same. CH_3I may be similarly treated and again gives very good agreement for all measured rotational constants.

Agreement between Tables III and V may be seen to be rather good. The C—H bond length and the H—C—H angle is slightly different for the two cases. However, the C—H distance is given by both as about constant for the three halides, and the H—C—H angle increases from CH_3Cl to CH_3Br with a considerable smaller increase to CH_3I. Values for the molecular parameters given by Table V are probably somewhat more accurate than those of Table III.

The change in bond distance with deuteration provides a good opportunity to study the effect of this variation on the electronic structure of a methyl halide. There is a very satisfying correlation between the effect of deuteration on the geometric parameters of methyl chloride and the change in quadrupole coupling constant reported by Simmons and Goldstein.[3] The magnitude of quadrupole coupling constant of Cl is approximately 0.7 Mc/sec smaller in CD_3Cl than in CH_3Cl, indicating an increase in the ionic character of the C—Cl bond of approximately 1 percent. This 1 percent increase in ionic character would be expected to increase the D—C—D angle by about 10′ as is observed. Both changes are presumably the result of a shortening of the C—D bond and hence an increased transfer of electropositive character from the hydrogens to carbon. A decreased electronegativity of 0.01 unit per each deuterium substitution fits reasonably well the observed decreases in quadrupole coupling in the methyl halides. The resulting increase in ionic character should be less in CH_3I than in CH_3Cl by about a factor of 2.5 because of the change in slope of the curve of electronegativity *versus* ionic character.[4] This agrees well with the observed ratio of three for the percentage changes in the quadrupole coupling in methyl chloride and methyl iodide upon deuteration.

The authors appreciate helpful discussions with Dr. B. P. Dailey on the subject of this paper, and the assistance of Dr. H. T. Minden with preparation of some of the molecules measured.

[3] J. W. Simmons and J. H. Goldstein, J. Chem. Phys. **20**, 122 (1952).

[4] L. Pauling, *Nature of the Chemical Bond* (Cornell University Press, Ithaca, New York, 1945).

THE JOURNAL OF CHEMICAL PHYSICS VOLUME 20, NUMBER 7 JULY, 1952

The Gaussian Approximation for the Probability Density of a Molecule in a Cell

GIORGIO CARERI
Istituto di Fisica dell' Università, Centro di Studio per la Fisica Nucleare del C. N. R., Roma, Italy
(Received July 10, 1951)

Kirkwood's integral equation of the free volume theory of liquids has been used to test the Gaussian approximation for the probability density $F(r)$ of a molecule in a cell. The approximation has been found to be good, even up to the critical point.

I. INTRODUCTION

IN a recent critique of the free volume theory of the liquid state, Kirkwood[1] showed the probability density function $F(r)$ for a molecule in a cell must satisfy an integral equation obtained by taking the minimum of the free energy with respect to $F(r)$. One sees then that the well-known Lennard-Jones and Devonshire[2] equation of state for dense gases and liquids is the first approximation to this integral equation, and better approximations are possible. Mayer and Careri[3] generalized Kirkwood's method including some empty cells and thus avoiding the communal entropy mistake. To get simple numerical results they assumed $F(r)$ to be a Gaussian, and used the "best" Gaussian taking the minimum of the free energy with respect to the Gaussian exponent. The object of this note is to test the worth of this Gaussian assumption with special emphasis on the critical point. No empty cells will be introduced.

II. INTEGRATION

Kirkwood's equation is

$$kT \ln F(r_i) = \sigma - \sum_{j \neq i} \int_{v_j} u(r_{ij}) F(r_j) d(j), \qquad (1)$$

where σ is a constant to be obtained from the normalization condition

$$\int_{v_i} F(r_i) d(i) = 1, \qquad (2)$$

and the other symbols have their usual significance.

[1] J. Kirkwood, J. Chem. Phys. **18**, 380 (1950).
[2] J. E. Lennard-Jones and A. F. Devonshire, Proc. Roy. Soc. (London) **163A**, 53 (1937); **165A**, 1 (1938).
[3] J. E. Mayer and G. Careri, J. Chem. Phys. **20**, 1001 (1952).

The Lennard-Jones and Devonshire approximation is obtained by using a δ-function at the origin, $r_j=0$, in the right-hand side of Eq. (1). In this paper a Gaussian, $F_1(r_j)$, is inserted in the right-hand side of Eq. (1), and the function obtained after integration; namely, the left-hand function, $F_2(r_j)$, is compared with the first approximation, F_1, used under the integral.

Following Mayer and Careri[3] we will use a normalized Gaussian,

$$F_1(r)=(\beta/2^{1/6}\pi^{1/2})^3\exp-(\beta/2^{1/6})^2r^2, \tag{3}$$

and a kind of compromise between a Morse and a Lennard-Jones potential,

$$u(r)=u_e\{\exp-12[r(x/2^{1/6})-1] -2\exp-6[r(x/2^{1/6})-1]\}, \tag{4}$$

where x is an expansion parameter,

$$x=2^{1/6}R/R_e=R/R_0=R^*/R_e. \tag{5}$$

Here R is a unit of length such that

$$R^3=v, \tag{6}$$

which is the volume per cell; R_e is the distance between two molecules at which the potential is $-u_e$; R_0 is the collision distance for zero energy, simply related[4] to R_e for the pure Lennard-Jones potential assumed in the last term of (5). We notice then that x^3 is v/v_0, with $v_0=R_0^3$, a familiar quantity to describe liquid properties. In the assumed face-centered packing, R^* is the distance between cell centers. We also use the coordinate system

$$\xi_i=x_i/R,\quad \eta_i=y_i/R,\quad \zeta_i=z_i/R,$$
$$r_{ij}=[(\xi_i-\xi_j)^2+(\eta_i-\eta_j)^2+(\zeta_i-\zeta_j)^2]^{\frac{1}{2}}. \tag{7}$$

In evaluating the integral in (1) the expression

$$I(\gamma,\delta)=\int_{vj}(\delta/2^{\frac{1}{2}}\pi y)^3\exp-[(r_j\delta/2^{\frac{1}{2}}y)^2 +(r_{ij}\gamma\delta/y)]d(j) \tag{8}$$
$$\cong(1-\gamma/\delta)\exp[\gamma^2/2-\gamma\delta]$$

is found to occur. The geometry is easy to understand from Fig. 1. Now define

$$J(y_{ij})=(1/u_e)\int_{vj}u(r_{ij})F_1(r_j)d(j), \tag{9}$$

and use (3) and (4) in (9), setting

$$\delta=\beta y_{ij}2^{\frac{1}{2}}, \tag{10}$$

$$\gamma=nx/\beta 2^{\frac{1}{2}},\quad n=12\quad\text{or}\quad 6. \tag{11}$$

One gets

$$J(y)=(1-6\times 2^{1/6}/\beta^2 y)\exp[36x^2/\beta^2-12\times y2^{-1/6}+12] -2(1-3\times 2^{1/6}/\beta^2 y)\exp[9x^2/\beta^2 -6\times y2^{-1/6}+6]. \tag{12}$$

[4] R. Fowler and E. A. Guggenheim, *Statistical Thermodynamics* (Cambridge University Press, London, 1939), p. 280.

TABLE I.

β^2	kT/u_e \ x =	1.25	1.30	1.35	1.40	1.44
25	½	248.00	135.00	73.80	41.70	
	1	104.00	57.10	33.90	20.80	14.40
22	½			131.00		
	1			56.10		
	2			4.08		

It is physically obvious that one has

$$J(0)\gg 1 \tag{13}$$

and

$$J(\infty)=0. \tag{14}$$

We now define the normalization factor,

$$H=\int_{vi}\exp\{-(u_e/kT)\sum_{j\neq i}J(y_{ij})\}d(i), \tag{15}$$

and write Eq. (1) as follows:

$$F_2(r_i)=(1/H)\exp\{-(u_e/kT)\sum_{j\neq i}J(y_{ij})\}. \tag{16}$$

To evaluate (15) and (16) numerically we will now make the two following assumptions: (a) only the first shell of 12 neighbors will contribute to the sum $\sum$; (b) $F_2(r_i)$ is spherically symmetrical.

Both assumptions seem to be reasonably good[5–7] for the purpose of this note. To find a relationship between y and r_i, one can easily see by elementary geometrical considerations that for r_i parallel to one cube edge the 12 neighbors can be split into three groups of four each, and for each group one has in our coordinate system one of the following:

$$y_{ij}=[r_0^2+2^{\frac{1}{2}}r_i+2^{\frac{1}{2}}]^{\frac{1}{2}}, \tag{17.1}$$

$$y_{ij}=[r_0^2-2^{\frac{1}{2}}r_j+2^{\frac{1}{2}}]^{\frac{1}{2}}, \tag{17.2}$$

$$y_{ij}=[r_0^2+2^{\frac{1}{2}}]^{\frac{1}{2}}. \tag{17.3}$$

Let us define as $J_1(r_i)$ the $J(y_{ij})$ one gets using (17.1), and similarly $J_2(r_i)$ and $J_3(r_i)$ using (17.2) and (17.3), and define again

$$g(r_i)=J_1(r_i)+J_2(r_i)+J_3(r_i). \tag{18}$$

It is now possible to evaluate $F_2(r_i)$ for r_i parallel to the cube edge, and the above assumption of symmetry enables us to perform the integral for the normalization factor. We write again Eqs. (15) and (16) as follows:

$$H=4\pi\int r^2\exp\{-(u_e/kT)4g(r)\}dr \tag{19}$$

and

$$F_2(r)=(1/H)\exp\{-(u_e/kT)4g(r)\}. \tag{20}$$

[5] I. Pirgogine and G. Garikian, J. Chem. Phys. **45**, 273 (1948).
[6] T. L. Hill, J. Phys. and Colloid Chem. **51**, 1219 (1947).
[7] Wentorf, Buchler, Hirschfelder, and Curtiss, J. Chem. Phys. **18**, 1484 (1950).

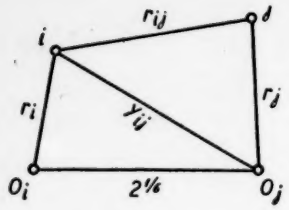

FIG. 1. Diagram showing the symbols used in the calculations. O_i and O_j are the cell centers of the two neighbor molecules i and j.

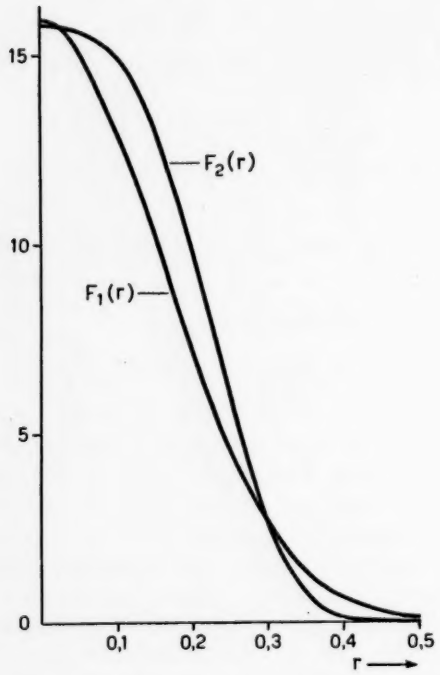

FIG. 2. The probability density *vs* the distance r from the cell center. $F_1(r)$ is the Gaussian with $\beta^2=25$. $F_2(r)$ is the probability density obtained by integration, at a reduced temperature $kT/u_e=1$, lattice parameter $x=1.43$ and using the Gaussian $F_1(r)$ with $\beta^2=25$.

The normalization factor H has been numerically evaluated by Eq. (19) in a few cases. Some $F_2(0)$ values are reported in Table I.

III. DISCUSSION

For reasonably large values of β^2 it is possible to pick up a pair of values of kT/u_e and x, namely, of the temperature and volume for which the agreement between the starting Gaussian and the $F_2(r)$ obtained is very close. In general, increasing the temperature and the volume the $F_2(r)$ gets broader as one must expect. However, at a volume and temperature corresponding to the critical point the Gaussian is still steep and the molecule remains inside the cell.

In order to find reasonable kT/u_e values we consider the first and the second derivatives. After long algebra one finds

$$[\partial F_2(r)/\partial r]_{r=0}=0 \tag{21}$$

and

$$[\partial^2 F_2(r)/\partial r^2]_{r=0}=-F_2(0)D(x,\beta)(8u_e/2^{1/6}kT), \tag{22}$$

where

$$\begin{aligned}D(x,\beta)&=[\partial J(y)/\partial y]_{y=2^{1/6}}+2^{-5/6}[\partial^2 J(y)/\partial y^2]_{y=2^{1/6}}\\&=12\times 2^{-1/6}\{(6x-36x^2\beta^{-2}-1)\exp 36x^2\beta^{-2}\\&\quad+12(1-x)-(3x-9x^2\beta^{-2}-1)\exp 9x^2\beta^{-2}\\&\quad+6(1-x)\}.\end{aligned} \tag{23}$$

On returning to Eq. (3) one finds

$$(\partial^2 F_1(r)/\partial r^2)_{r=0}=-2(\beta/2^{1/6})F_1(0), \tag{24}$$

so that

$$\begin{aligned}&[F_1(0)]^{-1}[\partial^2 F_1(r)/\partial r^2]_{r=0}\\&\qquad=[F_2(0)]^{-1}[\partial^2 F_2(r)/\partial r^2],\end{aligned} \tag{25}$$

only if we set

$$kT/u_e=(2^{13/6}/\beta^2)D(x,\beta). \tag{26}$$

Solutions of (26) occur only if D is positive, and this is always the case for x values of physical interest if $\beta^2\geq 20$, which is the condition necessary to safely integrate the value of r to infinity as shown in the previous paper. For the values of x, β for which D is positive one may find values of kT/u_e for which the ratio of the second derivative to the value of the function is the same at the origin for the Gaussian F_1 and for the next approximation F_2

This will give us a first reasonable kT/u_e value for a x, β pair. By successive approximations one can then find the values for which the two functions F_1 and F_2 are equal at $r=0$. This has been done for one case in the critical region, namely, for $x=1.44$, $kT/u_e=1$, and $\beta^2=25$. The Gaussian F_1 corresponding to this β value and the F_2 obtained are shown in Fig. 2. One sees the general shape of the two curves to be rather similar, the $F_2(2)$ being somewhat flatter at the origin then $F_1(2)$. As a matter of fact the second derivatives at the origin are, respectively, $F_1(0)=-560$ and $F_2(0)=-153$. The Gaussian starts down more steeply; therefore, owing to the normalization condition, it tails off more slowly. One can then be sure that the molecule will remain inside the cell, even up to the critical point, since this condition is already satisfied for the Gaussian.

ACKNOWLEDGMENT

The author is grateful to Professor J. E. Mayer, University of Chicago, Chicago, Illinois, for suggesting this problem and for criticism. He also expresses his appreciation to Professor M. Picone, Director, Istituto per le Applicazioni del Calcolo, Roma, for the numerical calculations, which have been done by his Institute.

The Diffraction of X-Rays by Liquid Alloys of Sodium and Potassium

N. S. GINGRICH AND R. E. HENDERSON
University of Missouri, Columbia, Missouri

(Received January 10, 1952)

Monochromatic x-ray diffraction patterns were taken of liquid alloys of sodium and potassium of seven different compositions at 115°C. Contrary to previous results, the present work does not show in a plot of position of main peak *vs* composition an inflection which had been taken as evidence for the existence of Na_2K molecules in the liquid. Fourier analyses made for five of the alloys gave distribution curves which prove that there are no compact molecules in these liquid alloys, though they do not rule out the possibility that there may be weakly associated groups of atoms.

INTRODUCTION

As in the case of elements in the liquid state, a study of the diffraction of x-rays can give information concerning the structure of liquids composed of more than one kind of atom. The early work of Zernike and Prins[1] and of Debye and Menke[2] led to the analysis of diffraction patterns from liquids composed of one kind of atom, giving as a result a curve showing the distribution of atoms about any one atom in the body of the sample. Numerous elements in the liquid state have been studied[3] this way, and all such studies show in the atomic distribution curve a first peak representing the concentration of nearest neighbors at a most probable distance approximately equal to the diameter of the atom. In the case of monatomic liquids such as sodium, potassium, or mercury, where nearest neighbors wander far from the original atom, this first peak is not discrete, showing the absence of any structure other than a time-averaged distribution governed largely by thermal motion of the atoms, by the impossibility of interpenetration of atoms, and by the existence of characteristic interatomic binding. On the other hand, studies with liquids such as phosphorus, chlorine, or oxygen disclosed the existence of a discrete first peak, indicating that the nearest neighbors were fixed relative to the origin atom. This means that these are molecular liquids.

Of the several experimental and theoretical attempts to deal with liquids of more than one kind of atom, perhaps the most fruitful approximate method is the one[4] which eventually led to the analysis of the structures of liquids such as alcohol[5] and carbon tetrachloride,[6] clearly showing discrete peaks in the distribution curves as one must expect for a molecular liquid. Extensive application of this theory has also been made to amorphous solids[7] which are generally polyatomic. Even though the theory is only approximate for polyatomic substances, it has been found adequate in sufficient cases to warrant its use to supply evidence on the question of whether in the liquid alloy of sodium and potassium molecules of one kind or another exist.

From their physical properties,[8] evidence for the molecular constitution of liquid alloys of sodium and potassium is conflicting, and statements can be found to the effect that there exist, or probably exist, molecules of NaK, Na_2K, NaK_2, and Na_nK, where n is greater than 1.45. The fact that Na_2K has been reported for the solid alloys may have influenced some of those who considered this problem. Reference has been found for two investigations on the diffraction of x-rays by the liquid alloys. The work of Banerjee[9] made use of filtered radiation, and the position of the main peak in the diffraction pattern was plotted as a function of alloy composition with the positions of the peaks for pure Na and pure K being taken from the work of Keesom. An inflection in this curve was interpreted as indicating the presence of Na_2K molecules. In the second investigation with x-rays, Heaps[10] sought in vain to find a change in the diffraction pattern to supply information regarding the change of resistance of the alloy in the presence of a magnetic field. It may be noted that for alloy of a given composition, Heaps found the main diffraction peak to occur at 9°30′, whereas Banerjee found it to occur at 11°28′.

EXPERIMENTAL

Alloy samples were prepared in thin-walled cylindrical Pyrex glass tubes of diameters from 1 mm to 3 mm chosen appropriately for the particular composition under study. Sodium and potassium cleaned in the manner used in earlier work[11] were introduced into an evacuated mixing chamber, shaken vigorously, and then poured partly into the thin-walled sample tube and partly into a side tube to supply material for the spectroscopic determination of composition of the alloy. The spectroscopist in charge of making this determination states that the percentage composition of the several alloys is known to within better than 2 percent

[1] F. Zernike and J. Prins, Z. Physik **41**, 184 (1927).
[2] P. Debye and H. Menke, Ergeb. d. Tech. Rontgenk. II (1931).
[3] N. S. Gingrich, Revs. Modern Phys. **15**, 90 (1943).
[4] B. E. Warren and N. S. Gingrich, Phys. Rev. **46**, 368 (1934).
[5] G. G. Harvey, J. Chem. Phys. **6**, 111 (1938).
[6] E. E. Bray and N. S. Gingrich, J. Chem. Phys. **11**, 351 (1943).
[7] B. E. Warren, J. Appl. Phys. **8**, 645 (1937).
[8] References to work on these properties can be found in the *Liquid-Metals Handbook* (Atomic Energy Commission and Department of Navy, 1950).
[9] K. Banerjee, Ind. J. Phys. **3**, 399 (1929).
[10] C. W. Heaps, Phys. Rev. **48**, 491 (1935).
[11] F. H. Trimble and N. S. Gingrich, Phys. Rev. **53**, 278 (1938).

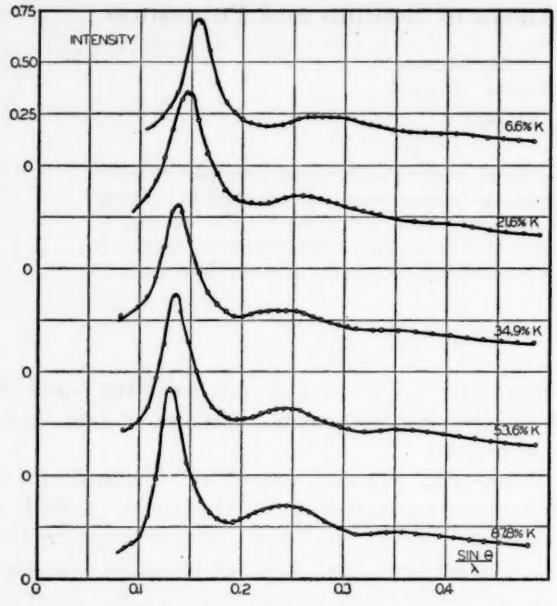

FIG. 1. Intensity *vs* $(\sin\theta)/\lambda$ for liquid alloys of sodium and potassium at 115°C for the compositions (atom percent) 87.8 percent K, 53.6 percent K, 34.9 percent K, 21.6 percent K, and 6.6 percent K.

in all cases. The cylindrical sample placed in a heater block at the center of a cylindrical camera was maintained at a temperature of 115°C (within 5°) in all cases. Two of the cameras used had radii of 9.20 cm and the third had a radius of 8.85 cm. Elaborate shielding protected the film from stray radiation. X-rays from a molybdenum target tube were monochromated by reflection from a rocksalt crystal to give a beam of wavelength 0.710A, and this beam passed through collimating slits to the sample and finally through a hole in the film to avoid scattering by the film. To keep the beam relatively free of short wavelength x-rays from second-order reflection, the x-ray tube was operated at a voltage less than 40 kv.

Two or more patterns were taken of each alloy, and seven different compositions in addition to samples of each of the two pure metals were studied. Microphotometering the films provided a measure of the intensity of x-rays as a function of the scattering angle, and the intensity patterns finally used were averages of duplicates. Since the patterns for the pure metals were closely identical to those previously obtained, they were not analyzed further, but the patterns for five alloys were corrected for absorption, polarization, and incoherent radiation as described elsewhere[3] in preparation for making a Fourier analysis of these determination. The uncorrected intensity curves are shown in Fig. 1, each one showing a fairly sharp main peak, a broad second peak, and a very weak indication of a broad third peak. The positions of the main peak as a function of alloy composition for seven alloys and the pure metals are plotted in Fig. 2 along with the values reported by Banerjee.

ANALYSIS OF PATTERNS

If in a liquid consisting of two kinds of atoms, the coherent scattering of both is very nearly the same, or if the coherent scattering of one is negligibly small, the analysis of the patterns may proceed essentially as in the case of a monatomic liquid without serious error, but when atoms such as sodium and potassium are mixed, the different contribution of each kind of atom must be taken into account. By introducing the concept of an average structure factor per electron and assuming that the structure factor for any atom is linearly proportional to this average electron structure factor, Warren, Krutter, and Morningstar[12] extended the simple theory to be applicable in this approximate form to molecular liquids. The equation they derive is

$$\sum 4\pi r^2 K_m \rho_m(r) = 4\pi r^2 \rho_0 \sum Z_m + \frac{2r}{\pi}\int_0^\infty si(s)\sin rs\,ds, \quad (1)$$

where $\sum$ denotes summation over all the atoms of the molecule; $\rho_m(r)$ = density of atoms of type m at a distance r from a given atom; f_m = atomic scattering factor of atom of type m; $f_e = \sum f_m / \sum Z_m$, the average f per electron; Z_m = atomic number of type m atom; $K_m = (f_m/f_e)$ average; $s = (4\pi \sin\theta)/\lambda$; 2θ = scattering angle; $i(s) = (I_e - \sum f_m^2)/f_e^2$; I_e = coherent scattering per molecule in electron units.

In the present case, the molecular structure of each alloy is considered unknown, and hence the average structure factor per electron is arbitrarily taken to be $f_e = (af_{Na} + bf_K)/(aZ_{Na} + bZ_K)$, where "$a$" is the atom fraction of sodium and "b" is the atom fraction of potassium. Similarly, it is assumed that $\sum f_m^2 = af_{Na}^2 + bf_K^2$, and the incoherent intensity is taken to be the sum of that due to sodium and that due to potassium in their respective proportions. With these assumptions

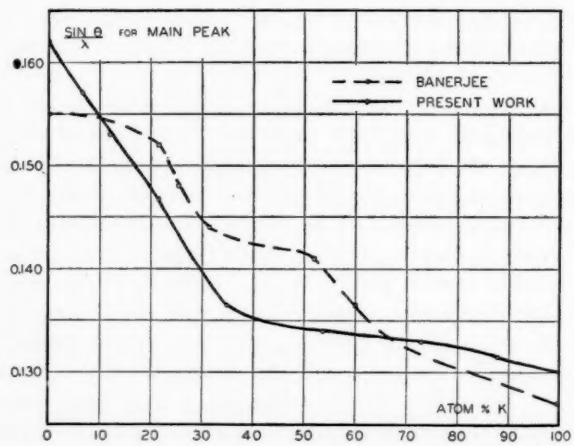

FIG. 2. Curves showing the position of the maximum of the first intensity peak as a function of alloy composition. Solid curve shows results of present work; dashed curve shows results reported by Banerjee.

[12] Warren, Krutter, and Morningstar, J. Am. Ceram. Soc. 19, 202 (1936).

it is then possible to proceed with the critical process of fitting the curve for independent coherent radiation to the corrected experimental curve, thus effectively putting it in electron units of intensity. The function $i(s)$ can then be determined, and with the aid of prepared cards and a planimeter the integral of Eq. (1) can be evaluated for a given value of r. One such operation supplies one point on the distribution curves of Fig. 3.

DISCUSSION OF RESULTS

The intensity curves of Fig. 1 are generally similar to those for the pure metals except for the locations of the peaks of intensity. In order to compare the results of the present work with that of Banerjee, Fig. 2 shows the position of the main peak as a function of alloy composition as determined in the two investigations. In the dashed curve showing Banerjee's results, the two end points were taken from work done by Keesom,[13] and it seems possible that slight differences in the techniques used in the different laboratories might account for irregularities in the curve near its two ends. But in this curve, from 30 to 50 atom percent K, the plateau depends heavily upon the accuracy of the one determination made for the 52 percent K alloy, and the claim made for the existence of Na_2K molecules was based upon the occurrence of this plateau at about the right composition to lend support to this hypothesis. In the present work, the curve of $(\sin\theta)/\lambda$ for the main peak as a function of alloy composition appears to be fairly well represented by two straight lines that intersect somewhere near 35 atom percent K. The fact that this occurs at approximately the same composition as Na_2K suggests that this may constitute significant evidence in support of the notion that this kind of molecule may occur in these alloys, but it should be pointed out that the relatively large contribution in intensity due to potassium as compared to sodium would tend to emphasize characteristics of the pattern due to potassium. Hence, it appears that the shape of the solid curve of Fig. 2 cannot be taken to supply unambiguous evidence for or against the existence of molecules in these liquid alloys. Finally, it can be noted that the value of $(\sin\theta)/\lambda$ obtained by Heaps (0.117) is less than that for pure potassium and cannot be plotted conveniently on Fig. 2. However, in his work he was primarily interested in detecting a change in the peak rather than in making an accurate determination of its position.

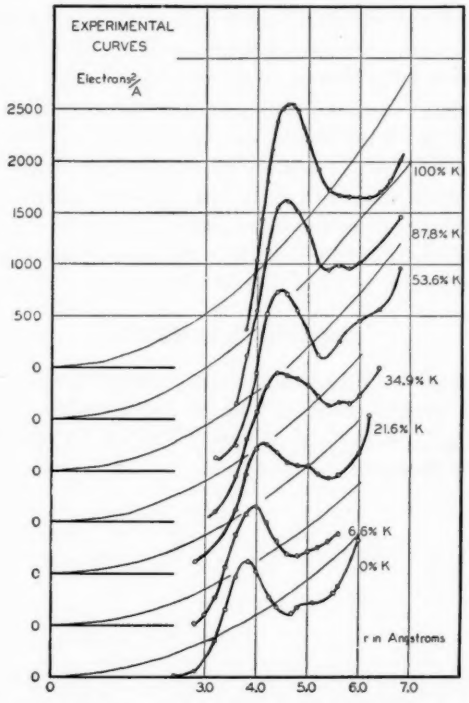

FIG. 3. Distribution curves showing $\Sigma 4\pi r^2 K_m \rho_m(r)$ in electrons²/A as a function of distance r in angstroms from origin for liquid alloys of sodium and potassium for the compositions (atom percent) of 0 percent K, 6.6 percent K, 21.6 percent K, 34.9 percent K, 53.6 percent K, 87.8 percent K, and 100 percent K. With each heavy curve showing the distribution as determined, there is a light parabolic curve for uniform average density of the sample.

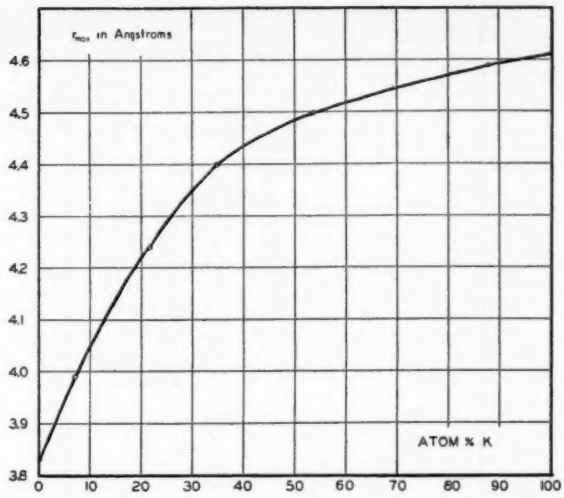

FIG. 4. Curve showing position r_{max} of the highest point in the first peak of the distribution curves for liquid alloys of sodium and potassium as a function of alloy composition.

Figure 3 presents a nest of distribution curves for pure sodium, alloys (in atom percent of potassium) of 6.6 percent, 21.6 percent, 34.9 percent, 53.6 percent, and 87.8 percent, and pure potassium as obtained with the aid of Eq. (1) above. The area under the curve between r and $r+dr$ gives a measure of the scattering matter at distance r from any given atom. Curves for the five alloys are presented for the first time, but for the pure metals the results of previous analyses[11, 14] were taken since the intensity patterns for them were closely the same as those taken in the earlier work. The positions of the maxima of the first peak of each curve

[13] W. H. Keesom, Proc. Roy. Acad. Amsterdam **30**, 341 (1927).

[14] C. D. Thomas and N. S. Gingrich, J. Chem. Phys. **6**, 659 (1938).

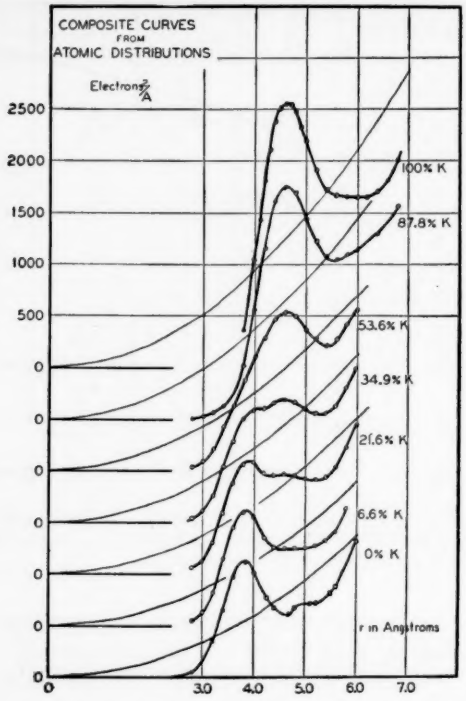

FIG. 5. Distribution curves for pure sodium and pure potassium shown together with composite curves obtained simply by adding the curves for sodium and potassium in proportionate amounts for the alloys for which experimentally determined curves are shown in Fig. 3.

are shown graphically in Fig. 4. The type of regularity is somewhat similar to that for the position of the first intensity peak shown in Fig. 2, but in general, the shape of the distribution curve is dependent upon the entire diffraction pattern rather than solely on the first intensity peak.

It is important to note that in the curves of Fig. 3 there appears to be no tendency in any of the alloys toward a discrete first peak as occurred, for example, in the case of liquid chlorine.[15] This can be taken as evidence that in these alloys there are no tightly bound molecules for which the distances between atoms in a molecule are considerably smaller than distances between atoms that are not in the same molecule. However, if there were some weak association of atoms into clusters of preferred grouping such that the interatomic distances within the group were only a few percent smaller than those occurring between atoms not in the same cluster, this analysis could neither establish nor deny their existence.

The distribution curves give a measure of how frequently various distances between scattering centers occur. In pure sodium, for example, one can think in terms of the average number of sodium atoms separated by a given distance. In the case of alloys, one would have distances between sodium atoms, distances between potassium atoms, and also distances between sodium and potassium atoms. The distribution curve for the alloy would therefore not be simply a proportionate superposition of the analogous curves for sodium and for potassium, but it is interesting to see how similar a composite curve is to the experimentally determined curve. This composite curve is shown in Fig. 5 and the rough similarity between these curves and those of Fig. 4 can be noted.

[15] C. C. Gamertsfelder, J. Chem. Phys. **9**, 450 (1941).

SUMMARY

Monochromatic x-ray diffraction patterns of seven liquid alloys of sodium and potassium at 115°C show locations of the main intensity peak which differ from those of previous work and whose positions, plotted as a function of alloy composition, give a curve that fails to show an inflection upon which it had been concluded earlier that Na_2K molecules exist in these alloys. While work of this kind would not disclose the existence of very weakly bound molecules or clusters whose interatomic distances are nearly the same as distances between atoms not in the same grouping, the five patterns analyzed definitely show that no permanent compact molecules exist in those liquid alloys.

ACKNOWLEDGMENT

It is a pleasure to acknowledge support for this work through grants made to one of the authors (N.S.G.) from the University of Missouri Research Council and from the Research Corporation.

Microwave Absorption and Molecular Structure in Liquids. IX. Measurement in Organic Halides at 10-Cm Wavelength*†

F. H. Branin, Jr.‡ and C. P. Smyth
Frick Chemical Laboratory, Princeton University, Princeton, New Jersey
(Received March 18, 1952)

The results of a systematic investigation of dielectric dispersion and absorption in the microwave region are discussed. Simple relations between the complex dielectric constant of an absorptive medium and the complex propagation constant of an electromagnetic wave within the medium are discussed in connection with a new interferometric method for measuring wavelength and absorption index directly within the medium. Results of measurements made at 10 cm wavelength by this method on twenty-five liquid organic halides are reported. The data of the present and previous measurements on these compounds are discussed in terms of distributions of relaxation times and, on the basis of absolute rate theory, the processes of dipole orientation and viscous flow in these liquids are compared.

INTRODUCTION

As part of a systematic investigation of the phenomena of dielectric dispersion and absorption in the microwave region,[1–8] this paper reports the results of a series of measurements made at a wavelength of 10 cm on twenty-five liquid organic halides. The purpose of the investigation was to apply recently developed techniques to the problem of determining the complex dielectric constants of polar liquids and so to obtain a large body of experimental data on dielectric dispersion and absorption in a region of the frequency spectrum which had previously been but little explored. Measurements were made at wavelengths of 1.27 cm,[2] 3.22 cm,[3] and 10.00 cm[1] on the homologous straight-chain alkyl bromides up to *n*-octadecyl bromide and certain other alkyl and aryl bromides over a temperature range from 0° to 75°. The static dielectric constants (at 520 kc), refractive indices, viscosities, and densities of these compounds were also measured.[6] Two new microwave methods of measurement were developed during the course of this work for use with both high loss and low loss media.†[3,6,9] The method used to obtain the results presented herein was based upon the measurement of the standing-wave pattern within the dielectric medium occupying a short-circuited section of coaxial transmission line. Since a detailed description of this method is to be published elsewhere, only a brief outline of the principles involved will be given here.

At microwave frequencies, since both storage and dissipation of electrical energy are involved when a wave is propagated through a polar dielectric, it is necessary to describe the dielectric properties of the medium in terms of a complex dielectric constant, $\epsilon^*=\epsilon'-j\epsilon''$, where ϵ' is the dielectric constant in its usual sense and ϵ'' is the dielectric loss factor. Because the complex dielectric constant cannot be measured directly when microwave propagation techniques are used, it becomes necessary to calculate ϵ^* from the complex propagation constant of the wave within the medium. The complex propagation constant for a wave traveling along the coordinate x in an absorptive medium is defined (in terms of the electric field component of a plane wave) by the equation $E=E_0e^{-\gamma x}=E_0e^{-\alpha x}\cdot e^{-j\beta x}$, where E_0 is an amplitude constant and $\gamma=\alpha+j\beta$ is the complex propagation constant; α is the attenuation constant and β is the phase constant. Since the wavelength, λ_d, within the medium is the distance between two points differing in phase by 2π radians, it follows that $\lambda_d=2\pi/\beta$. Using these definitions, it may be shown that for an absorptive dielectric, of zero magnetic susceptibility, which completely fills a waveguide or transmission line, the dielectric constant and loss factor may be calculated from the relations

$$\epsilon'=(\lambda_0/\lambda_d)^2[1-(\alpha/\beta)^2]+(\lambda_0/\lambda_c)^2, \quad (1)$$

and

$$\epsilon''=(\lambda_0/\lambda_d)^2[2\alpha/\beta], \quad (2)$$

where λ_0 is the free space wavelength and λ_c is the cut-off wavelength of the particular mode of wave-guide propagation in vacuum. For the fundamental (TEM) mode of propagation in coaxial transmission lines, the cut-off wavelength, λ_c, is infinite and so the second term of Eq. (1) vanishes. In this case, it is apparent that Eqs. (1) and (2), which now apply also to the plane

* This research was supported by the Office of Naval Research. Reproduction, translation, publication, use, and disposal in whole or in part by or for the United States Government is permitted.

† This paper is based upon a dissertation presented in January, 1950, by Franklin H. Branin, Jr., to the faculty of Princeton University in candidacy for the degree of Doctor of Philosophy.

‡ Present address: Los Alamos Scientific Laboratory, University of California, Los Alamos, New Mexico.

[1] Heston, Hennelly, and Smyth, J. Am. Chem. Soc. **70**, 4093 (1948).
[2] H. L. Laquer and C. P. Smyth, J. Am. Chem. Soc. **70**, 4097 (1948).
[3] Hennelly, Heston, and Smyth, J. Am. Chem. Soc. **70**, 4102 (1948).
[4] W. M. Heston, Jr. and C. P. Smyth, J. Am. Chem. Soc. **72**, 99 (1950).
[5] Heston, Hennelly, and Smyth, J. Am. Chem. Soc. **72**, 2071 (1950).
[6] Heston, Franklin, Hennelly, and Smyth, J. Am. Chem. Soc. **72**, 3443 (1950).
[7] Franklin, Heston, Hennelly, and Smyth, J. Am. Chem. Soc. **72**, 3447 (1950).
[8] Curtis, McGeer, Rathmann, and Smyth, J. Am. Chem. Soc. **74**, 644 (1952).
[9] W. H. Surber, Jr., J. Appl. Phys. **19**, 514 (1948).

wave propagation, become the microwave counterparts of the well-known optical relations,

$$\epsilon' = n^2(1-\kappa^2), \tag{3}$$

and

$$\epsilon'' = n^2(2\kappa), \tag{4}$$

or in complex form,

$$\epsilon^* = (n^*)^2 = [n(1-j\kappa)]^2, \tag{5}$$

where $n=\lambda_0/\lambda_d$ is the refractive index and $\kappa=\alpha/\beta$ is the absorption index.

EXPERIMENTAL METHODS

Of the numerous methods known for determining the complex dielectric constant at microwave frequencies,[1,2,6,9,10–16] those involving measurements made external to the dielectric medium require the use of unwieldy equations, whereas the direct measurement of absorption index and wavelength within the medium permits the use of Eqs. (1) and (2). The present technique, using an interferometric null method and a traveling probe immersed in the dielectric occupying a slotted section of coaxial line, permits both κ and λ_d to be measured directly and accurately, even in highly absorptive liquids. Three variations of this technique have been developed, two for measurements in high loss dielectrics and the third for measurements in low loss media.

Traveling Wave Method

When the dielectric-filled slotted line is terminated in a matched load so that no reflected wave is present, the traveling probe signal varies as $e^{-\alpha x}\cdot e^{-j\beta x}$ with increasing displacement away from the microwave generator, thus reproducing in relative amplitude and relative phase the characteristics of the incident or traveling wave. Using the apparatus indicated in Fig. 1, with a matched termination in place of the short circuit shown for the slotted line, both κ and λ_d can be measured absolutely and simultaneously by the following procedure.† The probe is first set at some convenient position and a null is then produced in the receiver by adjusting the phase and amplitude of the reference signal so that the signal from the probe is exactly canceled. The probe is next moved along the slotted line to a new position one wavelength away where an amplitude adjustment alone, either in the reference or probe signal channel, suffices to restore the null. If the amplitude adjustment be made without change of phase, then the probe displacement will be exactly one wavelength, λ_d, while the amplitude change will be exactly $e^{\alpha\lambda_d}$ or $e^{2\pi\kappa}$.

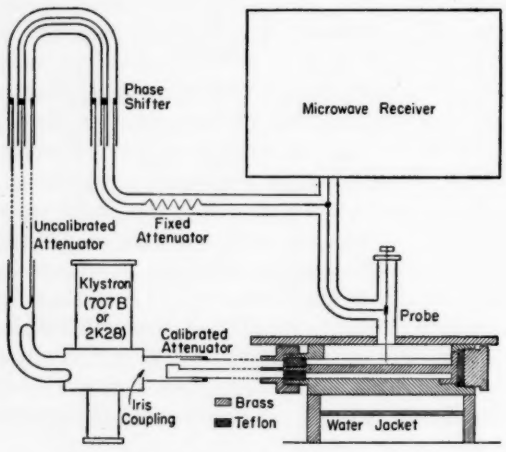

FIG. 1. Functional diagram of apparatus.

In order to provide a means of changing amplitude without change of phase, a piston attenuator[17–21] must be used, preferably placed in the probe signal channel so that the null-detection sensitivity, which is determined by the reference signal level, is kept constant. The piston attenuator consists of a traveling pick-up loop inside a wave guide which is operated beyond cut-off so that the wavelength is infinite and the phase constant zero. At the same time, the attenuation is exponential; hence, the pick-up loop displacement, y, required to restore the second null, is directly proportional to the absorption index according to the equation

$$\kappa = y(1/\lambda_c^2 - 1/\lambda_0^2)^{\frac{1}{2}} = 0.01831A, \tag{6}$$

where λ_c is the cut-off wavelength of the attenuator in vacuum and A is the attenuation in decibels.

With the traveling wave method, the measurements of both κ and λ_d are absolute because only linear displacements of the probe and of the pick-up loop are involved. Moreover, because of the sharpness of the null and the sensitivity of the receiver, excellent precision is obtained with respect to both the probe setting and the attenuator adjustment. However, the impracticability of constructing a matching termination suitable for use with the wide variety of materials to be investigated made it necessary to terminate the slotted line with a short circuit and base the measurements on the resulting standing wave pattern.

Standing Wave Method

The standing wave method, which is basically similar to the method reported by Drude[10] and by Brown,

[10] P. Drude, Z. physik. chem. **23**, 267 (1897).
[11] S. Roberts and A. von Hippel, J. Appl. Phys. **17**, 610 (1946).
[12] Brown, Hoyler, and Bierwerth, *Radio Frequency Heating* (D. Van Nostrand Company, Inc., New York, 1947), p. 218.
[13] C. G. Montgomery, "*Technique of Microwave Measurements*" (McGraw-Hill Book Company, Inc., New York, 1948), Chapter 10.
[14] T. W. Dakin and C. N. Works, J. Appl. Phys. **18**, 789 (1947).
[15] W. H. Surber, Jr. and G. E. Crouch, Jr., J. Appl. Phys. **19**, 1130 (1948).
[16] Collie, Hasted, and Ritson, Proc. Phys. Soc. (London) **60**, 145 (1948).
[17] D. E. Harnett and N. P. Case, Proc. Inst. Radio Engrs. **23**, 57 (1935).
[18] R. E. Grantham and J. J. Freeman, Am. Inst. Elec. Engrs., Technical Paper 4–50 (1947); Elec. Eng. **67**, 535 (1948).
[19] J. J. Freeman, J. Research Natl. Bur. Standards, **40**, 235 (1948).
[20] H. A. Wheeler, Monograph No. 8 (1949), Wheeler Laboratories, Great Neck, New York.
[21] C. G. Montgomery, reference 14, Chap. 11.

Hoyler, and Bierwerth,[12] incorporates a modification of the null technique previously described and can be used with the apparatus of Fig. 1. Assuming that the resistance of the short circuit termination for the slotted line is zero, it may be shown that the relative power, p, of the standing wave, as detected by the probe at a given distance, d, from the short circuit is given by the equation

$$p=\cosh 2\alpha d-\cos 2\beta d=\cosh 4\pi\kappa z-\cos 4\pi z, \qquad (7)$$

where $z=d/\lambda_d$ is the distance in wavelengths. Figure 2 illustrates this standing wave pattern for two different values of κ. From the figure, it is apparent that the absorption index can be uniquely determined from the power standing wave ratio, PSWR, defined as the ratio of the power at the first maximum to that at the first minimum from the short circuit. PSWR in decibels is determined by the substitution method[22] using the calibrated piston attenuator of Fig. 1; κ is then evaluated graphically using a curve calculated from Eq. (7).† Corrections for the finite resistance of the short circuit are then made nomographically.†

Since the minima of Fig. 2 are not spaced at integral half-wavelengths and since they cannot be located with adequate precision, particularly in high loss dielectrics, they are unsatisfactory for the determination of λ_d. However, by a proper application of the null technique, involving rapidly converging successive approximations, accurate measurements of wavelength can be made. Clearly, the validity of the λ_d measurement depends upon an exact correspondence between a one-wavelength displacement of the probe and a 360° phase shifted in the probe signal. This correspondence condition is fulfilled only for certain sets of points along the line where the incident and reflected electric waves are either in phase or out of phase.† Of four possible such sets of points, the set $z=N+\frac{1}{2}$, where $N=0, 1, 2, 3\cdots$, is best.

The object of the procedure for measuring λ_d is to establish the location of several points of this set by successive approximations, starting with the estimated position of the point $z=\frac{1}{2}$ obtained by applying a suitable correction factor to the measured position of the first minimum. Starting with the probe at the estimated $z=\frac{1}{2}$ point, a null is produced by proper adjustment of the reference signal. The probe is then moved into the region of the third minimum to a point where the null is restored by adjusting only the amplitude of the reference signal.§ The probe is next moved to the vicinity of the fifth minimum and the null again restored in like manner; the measurement may be repeated at succeeding odd minima as desired.

The distances between these null points are compared and, if the null points actually correspond to the points

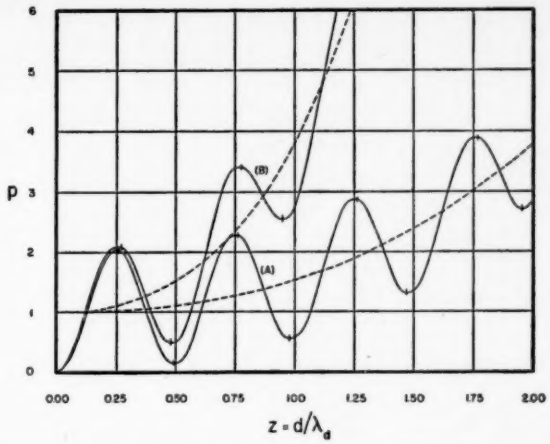

FIG. 2. Power standing wave pattern in short-circuited line filled with an absorptive dielectric. (A) $\kappa=0.08$; (B) $\kappa=0.16$. (Dashed line is $\cosh 4\pi\kappa z$.)

of the set $z=N+\frac{1}{2}$, then these distances will be equal. In such a case, λ_d is determined precisely. If the original probe setting was not exactly at the point $z=\frac{1}{2}$, successive null points will be spaced at unequal distances which, however, converge toward the correct value of λ_d.† Judging from the trend of this convergence, the initial probe setting may be corrected and a better approximation obtained. Usually, the desired precision is obtained after two or three trials.

In low loss media, ($\kappa<0.02$ or PSWR>25 db) the wavelength may be determined accurately enough from the distances between minima so that the null technique is unnecessary. At the same time, it is convenient to determine the absorption index from the breadths of successive minima.† In this method, the breadths of the minima, measured at some chosen multiple of the minimum standing wave power, are plotted as a function of distance from the short circuit. The absorption index is readily calculated from the slope of the line so obtained† and the short circuit resistance may be determined from the intercept.[6,7,23]

APPARATUS

Figure 1 is a functional diagram of the apparatus used for the present measurements. The dielectric-filled coaxial slotted line was machined from brass stock and then plated with gold to increase its conductivity and corrosion resistance. The center conductor was removable and carried either a short circuit termination, for use with the standing wave method, or a connector for attaching a matching device for use with the travelling wave method. Polytetrafluoroethylene ("Teflon") plugs were used to support the center conductor and to provide liquid tight seals. The ways for guiding the probe carriage were carefully machined and ground parallel to the center conductor to insure constant probe depth; the probe carriage was driven by a precision micrometer screw. The slotted

[22] C. G. Montgomery, reference 14, pp. 808–812.

§ In the standing wave method, it is preferable to vary the signal level of the reference signal rather than that of the probe signal in order to maintain null-detection sensitivity (see †).

[23] C. G. Montgomery, reference 14, pp. 505, 637.

TABLE I. Dielectric constants and dielectric loss factors at 10.00 cm.

	ϵ'					ϵ''				
	1.0°	25.0°	40.0°	55.0°	75.0°	1.0°	25.0°	40.0°	55.0°	75.0°
Ethyl bromide	10.20	9.24	...	...	...	0.80	0.60	...	...	...
n-Propyl bromide	8.57	7.97	7.48	7.06	...	0.93	0.66	0.53	0.44	...
i-Propyl bromide	9.88	9.33	8.86	8.30	...	1.02	0.69	0.55	0.46	...
n-Butyl bromide	7.18	6.74	6.44	6.20	...	1.15	0.79	0.63	0.51	...
i-Butyl bromide	7.38	6.90	6.60	6.24	...	1.07	0.74	0.59	0.46	...
s-Butyl bromide	9.52	8.75	8.30	7.90	...	1.46	0.98	0.78	0.62	...
n-Amyl bromide	6.15	5.95	5.77	5.58	5.27	1.10	0.79	0.63	0.51	0.38
n-Hexyl bromide	5.25	5.20	5.17	5.14	...	1.06	0.91	0.75	0.61	...
n-Heptyl bromide	4.57	4.53	4.50	4.47	4.42	1.06	0.86	0.75	0.67	0.51
n-Octyl bromide	4.10	4.14	4.17	4.18	...	0.97	0.84	0.75	0.67	...
n-Nonyl bromide	3.77	3.86	3.91	3.93	3.88	0.92	0.81	0.73	0.65	0.55
n-Decyl bromide	3.42	3.52	3.54	3.54	3.53	0.73	0.57	0.50	0.45	0.38
n-Dodecyl bromide[a]	3.00	3.20	3.26	3.29	3.28	0.64	0.58	0.55	0.50	0.40
n-Dodecyl bromide[b]	3.10	3.27	3.32	3.32	3.27	0.65	0.57	0.52	0.45	0.39
n-Dodecyl bromide[c]	3.25	3.36	3.40	3.40	3.40	0.66	0.57	0.49	0.41	0.41
n-Tetradecyl bromide[b]	...	3.08	3.10	3.11	3.26	...	0.53	0.45	0.40	0.29
n-Hexadecyl bromide	...	2.96	3.00	3.02	3.04	...	0.38	0.34	0.30	0.25
n-Octadecyl bromide	...	2.78	2.83	2.88	2.93	...	0.33	0.29	0.25	0.22
n-Octyl chloride	4.35	4.43	4.40	4.32	4.22	0.90	0.68	0.59	0.52	0.41
Cyclohexyl bromide	7.57	7.42	7.24	7.02	6.68	2.24	1.70	1.42	1.16	0.91
Chlorobenzene	5.73	5.50	5.26	5.06	...	0.88	0.64	0.50	0.39	...
Bromobenzene	5.17	5.08	5.02	4.86	4.71	1.12	0.76	0.61	0.48	0.38
α-Chloronaphthalene	3.97	4.16	4.22	4.29	4.35	1.06	0.86	0.75	0.64	0.52
α-Bromonaphthalene	...	3.76	3.90	4.00	4.04	...	0.81	0.77	0.71	0.56
Ethylene chloride	11.12	9.98	9.27	8.63	...	1.60	1.00	0.75	0.57	...
Ethylene bromide	...	4.65	4.61	4.58	...	...	0.46	0.37	0.31	...
Tetramethylene chloride	9.40	9.06	8.70	8.30	7.75	1.84	1.21	0.90	0.67	0.48

[a] 8.75 cm. [b] 10.60 cm. [c] 12.74 cm.

line was thermostated by means of a water jacket, circulating pump, and constant temperature water bath.

The signal source, tunable from 8.7 to 12.7 cm, was a 707B or 2K28 klystron oscillator; the microwave receiver, tunable over the same band, was of the superheterodyne type and used a 707B or 2K28 klystron for its local oscillator. Sensitivity of the system at 10 cm was 70 db below the full output of the piston attenuator of Fig. 1. Amplitude and frequency stability of the signal source and receiver were maintained by the use of electronically regulated power supplies. In addition, the receiver design incorporated automatic frequency control.

In the measurement of λ_0 (in air) or of λ_d in lossless dielectrics,[4] a precision of about ± 0.01 percent was obtainable with slightly lower accuracy. Measurement of λ_d in medium or low loss dielectrics with an accuracy of ± 0.1 percent was possible using both the traveling wave and standing wave methods, but in more highly absorptive media, the accuracy was somewhat less. The probable error in PSWR was about ± 0.1 db, corresponding to an error in $\log\kappa$ of ± 0.5 percent. Thus, the minimum instrumental error in ϵ' was about ± 0.2 percent and that in ϵ'' about ± 1.4 percent.

EXPERIMENTAL RESULTS

Measurements on twenty-five organic halides, purified by methods previously described,[5] were made by the standing wave method at temperatures from 1° to 75°C. A wavelength of $\lambda_0 = 10$ cm was used except in the case of *n*-dodecyl bromide where measurements were made at wavelengths of 8.75, 10.60, and 12.74 cm to test the frequency coverage of the apparatus. The calculated values of ϵ' and ϵ'' are reported in Table I at temperatures of 1°, 25°, 40°, and 55° in conformity with the data reported in previous papers of this series. The 75° values are also included for the compounds measured at this temperature.

DISTRIBUTION OF RELAXATION TIMES

According to Debye's theory of polar dielectrics,[24] the complex dielectric constant at any radian frequency ω is given by an equation of the form

$$\epsilon^* = \epsilon' - j\epsilon'' = \epsilon_\infty + \frac{\epsilon_0 - \epsilon_\infty}{1 + j\omega\tau}, \tag{8}$$

where ϵ_0 is the static or low frequency dielectric constant and ϵ_∞ is the so-called infinite frequency dielectric constant, while τ is the observed relaxation time, assumed to be the same for all molecules of a given kind. It is found experimentally, however, that few substances conform to Eq. (8); in general, it becomes necessary to assume that a distribution of relaxation times, $G(\tau)$, exists.

In order to focus attention on the process of dipole orientation exclusively, it is convenient to set aside the contributions of electronic and atomic polarization by normalizing all the data relative to the quantity $\epsilon_0 - \epsilon_\infty$. Accordingly, we have adopted the notation of

[24] P. Debye, *Polar Molecules* (Dover Publications, New York, 1945).

Fuoss and Kirkwood[25] in defining a complex quantity, Q^*, as follows

$$Q^*=J-jH=\frac{\epsilon'-\epsilon_\infty}{\epsilon_0-\epsilon_\infty}-j\frac{\epsilon''}{\epsilon_0-\epsilon_\infty}. \tag{9}$$

When this quantity is plotted as a function of frequency in the complex plane, it permits data for many different compounds to be compared directly since the plots have the same scale: $0<J<1$ and $0<H<\frac{1}{2}$. One such plot is illustrated in Fig. 3; the necessary values for ϵ_∞ have been estimated from the refractive indices.[4] In Table II the maximum values of H for each compound are listed. The fact that most of these maxima are definitely less than $\frac{1}{2}$ indicates the validity of the assumption of finite distributions of relaxation times since only in the case of a unique τ will the H *vs* J plot be a semicircle with $H_{\max}=\frac{1}{2}$.

Because microwave dispersion and absorption are cognate effects of the finite rate of dipole orientation in an alternating field, ϵ' and ϵ'' are interdependent functions of frequency.[26,27] In terms of $G(\tau)$, this fact may be expressed by the equations[26]

$$J(\omega)=\frac{\epsilon'-\epsilon_\infty}{\epsilon_0-\epsilon_\infty}=\int_0^\infty \frac{G(\tau)d\tau}{1+\omega^2\tau^2}, \tag{10}$$

$$H(\omega)=\frac{\epsilon''}{\epsilon_0-\epsilon_\infty}=\int_0^\infty \frac{\omega\tau G(\tau)d\tau}{1+\omega^2\tau^2}, \tag{11}$$

or, using the substitutions $F(s)=\tau G(\tau)$, $s=\ln(\tau/\tau_0)$ and $x=\ln(\omega_0/\omega)$, where $\tau_0=1/\omega_0$ is the most probable relaxation time,

$$J(x)=\int_{-\infty}^{+\infty} \frac{F(s)ds}{1+e^{2(s-x)}}, \tag{12}$$

$$H(x)=\int_{-\infty}^{+\infty} \frac{e^{s-x}F(s)ds}{1+e^{2(s-x)}}. \tag{13}$$

If $J(x)$ and/or $H(x)$ be known as a function of frequency, it is possible in principle to determine $F(s)$ from Eqs. (12) and/or (13). In practice, however, because of the paucity of data at several different frequencies, only the broadest generalizations can be made about the distribution functions.

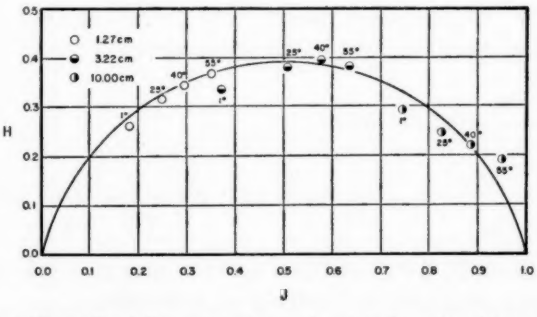

FIG. 3. Normalized dispersion-absorption data for *n*-hexyl bromide.

TABLE II. Maximum values of H.

	$H_{\max}$ 1.0°	25.0°	40.0°	55.0°
Ethyl bromide	0.44	0.45	...	...
n-Propyl bromide	0.44	0.43	0.45	0.48
i-Propyl bromide	0.49	0.50	0.49	0.50
n-Butyl bromide	0.40	0.43	0.43	0.44
i-Butyl bromide	0.44	0.48	0.48	0.50
s-Butyl bromide	0.47	0.49	0.49	0.48
t-Butyl bromide	0.47	0.48	0.49	0.50
n-Amyl bromide	0.38	0.39	0.41	0.41
n-Hexyl bromide	0.35	0.38	0.40	0.40
n-Heptyl bromide	0.36	0.36	0.37	0.37
n-Octyl bromide	0.35	0.34	0.35	0.36
n-Nonyl bromide	0.35	0.34	0.35	0.37
n-Decyl bromide	0.33	0.35	0.36	0.36
n-Dodecyl bromide	0.32	0.32	0.33	0.34
n-Tetradecyl bromide	0.37	0.35	0.33	0.35
n-Hexadecyl bromide	...	0.32	0.33	0.33
n-Octadecyl bromide	...	0.24	0.23	0.22
n-Octyl chloride	0.37	0.36	0.36	0.37
n-Octyl iodide	0.37	0.36	0.36	0.36
Cyclohexyl bromide	0.45	0.45	0.45	0.45
Chlorobenzene	0.45	0.46	0.47	0.48
Bromobenzene	0.45	0.46	0.47	0.48
α-Chloronaphthalene	0.39	0.44	0.47	0.48
α-Bromonaphthalene	...	0.40	0.40	0.42
Ethylene chloride	0.45	0.47	0.48	0.49
Ethylene bromide	...	0.41	0.43	0.45
Tetramethylene chloride	0.40	0.43	0.45	0.47

Of the four symmetrical distribution functions which have been proposed[25,28–31] those of interest for our purposes are the Cole and Cole function,[28] hereafter designated $C-C$,

$$F(s)=\frac{1}{2\pi}\frac{\sin\alpha\pi}{\cosh(1-\alpha)s-\cos\alpha\pi}, \tag{14}$$

and the Wagner-Yager function,[29,30] hereafter designated $W-Y$,

$$F(s)=\frac{b}{\pi^{\frac{1}{2}}}\exp(-b^2s^2), \tag{15}$$

in which α and b are adjustable breadth parameters. The H *vs* J curves corresponding to these two distribution functions are shown in Figs. 4 and 5. Although, as Kauzmann has pointed out,[32] the shapes of these distribution curves are similar there are certain criteria for distinguishing between them. For example, the limiting slopes of the H *vs* J curves differ at $x=\pm\infty$. In the case of the $C-C$ function, where the H *vs* J

[25] R. M. Fuoss and J. G. Kirkwood, J. Am. Chem. Soc. **63**, 385 (1941).
[26] H. Kramers, Atti Congr. dei Fisici, Como, 545 (1927).
[27] H. Fröhlich, *Theory of Dielectrics* (Oxford Press, London, England, 1949), pp. 4–9.
[28] K. S. Cole and R. H. Cole, J. Chem. Phys. **9**, 341 (1941).
[29] K. W. Wagner, Ann. Physik **40**, 817 (1913); Arch. Elektrotech. **3**, 83 (1914).
[30] W. A. Yager, Physics, **7**, 434 (1936).
[31] J. G. Kirkwood and R. M. Fuoss, J. Chem. Phys. **9**, 329 (1941).
[32] W. Kauzmann, Revs. Modern Phys. **14**, 12 (1942).

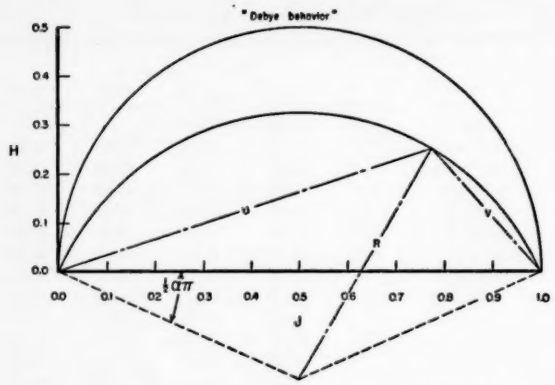

FIG. 4. Normalized dispersion-absorption curves for Cole and Cole distribution function.

curves are circular arcs defined by the equation[28]

$$Q^*=1/[1+(j\omega\tau)^{1-\alpha}], \tag{16}$$

the limiting slopes are always finite except when $\alpha=0$, in which case the Debye equation applies. The $W-Y$ function, on the contrary, leads to H *vs* J curves having infinite limiting slopes for all values of the parameter b as shown in Fig. 5. Another criterion for distinguishing between the $C-C$ and $W-Y$ functions is the relation between $H_{\max}$ and $(d\ln(v/u)/dx)_{\max}$ where the parameters v and u are defined in Fig. 4. These relations are shown in Figs. 6 and 7. Although Fig. 7 appears to provide the more sensitive distinction, actually it does not because the errors in evaluating $(d\ln(v/u)/dx)_{\max}$ are greater than those in evaluating $(dJ/dx)_{\max}$ as indicated by the equation

$$\left(\frac{d\ln(v/u)}{dx}\right)_{\max}=-\frac{(dJ/dx)_{\max}}{H_{\max}{}^2+1/4}. \tag{17}$$

A related criterion is based upon the relation[28]

$$v/u=(\omega\tau_0)^{1-\alpha}, \tag{18}$$

from which it follows that

$$\ln(v/u)=(1-\alpha)\ln\omega\tau_0=(\alpha-1)x. \tag{19}$$

Thus, a plot of $\ln(v/u)$ *versus* x or of $\log(v/u)$ *versus* $\log\lambda_0$ should give a straight line of slope $(\alpha-1)$ if the $C-C$ function applies.[7] Moreover, the value of α so obtained should agree with the observed value of $H_{\max}$ according to the equation

$$H_{\max}=\frac{1}{2}\frac{\cos(\alpha\pi/2)}{1+\sin(\alpha\pi/2)}. \tag{20}$$

Attempts to apply these criteria to the presently available data were unfortunately unsuccessful in making a clear distinction between the two functions because of insufficient frequency coverage.

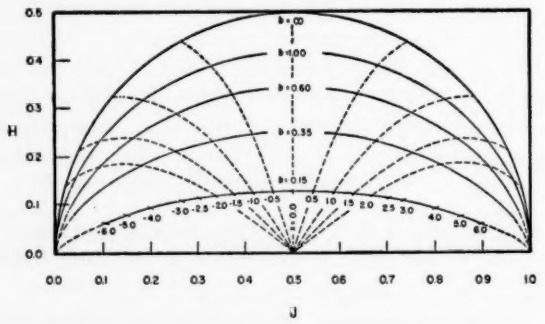

FIG. 5. Normalized dispersion-absorption curves for Wagner-Yager distribution function.

DIPOLE ORIENTATION AS A RATE PROCESS

Treating dipole orientation as a rate process, the Eyring rate equation[33] gives the relation for K, the number of times per second a dipole becomes sufficiently activated to surmount the free energy barrier, $\Delta F^\ddagger$ kilocalories per mole, separating a given orientation from an adjacent one

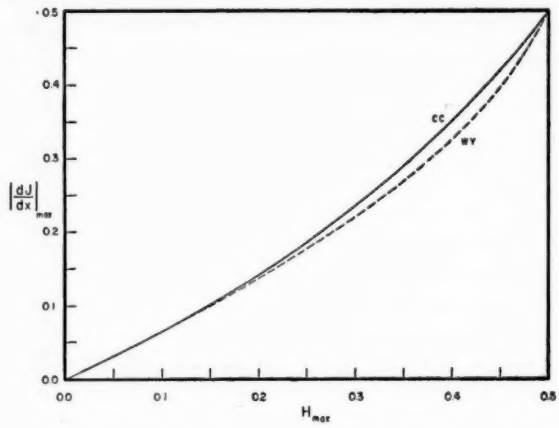

FIG. 6. Plot of $|dJ/dx|_{\max}$ *versus* $H_{\max}$ for Cole and Cole ($C-C$) and for Wagner-Yager ($W-Y$) distribution functions.

$$K=\frac{kT}{h}\exp(-\Delta F^\ddagger/RT). \tag{21}$$

Since the relaxation time is the reciprocal of K, it follows that the most probable relaxation time is

$$\tau_0=\frac{h}{kT}\exp(\Delta F_0^\ddagger/RT)$$
$$=\frac{h}{kT}\exp[(\Delta H_0^\ddagger/RT-\Delta S_0^\ddagger/R)], \tag{22}$$

where $\Delta F_0^\ddagger$, $\Delta H_0^\ddagger$, and $\Delta S_0^\ddagger$ are the most probable free energy, enthalpy and entropy of activation.

In calculating these thermodynamic quantities, the data for the organic halides[1-2,5] were used to obtain graphically from the H *vs* J plots the ratio v/u at each wavelength; plots of $\log(v/u)$ *versus* $\log\lambda_0$ were then

[33] H. Eyring, J. Chem. Phys. 4, 283 (1936).

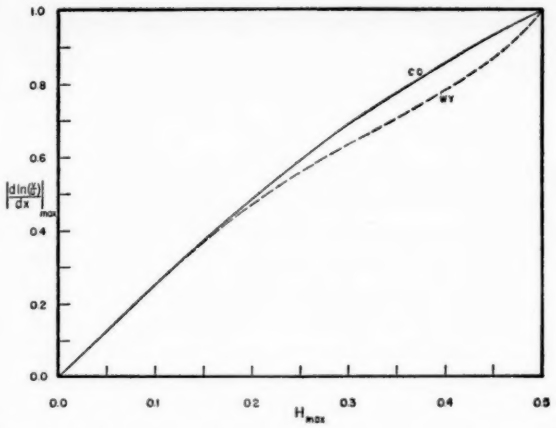

FIG. 7. Plot of $|d \ln(v/u)/dx|_{\max}$ *versus* $H_{\max}$ for Cole and Cole $(C-C)$ and for Wagner-Yager $(W-Y)$ distribution functions.

made and from the intersections of these curves with the ordinate $\log(v/u)=0$, the so-called "critical wavelengths," $\lambda_m=2\pi c/\omega_0=2\pi c\tau_0$, were determined. From these critical wavelengths, the most probable free energies of activation were calculated according to the equation

$$\Delta F_0^{\ddagger}=RT\ln\left(\frac{\lambda_m kT}{2\pi ch}\right)=2.303RT\log(0.1105\lambda_m T). \quad (23)$$

The most probable enthalpies of activation were then obtained from the average slopes of the curves of $\log(\lambda_m T)$ *versus* $1/T$ since it may be shown that

$$\Delta H^{\ddagger}_0=2.303Rd\log(\lambda_m T)/d(1/T). \quad (24)$$

Finally, the most probable entropies of activation were determined from the relation $\Delta F_0^{\ddagger}=\Delta H_0^{\ddagger}-T\Delta S_0^{\ddagger}$.

The critical wavelengths determined in this way agree well with those previously reported[3] except for some of the longer molecules where the 10 cm data, which were previously unavailable, require less extrapolation and therefore give more dependable results; the critical wavelengths are shown in Fig. 8 for the straight-chain bromides only. The free energies and enthalpies of

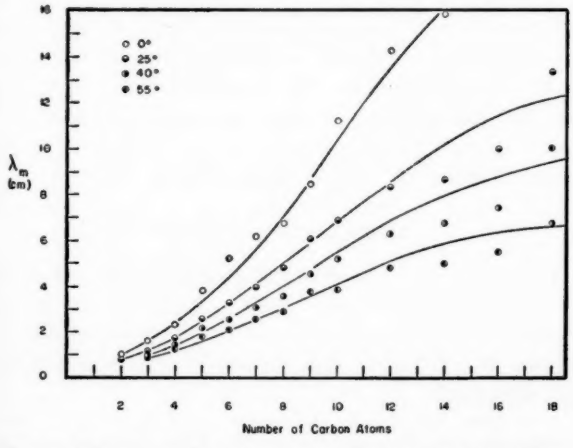

FIG. 8. Critical wavelengths for straight chain alkyl bromides.

TABLE III. Free energies and enthalpies of activation for dipole rotation (kcal/mole).

	$\Delta F_0^{\ddagger}$ 1.0°	25.0°	40.0°	55.0°	$\Delta H_0^{\ddagger}$
Ethyl bromide	1.86	1.89	...	...	1.53
n-Propyl bromide	2.11	2.13	2.17	2.22	1.30
i-Propyl bromide	1.97	2.04	2.09	2.16	1.05
n-Butyl bromide	2.30	2.38	2.42	2.46	1.49
i-Butyl bromide	2.21	2.31	2.38	2.44	1.01
s-Butyl bromide	2.22	2.27	2.32	2.38	1.24
t-Butyl bromide	2.11	2.17	2.23	2.26	1.33
n-Amyl bromide	2.58	2.62	2.67	2.70	1.92
n-Hexyl bromide	2.76	2.77	2.78	2.82	2.29
n-Heptyl bromide	2.86	2.89	2.91	2.94	2.36
n-Octyl bromide	2.90	3.00	3.00	3.02	2.29
n-Nonyl bromide	3.02	3.13	3.14	3.20	2.34
n-Decyl bromide	3.18	3.21	3.23	3.22	2.84
n-Dodecyl bromide	3.31	3.33	3.34	3.36	3.07
n-Tetradecyl bromide	3.36	3.35	3.39	3.40	3.21
n-Hexadecyl bromide	...	3.44	3.45	3.46	3.30
n-Octadecyl bromide	...	3.61	3.64	3.59	3.44
n-Octyl chloride	2.75	2.83	2.84	2.88	2.06
n-Octyl iodide	3.22	3.22	3.28	3.32	2.56
Cyclohexyl bromide	2.66	2.76	2.83	2.91	1.47
Chlorobenzene	2.44	2.47	2.48	2.52	2.06
Bromobenzene	2.71	2.75	2.78	2.82	2.24
α-Chloronaphthalene	3.10	3.18	3.24	3.28	2.16
α-Bromonaphthalene	...	3.48	3.51	3.55	2.84
Ethylene chloride	2.23	2.23	2.26	2.25	2.11
Ethylene bromide	...	2.73	2.71	2.58	4.03
Tetramethylene chloride	2.38	2.41	2.42	2.43	2.11

activation are given in Table III, while the free energies and entropies of activation are shown in Figs. 9 and 10 for the straight-chain bromides only.

These data, together with those of Table II, show some interesting features. Molecules not far from spherical in shape, such as those of isopropyl, isobutyl, sec.-butyl, and tert.-butyl bromides, have values of $H_{\max}$ closely approaching 0.5 and therefore have H *vs* J curves which are nearly semicircular, approximating Debye behavior. Accordingly, these molecules must have very narrow distributions of relaxation times and correspondingly narrow distributions of free energies of activation. The straight-chain molecules, on the other hand, have values of $H_{\max}$ which decrease somewhat regularly with increasing molecular size, a fact

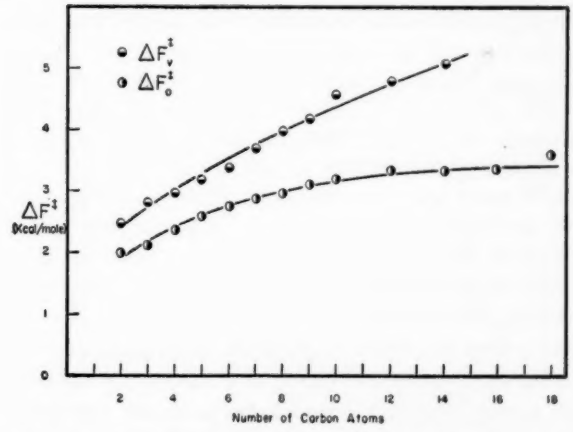

FIG. 9. Free energies of activation for dipole orientation and for viscous flow in straight chain alkyl bromides st 25°C.

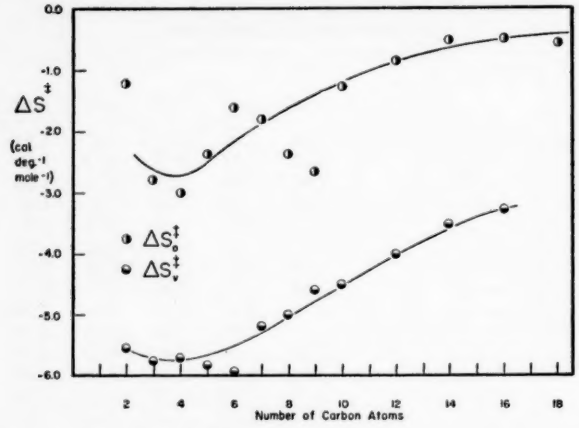

FIG. 10. Entropies of activation for dipole orientation and for viscous flow in straight chain alkyl bromides.

which indicates increasingly broad distributions both of relaxation times and of free energies of activation. These results are to be expected, since an increase of chain length gives rise not only to an increase in the number of degrees of freedom per molecule but also to an increase in the number of ways in which neighboring molecules can overlap and entangle each other. Both of these factors will greatly increase the total number of possible molecular configurations, and since each such configuration may be supposed to have, in general, a different free energy of activation for dipole orientation, it is logical to expect that a distribution of free energies will occur.

As might be expected, $\Delta F_0^{\ddagger}$ increases with chain length and decreases with approach to spherical shape, as in the case of the isomeric propyl and butyl bromides. Moreover, the distribution of free energies of activation decreases in breadth as the temperature rises, indicating that increasing thermal agitation favors a predominance of those configurations which have more nearly equal free energies of activation. At the same time, the most probable free energy of activation increases slightly with rising temperature, but there is no apparent explanation for this behavior.

In general, the most probable enthalpies of activation are less than the corresponding free energies so that, in every case but one, the most probable entropies of activation are negative. This finding is in disagreement with some of the earlier results,[3] but the errors involved in calculating the entropy values are so large that their general trend may be more important than their magnitude, or even their sign in the case of small values. Moreover, the arbitrary nature of a "most probable entropy of activation" as calculated by the procedure outlined above must be recognized for there is no assurance that the free energies and enthalpies of activation for each process of dipole orientation are paired in such a way that the actual most probable entropy of activation corresponds to that calculated.

The comparison of dipole orientation with the process of viscous flow[3] is based upon the Eyring equation,[34]

$$\eta = \frac{hN}{V} \exp(\Delta F_v^{\ddagger}/RT), \tag{25}$$

where N is Avogadro's number, V is the molar volume, and $\Delta F_v^{\ddagger}$ is the molar free energy of activation. Since viscous flow presumably involves not only translational motion but also rotational motion similar to that occurring in dipole orientation, it is to be expected that the free energies of activation for these two processes will show similar dependencies upon structure but with $\Delta F_v^{\ddagger}$ being larger than $\Delta F_0^{\ddagger}$ as shown in Fig. 9. Although the very nature of viscosity measurements precludes the possibility of obtaining direct evidence for the existence of distributions of free energies of activation, we may infer from the present dielectric measurements that such distributions do exist for viscous flow. Moreover, since translational motion is involved in addition to rotational motion, it is likely that these distribution functions for viscous flow will exhibit even greater breadth than do those for dielectric relaxation in a given substance.

Since it is known that there is a finite distribution of free energies of activation for dielectric relaxation, it is very probable that finite distributions of both enthalpies and entropies of activation also exist. Accordingly, certain molecular configurations will have either larger or smaller entropies of activation than the most probable (calculated) value while other configurations will have entropies of opposite sign. All that can be concluded from the present data, therefore, is that, at least for the smaller molecules, the most probable configurations involved in dipole orientation have negative entropies in the activated state. From this it follows that for these configurations the activated state is one of greater order than the normal state. This may be interpreted as indicating the existence of cooperative orientation of the molecules resulting either from steric forces or from dipole-dipole interactions, with the dipoles being more nearly aligned with each other in the activated state. As the molecular size increases, however, dipole-dipole interaction decreases because of the dilution effect of the hydrocarbon segments of the molecules; presumably, the cooperative orientation is likewise diminished so that the magnitude of the (calculated) negative entropy of activation decreases while its sign may even become positive.

ACKNOWLEDGMENT

The authors wish to acknowledge the assistance given by their colleagues on this project in purifying many of the materials. The assistance of D. M. Olson and L. C. Osborn in preparing the drawings is also gratefully acknowledged.

[34] Glasstone, Laidler, and Eyring, *The Theory of Rate Processes* (McGraw-Hill Book Company, Inc., New York, 1941), p. 544 *ff.*

The Time Dependence of the Potential in Electrode Reactions*

WILLIAM R. BUSING† AND WALTER KAUZMANN
Frick Chemical Laboratory, Princeton University, Princeton, New Jersey
(Received July 19, 1951)

Changes in the potential of an electrode with time during electrolysis at constant current are controlled by two factors: (1) the charging and discharging of the double layer capacitor (causing "capacitive" changes) and (2) alteration of the composition and other properties of the electrode and the adjacent solution (causing "non-capacitive" changes). Equations are derived for the capacitive changes in potential, assuming that the current-voltage relation across the electrode surface is given by Tafel's law.

An experimental study has been made of the potential accompanying the evolution of oxygen from 1N KOH at a platinum anode. When the current was held constant the potential increased slowly with time. When the current was interrupted the potential rapidly decreased, the decay being faster the higher the initial potential. The decay generally followed the above-mentioned equations for a capacitive change in potential, thus making it possible to evaluate effective Tafel constants of the electrode at various stages during electrolysis. These constants were found to depend very much on the time and on the current density, indicating that the electrode surface undergoes important changes. The behavior of the potential on increasing or decreasing the current has also been studied. This too reflects changes in the electrode surface.

Most of these variations can be understood if it is assumed that the electrode surface is non-uniform, the current being carried by relatively few active centers. The non-uniformity is similar to that encountered in ordinary catalysis, but is more complex since the same centers may not be active at all potentials. A simple graphical method of dealing with such a non-uniformity has been developed. It is based on the assumption that Tafel's law is valid for each microscopic element of the surface, and allows the Tafel constants to vary from one element to another. The electrode as a whole may then no longer obey Tafel's law. The concepts of poisoning and promotion, so important in catalysis, are readily incorporated and explain most of the observed results in a direct manner.

THE difference in potential at an electrode-electrolyte interface is not a function of the current density alone, but changes with time during the flow of the current.[1–6] Most theories of overvoltage[7–13] do not treat this time dependence explicitly; at best they discuss it in a qualitative manner. Much of the experimental data has been obtained by techniques which supposedly eliminate the factors responsible for the time dependence. In one common method a constant current is allowed to flow until the potential reaches a steady value. In another method the potential is measured at some definite time after turning on the current. Such methods obviously give an incomplete description of what is happening at the electrode.

This paper presents the results of an experimental and theoretical study of the time dependence of the potential for a typical electrode reaction.

PART I. EXPERIMENTAL OBSERVATIONS WITH PLATINUM ANODES IN AQUEOUS POTASSIUM HYDROXIDE

Apparatus and Method

The electrolysis was performed in a 120-ml Pyrex cell, the construction of which is shown in Fig. 1. The arms of a U-tube formed the anode and cathode compartments. At a point opposite the anode position a circulatory tube was cross-connected. Just above the anode a second tube was connected leading to the half cell compartment and to an overflow tube. A small glass propeller driven through the stirrer opening provided a continuous flow of the electrolyte through the circulation tube and past the electrode under study. This stirrer was operated throughout the experiments, although no evidence was obtained to indicate that stirring had any significant effect on the potential.

The salt bridge of a saturated calomel reference electrode, plugged with agar to prevent siphoning, was immersed in the electrolyte at the half cell opening. All potentials are reported with reference to this saturated

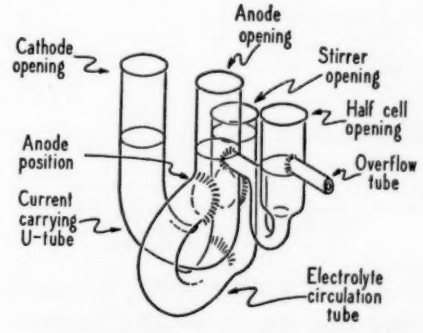

FIG. 1. The electrolysis cell.

* This article is based upon a thesis submitted by William R. Busing in partial fulfillment of the requirements for the degree of Doctor of Philosophy at Princeton University.

† Present address: Sterling Chemistry Laboratory, Yale University, New Haven, Connecticut.

[1] E. Baars, Sitzber. Ges. Beforder. ges. Naturw. Marburg **63**, 213 (1928).
[2] A. Hickling and F. W. Salt, Trans. Faraday Soc. **36**, 1226 (1940).
[3] J. H. Bartlett, Trans. Electrochem. Soc. **87**, 521 (1945).
[4] Y. M. Kolotyrkin, J. Phys. Chem. (USSR) **20**, 667 (1946); Chem. Abstracts **41**, 343d (1947).
[5] J. O'M. Bockris, Trans. Faraday Soc. **43**, 417 (1947).
[6] A. Hickling and S. Hill, Faraday Soc. Disc. **1**, 236 (1947).
[7] J. Tafel, Z. physik. Chem. **54**, 641 (1905).
[8] T. Erdey-Gruz and M. Volmer, Z. physik. Chem. **150**, 203 (1930).
[9] Eyring, Glasstone, and Laidler, J. Chem. Phys. **7**, 1053 (1939).
[10] G. E. Kimball, J. Chem. Phys. **8**, 199 (1940).
[11] Kimball, Glasstone, and Glassner, J. Chem. Phys. **9**, 91 (1941).
[12] Glasstone, Laidler, and Eyring, *The Theory of Rate Processes* (McGraw-Hill Book Company, Inc., New York, 1941).
[13] A. Hickling and F. W. Salt, Trans. Faraday Soc. **38**, 474 (1942).

calomel electrode without correction for the liquid junction potential, the "European" sign convention being followed. The reported potentials may be referred to the normal hydrogen electrode by adding 0.242 volt; this includes a correction of 0.007 volt for the junction potential of 1N KOH.

Connection of the reference electrode above the anode and out of the path of the current reduced the ohmic potential somewhat. The elimination of the remainder of this component was accomplished by the commutator method. No Luggin capillary was thus necessary.

Fresh electrolyte was continuously introduced into the cathode opening and withdrawn through the overflow tube at a rate of about 200 ml per hour. This flow also served to prevent the diffusion of the potassium chloride from the half cell to the anode compartment.

The cell was immersed in a thermostat and maintained at 20.0°C $\pm 0.1°$ throughout the experiments.

The circuit used for current supply and potential measurement was essentially that of the electronic commutator described by Hickling,[14] although a few modifications were made. The connections between the various units are shown in Fig. 2.

Current was supplied to the electrolysis cell from the 180-volt main battery which was connected in series with the interrupter and the milliammeter. The function of the interrupter was to break the circuit for calibrated time intervals ("off-times") ranging from 2×10^{-5} to 6×10^{-3} second. In order to measure the decay of the potential immediately following a decrease in the current density the interrupter was provided with a variable by-pass resistor so that a predetermined fraction of the current could be allowed to flow during the off-time. Current was measured with the milliammeter, which was provided with a calibrated shunt to permit readings up to 50 milliamperes.

The potentiometer together with the indicator served to measure the lowest value to which the potential fell during the off-time. A detailed description of the method is given elsewhere.[15] The potentiometer was connected in series with two cadmium cells to extend the range to 3 volts. A galvanometer was used with an external standard cell for calibration purposes. This instrument was also used to balance the potentiometer in the few cases in which direct readings were made. A switch was provided in the indicator circuit to make the necessary connections for this type of measurement. It was found that a 2-μf by-pass condenser was needed across the potentiometer circuit to prevent its interfering with the wave form of the transient.

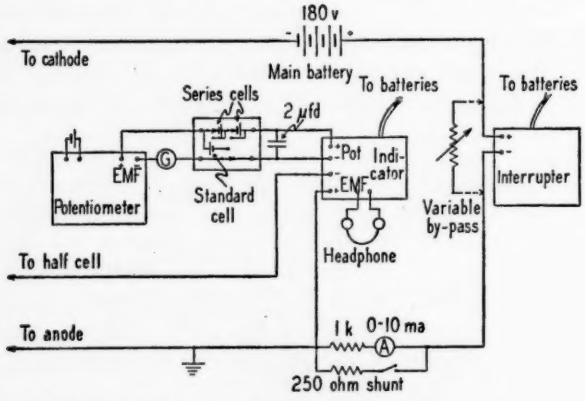

FIG. 2. Circuit used in measuring the potential.

The cathode consisted of smooth platinum foil approximately 2 cm² in area. The anodes were also constructed of smooth platinum and ranged in area from .02 to 8 cm². The smaller electrodes consisted of a short wire sealed into soft glass tubing while for the larger ones a piece of foil was attached to the wire.

Prior to each experiment the anode under study was pickled in boiling concentrated hydrochloric acid, a procedure recommended by Hickling and Hill.[6] The time of pickling was generally about five minutes, but no significant difference was observed between experiments preceded by one minute and by thirty minutes of pickling.

The electrolyte was prepared from cp potassium hydroxide and ordinary distilled water. Preliminary experiments indicated that the presence of small amounts of carbonate would not appreciably affect the results.

In these experiments no effort was made to keep the solution saturated with oxygen or to exclude hydrogen from the anode. The potential changes observed are, for the most part, too large to be accounted for by changes in the oxygen concentration, and Hickling and Hill[6] have shown that at the current densities used the presence of hydrogen has little effect on the anodic overpotential.

Theoretical Basis for the Experimental Approach

Electrode-electrolyte interfaces have relatively large electrical capacities arising from the proximity of the two conducting phases which are, in effect, insulated from one another.[16–19] The insulation is provided by the slowness of the chemical processes which transfer charge across the interface and need not depend on a layer of gas or other dielectric. The equivalent electrical circuit of the phase boundary is a capacitor (the double layer) in parallel with a resistor (the electrode reaction). The resistor is generally nonlinear, its characteristics being determined by the way in which the rate of the electrode reaction depends on the potential.

In the double layer the experimentally measured *external current* is split into two components, the *capacitive current* (which accumulates charge in the

[14] A. Hickling, Trans. Faraday Soc. **33**, 1540 (1937).
[15] W. R. Busing, thesis (Princeton University, 1949). See also reference 14.
[16] G. Gouy, J. phys. radium (4) **9**, 457 (1910).
[17] D. L. Chapman, Phil. Mag. **25**, 475 (1913).
[18] D. C. Grahame, J. Am. Chem. Soc. **68**, 301 (1946); Chem. Revs. **41**, 441 (1947).
[19] J. D. Ferry J. Chem. Phys. **16**, 737 (1948).

double layer) and the *reaction current* (consisting of charge carried across the interface by the electrode process).

The object of most of the theories of overvoltage has been to relate the potential to the reaction rate and thus to the current density. The current involved in these theories is therefore the reaction current. It is identical with the external current only under conditions for which the capacitive current is negligible.

For a short time after a change in the external current the potential is controlled almost entirely by the charge or discharge of the capacitor. Under these conditions the time dependence will be called *capacitive*. Many experimental data exist, however, that describe changes in potential with time which are too slow to be accounted for by the charging or discharging of a capacitor of reasonable size.[1–6] Such changes with time will be called *noncapacitive*. In order to describe such a change in potential formally in terms of a capacitor in parallel with a resistor, one must permit the properties of the resistor to change with time. This implies a change in the chemical or physical nature of the system. For instance, there might be a depletion of the reactants or an accumulation of products either in the bulk of the solution or near the interface, a factor which has been found to be important in many instances. But in the experiments to be described here, as well as in many other instances, the noncapacitive changes in potential persist even though concentration changes of this kind are believed to have been eliminated. Here the electrode itself must be altered in some way during the course of the reaction, either by some bulk change, such as the absorption of liberated gas, or by a surface change, such as the formation of a layer of some compound.

The capacitive potential changes may be treated quantitatively by making some assumptions concerning the properties of the double layer capacitor and the resistor in parallel with it.[20] There is much experimental and theoretical evidence indicating that, at potentials far from the equilibrium potential, the current-voltage relation has the form of the Tafel equation,[7]

$$V=a+b\log I_r, \tag{1}$$

where I_r is the reaction current density, V is the potential of the electrode, and a and b are constants. In practice V must be defined with reference to some standard electrode, and the value of a depends on this choice. It is convenient to use natural logarithms here:

$$V=a+b'\ln I_r, \tag{1'}$$

where $b'=b/2.303$.

We shall assume that this equation describes the behavior of the resistor. The constants a and b in this equation will be assumed to be independent of time, at least for the short intervals during which the capacitor charges or discharges. The capacity of the double layer, C, will be assumed to be a constant given by

$$CdV=dQ, \tag{2}$$

where Q is the charge accumulated by the double layer.

Dividing (2) by the time differential, dt, replacing dQ/dt by (I_e-I_r), where I_e is the experimentally measured external current, and eliminating dV/dt by means of (1'), we find

$$dI_r/[I_r(I_e-I_r)]=dt/b'C. \tag{3}$$

Case I. Decay of the Potential Immediately Following an Interruption in the External Current

Suppose the external circuit is broken after a current has been flowing for a long time. Under these conditions (3) becomes

$$-dI_r/I_r^2=dt/b'C. \tag{4}$$

Let I_{e1} be the external current just before the interruption. I_{e1} is also equal to the reaction current both before and immediately after this interruption. Then integration of (4) gives

$$1/I_r=t/b'C+1/I_{e1}. \tag{5}$$

Here t is measured from the time of the interruption. Substituting in (1')

$$V=K-b'\ln(t+bC/I_{e1}), \tag{6}$$

where

$$K=V_1+b'\ln bC/I_{e1},$$

and V_1 is the value of the potential just before the interruption. Note that V_1 is related to I_{e1} by the Tafel equation, (1').

A plot of V against $\log t$ is shown in Fig. 3. It may be seen that the curve has two asymptotes because for $t\ll b'C/I_{e1}$ Eq. (6) reduces to $V=V_1$, while for $t\gg b'C/I_{e1}$ it becomes

$$V=K-b'\ln t=K-b\log t.$$

This second asymptote has a slope of $-b$ and intersects the first where $\log t=\log b'C/I_{e1}$.

Thus the Tafel b can be found from the asymptote of a plot of the decaying potential against $\log t$. *This pro-*

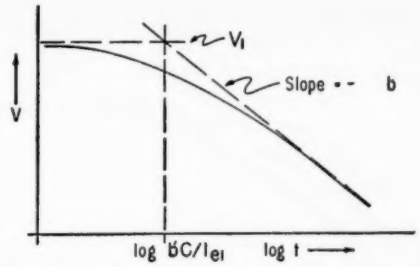

FIG. 3. The theoretical decay of the potential immediately following an interruption in the external current.

[20] This section is an extension of the treatment of the decay of potential which was first given by G. Armstrong and J. A. V. Butler, Trans. Faraday Soc. **29**, 1261 (1933).

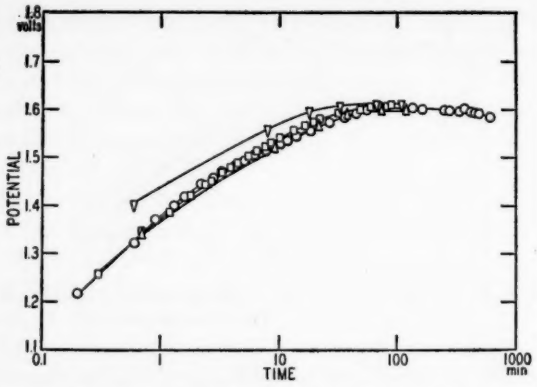

FIG. 4. The increase of the potential with time in a series of identical experiments at a constant current density of 10^{-1} amp/cm².

vides a rapid means of measuring b and should give a value much more characteristic of the instantaneous state of the surface than is the b obtained from the more usual plot of V against logI.

Case II. Change of the Potential Immediately Following a Change in the External Current

If the external current is changed abruptly from I_{e1} to I_{e2} where I_{e2} is not zero, (3) may be integrated directly, and by substituting the initial conditions, which are the same as for Case I, and using (1′) we get:

$$V=V_1+(I_{e2}/C)t \\ -b' \ln\{1+(I_{e1}/I_{e2})[\exp(I_{e2}t/b'C)-1]\}. \quad (7)$$

Equation (7) may also be written

$$V=V_2+(I_{e2}/C)t-b' \ln[I_{e2}/I_{e1}-1+\exp(I_{e2}t/b'C)], \quad (8)$$

where V_2 is the potential related to I_{e2} by the Tafel equation, (1).

Case III. Recovery of the Potential Following an Interruption in the External Current

If a steady current is interrupted for a short time and then restored to its original value the recovery of the potential is easily calculated from the results of Cases I and II. Let I_{e0} be the interrupted external current, V_0 the potential before interruption, I_{r1} the reaction current at the instant the external current is restored, and τ the duration of this interruption. Then from (5) we have

$$1/I_{r1}=\tau/bC+1/I_{e0}. \quad (9)$$

When the circuit is closed the recovering potential is given by (8) if I_{e1}, I_{e2}, and V_2 are replaced by I_{r1}, I_{e0}, and V_0, respectively. Eliminating I_{r1} with the aid of (9) it follows that

$$V=V_0+(I_{e0}/C)t-b' \ln[I_{e0}\tau/b'C+\exp(I_{e0}t/b'C)]. \quad (10)$$

t in this equation is measured from the instant I_{e0} is restored.

It may be shown that when t is small the potential recovers linearly. If this linear increase persisted the potential would reach its original value in time t' where

$$t'=(b'C/I_{e0}) \ln[(I_{e0}\tau/b'C)+1]. \quad (11)$$

After t' the potential given by (10) differs only slightly from V_0 so that t' provides an approximate measure of the time which should be required for the potential to recover after an interruption τ.

Results

The experiments described here are confined to the anodic decomposition of normal potassium hydroxide solutions at smooth platinum electrodes. Measurements were made of (1) the increase of the potential with time at constant current density; (2) the decay of the potential when the circuit was broken; (3) the recovery of the potential following an interruption; and (4) the changes in the potential which accompany an increase or decrease in the externally supplied current.

Increase of the Potential with Time at Constant Current Density

When a constant current density was supplied to the system, the potential increased at first rapidly and then more slowly. Figure 4 shows the results obtained in a series of identical experiments when the current density was 10^{-1} amp/cm², while in Fig. 5 curves representative of experiments at 1, 10^{-1}, 10^{-2}, and 10^{-3} amp/cm² are plotted.

The potentials were measured with the electronic commutator and the times recorded to the nearest 0.1 minute. The points plotted in Fig. 4 are the readings obtained with the interrupter set for the shortest off-time, which was about 18 μsec. The actual potentials were therefore somewhat higher than these. In Fig. 5 the true potentials for 1 and 10^{-1} amp/cm² are shown by the dashed curves which have been estimated from a few extrapolated points. (The method of extrapola-

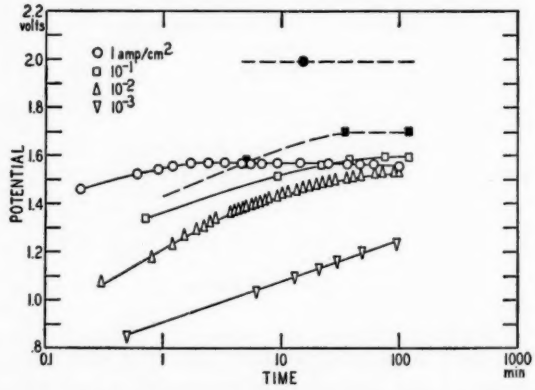

FIG. 5. The increase of the potential with time at constant current density. The open points are measured values obtained 18 μsec after the current was interrupted while the solid ones have been obtained by extrapolation and represent the true potential while the current is flowing.

tion is outlined below.) At current densities of 10^{-2} and 10^{-3} amp/cm², the extrapolated potentials did not differ by more than 0.01 volt from the measured values.

The general characteristics of the curves of increasing potential may be seen from Fig. 5. Initially the increase was approximately linear with logarithmic time, and for the experiments at 1, 10^{-1}, and 10^{-2} amp/cm² the potential levels off to a more or less constant value in 100 min or less. The steady state is reached more rapidly at the higher current densities. In the experiments with a current density of 10^{-3} amp/cm² the curves had not leveled off at 200 minutes.

It will be seen from Fig. 5 that after 25 minutes the measured potential associated with a current density of 1 amp/cm² was actually *lower* than that for 10^{-1} amp/cm². This apparently paradoxical behavior is a manifestation of the "crossing" of decay curves which will be discussed below. The extrapolated potentials were in the expected order.

Decay of the Potential Immediately Following an Interruption in the External Current

Equation (6) describes the theoretical behavior of the potential following a break in the external current. In order to test this equation, experiments were performed using the electronic commutator to measure the potentials between 2×10^{-5} and 6×10^{-3} seconds after an interruption in the current. A few measurements were also made after several seconds.

In Figs. 6 and 7 are shown the results of experiments in which the initial current densities, I_{c1}, are 10^{-3} and 10^{-2} amp/cm². According to Eq. (6) it should be possible to find a constant, $b'C/I_{c1}$, such that a plot of the potential against $\log(t+b'C/I_{c1})$ will give a straight line. In Figs. 6 and 7, $b'C/I_{c1}$ has been determined by trial and error and it will be seen that in these examples the points can be made to lie on a straight line as the theory predicts. The value of b' can then be found from the slope of the resulting line and C can be calculated

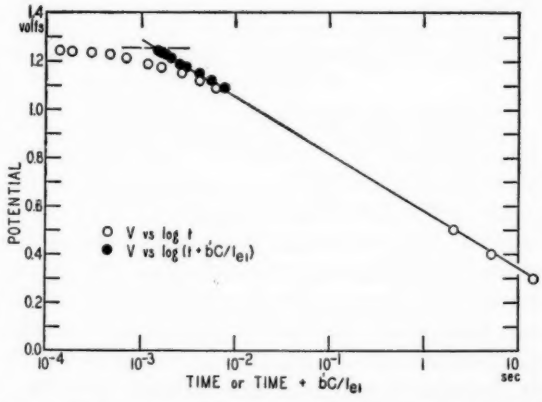

FIG. 6. The decay of the potential immediately following an interruption in the external current. The current before the interruption was 10^{-3} amp/cm². The following data were obtained from this plot: $b'C/I_{c1}=1.40\times10^{-3}$ sec, $V_1=1.252$ volts, $b=0.234$ volts, $C=13.8$ μfd/cm².

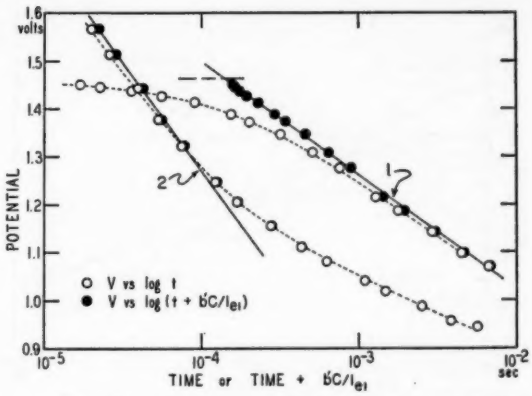

FIG. 7. The decay of the potential immediately following an interruption in the external circuit. For curve 1 the current before interruption was 10^{-2} amp/cm². From this plot the following data were obtained: $b'C/I_{c1}=1.40\times10^{-4}$ sec, $V_1=1.462$ volts, $b=0.233$ volts, $C=13.8$ μfd/cm². For curve 2 the current before interruption was 1 amp/cm². If it is assumed that $C=12.7$ μfd/cm² (which is the average of values obtained at lower current densities), then the data for times less than 10^{-4} sec, satisfy Eq. (6) with $b'C/I_{c1}=2.5\times10^{-6}$ sec, $V_1=1.985$ volts, $b=0.445$ volts.

since I_{c1} is known. Extrapolation of the straight line to zero time (i.e., to $\log b'C/I_{c1}$ on the $\log(t+b'C/I_{c1}$ scale)) gives the initial potential, V_1.

Figure 6 shows that for an initial current density of 10^{-3} amp/cm², Eq. (6) is satisfied until at least 14 seconds after the interruption. Using a Lindemann electrometer, Armstrong and Butler[20] found a similar logarithmic relationship for the decay of the potential between 1 and 200 seconds after anodic current densities of approximately 10^{-3} amp/cm² were interrupted. Equation (6) must, of course, fail when the potential has decayed to the reversible oxygen potential (0.16 volt for our cell). Our potentials are well above this, however.

Figure 7 also shows the decay of the potential from an initial current density of 1 amp/cm². It is seen that the results deviate considerably from the theory. In general, this was found to be the case whenever the initial current density was greater than 10^{-2} amp/cm². For this reason, and also because $b'C/I_{c1}$ becomes small as I_{c1} is increased, it was not feasible to determine this constant by trial and error at these current densities. Presumably the method would be satisfactory if potential measurements could be made at shorter time intervals, for which t would be comparable with $b'C/I_{c1}$. In order to determine this constant from the data available at present, an alternative procedure was adopted when I_{c1} had these higher values. C is assumed to be the average of the values found at lower initial current densities. $b'C/I_{c1}$ is then adjusted until the value of b' in this constant is the same as that obtained from the initial slope of the curve which results when the potentials are plotted against $\log(t+b'C/I_{c1})$. At short times the resulting points lie on a straight line as the theory predicts, but after longer intervals the observed potentials are considerably higher than those required by Eq. (6). V_1 may be found by extrapolation of the line as before.

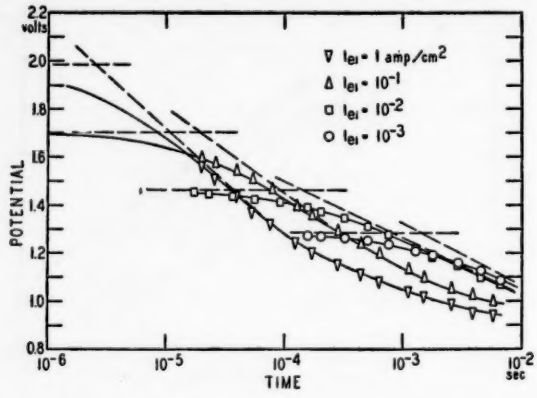

FIG. 8. The decay of the potential immediately following an interruption in the external current for various values of this current.

The data for the decay of the potential with initial current densities of 1, 10^{-1}, 10^{-2}, and 10^{-3} amp/cm² have been plotted together in Fig. 8 so that the results may be compared. For the decay from an initial current density of 1 amp/cm² the theoretical curve has been extended to include times of 10^{-6} seconds. The theoretical asymptotes have also been drawn. It will be noted that the higher initial current densities are associated not only with high initial potentials but also with large values of b as shown by the steeper negative slopes. *This results in a crossing of the decay curves.* For the curves corresponding to initial current densities of 1 and 10^{-1} amp/cm², this crossing is seen to occur at about 1.4×10^{-5} sec, which is earlier than the first reading possible with our equipment. For this reason our earliest measured potential at a current density of 1 amp/cm² (in Fig. 5) is lower than the earliest value found at 10^{-1} amp/cm².

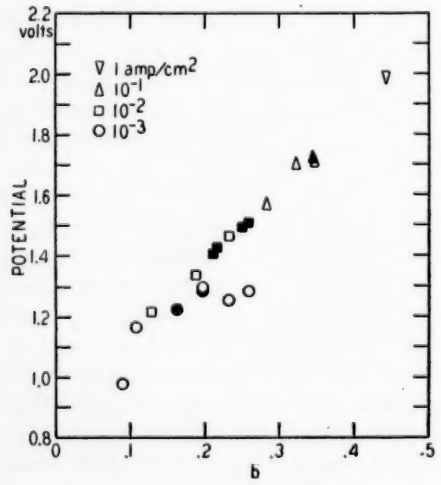

FIG. 9. The relationship between the initial potential and b as determined from the decay of the potential. The solid points represent results obtained a short time after the current density was increased or decreased.

The Change of the Tafel a and b During Electrolysis

The slow noncapacitive potential change shown, for example, in Fig. 4 is presumably a reflection of changes with time of the constants a and b in the Tafel equation. The value of b at any moment can be measured conveniently by breaking the circuit and interpreting the subsequent rapid decay of the potential by means of Eq. (6). The value of a at the same moment can be found by multiplying this b by log$I$ and subtracting from the initial potential.

In general, it was found that the values of both a and b increased as the potential increased with time. In Fig. 9, the potentials just prior to the interruption of the current V_1, are plotted against the values of b measured from the subsequent decay. This plot includes points determined at four different current densities. It is seen that when plotted in this way all of the points fall approximately along a single locus. Also included are some results (indicated by filled-in symbols) which were measured subsequent to an increase or decrease in the current density. These points have the same locus as the others.

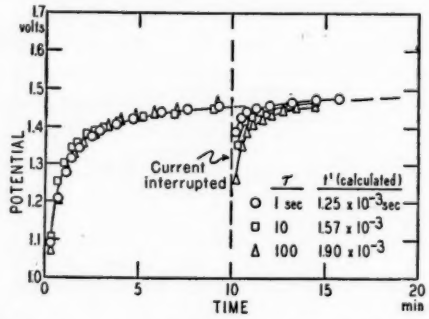

FIG. 10. The recovery of the potential following interruptions in the external current of various durations, τ. I' is the recovery time calculated using Eq. (11), which assumes only capacitive effects.

The Tafel a values are readily found from Fig. 9. In the steady state, a seems to be the same at all current densities.

Recovery of the Potential Following an Interruption in the Current

It has been seen that when the external circuit is broken, the decay of the potential can be fairly well described by Eq. (6), which has been derived on the assumption of a reaction current which obeys the Tafel equation and a constant double layer capacitance. Thus, after an interruption of known duration, the potential which is reached can be calculated. One would therefore expect that, using the same assumption, it should be possible to predict the increase in potential with time when the current is re-established. In this way Eq. (10) has been derived to describe the recovery of the potential after such an interruption in the current. The experiments to be described below show that this equation is not adequate to explain the slow increase in potential

which is observed. An interpretation of the deviations will be reserved for Part II.

After a current of 10^{-2} amp/cm^2 had been passed through the system for ten minutes, the circuit was broken for time intervals, τ, ranging from 1 to 100 seconds, and then restored. The changes in potential were followed with the electronic commutator as in the experiments on the increase of the potential with time. The results for interruption times of 1, 10, and 100 seconds are shown in Fig. 10 in which the dashed curve indicates the change in potential when there is no interruption. Also tabulated are the approximate recovery times, t', which were calculated from Eq. (11) using constants determined from the experiments on the decay of the potential. While the longest of the calculated times is 1.9×10^{-3} seconds, it will be seen that in none of the experiments did the recovering potential reach the dashed curve until about two minutes after the current was restored.

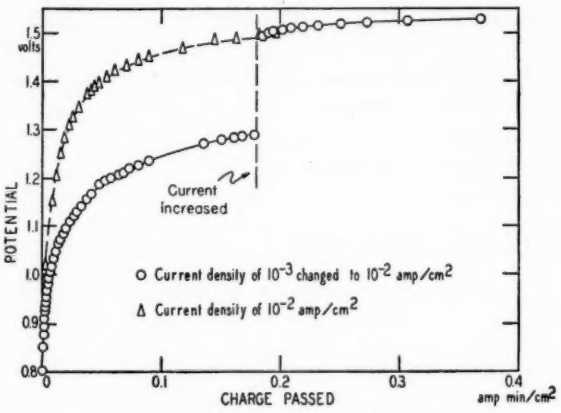

FIG. 11. Changes in the potential when the current density is increased.

It is interesting to note that the recovery curves for 1, 10, and 100 seconds are approximately evenly spaced. That is to say, at a given time the deviation from the calculated potential is approximately proportional to the logarithm of the time of interruption. An interpretation of this behavior will be given in Part II.

Changes in the Potential when the Current is Increased or Decreased

A series of experiments was performed in which the current was maintained constant for some time and then increased or decreased to a new value. The changes in potential were observed with the electronic commutator as before. Figure 11 illustrates the behavior of the potential following an increase in the current density from 10^{-3} to 10^{-2} amp/cm^2. In order to make the curves at different current densities more nearly comparable, the abscissa measures charge passed rather than time. Included on the same plot is a dashed curve showng the potential observed when the higher current density is maintained throughout the experiment. It

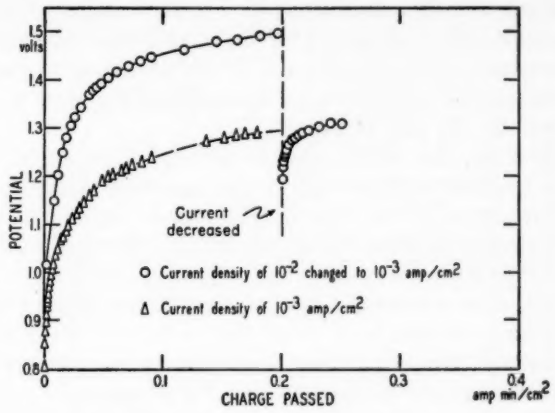

FIG. 12. Changes in the potential when the current density is decreased.

will be seen that immediately following the increase in current, the potential had a value very close to that which would have been reached had the higher current been flowing from the start. For a short time thereafter the potential rose slightly more rapidly than the dashed curve and then became parallel with it.

In an analogous experiment involving a decrease in current density, the potential varied in the remarkable way shown in Fig. 12. Here again the abscissa gives the charge passed. A dashed curve is plotted showing the potential observed if the lower current density was maintained throughout the experiment. When the

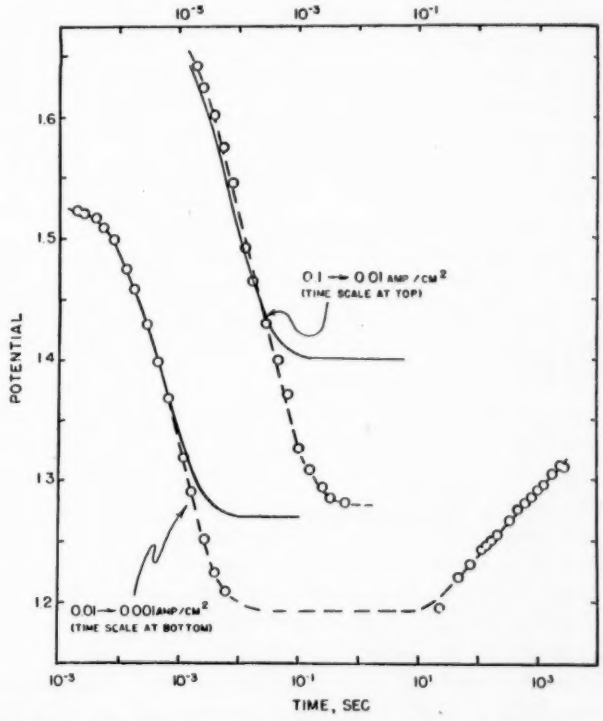

FIG. 13. Changes in potential following a decrease in current density. The solid curves are calculated from Eq. (7), using the following constants: upper curve, $V_1=1.719$ volts, $b=0.313$ volts, $b'C/I_{s1}=1.9\times10^{-5}$ sec; lower curve, $V_1=1.541$, $b=0.272$, $b'C/I_{s1}=1.4\times10^{-4}$ sec.

current was decreased from 10^{-2} to 10^{-3} amp/cm², the potential fell to about 0.1 volt *below* this curve and then increased rapidly to approach it. This increase was approximately linear with the logarithm of the time as is shown by the plot of Fig. 13.

Because this result was completely unexpected, it was thought that perhaps it was somehow due to the interruptions in the current necessary to the commutator method of potential measurement. For this reason the experiment was repeated using the direct method which does not require such interruptions. Except for an ohmic increment of about 0.02 volt included in the measured potential, the phenomenon was identical with that observed by the commutator method.

This phenomenon has been observed by Baars[1] and also by Kolotyrkin.[4] Its significance will be discussed in Part II.

Decay of the Potential Immediately Following a Decrease in the Current Density

Because of the peculiar result described above, it appeared advisable to study in detail the decay of the potential when the current density was decreased to a new value. The measurements were made with the electronic commutator by connecting a variable by-pass resistor across the interrupter as described above. Figure 13 shows the results obtained when the current was reduced from 10^{-1} to 10^{-2} amp/cm² and from 10^{-2} to 10^{-3} amp/cm². The solid lines are the theoretical curves derived from Eq. (7), the constants V_1, b', and C being determined from decay curves (with $I_{c2}=0$) measured just prior to, and again just after each experiment. Since the current did not fall to zero during the measurements, a small ohmic drop is included in the potential. This is negligible at 10^{-3} amp/cm² but probably accounts for the discrepancy of about 0.1 volt between the calculated and observed potentials at 10^{-2} amp/cm² at times shorter than 10^{-4} sec.

The observed potentials follow the calculated decay curves for 10^{-4} or 10^{-3} sec but then fall below them, leveling off after about 10^{-2} sec at values considerably below the predicted ones. A very slow increase in potential then takes place.

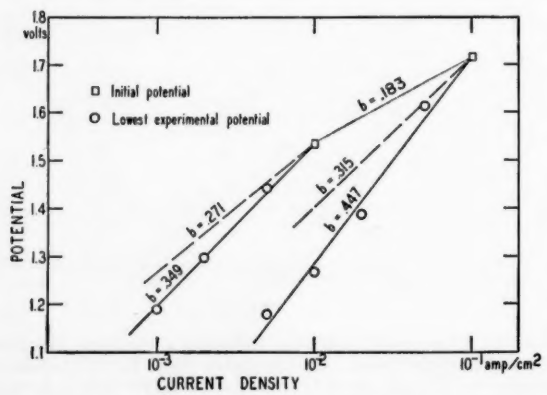

FIG. 14. The relationship between three ways of determining b.

A series of similar decay experiments was performed with various initial and final current densities. If the minimum value of the potential following the reduction in current is plotted against the logarithm of the final current density (correcting the potential, if necessary, for the ohmic drop), a straight line is obtained in agreement with Tafel's law (Fig. 14). The value of b obtained from the slope of this line differs considerably from the values found in other ways. Figure 14 also shows the relationship between three ways of determining this constant. The two initial potentials which were used are plotted against the logarithms of the corresponding initial currents, $\log I_{c1}$, while the subsequent minimum values of the potentials are plotted against the logarithms of the final currents, $\log I_{c2}$. In both series of experiments the initial current had flowed for a sufficient time to allow the potential to become constant. The dotted line joining the two initial points in Fig. 14 therefore gives a Tafel b value, 0.183 volt, which should and does agree with that found between the same current densities by Hickling and Hill,[6] who used "steady state" potentials in their study of the oxygen overpotential on smooth platinum. Still different values of b are obtained by the analysis of the decay of the potential when the final current, I_{c2}, is zero. The corresponding slopes are indicated by the dashed lines in Fig. 14.

PART II. THEORETICAL INTERPRETATIONS

Electrode Processes as Reactions on Non-Uniform Surfaces

The chemical reactions which occur at electrode surfaces during the passage of an electric current differ from other surface reactions only in that they are accompanied by the transfer of electrical charge into or out of the electrode. Their rates are therefore related to the current density and to the electrical potential—variables which do not have to be considered in other processes occurring at surfaces. Allowing for this complication, we can expect that the concepts which are used in studying ordinary surface reactions might profitably be exploited in the investigation of electrode processes.

The many steps involved in any electrode reaction may be divided into two classes: (1) processes which occur at the electrode surface or within molecular dimensions thereof and (2) diffusion processes which take place at somewhat greater distances from the electrode. In general, the rate-determining step may belong to either class depending on the relative rates of the reactions at the surface and of the diffusion processes. While diffusion is the limiting process under many conditions it can hardly be invoked in order to explain our results for the anodic decomposition of potassium hydroxide. For example, at a constant current density of 10^{-3} amp/cm² the potential increased almost linearly with the logarithm of the time from 0.86 volt at 0.5

minute to 1.24 volts at 95 minutes (Fig. 5). It is difficult to believe that this increase in potential is caused by changes in the concentration of the reactants or products in the solution. Such an assumption would imply that the concentration at the anode changed by a factor of more than 10^6 over a period of 95 minutes. Even if concentration changes of this order of magnitude were to take place, it is unreasonable to expect that it should require more than 95 minutes to establish steady state concentrations. Attempts to explain the results of other experiments described in Part I as the consequences of concentration changes lead to even greater difficulties. The strong dependence of the potential on the electrode material also provides evidence that the rate-determining step occurs at the electrode surface rather than in the solution.[6] We shall find that the behavior observed in our experiments can be given a relatively simple interpretation in this way.

As long as we are always dealing with the same chemical reaction at an electrode, the rate of the reaction during an experiment performed at constant current must remain constant. Assuming that the rate-determining process occurs at the electrode surface, an increase in the potential at a constant current density may be described as a decrease in the *catalytic activity* of the electrode. Similarly a decrease in the potential implies an increase in activity.‡ We shall say that an electrode whose activity has been decreased has been *poisoned* and one whose activity has been increased has been *promoted*.

Experiments in catalysis and adsorption provide convincing evidence that most surfaces are highly non-uniform.[21–24] In the light of what is known today of the microscopic structure of solids it would be surprising if this were not so. Metallic surfaces which are thought to be relatively uniform have been prepared from single crystals,[25] but such surfaces are not likely to be found ordinarily. We thus have every reason to believe that our electrodes, like other surfaces, are non-uniform, in that the activity as defined above varies from point to point. This means that at a given potential the reaction proceeds more rapidly on some elements of the surface than on others. The observed current density will be the average of the contributions from each element. The non-uniformity of an electrode surface will generally be more complex than that of a catalyst, however, because the surface elements which are the most active at one potential are not necessarily those which would be the most active at another potential. A graphical method of dealing with such a distribution of activities will now be developed.

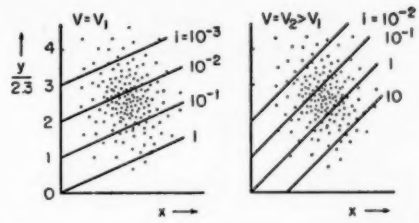

FIG. 15. Representation of the distribution of Tafel constants for a non-uniform electrode surface. The straight lines are contours of equal microscopic current density. The two plots represent the situation at different electrode potentials.

Graphical Representation of the Electrochemical State of a Non-Uniform Surface

We shall assume that at each element of area of the electrode surface the potential V of the electrode is related to the local current density, i, accompanying the electrode reaction, by Tafel's law,

$$V=a+b' \ln i, \tag{12}$$

where a and b' are constants for that element. The assumption of the validity of Tafel's law ought to lead to results of general interest since a law of this form is found experimentally for a number of important electrode reactions, and an expression of this general form is derivable theoretically from several widely different points of view.[7–12] The constants a and b' may be given different theoretical interpretations depending on which of these points of view one chooses, but this need not concern us here.§

Equation (12) may be rewritten in the form

$$y=Vx-\ln i=Vx+\gamma, \tag{13}$$

where $y=a/b'$, $x=1/b'$, and $\gamma=-\ln i$.

The potential V of the electrode will, by the laws of electrostatics, have the same value over the entire electrode surface—it being assumed that the experiment is so arranged that ohmic drops in the electrode are negligible. Therefore, the local current density i will vary from point to point on the surface only if the values of the constants x and y vary from point to point. Imagine the surface of the electrode to be divided into many elementary regions of equal area, each region being sufficiently small that the quantities x and y characterizing it can be considered as constant throughout the region. The state of electrochemical activity of the surface can then be represented con-

‡ Baars (see reference 1) and Masing and Laue (Z. physik. Chem. 178, 1 (1936)) have made similar proposals to explain the increase in the hydrogen overvoltage with time. Hickling and Salt (see reference 13) have discussed the role of the electrode in catalyzing the recombination of liberated atoms. Our use of the term "catalytic activity" is intended to be taken in a more general sense, however. The activity of an electrode is a measure of its ability to facilitate the rate-determining process, whatever that may be.

[21] Schwab, Taylor, and Spence, *Catalysis* (D. Van Nostrand Company, Inc., New York, 1937), pp. 280–295.

[22] H. S. Taylor, in *Advances in Catalysis*, edited by Frankenburg, Komarewsky and Rideal (Academic Press, Inc., New York, 1948), Vol. I, pp. 1–26.

[23] G. Halsey and H. S. Taylor, J. Chem. Phys. **15**, 624 (1947).

[24] R. Sips, J. Chem. Phys. **16**, 490 (1948).

[25] H. Leidheiser, Jr. and A. T. Gwathmey, J. Am. Chem. Soc. **70**, 1200 (1948).

§ Approaches analogous to the one we shall use are possible starting with different functional relations between V and i, e.g., $V=V_0+Ai$. There is not even any need to restrict oneself to equations containing only two parameters.

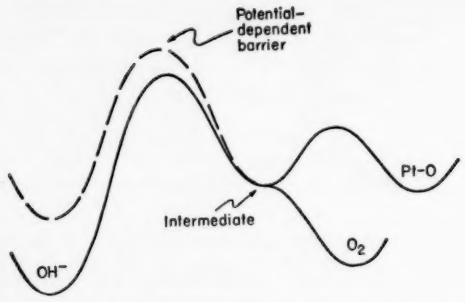

FIG. 16. A possible energy diagram for the evolution of oxygen and the formation of oxide. The dashed curve shows the effect of increasing the potential.

veniently by a plot in which x and y are the abscissa and ordinate and in which the pairs of (x, y) values for all elementary areas are indicated by dots. Any electrode surface would in this way correspond to a cloud of points in the x, y plane (see Fig. 15). A distribution function $S(x, y)$ can now be constructed such that $S(x, y)dxdy$ is the fraction of the electrode surface whose Tafel parameters lie in the range $x, x+dx$; $y, y+dy$. If this distribution function were known for a surface, the electrochemical behavior of the surface could be determined.

The observed average current density for the entire electrode will be given by

$$I=\int\int S(x, y)i(V, x, y)dxdy, \qquad (14)$$

where the integration is over all values of x and y. This is the fundamental equation relating the observed current density to the electrode potential.

An x, y diagram of this kind has the property that, if a straight line of slope V and intercept γ at $x=0$ is drawn, all regions whose representative points fall on this line will carry the same current density, $i=e^{-\gamma}$, when the electrode potential is V. Such lines therefore represent contours of constant current density in the x, y plane. (See Fig. 15.) For an electrode at a specified potential, these contours form a family of parallel lines. If these lines are equally spaced they will represent current densities differing by constant multiples (i_0, 10 i_0, 100 i_0, etc.), with lines of higher current density lying toward the bottom of the diagram.

The line

$$y=Vx-\ln I, \qquad (15)$$

in the x, y diagram will be called the *current line*. The position of this line relative to the distribution S will indicate which parts of the distribution carry most of the current. It is easy to see that, because of the exponential dependence of i on $-\gamma$, the current line will always tend to pass through the lower part of the region of the x, y plane covered by the distribution S. This means physically that, regardless of the value of the potential, most of the current tends to be carried by points near the lower half of the circumference of the distribution. These therefore represent the most active parts of the electrode. Furthermore, since the slope of the current line changes with the potential of the electrode, this line will intersect different parts of the circumference at different potentials. Therefore, the parts of the electrode which are the most active (i.e., carry the highest current density) at low potentials may not be the same as those which are most active at high potentials.

The integration of Eq. (14) for a simple distribution function is outlined in the Appendix to this paper. This integration shows that even if it were possible to measure the current-voltage relationship without changing the electrode surface, a broad distribution would cause considerable deviations from Tafel's law. It will be shown below, however, that most of the observed deviations are not caused by this but are related to changes in the distribution which invariably seem to occur during the experimental observations.

It is interesting at this point to try to make a rough estimate of the range of values of x and y over which the distribution S may extend for an actual electrode. We may do this either by referring to the variations in a and b' actually observed with, say, platinum electrodes under various experimental conditions, or by examining some of the theoretical factors which might determine the values of these constants.

The experiments reported in Part I gave values of $b'(=b/2.3)$ for the discharge of OH^- on platinum anodes varying between about 0.05 and 0.20 volt. The range of variation of a amounts to eight tenths of a volt. From these figures it is probable that distributions occur in which x ranges from 5 to 20 volts^{-1} and y has values varying by ten or more.

According to the slow discharge theory of overvoltage,[9] the constant a is given by

$$a=\Delta F^{\ddagger}/n\mathfrak{F}-\ln K, \qquad (16)$$

where $\Delta F^{\ddagger}$ is the standard free energy of activation of the rate-controlling step, n is the number of electrons transferred in this step, $\mathfrak{F}$ is the electrochemical equivalent of charge, and K is a constant which should not vary significantly over the electrode surface. The con-

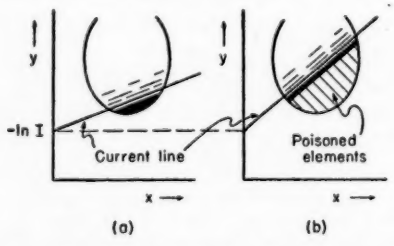

FIG. 17. Increase of potential with time at constant current density due to the poisoning of the most active surface elements. The ellipse shows the effective perimeter of the distribution function S. (a) represents the surface immediately after the current is turned on, while (b) represents the surface after the current has been allowed to flow for some time. The current density carried by each element is indicated by the depth of the diagonal shading adjoining the current line.

stant b' is given by

$$b'=RT/\alpha n\mathfrak{F}=0.024/n\alpha \text{ volts at } 293°\text{K}, \quad (17)$$

where α is the fraction of the electrode potential which acts in reducing the activation energy of the rate-controlling step. If $n=1$, a change in α of only 0.1 will cause x to change by 4 volts^{-1}. Similarly, a variation in $\Delta F^{\ddagger}$ by 23,000 cal/mole will result in a variation in a of 1 volt. Again we may expect distributions in which x has a range of 10 volts^{-1} or more and the variation in y may be of the order of ten.

Interpretation of the Behavior of Platinum Anodes in the Electrolysis of Potassium Hydroxide

From the fact that at constant current density the potential of a platinum anode increases with time (Figs. 4 and 5) we must conclude that the activity of the electrode decreases during the electrolysis. Such an over-all decrease must be the net result of variations in the activity of the individual surface elements. It has been assumed that these activities are described by Eq. (13) where the constants x and y are characteristic of each element. A change in the activity of this surface element must then be interpreted as a variation in the value of either x or y or both and the element is subsequently represented by a new position on the x, y diagram. The over-all change in the electrode is thus reflected in a change in the distribution function $S(x, y)$.

Mechanism of the Poisoning of the Platinum Anode

It has been proposed by Hoar[26] that the change in the potential with time at a platinum electrode in alkali is caused by the formation of oxide on the platinum surface, either as a monolayer or as a multilayer. If all of the current which passes through the system results in the formation of oxide, a monolayer would be formed in about one thousandth of the time observed for the steady state potential to be reached. Furthermore, the observed evolution of oxygen gas is ample proof that not all of the current is involved in oxide formation. Accepting the highly reasonable proposal of Hoar, a mechanism is therefore required whereby no more than one thousandth of the oxygen formed becomes bonded to the surface. This requirement seems to preclude the possibility that the oxide responsible for the poisoning is an intermediate in oxygen formation. Then the mechanism of poisoning must involve a reaction sequence similar to that represented by the energy diagram of Fig. 16, in which the barrier on the left represents the most difficult step in the potential dependent process. (The dashed curve indicates the effect which a change in the potential will have on the energy diagram.) The intermediate formed (possibly adsorbed hydroxyl radicals) may then either react to form oxygen gas, a process which probably requires little activation energy, or it may contribute to the chemisorbed layer responsible for poisoning. It is expected that an activation energy will be associated with this latter process.[27] The supposition that molecule formation proceeds at least a thousand times faster than chemisorption is made plausible by the difference in the activation energies required for these processes.

[26] T. P. Hoar, Proc. Roy. Soc. (London) **A142**, 628 (1933).

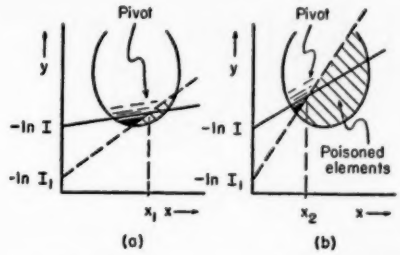

FIG. 18. Decay of the potential immediately following an interruption in the external current. I_1 is the current just before the circuit is opened, while I is the reaction current responsible for the decay of potential after the interruption. (a) represents the distribution a short time after the start of electrolysis when only a small fraction of the surface is poisoned. (b) corresponds to a later time with much more extensive poisoning. It is evident that x_1, the effective value of x controlling the decay of potential in (a), will be greater than x_2, which controls the decay in (b). This accounts for the observed tendency of the Tafel b to increase during an electrolysis.

If this picture is correct, then it must be true that the most active regions of the electrode surface are the most rapidly poisoned, since these are more frequently exposed to the active intermediate. Therefore, the increase in the potential of the electrode with time as the electrolysis proceeds is not due to a general migration of the entire distribution across the x, y diagram, but results almost entirely from the removal of only the most active centers. The situation is illustrated in Fig. 17 where the ellipse gives the effective perimeter of the original distribution function S. The diagonally shaded area represents regions which have been poisoned and the uniformly darkened area represents regions carrying the highest local current density. With the passage of time the current line rotates slowly across the distribution, inactivating regions of the electrode as it passes over their representative points. The increasing slope is reflected in the increase in potential which is observed.

Interpretation of the Increase with Time of Tafel's b During an Electrolysis

It was shown in Part I that when the circuit was opened after various times of electrolysis, the discharge of the electrode double layer led to a rapid decay in the potential. The rate of this decay was found to be greater the longer the electrolysis had been allowed to proceed before opening the circuit. It was shown that this behavior arises from the increase with time of the effective Tafel b.

The considerations of the previous section offer a

[27] S. Brunauer, *The Adsorption of Gases and Vapors* (Princeton University Press, Princeton, New Jersey, 1943), Vol. I, p. 4.

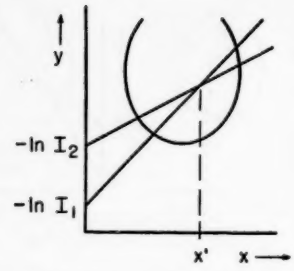

FIG. 19. The steady state current lines at two current densities. x' corresponds to the apparent value of b obtained from a Tafel plot.

straightforward explanation of this fact. If the external circuit is broken after the poisoning has proceeded for a short time, the potential falls because of the discharge of the double layer capacitor. The slope of the current line therefore decreases. The areas which are important for carrying the reaction current during the subsequent decay will then be those in the vicinity of the lowest point of the *unpoisoned* area of the distribution, as shown in Fig. 18(a). The rate of decay will correspond in effect to the mean value of b associated with these centers. During decay the current line tends to "pivot" about a point in this region. As the poisoning proceeds further, the area of importance to the decay process (i.e., the "pivot point") moves to the left—that is, toward smaller values of x and larger values of b [Fig. 18(b)]. The observed increase in b with time of electrolysis undoubtedly arises in this way. The changes in a can be similarly explained.

Stability of the Poisoned Electrode. Validity of Tafel's Law for Steady States

Associated with each region of the electrode surface there is a free energy of adsorption which determines the fraction of the region covered by a monolayer of oxide and hence the extent of the poisoning at equilibrium. This free energy will vary from one region to another because of the non-uniformity of the surface; it is probable that areas which poison most rapidly are those which form the most stable oxides. The equilibrium amount of oxide formed will depend also on the potential, so that on some areas the oxide will be stable only when the potential is high and the accompanying poisoning will persist only as long as the potential remains high. The well-known results of catalytic studies make it reasonable to suppose that on areas which are good current carriers the poisoning will be stable at low potentials, while the less effective centers will not be deactivated unless the potential is high.

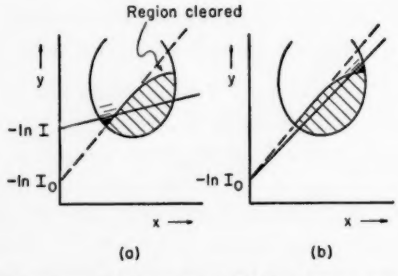

FIG. 20. Recovery of the potential following an interruption in the external current. (a) I_0 is the original current density. I is the reaction current at some time during the interruption. (b) represents the situation after re-establishing the external circuit. The potential (slope of the current line) is lower than the value before interrupting the circuit.

As the poisoning proceeds during an electrolysis at constant current, the potential increases because most of the current is carried by less and less active regions on the electrode. Eventually, the electrode reaction may occur at regions on which no oxide can form because the oxide on these regions is not stable at the prevailing potential. Under these conditions no further poisoning can occur, the potential becomes constant, and the electrode reaches a steady state.

What are the conditions under which the steady state potential is related to the observed macroscopic current density, I, according to Tafel's law? As can be seen from Fig. 19 the portions of the electrode surface which are important in determining the steady state potential are not the same at different current densities. Tafel's law will hold if there are constants, x' and y', such that for all values of I and the associated steady state potentials, V, we can write

$$y' = x'V + \ln I.$$

This is only possible if all the steady state current lines $y = xV + \ln I$ intersect at the common point x', y', giving for the over-all Tafel constants, $a = y'/x'$, $b' = 1/x'$. Such an intersection would be quite fortuitous if there is a broad distribution susceptible to a considerable amount of poisoning, and the values of a and b' which it yields have no simple physical significance. At best these values indicate the approximate location of the distribution on the x, y plane, but it is possible for an intersection to lie well outside the actual distribution.

Thus, even though Tafel's law may be valid on the microscopic scale, it is easily possible for it to fail on the macroscopic scale when applied to the steady states of a non-uniform electrode, as is so often done. Even if it does fit steady state data it may not be particularly significant.

Recovery of the Potential Following an Interruption in the Current

If after the poisoning has proceeded for some time the external circuit is broken for a short interval, the potential will decay to a value which may be predicted from the considerations of Part I. We should expect that at this lower potential some of the oxide responsible for the poisoning will be unstable and will decompose [Fig. 20(a)]. This will occur primarily on the less active regions whose representative points are toward the top of the x, y diagram. When the circuit is again closed the surface elements which have been cleared

during the interruption will be available for carrying current, and the potential will therefore be somewhat below the value which it had previously attained [Fig. 20(b)]. As the oxide is replaced, however, the potential will slowly recover, as is experimentally observed (Fig. 10).

The oxide being more stable on some areas than on others, the amount which is removed during an interruption of current depends on the lowest value reached by the potential. Over any small range of potentials this dependence should be more or less linear. Since the decay of the potential during the interruption is approximately linear in the logarithm of the time, the area cleared of oxide would be expected to vary in a similar fashion. The observed logarithmic dependence of the recovering potentials on the time of interruption of the current (Fig. 10) is, therefore, what one would expect.

Changes in the Potential when the Current is Increased or Decreased. Indications of Catalytic Promotion

Suppose that the current is increased after the steady state potential has been reached at some current density. The amount of oxide which has formed at the lower current density will be less than the equilibrium amount corresponding to the higher current density. The potential should therefore increase for some time until a new steady state is reached. This is what is observed with platinum anodes.

The results obtained following a decrease in the current are, however, not so easily interpreted. In this case the potential first falls when the current is reduced, and then *rises* slowly to a new steady state (Fig. 12). In order to account for this it is necessary to introduce new postulates.

Catalytic experiments have shown that an interface between two solid phases frequently has enhanced reactive properties. Thus the introduction of a small quantity of K_2O in an iron catalyst greatly increases its effectiveness in catalyzing the decomposition of ammonia,[27] presumably because of the greater activity of the interfaces produced. The reduction of packed black copper oxide by hydrogen starts at a point and spreads through the entire mass[28] because the reduction takes place more easily at the interface than in the pure oxide. An area with increased activity due to such a nearby disturbance is said to be *promoted*. In the light of these results it is not unreasonable to expect that a boundary between platinum oxide and a clean metal surface may contain a number of centers which have been promoted and therefore possess enhanced current-carrying properties.

Our results can be explained if it is assumed that the attachment of an oxygen atom to an active area not only deactivates this area but may also alter the activity of adjoining sites on the surface. The characteristics of these neighboring areas will probably be altered at random but at least a small fraction of them may thereby have their current-carrying ability enhanced.

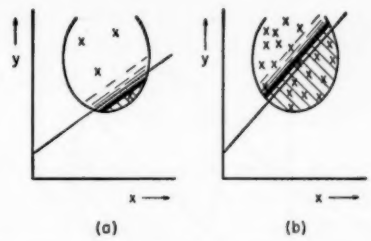

FIG. 21. Representation of a non-uniform electrode showing promoted centers. (a) shows the situation a short time after the electrolysis is started. (b) represents the electrode after a longer time. More oxide has been formed and therefore a larger number of elements have been promoted. The elements promoted to the lower right contribute significantly to the current density causing the current line to pass below those elements which would otherwise be most important.

These altered areas have been represented in the diagram of Fig. 21(a) by crosses, the random distribution of which is in accordance with the postulate. When only a small amount of poisoning has occurred, there are only a few of these areas with new characteristics but their number increases as more of the surface is poisoned. Centers which are shifted to regions of high y or low x have poor current-carrying properties but those which appear below the current line in the x, y plane will make important contributions to the total current. Their effect is taken into account diagrammatically [Fig. 21(b)] by shifting the current line downward slightly so that the intercept again corresponds to the true total current.

In the experiments which have thus far been discussed, the effect of the poisoning has greatly outweighed that of the promotion since only relatively few of the altered areas were important. For this reason the new postulate will not appreciably affect the foregoing qualitative interpretations. The behavior of the potential when the current is decreased does depend sig-

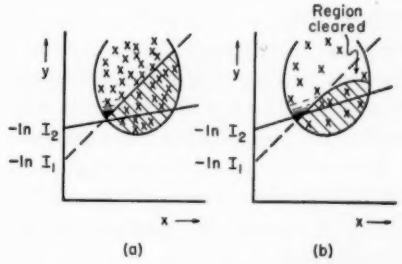

FIG. 22. The changes in potential following a decrease in current density. (a) represents the electrode immediately after a decrease from I_1 to I_2. The large number of promoted centers contribute significantly to the current. (b) shows the situation at a later time. Many of the promoted centers have been lost because some of the oxide is unstable at the lower potential. Since they no longer contribute to the current, the potential must be increased to maintain I_2.

[27] R. N. Pease and H. S. Taylor, J. Phys. Chem. **24**, 241 (1920).
[28] R. N. Pease and H. S. Taylor, J. Am. Chem. Soc. **43**, 2179 (1921).

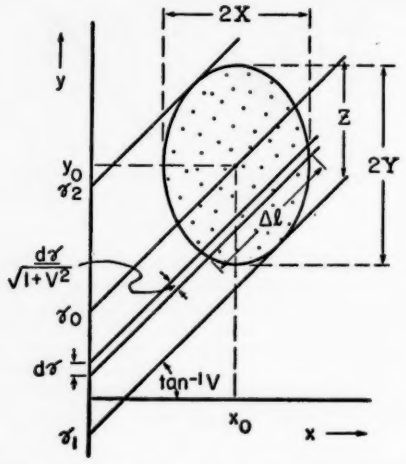

FIG. 23. Constants appearing in the treatment of the uniform elliptical distribution.

nificantly on these promoted centers, however. Figure 22(a) shows the situation immediately after the current is decreased from I_1 to I_2. The current line for I_2 is drawn somewhat below the best areas because of the contribution of the large number of promoted centers present. The existence of these promoted areas depends in turn upon the large amount of oxide which formed at the higher current density. At the new lower potential, however, some of this oxide will be unstable and as time proceeds it will disappear [Fig. 22(b)]. This will result in a corresponding removal of some of the promoted centers and for this reason the potential must rise to maintain the current at a constant value. In this way, the effect which was observed experimentally can be understood.

If the activation energy for the removal of the unstable oxide is uniformly distributed over a large range of values, it would be expected that the removal of this oxide would be approximately linear with the logarithm of the time. The loss of promoted centers and the ultimate rise in potential following a decrease in current would be expected to occur in a similar manner. Such a result was found experimentally, as Fig. 13 shows.

An interesting point concerning this observed effect is that it shows the properties of an electrical inductance. The passage of a high current tends to oppose a decrease in this current when the potential is lowered. Inductive components have previously been found in alternating current impedance measurements made on the giant axon of the squid.[29] Although other explanations for this behavior have been given,[30] it is possible that it could be caused by phenomena analogous to those observed here.

Further Interpretations

Four other effects described in Part I remain to be discussed from the point of view developed here. The first of these ((1) below) can be given a fairly plausible explanation; the other three ((2), (3), and (4)) cannot be understood without further postulates.

(1). Equation (6) fails to describe the decay of the potential after the passage of large currents (Figs. 7 and 8). This is probably caused by a decrease in the effective Tafel b during the decay. This, in turn, is just what we should expect to accompany any decrease in the poisoning made possible by the lowered potential. That is, the pivot point about which the current line rotates during decay does not stay fixed but moves to the right in the x, y diagram as active centers reappear in the poisoned region.

(2) The Tafel b values obtained from the potentials immediately before and after a sudden decrease in the current were about 30 percent larger than those obtained from the decay curves when the circuit was completely opened (Figs. 13 and 14). This could be accounted for qualitatively if the extent of poisoning changed during the decay period, as was just postulated, since such a change ought to be less when the current is flowing than when the circuit is completely open. But the fact that Eq. (6) describes the decay very well at low current densities seems to make the possibility of such a change in the pivot point doubtful.

(3) When currents are allowed to flow until the potential has become steady—as is the usual procedure in studying the current-voltage relation—much smaller values of Tafel's b are found than those mentioned in (2), above (Fig. 14).

(4) The Tafel b which controls the decay of the potential on opening the circuit depends much more on the electrode potential which just preceded the interruption than on the corresponding current density (Fig. 9).

We can see no simple interpretation of (2), (3), and (4) in terms of the concepts presented in this paper. These observations tell something about the general relationships of the current lines and their pivot points to the distribution; we cannot yet say why these relationships should be as they are. They seem to be controlled by the rates of poisoning and of recovery from poisoning—factors about which we still need more information.

Complications in electrode behavior therefore exist which our theory in its present stage can do little more than describe.

APPENDIX

The Current-Voltage Relation Arising from a Typical Distribution Function

In order to have a more precise picture of the effect of nonuniform surfaces on electrode behavior we shall give a quantitative application of Eq. (14) and its consequences. Fortunately, it is possible to evaluate the integral appearing in this equation if one uses a model distribution function which ought to illustrate many features of actual electrode surfaces.

[29] K. S. Cole, J. Gen. Physiol. **25**, 29 (1941).
[30] T. Teorell, Nature **162**, 961 (1948).

Consider the elliptical region, R, of the x, y plane defined by the equation

$$\left(\frac{x-x_0}{X}\right)^2+\left(\frac{y-y_0}{Y}\right)^2=1. \tag{18}$$

We shall assume that the distribution function $S(x, y)$ is constant inside this region and zero everywhere else. This distribution is shown in Fig. 9. From the condition $\int\int S dx dy=1$ we see that inside R

$$S=1/\pi XY. \tag{19}$$

x_0 and y_0 are thus the mean values of x and y in the distribution and $2X$ and $2Y$ give the range over which the distribution falls. Applying Eqs. (13) and (14),

$$I=\int\int_R Si dx dy=(1/\pi XY)\int\int_R e^{-\gamma} dx dy. \tag{20}$$

This integral may be evaluated by recalling that all points along the line $y=Vx-\gamma$ carry the same current density and by treating γ as the independent variable. Therefore,

$$I=(1/\pi XY)\int_{\gamma_1}^{\gamma_2} e^{-\gamma}\frac{\Delta l d\gamma}{(1+V^2)^{\frac{1}{2}}}, \tag{21}$$

where Δl is the length of the segment of the line $y=Vx-\gamma$ lying inside the ellipse and γ_1 and γ_2 are the values of γ for which the lines $y=Vx-\gamma$ are tangent to the ellipse (see Fig. 23). Let us make the substitutions,

$$Z^2=X^2V^2+Y^2,$$
$$\gamma_0=y_0-x_0V,$$
$$Z\cos\theta=\gamma-\gamma_0.$$

The geometrical significance of Z and γ_0 are indicated in Fig. 23. It is readily found that

$$\Delta l=(1+V^2)^{\frac{1}{2}}(2XY/Z)\sin\theta,$$

and

$$I=(e^{-\gamma_0}/\pi)\int_0^{\pi}\exp(-Z\cos\theta)(1-\cos 2\theta)d\theta$$
$$=e^{-\gamma_0}[\mathcal{I}_0(Z)-\mathcal{I}_2(Z)]=\frac{2\exp(x_0V-y_0)}{Z}\mathcal{I}_1(Z), \tag{22}$$

where $\mathcal{I}_n(Z)$ is the Bessel function of order n with imaginary argument.[31] Equation (22) takes simpler forms in the special cases of very small and very large values of Z, $Z\ll 1$ giving

$$\mathcal{I}_1(Z)\cong Z/2,$$

and $Z\gg 1$ giving

$$\mathcal{I}_1(Z)\cong[e^Z/(2\pi Z)^{\frac{1}{2}}](1-3/8Z-15/16Z^2-\cdots).$$

Thus if we have a very narrow distribution ($Z\ll 1$) we will find

$$I\cong\exp(x_0V-y_0),$$

or

$$V\cong(1/x_0)\ln I+(y_0/x_0), \tag{23}$$

which is Tafel's law, as we should of course expect under these conditions. The current line, $y=Vx-\ln I$, goes through the center of the distribution.

On the other hand, if the distribution is broad ($Z\gg 1$) we find

$$I\cong(2/\pi Z^3)^{\frac{1}{2}}\exp(Z-\gamma_0)$$

or

$$\ln I\cong(X^2V^2+Y^2)^{\frac{1}{2}}-x_0V+y_0+\tfrac{1}{2}\ln 2/(X^2V^2+Y^2)^{\frac{3}{4}}\pi. \tag{24}$$

The over-all current-voltage relation no longer follows Tafel's law. Evidently the average current line lies a vertical distance $(Z+\frac{1}{2}\ln 2/Z^3\pi)$ below the center of the distribution. For large values of Z the logarithmic term becomes relatively unimportant compared with Z itself. Since Z is the vertical distance from the center of the distribution to the lower tangent line (see Fig. 23), we see that as Z increases, the average current line approaches the lower perimeter of the distribution. This result can be expected to be true of all distributions, regardless of their shapes.

Let us denote by λ the ratio of the distance of the current line from the center of the distribution to the distance from the center to the perimeter. That is,

$$\lambda=(-\ln I-\gamma_0)/Z. \tag{25}$$

This ratio is a measure of the deviation from Tafel's law due to the distribution. If λ is zero the current line passes through the center of the distribution and Tafel's law will be valid, while if λ is unity the current line is tangent to the lower edge of the distribution and Tafel's law is not obeyed. The calculated dependence of λ and Z as found from Eqs. (22) and (25) is

Z	0	1	3	10	30	100
λ	0	0.12	0.32	0.63	0.82	0.92.

Evidently the effect of the distribution in causing deviations from Tafel's law begins to become serious when Z is greater than about 3. We have seen, however, that on platinum anodes there is experimental evidence for variations in xV and y amounting to 5 or 10 or more, leading to values of Z much larger than 3. The distribution must therefore play an important part in modifying the instantaneous current-voltage relation for platinum anodes. As yet no experimental method has been devised to measure this relationship without causing changes in the distribution. The results of this appendix do serve to show, however, that it is essential to take the distribution into account in interpreting our experiments.

[31] See, for example, H. Jeffreys and B. S. Jeffreys, *Methods of Mathematical Physics* (The Cambridge University Press, New York, 1946), Chapter 21, especially Eq. (2), p. 542; Eq. (54), p. 547; Eq. (8), p. 550; Eq. (13), p. 552.

Statistical Theory of Networks of Non-Gaussian Flexible Chains*

MING CHEN WANG AND EUGENE GUTH
University of Notre Dame, Notre Dame, Indiana
(Received January 14, 1952)

The aim of this paper is to develop a selfconsistent theory of rubber-like materials consisting of networks of non-Gaussian chain molecules. Three kinds of series developments are derived for the distribution function of perfectly flexible single chains from the Fourier integral solution of Rayleigh; namely, (1) long chains with actual extension much less than the maximum extension, (2) long chains with actual extension comparable to the maximum extension, and (3) short chains. In the non-Gaussian network theory, the leading term of the series (2) is used as the starting point for the individual chains of the network. Calculations are made for the case where the free junctions are moving with no restriction, and for the case where the free junctions are assumed to be at their most probable positions. The final expressions of the elastic energy for the two cases are compared, and it is shown that the percentage difference of the two expressions is of the order $1/n$ (n being the average number of links per chain), which is negligible for sufficiently large n. Finally an expression of the elastic energy is obtained with the assumption that all junctions are fixed and is shown to be, in general, a function of three strain invariants. The interdependence of the coefficients of the invariants is shown. Comparison of theory and experiment is given. Because of the interdependence of the coefficients only part of the observed deviations from Gaussian theory can be explained by our molecular theory. The remaining discrepancies must be ascribed to van der Waals forces. This should show up in the (not yet investigated) temperature dependence of these discrepancies.

I. INTRODUCTION

IN the network theory of rubber elasticity as developed by James and Guth[1] one distinguishes between two types of statistical problems concerning (1) the single chains, which constitute the segments of the network, and (2) the whole cross-linked network.

Problem (1) was solved in a simple manner for arbitrarily large extensions of perfectly flexible chains. The simplicity of the solution was achieved by considering instead of the distribution function its Laplace transform. A generalized partition function (p.f.) was set up which is essentially the statistical analog of the Gibbs free energy function for a single chain stretched by equal and opposite forces at its two ends. From this generalized p.f. we obtain by differentiation the (average) extension of the chain as a function of the (given) stress. The more conventional approach to problems of this type starts from the usual p.f., which is essentially the statistical analog of the Helmholtz free energy function, for a single chain constrained to a constant extension by fixing its two ends. From this usual p.f. we obtain by differentiation the (average) force acting on the two ends of the chain as a function of the (given) extension of the chain.

In reference 1(c) it was proved that the preceding two approaches lead to consistent stress-strain-temperature relationships only in the *limit* of a *large* number of links, i.e., *the existence of a unique equation of state is a limit properly* just as is the existence of phase transitions. However, while the limit character of the existence of phase transitions is quite well known, this does not seem to be the case for the limit character of the existence of an equation of state. As a matter of fact, reference 1(c) published in 1943 seems to contain the first explicit proof of this limit character. Naturally then, for the approach by means of the usual p.f. method, one needs only the limiting or asymptotic form, for a large number of links, of the distribution (=partition) function. The use of a more accurate or of the exact distribution function is obviously superfluous. We wish to emphasize this point because Treloar[2] used the exact distribution function, not realizing its superfluous character in statistical mechanics.

The above condition for the existence of an equation of state is a necessary one. The sufficient condition is that the dimensions of the system should show negligible fluctuations if subjected to a constant force, and conversely.

Problem (2), pertaining to the whole cross-linked network, has been solved completely for the case in which the distribution function of the segments can be approximated by its (dominant) Gaussian term.[1] The statistical properties of such a Gaussian network, consisting of segments with Gaussian distribution functions, have been studied in detail.[3] The theory of the process of cross-linking (cure) leading to Gaussian networks has been developed.[4] More recently, a simplified presentation of the network theory of rubber elasticity has been given together with a critical discussion of other (non-network) theories of rubber elasticity.[5] In all these papers, the Gaussian network has been treated by means of the usual partition (=distribution) function method.

For a whole network an equation of state will exist

* Supported in part by ONR. The chief results of this paper were presented at the November, 1950, Chicago meeting of the American Physical Society; *cf.* Phys. Rev. **81**, 302(A) (1951).

[1] (a) E. Guth and H. M. James, Ind. Eng. Chem. **33**, 624 (1941); (b) H. M. James and E. Guth, Phys. Rev. **59**, 111 (1941); (c) H. M. James and E. Guth, J. Chem. Phys. **11**, 455 (1943).

[2] (a) L. R. G. Treloar, Trans. Faraday. Soc. (London) **42**, 77 (1946); (b) L. R. G. Treloar, *The Physics of Rubber Elasticity*, (Clarendon Press, Oxford, England, 1949), pp. 99–100, Eqs. (6.5).

[3] Cf. reference 1(c), particularly the appendix, and H. M. James, J. Chem. Phys. **15**, 651 (1947).

[4] H. M. James and E. Guth, J. Chem. Phys. **15**, 669 (1947).

[5] (a) Guth, James, and Mark, *Advances in Colloid Science* (Interscience, Publishers, New York, 1946), Vol. II; (b) H. M. James and E. Guth, J. Polymer Sci. **4**, 153 (1949).

as long as the total number of links is large, even if the segments between junctions are short.

For imperfectly flexible chains, methods to obtain distribution functions have been developed by James and Guth in 1943[6] and later, apparently independently, by Kubo.[7]

In contrast to this very satisfactory theory of Gaussian networks, the theory of non-Gaussian networks consisting of non-Gaussian segments is in a very rudimentary state. An approximate theory was developed by James and Guth.[1(a),1(c)] In this theory, the set of three independent hypothetical Gaussian chains parallel to the coordinate axes (to which the real network was proved to be equivalent for the purposes of deriving an equation of state) is replaced by a similar set of non-Gaussian chains. The subsequent analysis follows exactly as for the Gaussian network. The resulting stress-strain-temperature relationship contains two constants, the first of which determines the vertical scale or the modulus in the Gaussian region of low strains, while the second constant measures the maximum extensibility of the chains, and hence, of the network. It was pointed out by James and Guth that the maximum extensibility is proportional to the square root of the chain length. Since the modulus is inversely proportional to the chain length, there is only one independent parameter in the James-Guth theory.

Treloar[8] has attempted to give an improved theory for non-Gaussian networks. As his model, he takes the Flory-Rehner tetrahedron. This "network" consists of only four chains with one junction (cross-link). It was explained in reference 5 why the Flory-Rehner model (in spite of being only a rudimentary representation of a network) leads to the same stress-strain-temperature relationship as the complete network theory does, but only in the Gaussian approximation.

The inadequacy of Gaussian theory to explain the growing amount of experimental data, especially in the recent years, is obvious. There are two main kinds of deviations from the Gaussian theory. One kind of deviation, usually large, occurs in the region of large deformations, such as the upward turning of the stress-strain curve (or the well-known *S*-shape). The other kind, smaller but still observable, occurs in the region of moderate deformations and shows up when one tries to explain deformations of various types (such as simple elongation, shear, compression, etc.) simultaneously. These latter deviations have been described phenomenologically by a generalization to large deformations of the usual theory of elasticity, which considers (infinitesimally) small deformations only. This generalization is due to Mooney[9] and was extensively developed lately by Rivlin[10] and very recently by Green and Shield,[11] who gave a simplified account of the theory using tensor notations.[12]

In this theory of large deformations the elastic energy depends on two (three for compressible materials) so-called strain invariants. In the Gaussian theory of rubber elasticity only one of these strain invariants enters. In Mooney's theory the coefficients of the two strain invariants can be adjusted independently to represent the experimental data.

The present paper was undertaken to develop a more precise and self-consistent molecular non-Gaussian theory. This network theory leads naturally to a theory of large deformations in which the elastic energy is a function of the two (three) strain invariants as in Mooney's and Rivlin's phenomenological theory. In contrast to the phenomenological theory, however, in our molecular theory the coefficients of the strain invariants are not any longer independent of each other and they are all, of course, proportional to the absolute temperature just as the modulus in the Gaussian theory is. The interdependence of the coefficients makes it impossible to explain the experimental data solely on the basis of this generalized molecular theory of rubber elasticity. This situation leads to the prediction, that at least part of the observed deviations from the Gaussian network theory must be due to inter- and intramolecular forces, which are neglected in the present molecular theory of rubber elasticity (ideal rubber). All observed deviations from the Gaussian theory were obtained at room temperature. It is to be expected that investigations of the temperature dependence of these deviations will reveal deviations of the coefficients of the invariants from the simple proportionality with absolute temperature and thus indicate the dependence of the deviations upon the van der Waals (molecular) forces. Such experimental investigations have been started in the Polymer Physics laboratory at the University of Notre Dame. Also a theory has been developed by James and Guth[13] which does take into account the van der Waals forces in a rubber network (real rubber: analog of real gas).

After the present work has been in progress we noticed a paper by Ishihara[14] which starts to develop a

[6] H. M. James and E. Guth, J. Chem. Phys. **11**, 531 (1943).
[7] R. Kubo, J. Phys. Soc. Japan, **2**, 47 (1947); and **3**, 119 (1948).
[8] L. R. G. Treloar, Trans. Faraday. Soc. (London) **42**, 83 (1946).
[9] M. Mooney, J. Appl. Phys. **11**, 582 (1940).
[10] R. S. Rivlin, Phil. Trans. Roy. Soc. (London) **A240**, 459 and 491 (1948), and later papers.
[11] A. E. Green and R. T. Shield, Proc. Roy. Soc. (London) **A202**, 407 (1950); and Phil. Trans. Roy. Soc. (London) **A244**, 47 (1951).
[12] For a modern account of tensor notations in the theory of elasticity, *cf.* L. Brillouin, *Les Tenseurs en Mécanique et en Élasticité* (Dover Publications, New York, 1946).
[13] E. Guth and H. M. James, Phys. Rev. **81**, 302(A) (1951).
[14] A. Ishihara, J. Phys. Soc. Japan **3**, 289 (1948). *Note added at proof:*—A new interesting paper by Ishihara, Hashitsume, and Tatibana, J. Chem. Phys. **19**, 1508 (1951), is more complete and includes comparison with experiment. They put the free junctions into their most probable positions. However, their discussion is still less complete than ours. Their comparison of theory and experiment does not seem to have been extensive enough to show up the discrepancies we found.

non-Gaussian network theory. His treatment, however, is less complete than ours, and no attempt has been made by him to compare theory with experiment. Essentially he assumes all junctions as fixed in space and derives the first two terms of our expression (4.11).

II. NON-GAUSSIAN DISTRIBUTION FUNCTIONS FOR PERFECTLY FLEXIBLE SINGLE CHAINS

In this section we give a brief account of the distribution functions for non-Gaussian single chains. Various kinds of series developments are made starting from the same generally valid formula, namely, the Fourier integral representation, first derived by Rayleigh.[15] The development for long Gaussian chains (actual extension small compared to maximum extension) is, of course, a special case of the general central limit theorem. The development for long non-Gaussian chains (actual extension of the same order as maximum extension) does not seem to have been derived in the literature on probability theory. The nature of the deviations from the Gaussian behavior is best seen for a one dimensional chain and is discussed briefly in Note 1 of Appendix. The starting point for the approximations is here simply the binomial formula (equivalent to symmetric random walk in one dimension). The various approximations can be obtained using the familiar Stirling approximation for factorials.

(A) Exact Formula in Form of a Fourier Integral

A perfectly flexible chain can assume a number of configurations without changing the positions of the ends of the chain. This problem is equivalent to the problem of random flights. In the latter case, a particle makes a given number of steps to reach a point at a certain distance from the starting point. There are a number of ways to get to that point. We shall sketch briefly a simple derivation of Rayleigh's Fourier integral solution of this problem.

Let n be the number of links, each of length l, and $\mathbf{r}$ be the vector from one end of the chain to the other. First we consider the probability, $P_n(x, y, z)dxdydz$, of finding the projection of $\mathbf{r}$ along the coordinate axes between x and $x+dx$, etc. The function $P_n(x, y, z)$ is, of course, a function of the magnitude r only, since everything is spherically symmetric. By definition,

$$\int\int\int_{-\infty}^{+\infty} e^{iux+ivy+iwz}P_n(x, y, z)dxdydz = \langle e^{iux+ivy+iwz}\rangle_{Av}. \quad (2.1)$$

If λ_k, μ_k, ν_k are the projections of the kth link so that

$$x=\sum_{j=1}^{n}\lambda_j, \quad y=\sum_{j=1}^{n}\mu_j \quad \text{and} \quad z=\sum_{j=1}^{n}\nu_j,$$

then

$$\langle e^{iux+ivy+iwz}\rangle_{Av} = \langle\prod_{j=1}^{n} e^{iu\lambda_j+iv\mu_j+iw\nu_j}\rangle_{Av}=\langle e^{iu\lambda+iv\mu+iw\nu}\rangle_{Av}{}^{n}, \quad (2.2)$$

since the orientations of the different links are not correlated. In the last average of (2.2), λ, μ, ν are the projections of any one link. The quantity $(u\lambda+v\mu+w\nu)$ is just the scalar product of the two vectors $\boldsymbol{\varrho}$ and $\mathbf{l}$, whose magnitudes are given by

$$\rho^2=u^2+v^2+w^2 \quad \text{and} \quad l^2=\lambda^2+\mu^2+\nu^2,$$

or simply ρh, where h is the projection of $\mathbf{l}$ on $\boldsymbol{\varrho}$. Thus,

$$\langle e^{iu\lambda+iv\mu+iw\nu}\rangle_{Av}=\langle e^{i\rho h}\rangle_{Av}=\int_{-l}^{+l} e^{i\rho h}\psi(h, l)dh, \quad (2.3)$$

where the probability $\psi(h, l)dh$ that the projection of a link of length l on a given line lies between h and $h+dh$ is given by the ratio

$$\frac{\text{area of spherical surface of radius } l \text{ enclosed between two parallel planes at distances } h \text{ and } h+dh \text{ from origin}}{\text{total area of spherical surface of radius } l} = \frac{2\pi l dh}{4\pi l^2}=\frac{dh}{2l}. \quad (2.4)$$

If (2.4) is used, Eq. (2.3) gives immediately

$$\langle e^{iu\lambda+iv\mu+iw\nu}\rangle_{Av}=\frac{\sin l\rho}{l\rho}. \quad (2.5)$$

Combining Eqs. (2.1), (2.2), and (2.5), and taking the Fourier transform of (2.1), we get

$$P_n(x, y, z) = (1/8\pi^3)\int\int\int_{-\infty}^{+\infty} e^{-iux-ivy-iwz}\left(\frac{\sin l\rho}{l\rho}\right)^n dudvdw.$$

For a fixed value of ρ, the above integral is an average of the same type as that given by (2.3). Therefore,

$$P_n(x, y, z)=(1/8\pi^3)\int_0^{\infty} 4\pi\rho^2 d\rho \times\left(\frac{\sin l\rho}{l\rho}\right)^n\int_{-\rho}^{+\rho} e^{-irg}\psi(g, \rho)dg, \quad (2.6)$$

where g is the projection of $\boldsymbol{\varrho}$ on $\mathbf{r}$. Equation (2.6) shows explicitly that the probability $P_n(x, y, z)$, which we shall call $C(r)$ in the sequel, is a function of r only.

[15] Lord Rayleigh, Phil. Mag. 37, 321 (1919).

Using (2.3) and (2.5), we get from (2.6) the final result

$$C(r)=(1/2\pi^2 l^3 r)\int_0^\infty s\sin rs\,(\sin s/s)^n ds, \quad (2.7)$$

where r is now in units of l. Rayleigh derived the above expression by means of the well-known discontinuous integral of Dirichlet. The two derivations are, of course, essentially the same. The above derivation can be easily generalized to any number of dimensions. The k-dimensional analog of (2.7) is

$$C(r)=\frac{1}{(2\pi)^{k/2}l^k r^{(k-2)/2}}\int_0^\infty s^{k/2}J_{(k-2)/2}(rs)\times\left[\frac{\Gamma(k/2)2^{(k-2)/2}J_{(k-2)/2}(s)}{s^{(k-2)/2}}\right]^n ds,$$

which is due to G. Pólya.[16] One notices that the formula is simpler for odd dimensions than for even ones, a fact which is true for many kinds of physical problems, such as wave propagation.

The integral solution (2.7) is exact, but it is not immediately applicable to practical problems. In the following we shall give different kinds of series developments for the integral both for large n and for small n. In the limit of large n we consider the two cases where $r\ll n$ and $r\sim n$ (r comparable to n).

(B) Series Development for $n\gg 1$ and $r\ll n$.

The development for the case $r\ll$n is essentially due to Rayleigh.[15] To get his result, we develop $\log(\sin s/s)^n$ in a power series of s, i.e.,

$$\log\left(\frac{\sin s}{s}\right)^n=-n\sum_{k=1}^\infty\frac{B_{2k-1}(2s)^{2k}}{(2k)!2k},$$

where the B's are the Bernoulli numbers. Then

$$\left(\frac{\sin s}{s}\right)^n=\exp(-ns^2/6)\exp-n\sum_{k=2}^\infty\frac{B_{2k-1}(2s)^{2k}}{(2k)!2k}$$
$$=\exp(-ns^2/6)\left(1-\frac{ns^4}{180}-\frac{ns^6}{2835}+\frac{7n^2-12n}{453600}s^8\cdots\right). \quad (2.8)$$

Putting (2.8) into (2.7) and integrating term by term, the first term of the integral gives

$$\int_0^\infty s\sin rs\exp(-ns^2/6)ds=\frac{3}{2n}\left(\frac{6\pi}{n}\right)^{\frac{1}{2}}r\exp(-3r^2/2n). \quad (2.9)$$

[16] G. Pólya, Vierteljahrsschrift Naturforsch. Ver. Zürich, **59** (1919).

The rest of the terms can be obtained in the following way: for k even,

$$\int_0^\infty s^{k+1}\sin rs\exp(-ns^2/6)ds$$
$$=(-1)^{k/2}\left(\frac{d}{dr}\right)^k\int_0^\infty s\sin rs\exp(-ns^2/6)ds$$
$$=\frac{3}{2n}\left(\frac{6\pi}{n}\right)^{\frac{1}{2}}(-1)^{k/2}\left(\frac{d}{dr}\right)^k r\exp(-3r^2/2n)$$
$$=\frac{3}{2n}\left(\frac{6\pi}{n}\right)^{\frac{1}{2}}(-1)^{k/2}\left\{r\left(\frac{d}{dr}\right)^k+k\left(\frac{d}{dr}\right)^{k-1}\right\}\times\exp(-3r^2/2n). \quad (2.10)$$

Now if we let

$$y=(3/n)^{\frac{1}{2}}r, \quad (2.11)$$

Eq. (2.10) becomes (with k even)

$$\int_0^\infty s^{k+1}\sin rs\exp[(-ns^2)/6]ds$$
$$=\frac{3}{2n}\left(\frac{6\pi}{n}\right)^{\frac{1}{2}}(-1)^{k/2}\left(\frac{3}{n}\right)^{(k-1)/2}\exp(-y^2/2)\times\{yH_k(y)-kH_{k-1}(y)\}, \quad (2.12)$$

where the H's are the Hermite polynomials which are defined as

$$H_n(y)=(-1)^n\exp(y^2/2)(d/dy)^n\exp(-y^2/2).$$

Using Eqs. (2.8), (2.9), (2.11), and (2.12), we get the series for the integral (2.7)

$$C\left[\left(\frac{n}{3}\right)^{\frac{1}{2}}y\right]=\frac{3}{4\pi nl^3}\left(\frac{6}{\pi n}\right)^{\frac{1}{2}}\exp(-y^2/2)\times\left\{1-\frac{1}{20n}\left(H_4-\frac{4H_3}{y}\right)+\frac{1}{105n^2}\left(H_6-\frac{6H_5}{y}\right)+\left(\frac{1}{800n^2}-\frac{3}{1400n^3}\right)\left(H_8-\frac{8H_7}{y}\right)\cdots\right\}.$$

On going back to the variable r, the last series becomes

$$C(r)=\frac{3}{4\pi nl^3}\left(\frac{6}{\pi n}\right)^{\frac{1}{2}}\exp(-3r^2/2n)\times\{1-3(5-10r^2/n+3r^4/n^2)/20n+(1015-9660r^2/n+13734r^4/n^2-5364r^6/n^3+567r^8/n^4)/5600n^2-9(315-1260r^2/n+1134r^4/n^2-324r^6/n^3+27r^8/n^4\cdots)/1400n^3\cdots\}. \quad (2.13)$$

(C) Series Development for $n \gg 1$ and $r \sim n$

The development for the case $r \sim n$ and n large is obtained by the method of steepest descents. We first write

$$\int_0^\infty s \sin rs \, (\sin s/s)^n ds = (1/2i) \int_{-\infty}^{+\infty} \left(e^{ist} \frac{\sin s}{s} \right)^n s ds, \quad (2.14)$$

where t is the fractional extension r/n. It can be shown that the function,

$$\varphi(s) = \exp(ist) \sin s/s, \quad (2.15)$$

is analytic in the entire finite complex plane; therefore, the integrand of (2.14) must be analytic in the same region. The saddle point, given by the condition

$$(d/ds) \log \varphi(s) = 0,$$

can be shown to be the point $s = iy_0$ on the positive imaginary axis with

$$\coth y_0 - 1/y_0 = \mathfrak{L}(y_0) = t, \quad (2.16)$$

where $\mathfrak{L}(y_0)$ is the Langevin function. The direction of the steepest descent at the saddle point, determined by the requirement that

$$[(d/ds)^2 \log \varphi(s)]_{s=iy_0} (s - iy_0)^2$$

must be real and negative, is the line parallel to the real axis. Thus the integral (2.14) can be approximated by

$$\begin{aligned}(1/2i) &\int_{-\infty}^{+\infty} [\varphi(x+iy_0)]^n (x+iy_0) dx \\ &= \{y_0[\varphi(iy_0)]^n/2\} \int_{-\infty}^{+\infty} \times (1 - nk_2x^2/2 + nk_4x^4/24 \cdots) dx \\ &= \{y_0[\varphi(iy_0)]^n/2\} \int_{-\infty}^{+\infty} \exp(-nk_2x^2/2) \times \{1 + n(k_4 - 3nk_2^2)x^4/24 \cdots\} dx, \quad (2.17)\end{aligned}$$

where k_2 and k_4 are given by

$$\begin{aligned} k_2 &= 1 - t^2 - 2t/y_0, \\ k_4 &= 3nk_2^2 - (5 - 14t^2 + 9t^4 - 22t/y_0 \\ &\qquad + 30t^3/y_0 - 2/y_0^2 + 30t^2/y_0^2 + 6t/y_0^3). \end{aligned} \quad (2.18)$$

The last equality of (2.17) is justified if we keep terms up to x^4 only. Equation (2.16) gives the functional dependence of y_0 on t; i.e.,

$$y_0 = \mathfrak{L}^{-1}(t), \quad (2.19)$$

where $\mathfrak{L}^{-1}$ is the inverse Langevin function. Integrating (2.17) and making use of (2.15), (2.18), and (2.19), we get the final result

$$C(r) = \frac{1}{4\pi n l^3} \left(\frac{2}{\pi n} \right)^{\frac{1}{2}} \left[\frac{\sinh \mathfrak{L}^{-1}(t)}{\mathfrak{L}^{-1}(t) \exp[t\mathfrak{L}^{-1}(t)]} \right]^n \times \left[\frac{\mathfrak{L}^{-1}(t)}{t} \left\{ 1 - t^2 - \frac{2t}{\mathfrak{L}^{-1}(t)} \right\}^{-\frac{1}{2}} \right] \left[1 + \frac{q(t)}{n} \cdots \right] \quad t = r/n, \quad (2.20)$$

with $q(t) = (k_4 - 3nk_2^2)/8k_2^2$. The above development is valid for the entire range $0 \leq t \leq 1$, while the development (2.13) is good only for $t \ll 1$.

In connection with the elastic properties of long chain molecules, we are interested essentially in the quantity $\log C(r)$. Thus, it is clear that the first square bracket in (2.20) gives the main contribution, and the contribution from each successive bracket is only of the order $1/n$ of the contribution from the preceding bracket.

(D) Series Development for Small n (Finite Series)

A simple development for the other extreme case, n small, may not be out of place here. The integral (2.7) may be written in the form

$$C(r) = (-i/4\pi^2 l^3 r) \int_\Gamma s \exp(irs) \, (\sin s/s)^n ds. \quad (2.21)$$

The path Γ is the whole real axis (in its positive direction) except that the region around the origin is replaced by a small half circle in the upper half plane. This little deformation of the path is allowable since the integrand is analytic around the origin. Now we use the development

$$\sin^n s = (1/2^n i^n) \sum_{\tau=0}^{n} (-1)^\tau \binom{n}{\tau} \exp(ins - i2\tau s). \quad (2.22)$$

Putting (2.22) in (2.21), and interchanging summation with integration, we have

$$C(r) = (-1/2^{n+2} i^{n-1} \pi^2 l^3 r) \sum_{\tau=0}^{n} (-1)^\tau \times \binom{n}{\tau} \int_\Gamma e^{i(n-2\tau+r)s}/s^{n-1} ds. \quad (2.23)$$

The integral in (2.23) can be evaluated by using the relation

$$\int_\Gamma (e^{ias}/s^k) ds = \begin{cases} 0 & a > 0 \\ -2\pi i^k a^{k-1}/(k-1)! & a \leq 0. \end{cases} \quad (2.24)$$

Thus from (2.23) we get, using (2.24),

$$C(r)=[1/2^{n+1}(n-2)!\pi l^3 r]\sum_{k=0}^{k\leq(n-r)/2}(-1)^k \times\binom{n}{k}(n-2k-r)^{n-2}. \quad (2.25)^{17}$$

This series contains, as special cases, the expressions given by Rayleigh[14] and Chandrasekhar[18] for the first few values of n. We shall give another derivation of Eq. (2.25) later.[19] The series (2.25) was used by Treloar.[2(b)] However, for large n this series is not practicable. For small n, on the other hand, no unique equation of state exists as discussed in the introduction.

(E) Imperfectly Flexible Chains

One can make similar developments for imperfectly flexible chains, but usually it involves more complicated calculations. For a model corresponding to random walk on diamond lattice, James and Guth have obtained an expression (unpublished) equivalent to the first square bracket of Eq. (2.20) in the case of perfectly flexible chains, i.e.,

$$C(r)\sim[\{2\exp(-2f/t)\,(\sinh^2 f+5/8 +\cosh f\sinh f/t)\}^{1/2(3)^{\frac{1}{2}}}]^n, \quad (2.26)$$

where $t=r(3)^{\frac{1}{2}}/n$ and f is a function of t, which is given by

$$t=\sinh f/(\sinh^2 f+1/4)^{\frac{1}{2}}.$$

III. NETWORK OF PERFECTLY FLEXIBLE NON-GAUSSIAN CHAINS

We shall first derive the distribution function of a network of non-Gaussian chains both for the real case that the free junctions are not restricted in motion, and for the idealized case that the free junctions are restricted to their most probable positions. Then we compare the results of the two cases, and show that the error committed by fixing the free junctions at their most probable positions is of higher order of small quantities. Therefore, it is permissible, for our purpose, to assume that all the free junctions are at their most probable positions. This is, then, just a special case of a model with all junctions fixed.

(A) Free Junctions with Unrestricted Motion

We have shown in Section II(C) that, in the limit of large n, the single chain distribution function is given by the first square bracket of Eq. (2.20), i.e.,

$$C(r)=[\sinh\mathfrak{L}^{-1}(t)/\mathfrak{L}^{-1}(t)\exp\{t\mathfrak{L}^{-1}(t)\}]^n;\quad t=r/n. \quad (3.1)$$

If t, the fractional extension, is small, we develop the function in (3.1) and get the series

$$C(r)=[\exp(-3t^2/2)(1-9t^4/20\cdots)]^n =\exp(-3nt^2/2)(1-9nt^4/20\cdots) =\exp(-3r^2/2n)(1-9r^4/20n^3\cdots). \quad (3.2)$$

The first term is the well-known Gaussian term, and the second term should be the main correction for non-Gaussian behavior.

For a network of such chains, the configuration function is simply the double product

$$\prod_{\tau>\nu}\prod C(r_{\tau\nu})=\prod_{\tau>\nu}\prod\exp(-3r_{\tau\nu}^2/2n_{\tau\nu}) \times(1-9r_{\tau\nu}^4/20n_{\tau\nu}^3), \quad (3.3)$$

where the indices τ and ν denote the end points of a definite chain. The product extends over all the junctions, free or fixed. A further approximation consists in replacing the double product

$$\prod_{\tau>\nu}\prod(1-9r_{\tau\nu}^4/20n_{\tau\nu}^3) \quad \text{by} \quad (1-\sum_{\tau>\nu}\sum 9r_{\tau\nu}^4/20n_{\tau\nu}^3);$$

then we have

$$\prod_{\tau>\nu}\prod C(r_{\tau\nu})\simeq\exp(-\sum_{\tau>\nu}\sum 3r_{\tau\nu}^2/2n_{\tau\nu}) \times(1-\sum_{\tau>\nu}\sum 9r_{\tau\nu}^4/20n_{\tau\nu}^3). \quad (3.4)$$

Now since the free junctions are movable, we have no knowledge of their positions. Therefore, we have to integrate the expression (3.4) over all the coordinates of the free junctions. Thus we get the final configuration function

$$C(x_{p+1}\cdots z_s)=\int_{-\infty}^{+\infty}\cdots\int dx_1dy_1dz_1\cdots dx_pdy_pdz_p \times\exp(-\sum_{\tau>\nu}^{s}\sum^{s}3r_{\tau\nu}^2/2n_{\tau\nu})(1-\sum_{\tau>\nu}^{s}\sum^{s}9r_{\tau\nu}^4/20n_{\tau\nu}^3), \quad (3.5)$$

where we assume that the junctions are indexed in such an order that the first p are the free ones and the remaining $s-p$ are the fixed ones. The distance $r_{\tau\nu}$ is, of course, given by

$$r_{\tau\nu}^2=(x_\tau-x_\nu)^2+(y_\tau-y_\nu)^2+(z_\tau-z_\nu)^2. \quad (3.6)$$

The integrations in (3.5) are all elementary, but laborious. After integrating over the free junctions, C will be a function of the coordinates of the fixed junctions only. If we consider a deformation which changes a unit cube to a parallelopiped of dimensions L_x, L_y, L_z, then for the fixed junctions the following relations

[17] This series is the analog of the binomial formula in the one-dimensional case. We shall show in Note 1 of the Appendix how one can derive the series equivalent to (2.13) and (2.20) for the one-dimensional case from the binomial formula.

[18] S. Chandrasekhar, Revs. Modern Phys. **15**, 1 (1943).

[19] See Note 2 of the Appendix.

will hold,

$$x_\alpha = x_\alpha^{(0)} L_x; \quad y_\alpha = y_\alpha^{(0)} L_y; \quad z_\alpha = z_\alpha^{(0)} L_z; \quad (3.7)$$

where $x_\alpha^{(0)}$, $y_\alpha^{(0)}$, and $z_\alpha^{(0)}$ denote the values in the undeformed state. Inserting (3.7) into (3.5), we get the final result for C in the form

$$C(L_x, L_y, L_z) = \exp[-K(L_x^2+L_y^2+L_z^2)/2] \times\{1-\delta_1-\delta_2(L_x^2+L_y^2+L_z^2) -3H(L_x^4+L_y^4+L_z^4)/20 -3G(L_x^2L_y^2+L_y^2L_z^2+L_z^2L_x^2)/10\}. \quad (3.8)$$

Here the constants are defined as follows:[20]

$$\left.\begin{aligned}
&\delta_1=\sum_k^p\sum_r^p 3D_{k-1,\,k-1}^{(k-1)}D_{r-1,\,r-1}^{(r-1)}/4D_{kk}^{(k)}D_{rr}^{(r)}\{\sum_i^k G_{ik}^2G_{ir}^2\sum_{j\neq i}^s 1/n_{ij}^3 \\
&\qquad +\sum_{i\neq j}^k\sum^r [G_{ik}^2G_{jr}^2-2G_{ik}^2G_{ir}G_{jr}-G_{ik}G_{jk}(G_{ir}-G_{jr})^2]/n_{ij}^3\}, \\
&\delta_2=\sum_r^p [\sum_{\tau>\nu}^s\sum^s (x_{\tau\nu}^{(0)2}+y_{\tau\nu}^{(0)2}+z_{\tau\nu}^{(0)2})(C_{\tau r}-C_{\nu r})^2/2n_{\tau\nu}^3]/\sum_{\tau>\nu}^s\sum^s [(C_{\tau r}-C_{\nu r})^2/n_{\tau\nu}], \\
&K=\sum_{\tau>\nu}^s\sum^s (x_{\tau\nu}^{(0)2}+y_{\tau\nu}^{(0)2}+z_{\tau\nu}^{(0)2})/n_{\tau\nu}, \\
&H=\sum_{\tau>\nu}^s\sum^s (x_{\tau\nu}^{(0)4}+y_{\tau\nu}^{(0)4}+z_{\tau\nu}^{(0)4})/n_{\tau\nu}^3, \\
&G=\sum_{\tau>\nu}^s\sum^s (x_{\tau\nu}^{(0)2}y_{\tau\nu}^{(0)2}+y_{\tau\nu}^{(0)2}z_{\tau\nu}^{(0)2}+z_{\tau\nu}^{(0)2}x_{\tau\nu}^{(0)2})/n_{\tau\nu}^3.
\end{aligned}\right\} \quad (3.9)$$

The $x_{\tau\nu}^{(0)}$, etc., are in turn defined by

$$x_{\tau\nu}^{(0)} = x_\tau^{(0)} - x_\nu^{(0)}, \quad \text{etc.},$$

with

$$x_\tau^{(0)} = \sum_{\beta=p+1}^s C_{\tau\beta}x_\beta^{(0)}, \quad \text{etc.} \quad (3.10a)$$

The $x_\tau^{(0)}$ defined above is not the actual x-coordinate of the τth junction in the undeformed state unless $\tau>p$, since the positions of the free junctions are unknown. It is just defined by the quantities on the right-hand side of (3.10a). If we multiply both sides of the above equation by L_x and use (3.7), we have

$$x_\tau^{(0)}L_x = \sum_{\beta=p+1}^s C_{\tau\beta}x_\beta, \quad \text{etc.}$$

Here we can again define the quantiy $x_\tau^{(0)}L_x$ by x_τ, so we have

$$x_\tau = \sum_{\beta=p+1}^s C_{\tau\beta}x_\beta, \quad \text{etc.} \quad (3.10b)$$

The $C_{\tau\nu}$'s above are given by

$$C_{\tau\nu}=\left\{\begin{array}{lll}
0 & & \tau>p \\
G_{\tau\nu} & \nu\leq p & \tau\leq p \\
J_{\tau\nu} & \nu>p & \tau\leq p \\
1 & & \tau=\nu \\
0 & & \tau>\nu
\end{array}\right\} \quad \tau<\nu \quad (3.11)$$

and

$$G_{\tau\nu}=\left\{\begin{array}{ll}
-\Delta_{\tau\nu}/D_{\nu-1,\,\nu-1}^{(\nu-1)} & \tau<\nu \\
1 & \tau=\nu \\
0 & \tau>\nu
\end{array}\right\},$$

where $\Delta_{\tau\nu}$ is the determinant obtained by replacing the τth column of $D_{\nu-1,\,\nu-1}^{(\nu-1)}$ by the column $\gamma_{1\nu}, \gamma_{2\nu}\cdots\gamma_{\nu-1,\,\nu}$. The quantity $J_{\tau\nu}$ in (3.11) is defined by James[21] as $C_{\tau\nu}$. All the rest of the undefined symbols have the same meaning as in James' paper mentioned above. In deriving (3.8), we have also assumed that the network is isotropic in the unstrained state; i.e.,

$$\sum_{\tau>\nu}^s\sum^s x_{\tau\nu}^{(0)2}/n_{\tau\nu} = \sum_{\tau>\nu}^s\sum^s y_{\tau\nu}^{(0)2}/n_{\tau\nu} = \sum_{\tau>\nu}^s\sum^s z_{\tau\nu}^{(0)2}/n_{\tau\nu}, \quad (3.12a)$$

$$\sum_{\tau>\nu}^s\sum^s x_{\tau\nu}^{(0)4}/n_{\tau\nu}^3 = \sum_{\tau>\nu}^s\sum^s y_{\tau\nu}^{(0)4}/n_{\tau\nu}^3 = \sum_{\tau>\nu}^s\sum^s z_{\tau\nu}^{(0)4}/n_{\tau\nu}^3, \quad (3.12b)$$

$$\sum_{\tau>\nu}^s\sum^s x_{\tau\nu}^{(0)2}y_{\tau\nu}^{(0)2}/n_{\tau\nu}^3 = \sum_{\tau>\nu}^s\sum^s y_{\tau\nu}^{(0)2}z_{\tau\nu}^{(0)2}/n_{\tau\nu}^3 = \sum_{\tau>\nu}^s\sum^s z_{\tau\nu}^{(0)2}x_{\tau\nu}^{(0)2}/n_{\tau\nu}^3. \quad (3.12c)$$

As a simple example, let us calculate the configuration function of the tetrahedral "network" (Flory-

[20] When the range of the summation index is not given, it is to be taken as extending from unity to the upper limit indicated.

[21] See reference 3, Eq. (2.10), with $i=\tau$ and $\alpha=\nu$.

Rehner model) by means of (3.8). This "network" consists of four chains of n links each starting from four fixed junctions at the corners of a regular tetrahedron and meeting at one free junction. Thus $p=1$, $s=5$, $n_{12}=n_{13}=n_{14}=n_{15,}=n$, and all other $n_{\tau\nu}=0$. From the definitions given above, one can show easily that for this case

$$\delta_1=3/16n; \quad \delta_2=K/8n.$$

Thus,

$$C(L_x, L_y, L_z)=\exp[-K(L_x^2+L_y^2+L_z^2)/2] \times\{1-3/16n-K(L_x^2+L_y^2+L_z^2)/8n -3H(L_x^4+L_y^4+L_z^4)/20 -3G(L_x^2L_y^2+L_y^2L_z^2+L_z^2L_x^2)/10\}. \quad (3.13)$$

For this simple model one can get (3.13) very easily also by direct calculation. Let $\mathbf{S}$ and $\boldsymbol{\varrho}_i$ be the vectors from the center of the tetrahedron to the free junction and to the ith fixed junction, respectively, and ρ be the length of the four $\boldsymbol{\varrho}_i$'s. Then,

$$r_i^2=S^2+\rho^2-2\mathbf{S}\cdot\boldsymbol{\varrho}_i. \quad (3.14)$$

The equivalent form of (3.5) for this case is

$$C=\int\int\int S^2dSd\Omega\exp(-3\sum_{i=2}^{5} r_i^2/2n)(1-9\sum_{i=2}^{5} r_i^4/20n^3)$$

$$d\Omega=\sin\theta d\theta d\phi, \quad (3.15)$$

where S, θ, ϕ are the spherical coordinates of the free junction. One can show that

$$\sum_{i=2}^{5}\mathbf{S}\cdot\boldsymbol{\varrho}_i=0$$

and

$$\sum_{i=2}^{5}(\mathbf{S}\cdot\boldsymbol{\varrho}_i)^2=4S^2\rho^2/3.$$

Using these relations together with Eq. (3.14), one finds that the integrand of (3.15) is spherically symmetric. Therefore,

$$C=4\pi\int^{\infty} S^2dS\exp[-6(\rho^2+S^2)/n] \times[1-9(\rho^4+S^4+10\rho^2S^2/3)/5n^3] \simeq\exp(-6\rho^2/n)[(1-3/16n)-3\rho^2/2n^2-9\rho^4/5n^3]. \quad (3.16)$$

Now, using (3.7) and (3.12),

$$\rho^2=\sum_{i=2}^{5}(x_i^2+y_i^2+z_i^2)/4=\sum_{i=2}^{5}(x_i^{(0)2}L_x^2+y_i^{(0)2}L_y^2+z_i^{(0)2}L_z^2)/4$$

$$=\sum_{i=2}^{5}(x_i^{(0)2}+y_i^{(0)2}+z_i^{(0)2})(L_x^2+L_y^2+L_z^2)/12$$

$$=nK(L_x^2+L_y^2+L_z^2)/12,$$

and

$$\rho^4=\sum_{i=2}^{5}(x_i^2+y_i^2+z_i^2)^2/4=n^3H(L_x^4+L_y^4+L_z^4)/12 +n^3G(L_x^2L_y^2+L_y^2L_z^2+L_z^2L_x^2)/6.$$

Inserting the last two expressions into (3.16), we get (3.13) exactly.

(B) Free Junctions Restricted to Most Probable Positions

The configuration function of the network as a function of the coordinates of both the free and the fixed junctions is given by (3.4); i.e.,

$$C=\exp\{-3\sum_{\tau>\nu}^{s}\sum^{s}[(x_\tau'-x_\nu')^2+(y_\tau'-y_\nu')^2 +(z_\tau'-z_\nu')^2]/2n_{\tau\nu}\}\{1-9\sum_{\tau>\nu}^{s}\sum^{s}[(x_\tau'-x_\nu')^2 +(y_\tau'-y_\nu')^2+(z_\tau'-z_\nu')^2]^2/20n_{\tau\nu}^3\}. \quad (3.17)$$

We use x', y', z' here in order to distinguish these coordinates from the x, y, z defined in (3.10a) (which will appear later).

If the free junctions are at their most probable positions, we should have

$$\partial C/\partial x_i'=0 \quad \text{or} \quad \partial\log C/\partial x_i'=0 \quad i=1, 2\cdots p.$$

From (3.17) we get, for the last condition,

$$\sum_{\nu}^{s}\{(x_\nu'-x_i')/n_{\nu i}+3(x_\nu'-x_i')[(x_\nu'-x_i')^2 +(y_\nu'-y_i')^2+(z_\nu'-z_i')^2]/5n_{\nu i}^3\}=0 \quad i=1, 2\cdots p.$$

These p equations and the other two similar sets for the y and z coordinates together form a system of $3p$ equations from which one gets the most probable values of x_1', y_1', $z_1'\cdots x_p'$, y_p', z_p' as functions of the fixed junction coordinates. It is impossible to solve the system exactly; therefore, we shall first drop the term with $n_{\nu i}^3$ and get a solution in first approximation. This is just the solution for the Gaussian case given by James.[22] Putting these approximate values of $x_1'\cdots z_p'$ into the terms omitted previously and solving the equation again, we get

$$x_i'=\sum_{\alpha=p+1}^{s} C_{i\alpha}x_\alpha+3\Gamma^{i\to fx}/5\Gamma, \quad (3.18)$$

where Γ is defined in reference 3, and $\Gamma^{i\to fx}$ is the determinant obtained by replacing the ith column of Γ by the column f_{1x}, $f_{2x}\cdots f_{px}$, which is defined as

$$f_{kx}=L_x\sum_{\tau}^{s}(x_\tau^{(0)}-x_k^{(0)})[(x_\tau^{(0)}-x_k^{(0)})^2L_x^2 +(y_\tau^{(0)}-y_k^{(0)})^2L_y^2+(z_\tau^{(0)}-z_k^{(0)})^2L_z^2]/n_{\tau k}^3. \quad (3.19)$$

Using this expression for f_{kx} in (3.18), we get

$$x_i'=x_i+\epsilon_{ix}, \quad (3.20)$$

where x_i is defined by (3.10), and

$$\epsilon_{ix}=3L_x(\Gamma^{i\to X_x}L_x^2+\Gamma^{i\to Y_x}L_y^2+\Gamma^{i\to Z_x}L_z^2)/5\Gamma. \quad (3.21)$$

Here $\Gamma^{i\to X_x}$ is the determinant obtained by replacing the ith column of Γ by the column X_{1x}, $X_{2x}\cdots X_{px}$, and similarly for $\Gamma^{i\to Y_x}$ and $\Gamma^{i\to Z_x}$. X_{kx}, Y_{kx}, and Z_{kx} are

[22] See reference 3, Eq. (2.8).

defined as follows:

$$X_{kx}=\sum_{\tau}^{s}(x_\tau^{(0)}-x_k^{(0)})^3/n_{\tau k}^3, \tag{3.22a}$$

$$Y_{kx}=\sum_{\tau}^{s}(x_\tau^{(0)}-x_k^{(0)})(y_\tau^{(0)}-y_k^{(0)})^2/n_{\tau k}^3, \tag{3.22b}$$

$$Z_{kx}=\sum_{\tau}^{s}(x_\tau^{(0)}-x_k^{(0)})(z_\tau^{(0)}-z_k^{(0)})^2/n_{\tau k}^3. \tag{3.22c}$$

We will now put the most probable values of the free junction coordinates, given by (3.20), into (3.17), and keep enough terms for the present approximation. Then, again assuming isotropy, we get

$$\begin{aligned}C(L_x, L_y, L_z)=&\exp[-K(L_x^2+L_y^2+L_z^2)/2]\\&\times\{1-3H'(L_x^4+L_y^4+L_z^4)/20\\&-3G'(L_x^2L_y^2+L_y^2L_z^2+L_z^2L_x^2)/10\},\end{aligned} \tag{3.23}$$

where

$$\begin{aligned}H'=H+\frac{12}{\Gamma}\Bigg\{&\sum_{i}^{p}\sum_{>i}^{p}\frac{x_i^{(0)}-x_j^{(0)}}{n_{ij}}(\Gamma^{i\to X_x}-\Gamma^{j\to X_x})\\&+\sum_{i}^{p}\sum_{\alpha=p+1}^{s}\frac{x_i^{(0)}-x_\alpha^{(0)}}{n_{i\alpha}}\Gamma^{i\to X_x}\Bigg\},\end{aligned} \tag{3.24a}$$

$$\begin{aligned}G'=G+\frac{6}{\Gamma}\Bigg\{&\sum_{i}^{p}\sum_{>i}^{p}\frac{x_i^{(0)}-x_j^{(0)}}{n_{ij}}(\Gamma^{i\to Y_x}-\Gamma^{j\to Y_x})\\&+\sum_{i}^{s}\sum_{\alpha=p+1}^{p}\frac{x_i^{(0)}-x_\alpha^{(0)}}{n_{i\alpha}}\Gamma^{i\to Y_x}\Bigg\}.\end{aligned} \tag{3.24b}$$

Since the coordinate differences occurring in X_{kx}, Y_{kx}, and Z_{kx} are of odd power, the difference between H' and H is small compared with H, and the same is true for G' and G. In fact, for the regular cubic network or the tetrahedron network, X_{kx}, etc., are zero; therefore, $H'=H$ and $G'=G$.

(C) Comparison between the Two Cases Treated in Sections (A) and (B)

The two configuration functions for the cases considered in (A) and (B) are given by (3.8) and (3.23), respectively. Since the stress-strain relation can be derived from the so-called elastic energy function, which is essentially log$C$, we will take the log of the two expressions and then carry through the comparison. From (3.8) and (3.23), we get

$$\begin{aligned}\log C=&-(K+2\delta_2)(L_x^2+L_y^2+L_z^2)/2\\&-3H(L_x^4+L_y^4+L_z^4)/20\\&-3G(L_x^2L_y^2+L_y^2L_z^2+L_z^2L_x^2)/10+\text{constant}\end{aligned} \tag{3.25a}$$

and

$$\begin{aligned}\log C=&-K(L_x^2+L_y^2+L_z^2)/2\\&-3H'(L_x^4+L_y^4+L_z^4)/20\\&-3G'(L_x^2L_y^2+L_y^2L_z^2+L_z^2L_x^2)/10,\end{aligned} \tag{3.25b}$$

respectively. In getting (3.25) we have kept only the first term of the Taylor series expansion for $\log(1+x)$.

The two expressions (3.25a) and (3.25b) differ in two respects (apart from the unessential constant). First, the coefficients H and G are different from H' and G' as shown in (3.24); but we have indicated that the difference can probably be neglected compared with H and G themselves. The other difference is the additional term $2\delta_2$ in (3.25a). From the definitions of δ_2 and K in (3.9), we can see that the ratio $2\delta_2/K$ is of the order $1/n$. For the simple tetrahedral network, we have shown that $\delta_2=K/8n$; therefore, $2\delta_2/K=1/4n$. For the regular cubic network, the $x_\tau^{(0)}$'s, etc., defined in (3.10b) turn out to be the actual values of the coordinates of the junctions at their regular positions. Therefore, the quantity $(x_{\tau\nu}^{(0)2}+y_{\tau\nu}^{(0)2}+z_{\tau\nu}^{(0)2})$, or $r_{\tau\nu}^{(0)2}$, occurring in δ_2 and K is also the actual distance between the τth and the νth junctions in the undeformed state. Since the network is regular, all $r_{\tau\nu}^{(0)2}$'s are equal and so are the $n_{\tau\nu}$'s. Let the constant ratio $r_{\tau\nu}^{(0)}/n_{\tau\nu}$ be t, and all $n_{\tau\nu}$'s be n. Then it is easy to see that

$$\frac{2\delta_2}{K}=\frac{1}{n}\frac{\text{total number of free junctions}}{\text{total number of chains}}. \tag{3.26}$$

If the number of free junctions along one side of the cube is m, the total number of free junctions is m^3, and the total number of chains is $3m^2(m+1)$. Then (3.26) becomes

$$\frac{2\delta_2}{K}=\frac{1}{n}\frac{m}{3(m+1)}\quad\text{or}\quad\frac{1}{3n}\quad\text{for } m \text{ large.}$$

The tetrahedral network also fulfills the condition (3.26). One has here four chains and one free junction. Therefore, (3.26) gives

$$2\delta_2/K=1/4n,$$

which is what we got previously. Consequently, if n is large, the term $2\delta_2$ in (3.25a) can be neglected compared with the term K.

Thus we have shown that if we are willing to neglect differences of higher order of small quantities, we may treat the free junctions as fixed ones.

(D) All Junctions Fixed

If we treat all junctions as fixed ones, the calculation is more general as well as simpler. We start with the complete series expansion of the function in (3.1)

$$C(t)=\exp(-3nt^2/2)(1+\sum_{k=2}^{\infty}a_kt^{2k})^n,$$

where $a_2=-9/20$, etc. Then for the network

$$C=\prod_{\tau>\nu}^{s}\prod^{s}\exp(-3n_{\tau\nu}l_{\tau\nu}^2/2)(1+\sum_{k=2}^{\infty}a_k l_{\tau\nu}^{2k})^{n_{\tau\nu}}$$

and

$$\log C=-3\sum_{\tau>\nu}^{s}\sum^{s}n_{\tau\nu}l_{\tau\nu}^2/2$$
$$+\sum_{\tau>\nu}^{s}\sum^{s}n_{\tau\nu}\log(1+\sum_{k=2}^{\infty}a_k l_{\tau\nu}^{2k})$$
$$=\sum_{k=1}^{\infty}b_k\sum_{\tau>\nu}^{s}\sum^{s}n_{\tau\nu}l_{\tau\nu}^{2k}, \quad (3.27)$$

where $b_1=-3/2$, $b_2=a_2$, $b_3=a_3$ and all the other b_k's are polynomials of the constants a_k. The quantity $l_{\tau\nu}$ in (3.27) is, by definition,

$$l_{\tau\nu}^2=(r_{\tau\nu}/n_{\tau\nu})^2=[(x_\tau-x_\nu)^2+(y_\tau-y_\nu)^2+(z_\tau-z_\nu)^2]/n_{\tau\nu}^2.$$

Now if all junctions are fixed, (3.7) is true for all of them. Then, for all τ and ν,

$$l_{\tau\nu}^2=[(x_\tau^{(0)}-x_\nu^{(0)})^2L_x^2+(y_\tau^{(0)}-y_\nu^{(0)})^2L_y^2+(z_\tau^{(0)}-z_\nu^{(0)})^2L_z^2]/n_{\tau\nu}^2$$

and

$$l_{\tau\nu}^{2k}=\frac{1}{n_{\tau\nu}^{2k}}\sum_{i=0}^{k}\sum_{m=0}^{k-i}\frac{k!}{i!m!(k-i-m)!}$$
$$\times x_{\tau\nu}^{(0)2i}y_{\tau\nu}^{(0)2m}z_{\tau\nu}^{(0)2(k-i-m)}L_x^{2i}L_y^{2m}L_z^{2(k-i-m)}, \quad (3.28)$$

where $x_{\tau\nu}^{(0)}=x_\tau^{(0)}-x_\nu^{(0)}$, etc. If we again assume the isotropy conditions (3.12) and similar ones involving other combinations, it is obvious that the kth term in (3.27) will consist of combinations of the form

$(L_x^2+L_y^2+L_z^2)$ for $k=1$
$(L_x^4+L_y^4+L_z^4)$, $(L_x^2L_y^2+L_y^2L_z^2+L_z^2L_x^2)$ for $k=2$
$(L_x^6+L_y^6+L_z^6)$,
$(L_x^2L_y^4+L_y^2L_z^4+L_z^2L_x^4+L_x^4L_y^2+L_y^4L_z^2+L_z^4L_x^2)$,
$(L_x^2L_y^2L_z^2)$ for $k=3$, etc.,

since everything is symmetrical in x, y, z. It can be shown that all the above combinations can be expressed in terms of the three invariants

$$I_1=L_x^2+L_y^2+L_z^2;\quad I_2=L_x^2L_y^2+L_y^2L_z^2+L_z^2L_x^2;\quad I_3=L_x^2L_y^2L_z^2.$$

For example,

$$L_x^4+L_y^4+L_z^4=I_1^2-2I_2$$
$$L_x^6+L_y^6+L_z^6=I_1^3-3I_1I_2+3I_3$$
$$L_x^2L_y^4+L_y^2L_z^4+L_z^2L_x^4+L_x^4L_y^2+L_y^4L_z^2+L_z^4L_x^2=I_1I_2-3I_3.$$

Therefore, the whole expression (3.27) can be expressed as a function of the three invariants. Mooney[9] and Rivlin[10] have introduced a phenomenological theory in which the elastic energy is assumed to be expressible in terms of these three invariants.

Keeping the first two terms of the infinite series in (3.27), this equation has the final form

$$\log C=-K(L_x^2+L_y^2+L_z^2)/2-3H(L_x^4+L_y^4+L_z^4)/20-3G(L_x^2L_y^2+L_y^2L_z^2+L_z^2L_x^2)/10,$$

which is similar to (3.25). The constants K, H, and G are defined by (3.9), except here $x_{\tau\nu}^{(0)}$, etc., are the actual coordinate differences between the τth and the νth junctions in the undeformed state. These constants can be evaluated by assuming two distribution functions characterizing the statistical properties of the network. Following James and Guth,[4] let $F(n)dn$ be the number of chains per unit volume with number of links between n and $n+dn$ and let $G(n, t)dt$ be the fraction of these chains which have fractional extension between t and $t+dt$ in the undeformed state. Then

$$\left.\begin{aligned}K&=\int_0^\infty dn\int_0^1 dtF(n)G(n,t)nt^2\\ H&=(3/5)\int_0^\infty dn\int_0^1 dtF(n)G(n,t)nt^4\\ G&=H/3,\\ &\text{etc.}\end{aligned}\right\} \quad (3.29)$$

Here one also assumes that the network satisfies the isotropy condition (3.12) for all orientations of the axes. For the regular cubic network, both $F(n)$ and $G(n, t)$ are δ-functions. By definition

$$\int_0^\infty F(n)dn=N;\quad \int_0^1 G(n,t)dt=1,$$

where N is the total number of chains per unit volume. Thus, for the regular cubic network, (3.29) gives

$$K=Nnl^2;\quad H=3Nnl^4/5;\quad G=Nnl^4/5. \quad (3.30)$$

If we orient the axes in the directions of the chains, (3.12) is satisfied, but the values obtained for these constants, by direct calculation from (3.9), are

$$K=Nnl^2;\quad H=Nnl^4;\quad G=0,$$

which do not agree with (3.30). Therefore, the regular cubic network is not isotropic for all orientations of the axes.

All that we have derived in this Section III can be applied to cases of imperfectly flexible chains. Since we cannot work with the closed form (3.1), and have to start from the development (3.2), we can always make the same kind of development for imperfectly flexible chains. The difference will be only in the numerical coefficients, which do not affect the essential arguments in the calculation that follows. For example, for the diamond lattice model one can develop the expression

TABLE I.

	Perfectly flexible chain	Diamond lattice
b_1	$-3/2$	$-\sqrt{3}/4$
b_2	$-9/20$	$-11\sqrt{3}/64$
b_3	$-99/350$	$-609\sqrt{3}/2560$

(2.26) into the series

$$C(r)\sim\exp[-(3)^{\frac{1}{2}}r^2/4n][1-11(3)^{\frac{1}{2}}r^4/64n^3\cdots],$$

which can be used as the starting expression instead of (3.2).

IV. COMPARISON WITH EXPERIMENTS

For the following calculation we shall take the first three terms of Eq. (3.27). After inserting the constants and using the condition of isotropy, we get

$$\begin{aligned}\log C=&b_1\langle u^2\rangle I_1/3+b_2\langle u^4\rangle(I_1^2-2I_2)/5\\&+2b_2\langle u^4\rangle I_2/15+b_3\langle u^6\rangle(I_1^3-3I_1I_2+3I_3)/7\\&+3b_3\langle u^6\rangle(I_1I_2-3I_3)/35+2b_3\langle u^6\rangle I_3/35,\end{aligned}\quad(4.1)$$

where

$$\langle u^k\rangle=\int_0^\infty dn\int_0^1 dt F(n)G(n,t)nt^k.\quad(4.2)$$

Now the elastic energy W is given by

$$W=-kT\log[C(I_1,I_2,I_3)/C(3,3,1)],$$

where k is the Boltzmann constant, and T the absolute temperature. When (4.1) is used, we have

$$\begin{aligned}W=&-kT\{b_1\langle u^2\rangle I_1/3+b_2\langle u^4\rangle(I_1^2-4I_2/3)/5\\&+b_3\langle u^6\rangle(I_1^3-12I_1I_2/5)/7+\text{constant}\},\end{aligned}\quad(4.3)$$

where we have used the incompressibility condition $I_3=1$.

Mooney,[9] in his theory of large elastic deformations, assumes

$$W=C_1I_1+C_2I_2+\text{constant},\quad(4.4)$$

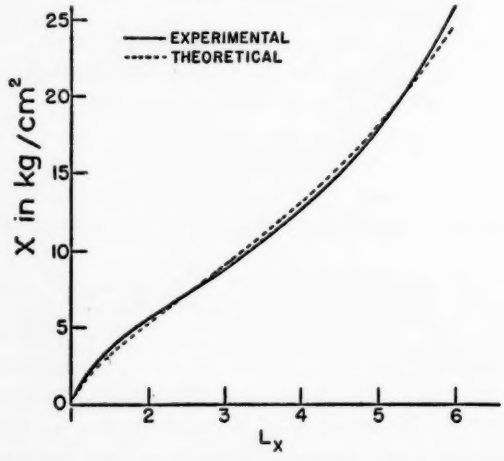

FIG. 1. Stress-strain curves for simple elongation. Experimental curve copied from reference 2(b) Fig. 5.1(a). Parameters for theoretical curve: $kTN=2.88$, $3/5\tilde{n}=0.007$.

and he also introduces terms with higher powers of the invariants in his general theory. However, he assumes all the coefficients C_1, C_2, etc., to be arbitrary constants. In our expression (4.3), the coefficients are not entirely independent. Once the distribution functions $F(n)$ and $G(n,t)$ are given, all the $\langle u^k\rangle$'s are determined; there are only a definite number of arbitrary coefficients, depending on the number of adjustable parameters in the assumed distribution functions.

For the function $G(n,t)$ we will use the expression given by James and Guth,[23] i.e.,

$$G(n,t)=4(3n/2)^{\frac{3}{2}}\pi^{-\frac{1}{2}}l^2\exp(-3nl^2/2),\quad(4.5)$$

and let us take

$$F(n)=N\delta(n-\tilde{n});\quad\int_0^\infty F(n)dn=N,\quad(4.6)$$

where $\delta(x)$ is the Dirac singular function normalized to unity, N the number of chains per unit volume and $\tilde{n}$ the average number of links per chain. Then we calculate the $\langle u^k\rangle$'s from (4.2), and obtain

$$\langle u^k\rangle=1\cdot3\cdots(k+1)N\tilde{n}^{1-k/2}/3^{k/2}.\quad(4.7)$$

Since here we use two adjustable parameters, N and $\tilde{n}$, in the distribution functions, we can leave two of the $\langle u^k\rangle$'s arbitrary. Therefore, if we are willing to neglect terms with $\langle u^6\rangle$ in (4.3), there is no need to make any assumption about the form of $F(n)$ and $G(n,t)$.

Rivlin[24] has shown that the principal components of stresses $t_i(i=x,y,z)$ associated with the pure homogeneous deformation of the material, for which the extension ratios are $L_i(i=x,y,z)$, are given by

$$t_i=2\left[L_i^2\frac{\partial W}{\partial I_1}-\frac{1}{L_i^2}\frac{\partial W}{\partial I_2}\right]+p\quad i=x,y,z,\quad(4.8)$$

where p is an arbitrary hydrostatic pressure. Subtracting one Eq. (4.8) from the other, we get

$$t_x-t_y=2(L_x^2-L_y^2)(\partial W/\partial I_1+L_z^2\partial W/\partial I_2),\quad(4.9)$$

in which the incompressibility condition has been used. When the expression (4.3) is used for W, Eq. (4.9) becomes

$$\begin{aligned}t_x-t_y=&-(2/3)kTb_1\langle u^2\rangle(L_x^2-L_y^2)\\&\times\{1+6b_2\langle u^4\rangle(I_1-2L_z^2/3)/5b_1\langle u^2\rangle\\&+9b_3\langle u^6\rangle(I_1^2-4I_2/5-4L_z^2I_1/5)/7b_1\langle u^2\rangle\}.\end{aligned}\quad(4.10)$$

For the case of a simple elongation along the x-axis, $L_y=L_z=1/(L_x)^{\frac{1}{2}}$ and $t_y=0$. Thus Eq. (4.10) reduces to

$$\begin{aligned}t_x=&-(2/3)kTb_1\langle u^2\rangle(L_x^2-1/L_x)\\&\times\{1+6b_2\langle u^4\rangle(L_x^2+4/3L_x)/5b_1\langle u^2\rangle\\&+9b_3\langle u^6\rangle(L_x^4+8L_x/5+8/5L_x^2)/7b_1\langle u^2\rangle\}.\end{aligned}\quad(4.11)$$

[23] See reference 4, Eq. (21).
[24] R. S. Rivlin, Phil. Trans. (London) **A, 241**, 379 (1948).

Here the quantity t_x is force per unit strained area. It is related to the force per unit unstrained area, X, by

$$t_x = X/L_yL_z = L_xX. \tag{4.12}$$

The stress-strain curve is usually plotted with X against L_x. The constants b_1, b_2, and b_3 in the foregoing equations have the values given in Table I.

Figure 1 shows the experimental stress-strain curve in comparison with the theoretical curve plotted by means of Eqs. (4.11) and (4.12) using (4.7) and the model of perfectly flexible chains. Figure 2 gives the theoretical curves for the deformations shear and 2-dimensional extension. The corresponding experimental curves are given in Fig. 3. By comparing Figs. 2 and 3, we notice immediately that our theoretical curves do not portray the experimental curves very well, but they do give the same qualitative behavior. In plotting Figs. 1 and 2, we have used the same numerical values for the parameters, since the experimental values are obtained from the same sample of rubber.

If the number of links of every segment of the network is known, one can calculate the most probable positions of all the free junctions and obtain an exact expression for the configuration function $C(L_x, L_y, L_z)$ by using the exact distribution function (3.1) instead of the development (3.2) for the single chains. If the network is not completely isotropic, the function $C(L_x, L_y, L_z)$ would be different for different orientations of the axes. However, there may be one particular orientation for which the isotropy conditions (3.12) are satisfied; then $C(L_x, L_y, L_z)$ will still be symmetric and the stress-strain relation will have a simple form. For the regular cubic network with axes parallel to the three sets of chains, the exact expression of $C(L_x, L_y, L_z)$ leads to the stress-strain relation, similar to (4.10),

$$t_x - t_y = M\{L_x\mathfrak{L}^{-1}(L_x\kappa) - (L_y\mathfrak{L}^{-1}(L_y\kappa)\}, \tag{4.13a}$$

which is, of course, just the expression obtained in the James-Guth non-Gaussian theory[1(e)]. Similarly for the tetrahedral network we can orient the axes so that the network satisfies (3.12) and obtain the simple exact stress-strain relation

$$t_x - t_y = M(L_x^2 - L_y^2)\frac{\mathfrak{L}^{-1}(p\kappa)}{p};\quad p = (L_x^2 + L_y^2 + L_z^2)^{\frac{1}{2}}. \tag{4.13b}$$

In both (4.13a) and (4.13b), the function $\mathfrak{L}^{-1}(x)$ is the inverse Langevin function, and M and κ are constant parameters. However, both models are not realistic, since they are not isotropic for all orientations of the axes.

We have also tried to represent the experimental data given by Rivlin and Sauders,[25] and Boonstra[26] by

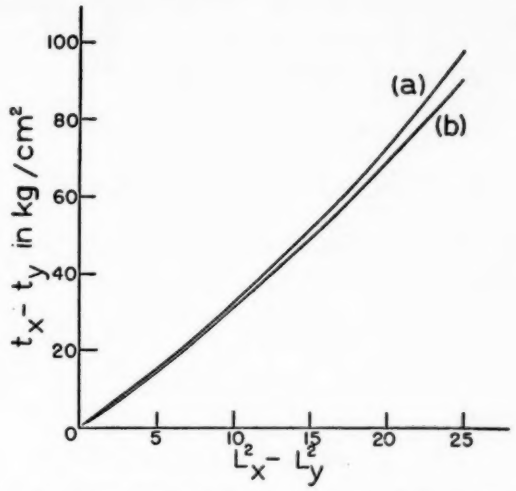

FIG. 2. Curves of Eq. (4.10) for (a) 2-dimensional extension, (b) shear. Parameters have same values as in Fig. 1.

our theoretical formula (4.3) for the elastic energy, but no agreement is found. In deriving Eq. (4.3), we have assumed that the network satisfies the isotropy condition (3.12) for all orientations of the axes, therefore, the quantities H and G defined by (3.9) are related by (3.29), i.e.,

$$H = 3G. \tag{4.14}$$

If we are willing to discard the relation (4.14) and to assume $H < G$, we can surmount one of the main difficulties in fitting the theory with those experiments. However, it does not seem reasonable to make this assumption. In fact, even if the network satisfies the isotropy condition for only one orientation of the axes, one can show that $H \geq G$. To simplify the notation, let

$$x_i = x_{rr}^{(0)}/n_{rr}^{\frac{1}{2}}$$

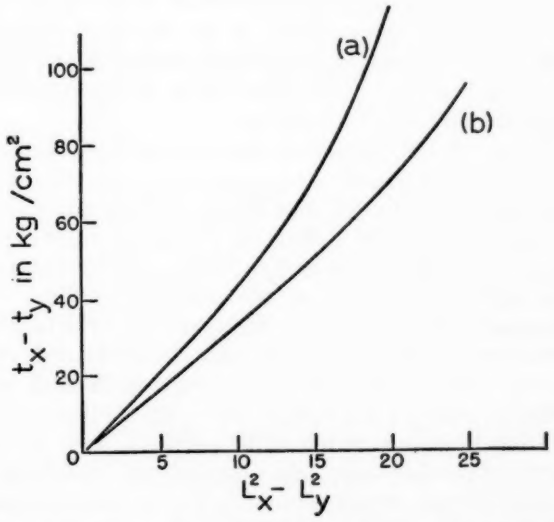

FIG. 3. Experimental curves, corresponding to the theoretical curves in Fig. 2, copied from reference 2(b) Fig. 5.7.

[25] R. S. Rivlin and D. W. Saunders, Phil. Trans. (London) **A243**, 251 (1951).
[26] B. B. S. T. Boonstra, J. Appl. Phys. **21**, 1098 (1950).

so that

$$H=3\sum_{\tau>\nu}^{s}\sum^{s} x_{\tau\nu}{}^{(0)4}/n_{\tau\nu}{}^{3}=3\sum_{i} x_i{}^{4},$$

$$G=3\sum_{\tau>\nu}^{s}\sum^{s} x_{\tau\nu}{}^{(0)2}y_{\tau\nu}{}^{(0)2}/n_{\tau\nu}{}^{3}=3\sum_{i} x_i{}^{2}y_i{}^{2}, \tag{4.15}$$

where the i-summation extends over all the chains. By symmetry,

$$\sum_{\substack{\text{all } i \text{ with}\\ x_i{}^2>y_i{}^2}} x_i{}^2(x_i{}^2-y_i{}^2)=\sum_{\substack{\text{all } i \text{ with}\\ y_i{}^2>x_i{}^2}} y_i{}^2(y_i{}^2-x_i{}^2).$$

Therefore,

$$\sum_{\substack{\text{all } i \text{ with}\\ x_i{}^2>y_i{}^2}} x_i{}^2(x_i{}^2-y_i{}^2)\geq\sum_{\substack{\text{all } i \text{ with}\\ y_i{}^2>x_i{}^2}} x_i{}^2(y_i{}^2-x_i{}^2)$$

or

$$\sum_{\substack{\text{all } i \text{ with}\\ x_i{}^2>y_i{}^2}} x_i{}^2(x_i{}^2-y_i{}^2)-\sum_{\substack{\text{all } i \text{ with}\\ x_i{}^2<y_i{}^2}} x_i{}^2(y_i{}^2-x_i{}^2)\geq 0,$$

which means

$$\sum_{\text{all } i} x_i{}^2(x_i{}^2-y_i{}^2)\geq 0. \tag{4.16}$$

Since H and G are given by (4.15), the inequality (4.16) means that $H\geq G$. The equality sign holds true only when $x_i{}^2=y_i{}^2$ for all i.

Since the coefficients of the strain invariants are not all independent of each other, we find that it is impossible to represent the experimental results of Rivlin *et al.* by the above molecular theory alone. Therefore, we believe that the inter- and intramolecular forces, neglected in the present molecular theory of ideal rubber, cause at least part of the deviations from Gaussian theory. It is hoped that experimental investigations on the temperature dependence of these deviations will give the actual temperature dependence of the coefficients of the strain invariants, which in our theory are assumed to be proportional to the absolute temperature just as in the Gaussian theory. In this way we may get some idea about the dependence of the deviations upon the van der Waals forces.

Although the agreement between the non-Gaussian statistical theory and the experiments is not very satisfactory, yet the theory does explain more or less quantitatively the general S-shape of the stress-strain curve. Before the advent of the (Gaussian) statistical theory, the upward curvature of the stress-strain curve was assumed to be due to crystallization. As late as in 1946, Flory[27] still upheld this older view. However, this view is not correct to be sure; the S-shape is changed very little by raising the temperature to 100°C, but crystallization is greatly reduced. In addition, both natural rubber [for instance, soft gum rubber containing 8 percent sulfur, *cf.* reference 1(c), Fig. 3] and synthetic rubber like GR-S give the S-shape, but they do not crystallize.

[27] P. J. Flory, Ind. Eng. Chem. **38**, 417 (1946) and Rubber Chem. and Tech. **19**, 552 (1946).

V. APPENDIX

Note 1. Derivation of the one-dimensional equivalents of Eqs. (2.13) and (2.20) from the binomial formula

It is well-known that the distribution for the one-dimensional random walk problem is the Bernoullian distribution, or the binomial formula,

$$W(r)=(1/2)^n n!/[(n+r)/2]![(n-r)/2]! \tag{5.1}$$

Using the Stirling approximation,

$$\log n!=(n+1/2)\log n-n+(1/2)\log 2\pi+O(1/n), \tag{5.2}$$

for all the factorials in (5.1), we get

$$\log W(r)=(1/2)\log[2/n\pi(1-t^2)]-(n/2)\{(1+t)\log(1+t)+(1-t)\log(1-t)\}+O(1/n),\quad t=r/n. \tag{5.3}$$

The quantity in the curly brackets is equal to

$$\int_0^t \log\frac{1+t}{1-t}dt$$

or

$$2\int_0^t \tanh^{-1}t\,dt.$$

The last integral can be evaluated by partial integration and gives

$$2\int_0^t \tanh^{-1}t\,dt=2\left\{t\tanh^{-1}t-\int_0^t t\,dt/(1-t^2)\right\}=2\log\{(1-t^2)^{\frac{1}{2}}\exp(t\tanh^{-1}t)\}. \tag{5.4}$$

Putting (5.4) into (5.3), we have

$$W(r)=(2/n\pi)^{\frac{1}{2}}[1/(1-t^2)^{\frac{1}{2}}\exp(t\tanh^{-1}t)]^n\times[(1-t^2)^{-\frac{1}{2}}][1+O(1/n)].$$

The distribution $W(r)$ is a discrete distribution, which has values only at even or odd r depending upon whether n is even or odd; therefore, $C(r)$, the probability per unit length, is equal to $W(r)/2l$. Thus we get

$$C(r)=[1/(2n\pi)^{\frac{1}{2}}l][1/(1-t^2)^{\frac{1}{2}}\exp(t\tanh^{-1}t)]^n\times[(1-t^2)^{-\frac{1}{2}}][1+O(1/n)],$$

which is the one-dimensional equivalent of Eq. (2.20). Feller[28] gave a series for large deviations from the Gaussian distribution, which is essentially a series development of the quantity in the second square bracket of the last equation.

If one takes more terms of the Stirling formula (5.2), and rearranges the terms in the last series for

[28] W. Feller, *Probability Theory and its Applications* (John Wiley and Sons, Inc., New York, 1950), Vol. 1, p. 147, Eq. (6.11). H. Cramér [Actualitès Scientifiques Paris No. 736, p. 5 (1938)] has given a more general formula for the integrated distribution function, which, however, is not useful for our purpose.

$C(r)$, one gets the series

$$C(r)=[1/(2n\pi)^{\frac{3}{2}}l]\exp(-r^2/2n)\times\{1-(3-6r^2/n+r^4/n^2)/12n+(45-660r^2/n+570r^4/n^2-108r^6/n^3+5r^8/n^4)/1440n^2\cdots\},$$

which is the one-dimensional equivalent of Eq. (2.13).

Note 2. Derivation of Eq. (2.25) from a recurrence relation

Equation (2.25) can be derived in an alternative way from a recurrence relation. This relation is of similar type as the fundamental integral equations of Boltzmann and Smoluchowski used in the theory of Brownian motion and of transport phenomena.

It is instructive to derive first the binomial formula (5.1) from a recurrence relation. Let us denote the distribution by $W_n(r)$ instead of $W(r)$ in order to show the dependence on n explicitly. Then the recurrence relation for $W_n(r)$ is given by the difference equation

$$W_n(r)=[W_{n-1}(r-1)+W_{n-1}(r+1)]/2.$$

The solution of this equation is

$$W_n(r)=(1/2)^n\sum_{i=0}^{n}\binom{n}{i}g(r+2i-n),$$

where g is an arbitrary function of its argument determined by the initial condition

$$W_1(r)=[\delta(r-1)+\delta(r+1)]/2,$$

where $\delta(x)$ is the Dirac singular function normalized to unity. Thus we get $g(x)=\delta(x)$, and

$$W_n(r)=(1/2)^n\sum_{i=0}^{n}\binom{n}{i}\delta(r+2i-n)=(1/2^n)n!/[(n+r)/2]![(n-r)/2]!.$$

The three-dimensional analog (2.25) of the binomial formula can be derived in a similar manner. Let $Q_n(h)dh$ be the probability that the projection of $\mathbf{r}$ along a given line lies between h and $h+dh$, where r and h are both in units of the link length l. Then

$$Q_n(h)dh=\int_h^\infty (dh/2r)C(r)4\pi r^2l^3dr. \qquad (5.5)$$

The factor $dh/2r$ comes from the same type of ratio as given by Eq. (2.4), and the remaining part under the integral just gives the probability of finding one end of the chain within the spherical shell of radii r and $r+dr$, while the other end is fixed at origin. The lower limit of the integral in (5.5) is due to the fact that any chain with extension, r, less than h cannot contribute to the integral.

Now the recurrence relation for $Q_n(h)$ is obviously

$$Q_n(h)=\int_{h-1}^{h+1}Q_{n-1}(x)dx/2,$$

since the projections on a given diameter of the points uniformly distributed on a sphere are also uniformly distributed. Differentiating the above equation, we get the following differential-difference equation,

$$dQ_n(h)/dh=[Q_{n-1}(h+1)-Q_{n-1}(h-1)]/2,$$

or

$$2dQ_{n+1}(h+1)/dh-Q_n(h+2)+Q_n(h)=0. \qquad (5.6)$$

By means of Boole's symbolical method,[29] Eq. (5.6) has the solution

$$Q_n(h)=[1/(2d/dh)^n]\sum_{\tau=0}^{n}(-1)^\tau\binom{n}{\tau}g(h+n-2\tau), \qquad (5.7)$$

where g is an arbitrary function to be determined by the initial condition

$$Q_1(h)=(1/\pi)\int_0^\infty \sin x\cos xh\,dx/x=(1/2\pi)\left\{\int_0^\infty \sin[(h+1)x]dx/x-\int_0^\infty \sin[(h-1)x]dx/x\right\}. \qquad (5.8)$$

From (5.7) we have

$$Q_1(h)=[1/(2d/dh)]\{g(h+1)-g(h-1)\}. \qquad (5.9)$$

Combining (5.8) and (5.9), we get

$$g(h)=(1/\pi)(d/dh)\int_0^\infty \sin xh\,dx/x=(-i/2\pi)(d/dh)\int_\Gamma \exp(ihx)dx/x, \qquad (5.10)$$

where the path Γ is the same as that in the integral of Eq. (2.24). Putting (5.10) into (5.7) and carrying out the integrations, the final form of $Q_n(h)$ becomes

$$Q_n(h)=[1/2^n(n-1)!]\sum_{k=0}^{k\le(n-h)/2}(-1)^k\binom{n}{k}\times(n-2k-h)^{n-1}, \qquad (5.11)$$

in which we have made use of Eq. (2.24). Irwin[30] and Hall[31] derived the series (5.11) long ago in connection with the theory of random sampling by different methods. Equation (5.5) gives

$$C(r)=(-1/2\pi l^3r)dQ_n(r)/dr. \qquad (5.12)$$

Putting (5.11) in (5.12), we get Eq. (2.25).

---

[29] *Cf.*, C. Jordan, *Calculus of Finite Differences* (Chelsea Publishing Company, New York, 1947), p. 616.
[30] J. O. Irwin, Biometrika **19**, 225 (1927).
[31] P. Hall, Biometrika, **19**, 240 (1927).

The Vapor Pressures and Critical Constants of Pure Ozone*

ARTHUR C. JENKINS AND CLAIR M. BIRDSALL
Laboratory of the Linde Air Products Company, a Division of Union Carbide and Carbon Corporation, Tonawanda, New York
(Received February 18, 1952)

Vapor pressures of pure ozone have been measured over the range −183°C to −30°C with an estimated accuracy of ±3 percent and are represented by the equation

$$\log P_{mm} = 8.25313 - \frac{814.941587}{T} - 0.001966943T.$$

The normal boiling point is −111.9°C±0.3°C. The critical temperature has been determined experimentally and found to be −12.1°C±0.1°C. The critical pressure derived from this critical temperature and the vapor pressure equation is 54.6 atmospheres absolute. Results are, in general, in good agreement with the meager data in the literature. The precision of the vapor pressure data is limited by the unstable nature of ozone and the necessarily small samples which must be used for measurements in the interests of safety.

I. INTRODUCTION

ASIDE from the low temperature measurements of Spangenberg,[1] the only experimental determinations of the vapor pressure of ozone given in the literature are those of Riesenfeld and Beja[2] who made measurements over the range −108.5°C to −169.0°C. Riesenfeld and Beja reported the boiling point as −111.5°C±0.5°C; this was the average of values obtained by them and by Riesenfeld and Schwab.[3] Briner and Biederman[4] gave −111.5°C±0.2°C as the boiling point; however, they made only one measurement at 730 mm pressure and extrapolated to 760 mm by means of the Riesenfeld and Beja vapor pressure data.

Riesenfeld and Schwab[3] have reported −5.0°C as the critical temperature. They made several series of measurements and obtained values ranging from −23°C to −5.0°C and concluded that the highest temperature was the correct one. In addition, Schwab[5] approximated the critical temperature as −5.0°C from the boiling point by means of the Guldberg rule, using a factor of 0.6 and a boiling point of −112.3°C. In another journal Riesenfeld[6] reported the observed critical temperature as −13°C but concluded that it was probably higher than this, "about −10°C."

Riesenfeld[7] used the law of corresponding states and the value of −5°C for the critical temperature to calculate the critical pressure of 65 atmospheres. It is of interest to note that the pressure computed from our vapor pressure equation for −5°C results in a pseudo critical pressure of 63.9 atmospheres.

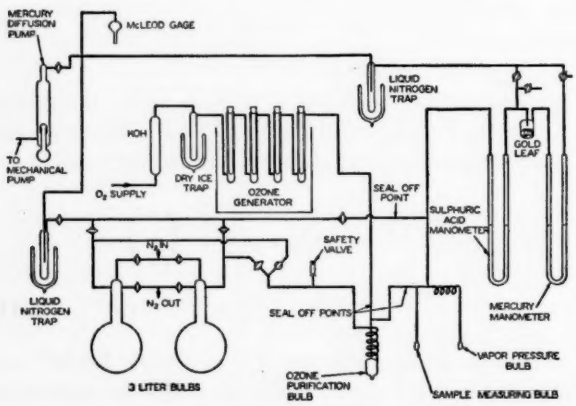

FIG. 1. Flow sheet of apparatus showing purification system and low range vapor pressure apparatus.

II. PREPARATION AND PURIFICATION OF OZONE

Ozone was prepared from oxygen in an all-glass ozonizer consisting of four Berthelot tubes in series, immersed in a water bath. The oxygen was passed through a copper oxide filled tube heated in an electric furnace to remove hydrocarbons. Following the copper oxide the oxygen passed through a KOH-filled tube and a trap immersed in dry ice and acetone to remove CO_2 and water vapor. Power for the ozonizer was supplied by a 15,000-volt sign transformer. The ozone-oxygen mixture, which contained approximately 3 percent ozone, was liquefied in a glass bulb immersed in liquid oxygen. Purification was accomplished by pumping off the oxygen after the method of Lainé.[8] This method involves the use of two three-liter bulbs which are alternately evacuated, filled with oxygen from the sample (and small quantities of ozone), purged with nitrogen, and re-evacuated. The method avoids the necessity of passing oxygen and ozone through the pumping system. The last traces of oxygen were removed by pumping directly on the sample, since the ozone vapor pressure at liquid oxygen temperatures is only 0.1 mm. A flow sheet of the entire apparatus is shown in Fig. 1. The use of stopcocks was avoided insofar as possible. Those which were necessary were lubricated with a mixture of polyperfluorovinylchloride and

* This work was performed under Contract NO(s) 10945 for the Bureau of Aeronautics, United States Navy.
[1] Anna Lise Spangenberg, Z. physik. Chem. **119**, 419 (1926).
[2] E. H. Riesenfeld and M. Beja, Medd. Netenskapsakademiens Nobelinstitut, **6**, No. 7, 1 (1923).
[3] E. H. Riesenfeld and G. M. Schwab, Z. Physik **11**, 12 (1922).
[4] Briner and Biederman, Helv. Chim. Acta **16**, 207 (1933).
[5] G. M. Schwab, Z. physik. Chem. **110**, 599 (1924).
[6] E. H. Riesenfeld, Naturwiss. **10**, 470 (1922).
[7] E. H. Riesenfeld, Z. Electrochem. **29**, 119 (1923).
[8] P. Lainé, Ann. Physik. **11**, 3, 461 (1935).

colloidal silica. After purification, break seals and seal off points were used in place of stopcocks. The criterion of purity was a constant vapor pressure at −183°C of 0.1 mm of mercury which checks closely with the value reported by Spangenberg.[1]

III. VAPOR PRESSURES

Since nonflammable cryostat liquids usable over the desired range are unobtainable, the vapor pressure bulb was enclosed in the copper block cryostat shown in Fig. 2. This cryostat consists of a $1\frac{3}{8}$-inch diameter copper block 8 inches long with a central drilled well for the vapor pressure bulb and a thermocouple well. The copper block was provided with an external copper cooling coil soldered in place and a Chromel wire heating coil enclosed in asbestos tubing. The block was suspended in an empty Dewar flask from a Transite top. Temperature control was obtained by passing cold gaseous nitrogen or liquid nitrogen through the coil to produce slow cooling and compensating with the

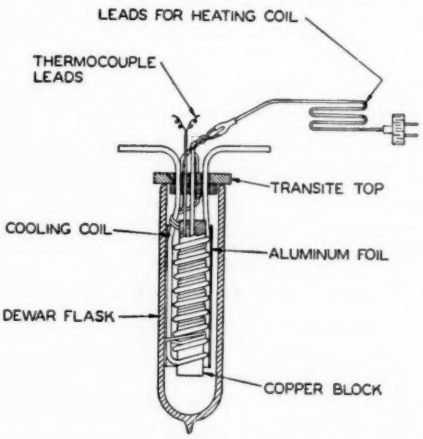

FIG. 2. Sectional view of the copper block cryostat.

heating coil. In the first series of measurements, temperatures were measured by means of a copper-constantan thermocouple in the well in the copper block. In subsequent measurements a thermocouple was located in the liquid ozone as shown in Fig. 3. Comparison of the two thermocouples showed that either location gave the same temperature.

Temperatures were determined by means of Leeds & Northrup Duplex, glass-insulated, 30-gauge copper-constantan thermocouples. Thermocouples were calibrated at the mercury freezing point, the CO_2 sublimation point, and at liquid oxygen temperatures, the last by comparison with a Bureau of Standards calibrated Leeds & Northrup platinum resistance thermometer. In addition, the thermocouples were compared with the resistance thermometer at the CO_2 sublimation point, where they checked to 0.02°C. Curves showing the deviation from the standard tables were plotted according to the directions given by Scott.[9] Temperatures

[9] Russel B. Scott, J. Research Natl. Bur. Standards **25**, 459, RP1339 (1940).

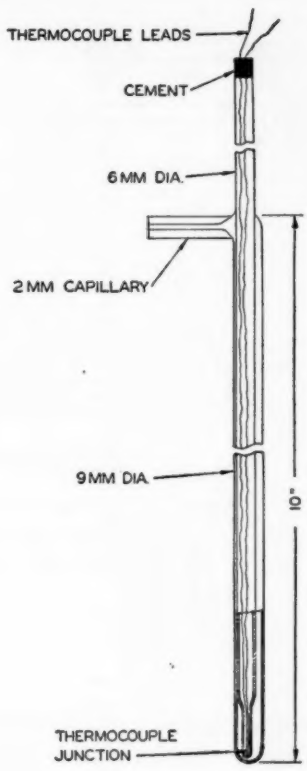

FIG. 3. Vapor pressure bulb used in low range measurements showing the location of the thermocouple.

could be read to ±0.03°C to ±0.05°C in the range of these measurements on the Wenner thermocouple potentiometer. Because of the danger of explosions the direct use of a resistance thermometer was not feasible, since these instruments cannot be considered expendable as are thermocouples.

The vapor pressure bulb was filled by condensing ozone from the purification bulb into the measuring bulb and from there into the vapor pressure bulb. The measuring bulb was necessary because the vapor pressure bulb could not be observed in its position in the cryostat. No stopcocks were used in this process, the transfer being accomplished by means of break-seals and seal-off points. After condensation in the vapor pressure bulb with the copper block at liquid oxygen temperature the ozone was repumped to remove any oxygen formed by decomposition, and its vapor pressure checked at this temperature. During the course of the measurements the ozone was cooled to approximately −183°C several times and repumped to insure continuous purity of the sample. The copper block cryostat proved to be very satisfactory for this purpose, since it could be cooled rapidly by passing liquid nitrogen through the coil.

Vapor pressures in the range −183°C to −100°C were measured by means of a sulphuric acid manometer and a mercury manometer in series. The sulphuric acid manometer prevented the ozone from coming in contact with the mercury. Pressures were read directly on this manometer up to its maximum range. Mano-

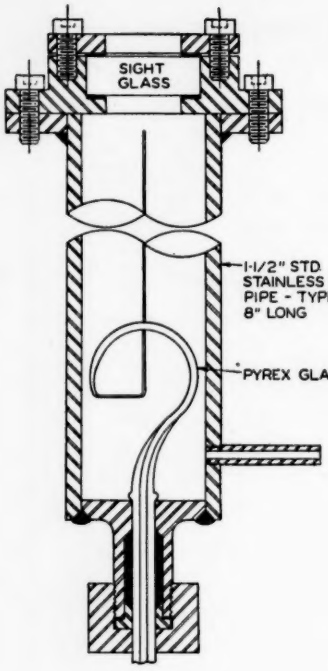

FIG. 4. Sickle gauge used in high range vapor pressure measurements.

metric heights were measured with a Gaertner cathetometer using two telescopes.

For the range −82°C to −30°C the vapor pressure bulb was equipped with a Pyrex glass sickle gauge which was enclosed in a stainless steel housing provided with a sight glass. The sickle gauge (shown in Fig. 4) was maintained at its zero setting by external nitrogen pressure. The pointer of the gauge was observed by means of a cathetometer and a mirror placed at a 45-degree angle above the sight glass. The sickle gauge was sensitive to pressure changes of less than 1 psi, well within the accuracy of the measurements in this range. The balancing nitrogen pressure was read on a calibrated test gauge which could be read to approximately 1 psi. Filling of the vapor pressure bulb was accomplished by means of a tee between the bulb and sickle gauge. After filling, this tee was sealed off while the ozone was being pumped at a low temperature. Two series of measurements were made in this range with separate ozone samples. Since the decomposition of two volumes of gaseous ozone results in three volumes of oxygen, points were taken on a rising temperature scale. This procedure, it is believed, confined any decomposed ozone to the sickle gauge area where it did not materially affect the vapor pressures. This was confirmed by measuring one point on a decreasing temperature scale, which should have resulted in a much higher pressure than that actually observed if any appreciable quantity of oxygen had been present.

The experimental vapor pressures are given in Table 1 and are compared with the pressures calculated by means of the following least-squares equation derived from 28 of the 30 measured points:

$$\log P_{mm} = 8.25313 - \frac{814.941587}{T} - 0.001966943T, \quad (T° = t°C + 273.15), \quad (1)$$

where P is in standard mm of mercury.

Omitting point 1, which shows a deviation of 27 percent but only 0.19 mm in pressure, the average percent deviation between observed and calculated points is 2.9 percent. Careful analysis of the data indicated that two points should be discarded. One of these (4b) was taken as a test point on a decreasing temperature scale and may have been affected by decomposition. The second (10b) was obviously greatly in error for reasons which could not be determined.

IV. CRITICAL TEMPERATURE AND PRESSURE

The critical temperature was determined by direct observation of the liquid meniscus. Pure ozone was condensed in a 3-mm i.d. Pyrex glass ampoule, which was sealed off under vacuum with the lower half immersed in liquid nitrogen. The ampoule was enclosed in a drilled 1-inch diameter copper block provided with longitudinal slits 3 mm wide for observation and a thermocouple well. After filling, the block and ampoule were transferred to a Freon 11 bath cooled to −150°C. The bath temperature was raised to the critical region and the temperature recorded at the point where the meniscus disappeared. Two series of measurements were made with two separate ampoules and different

TABLE I. Vapor pressures of liquid ozone.

Point	T°C	T°K	Pressure standard mm of mercury obs	calc Eq. 1	calc−obs	% Dev
0	−182.96	90.19	0.10	0.11	+0.01	+9.0
1	−173.83	99.32	0.90	0.71	−0.19	−27.0
2	−162.28	110.87	4.32	4.83	+0.51	+10.6
10	−161.32	111.83	5.34	5.57	+0.23	+4.1
14	−157.45	115.70	9.93	9.59	−0.34	−3.5
11	−155.19	117.96	12.80	12.97	+0.17	+1.3
4	−155.00	118.15	13.16	13.28	+0.12	+0.9
3	−143.38	124.77	28.84	29.92	+1.08	+3.6
5	−142.69	130.46	55.79	56.24	+0.45	+0.8
6	−137.60	135.55	94.59	94.34	−0.25	−0.3
7	−128.59	144.56	212.3	214.3	+2.0	+0.9
15	−126.68	146.47	256.8	252.0	−4.8	−1.9
8	−199.17	153.98	447.9	455.0	+7.1	+1.6
16	−119.17	153.98	469.3	455.0	−14.3	−3.0
12	−112.22	160.93	723.7	745.7	+22.0	+3.0
9	−112.03	161.12	734.1	756.3	+22.2	+2.9
13	−110.92	162.23	778.9	814.2	+35.3	+4.3
17	−109.63	163.52	914.7	887.4	−27.3	−3.1
18	−107.21	165.94	1090	1037	−53	−5.1
19	−101.86	171.29	1457	1441	−16	−1.1
6[b]	−81.85	191.30	4249	4142	−107	−2.6
1[b]	−78.87	194.28	5029	4748	−281	−5.9
7[b]	−65.98	207.17	8247	8164	−83	−1.0
2[b]	−57.17	215.98	11380	11353	−37	−0.3
8[b]	−49.24	223.91	14870	14900	+30	+0.2
9[b]	−43.53	229.62	17500	17881	+381	+2.1
3[b]	−38.05	235.10	20660	21083	+423	+2.0
5[b]	−35.77	237.38	22060	22536	+476	+2.1
...	−12.10[a]	261.05[a]	...	41484	...	...
			Points Discarded			
4[b]	−39.78	233.37	20510	20047	−463	−2.3
10[b]	−29.68	243.47	24690	26733	+2043	+7.7
			Average percent deviation (omitting point 1)			2.9

[a] Critical temperature.
[b] Sickle gauge apparatus.

gross densities. The disappearance of the meniscus was taken as the critical point. Observations were repeated until a drop in the observed critical temperature occurred, an indication of decomposition. The observer had no knowledge of the temperature when the critical point was noted but notified a second observer who recorded the thermocouple reading. Because of the deep blue color of both phases near the critical point the meniscus was not as easily observable as in the case of other liquids, and the usual critical opalescence was not seen. Results are given in Table II. The measured critical temperature is −12.1°C. It is believed that the second series is more reliable than the first, since the spread of the data is less, and experience obtained in the first series made detection of the meniscus easier. However, the average value of the two series checked to 0.1°C.

The critical pressure of ozone, calculated from Eq. (1) and our value of the critical temperature, is 54.6 atmospheres.

TABLE II. Critical temperature observations.

Series 1		
Disappearance of meniscus	−12.0°C	
Disappearance of meniscus	−11.6°C	
Disappearance of meniscus	−12.4°C	
Disappearance of meniscus	−16.4°C	Decomposition
Average temperature before decomposition	−12.0°C	
Series 2		
Disappearance of meniscus	−12.2°C	
Appearance	−12.4°C	
Disappearance	−12.2°C	
Appearance	−12.3°C	
Disappearance	−12.0°C	
Cooled to −18°C		
Disappearance of meniscus	−13.3°C	Decomposition
Best value of critical temperature	−12.1°C	

ACKNOWLEDGMENT

The authors extend their thanks to Professor James A. Beattie of the Massachusetts Institute of Technology for reviewing the manuscript and for many helpful suggestions.

THE JOURNAL OF CHEMICAL PHYSICS VOLUME 20, NUMBER 7 JULY, 1952

An Analysis of the Pressure Dependence of the Dielectric Constant of Polar Liquids*

I. S. JACOBS AND A. W. LAWSON
Institute for the Study of Metals, University of Chicago, Chicago, Illinois
(Received February 29, 1952)

The Onsager and Kirkwood theories of polar liquids have been used to analyze the available experimental data on the pressure dependence of the dielectric constant. It is found necessary in most cases to assume an appreciable decrease in the dipole moment arising from intramolecular distortion which may be large enough in some cases to more than compensate for the increase in effective moment caused by intermolecular compression. Quantitative estimates of these two factors are given, and their influence on binding energy and compressibility is discussed.

RECENTLY, Falkenhagen and Jacob[1] have compared the predicted values for the electrostrictive coefficients of liquids on the basis of the Clausius-Mosotti and Onsager theories of dielectric media. They propose to make an experimental test of their calculations by measuring the electrostrictive effect produced by ultrasonic waves. It is also possible, however, to determine these electrostrictive coefficients from the pressure variation of the dielectric constant. Such data are available from the work of Kyropoulos[2] and Danforth,[3] whose investigations predated the treatments of Onsager,[4] Kirkwood,[5] and Fröhlich[6] by some years. It is of interest, therefore, to see how these data fit into the various theoretical frameworks. This analysis parallels a similar analysis by Brown[7] of nonpolar fluids.

The pertinent equations are those of Onsager and of Kirkwood. Although the Clausius-Mosotti equation, as modified by Debye[8] for polar substances, works well for gases and dilute solutions, the density range with which we are concerned is too high to allow its application, and hence it has been excluded.

The Kirkwood formula for a pure polar liquid is

$$(\epsilon-1)/3=3\epsilon P_0\rho/M(2\epsilon+1), \tag{1}$$

where

$$P_0=4\pi N/3[\alpha+\mu\cdot\bar{\mu}/3kT]. \tag{2}$$

Here α is the optical polarizability; μ the moment of the molecule in the medium, somewhat different than μ_0 as a result of the polarizing reaction of the surround-

* It is a pleasure to acknowledge the support of the ONR.

[1] H. Falkenhagen and H. Jacob, Ann. Physik (6) **8**, 105 (1951).
[2] S. Kyropoulos, Z. Physik **40**, 507 (1926).
[3] W. E. Danforth, Jr., Phys. Rev. **38**, 1224 (1931).
[4] L. Onsager, J. Am. Chem. Soc. **58**, 1486 (1936).
[5] J. G. Kirkwood, J. Chem. Phys. **7**, 911 (1939); G. Oster and J. G. Kirkwood, J. Chem. Phys. **11**, 175 (1943).
[6] H. Fröhlich, Trans. Faraday Soc. **44**, 238 (1948); *Theory of Dielectrics* (Oxford University Press, London, 1949).
[7] W. F. Brown, Jr., J. Chem. Phys. **18**, 1200 (1950).
[8] P. Debye, *Polar Molecules* (Chemical Catalog Company, Inc., New York, 1929).

TABLE I.[a]

1 Source of data	2 Substance	3 T	4 $\epsilon_{p=0}$	5 $\frac{d\ln\epsilon}{d\ln\rho}$ Exp.	6 $2\left(\frac{\mu(1)}{\mu_0(1)}-1\right)$[b] Eq. (8)	7 $\frac{d\ln\mu_0^2}{d\ln\rho}$ Eq. (10)	8 Eq. (8) + Eq. (10)	9 $\frac{d\ln\mu\cdot\bar{\mu}}{d\ln\rho}$ Eq. (5)	10 $\frac{\partial^2\ln\epsilon}{\partial(\ln\rho)^2}$ Exp.
2	H_2O	20	80.79	1.34±0.02	0.63[c]	−0.20±0.02	+0.43	+0.35±0.02	−
2	$(CH_3)_2CO$	20	21.50	1.27±0.01	0.59[d]	−0.30±0.01	+0.29	+0.32±0.01	−
2	CH_3OH	20	33.79	1.05±0.02	0.54	−0.47±0.02	+0.07	+0.07±0.02	+
3	C_2H_5OH	0	27.8	0.88±0.02	0.60	−0.72±0.02	−0.12	−0.10±0.02	+
2	C_2H_5OH	20	25.71	0.98±0.01	0.60	−0.59±0.01	+0.01	0.00±0.01	+
3	C_2H_5OH	30	23.2	1.04±0.02	0.56	−0.52±0.01	+0.04	+0.07±0.02	+
3	$C_6H_{13}OH$	30	12.90	0.85±0.03	0.72	−0.85±0.03	−0.13	−0.12±0.03	+
3	$C_6H_{13}OH$	75	8.55	1.28±0.02	0.51	−0.28±0.02	+0.23	+0.44±0.02	−
3	$C_3H_5(OH)_3$	0	49.9	1.63±0.07	0.95	−0.19±0.07	+0.76	+0.67±0.07	+
3	$C_3H_5(OH)_3$	30	42.8	1.88±0.05	0.90	+0.02±0.05	+0.92	+0.93±0.05	+
3	C_6H_5Cl	30	5.41	1.04±0.02	0.16	−0.64±0.03	−0.48	+0.26±0.03	+
3	C_6H_5Cl	75	4.90	1.04±0.02	0.17	−0.55±0.03	−0.38	+0.30±0.03	+
3	C_6H_5Br	30	5.22	0.79±0.01	0.12	−1.29±0.02	−1.17	−0.13±0.01	0
3	C_6H_5Br	75	4.87	0.86±0.01	0.15	−1.06±0.01	−0.91	+0.00±0.01	+
2	$CHCl_3$	18.5	4.96	1.28±0.05	0.30	−0.18±0.08	+0.12	+0.69±0.07	+
2	$(C_2H_5)_2O$	20	4.33	1.78±0.02	0.20	+0.89±0.03	+1.09	+1.56±0.07	0
3	$(C_2H_5)_2O$	30	4.15	1.63±0.05	0.19	+0.69±0.08	+0.88	+1.37±0.07	+
3	$(C_2H_5)_2O$	75	3.82[e]	1.51±0.05[e]	0.20[e]	+0.62±0.09[e]	+0.82[e]	+1.28±0.07[e]	+

[a] Note good agreement between columns 8 and 9 above solid dividing line and poor agreement below. Substances above dividing line are all relatively highly associated.
[b] Values in column 6 were calculated assuming cubic packing except where noted.
[c] Diamond packing assumed.
[d] Zig-zag chain model assumed (see text).
[e] $P=500$ kg/cm².

ings; and $\bar{\mu}$ is the sum of μ and the moment induced by a representative molecule of fixed orientation in a neighboring spherical region of radius large relative to the range of intermolecular forces. According to Kirkwood, the value of $\mu\cdot\bar{\mu}$ in Eq. (3) is given approximately by

$$\mu\cdot\bar{\mu}=\mu_0^2[1+\textstyle\sum_i z_i\langle\cos\gamma_i\rangle]\left[1-\frac{2z_1\alpha}{d^3}\langle\cos\gamma_1\rangle\right]^{-2}, \quad (3)$$

where γ_i is the angle between the molecular axis of a molecule in the ith shell surrounding a fixed central molecule and the axis of the central molecule, z_i the number of particles in the ith shell, and d the distance between neighbors. Equation (3) is approximate to the extent that μ only differs from μ_0 because of its polarization in the dipole field of its first shell neighbors.

Experimentally, we find that at constant temperature $\ln\epsilon$ is very nearly a linear function of $\ln\rho$ over a range of several thousand atmospheres. (see Fig. 1) Consequently, we choose to compare the initial slopes of such curves with the theoretically predicted values of $d\ln\epsilon/d\ln\rho$. Simple differentiation of Eq. (1) yields for this derivative the following formula:

$$\frac{d\ln\epsilon}{d\ln\rho}=\frac{(\epsilon-1)(2\epsilon+1)}{2\epsilon^2+1}\left[1+\frac{d\ln P_0}{d\ln\rho}\right]. \quad (4)$$

Unfortunately, we are unable to predict the value of $d\ln P_0/d\ln\rho$, but we may estimate its numerical value by inserting the observed value of ϵ and $d\ln\epsilon/d\ln\rho$ in Eq. (4). Then since

$$\frac{d\ln\mu\cdot\bar{\mu}}{d\ln\rho}=\left[1+\frac{3kT\alpha}{\mu\cdot\bar{\mu}}\right]\frac{d\ln P_0}{d\ln\rho}, \quad (5)$$

we may evaluate the derivative and examine its value in the light of Eq. (3). For instance, if we assume that μ_0 and $z_i\langle\cos\gamma_i\rangle$ are independent of pressure, so that the variation in $\mu\cdot\bar{\mu}$ is controlled only by the increase in this quantity resulting from the decrease in d, then

$$\frac{d\ln\mu\cdot\bar{\mu}}{d\ln\rho}=2b/(1-b), \quad (6)$$

where

$$b=[\mu(1)-\mu_0(1)]\rho/\mu(1)\rho_0, \quad (7)$$

and the moments are evaluated at $P=1$ kg/cm². At atmospheric pressure, when $\rho=\rho_0$, we have simply

$$\frac{d\ln\mu\cdot\bar{\mu}}{d\ln\rho}=2\left(\frac{\mu}{\mu_0}-1\right). \quad (8)$$

In Table I we have listed the values of $d\ln\mu\cdot\bar{\mu}/d\ln\rho$ estimated from experimental values of $d\ln\epsilon/d\ln\rho$ from Eq. (5) as well as the values of this derivative estimated from Eq. (8).

The experimental results employed to obtain $(d\ln\epsilon/d\ln\rho)_T$ are those of Kyropoulos and Danforth, supplemented in the case of chloroform with recent compressibility data of Bridgman.[9] The optical data are from the International Critical Tables and the Landolt-Börnstein Tabellen.

The theoretical ratios $\mu(1)/\mu_0(1)$ were estimated in the following way from Eq. (3): A certain type of packing was assumed for the liquid, say simple cubic. Then the value of d was calculated from the density and the value of $z\langle\cos\gamma\rangle$ for the first shell was estimated

[9] P. W. Bridgman, Proc. Am. Acad. Arts Sci. 77, 129 (1949).

from the known dielectric constant. The ratio $\mu(1)/\mu_0(1)$ is then readily calculated. The values listed in Table I were obtained by assuming simple cubic packing for lack of a better model, except in the cases of water and acetone. For the former, diamond packing was assumed and for the latter a zig-zag chain of the type discussed by Fröhlich.[6] Unfortunately, the values are somewhat sensitive to the type of packing assumed, increasing for less dense packings and decreasing for those more dense. However, as we shall see below, simple cubic packing yields values consistent with Onsager's spherical molecule model in many cases.

Comparing now the two estimates of the quantity $d\ln\mu\cdot\bar{\mu}/d\ln\rho$ (recalling that the theoretical value assumes μ_0 and $z\langle\cos\gamma\rangle$ independent of pressure), we see that the theoretical value is appreciably larger than that estimated from experimental values for the highly associated liquids. We are invited, therefore, to seek the origin of the discrepancy by considering the effect of allowing either μ_0 or $(1+z\langle\cos\gamma\rangle)$ to vary with density. Returning to Eq. (3), we note that to remove the discrepancy either μ_0 or $(1+z\langle\cos\gamma\rangle)$ must decrease with increasing pressure.

We might expect that for highly associated liquids that $z\langle\cos\gamma\rangle$ would not change much with pressure or would increase slightly with more dense packing. We may gain some insight into the variation of $z\langle\cos\gamma\rangle$ by considering the form of the Kirkwood formula for the special case of spherical molecules, for which we may write

$$\epsilon-n^2=\frac{3\epsilon}{2\epsilon+n^2}\cdot\frac{n^2+2}{3}\cdot\frac{4\pi N\rho}{3M}\frac{\mu_0^2}{kT}(1+z\langle\cos\gamma\rangle). \quad (9)$$

This formula is just that derived originally by Onsager if we set $z\langle\cos\gamma\rangle=0$. For the pressure dependence of ϵ, we now have

$$\frac{d\ln\epsilon}{d\ln\rho}=\frac{(\epsilon-n^2)(2\epsilon+n^2)}{(2\epsilon^2+n^4)}\left[1+\frac{d\ln\mu_0^2(1+z\langle\cos\gamma\rangle)}{d\ln\rho}\right]+\frac{\epsilon+2n^2}{2\epsilon^2+n^4}\cdot\frac{(n^2-1)(n^2+2)}{3}. \quad (10)$$

If we assume, as before, that $d\ln\mu_0^2(1+z\langle\cos\gamma\rangle)/d\ln\rho$ is zero, we obtain values which again are too high except for the case of ethyl ether. If we assume $z\langle\cos\gamma\rangle$ is constant and calculate the values $d\ln\mu_0^2/d\ln\rho$ must have to force agreement with experiment, we obtain the numbers listed in column (7) of Table I. It is interesting to note that the Onsager model gives quite consistent results in the case of highly associated liquids for the value of $d\ln\mu\cdot\bar{\mu}/d\ln\rho$ calculated from the more general Kirkwood equation. For if we add column (6) and column (7), we obtain the values listed in column (8) which for the cases with large ϵ agree well with the values in column (9), calculated from Eq. (5).

By comparing the derivations of Eq. (3) and Eq. (9), the Onsager model permits us to give an approximate formula for $z\langle\cos\gamma\rangle$ namely,

$$z\langle\cos\gamma\rangle\cong 4\pi/3\cdot 1/f\cdot(\epsilon-1)/(2\epsilon+1), \quad (11)$$

where f is a number dependent on the type of packing and is determined by the equation

$$fNd^3=V, \quad (12)$$

where d is the distance between closest neighbors and V is the molal volume. In the case of water Eq. (11) estimates $z\langle\cos\gamma\rangle=1.37$. Pople[10] with a more refined model finds about 1.50. It is clear from Eq. (11) that in the limit of high ϵ, $z\langle\cos\gamma\rangle$ is independent of pressure as long as the type of packing does not change appreciably.

Accordingly, we are forced to conclude that in at least some cases the decrease of the effective dipole moment arising from intramolecular distortion plays an appreciable role in determining the variation of dielectric constant with pressure. In the case of water, for instance, if we assume that the OH distance is not changed but that the angle β between the OH bonds increases, the required change in angle to yield the observed change in μ_0 is 1.7° for 10,000 kg/cm². According to Pople's bendable bond theory, the corresponding change in the angle γ corresponding to this change in β is only about 0.2°, which is additional evidence in support of our conclusion that in general $z\langle\cos\gamma\rangle$ changes less rapidly with pressure than μ_0.

From an extremely naive point of view the values obtained for $d\ln\mu_0^2/d\ln\rho$ seem reasonable. For we may write

$$\boldsymbol{\mu}_0=\Sigma_i e_i\mathbf{d}_i, \quad (13)$$

and if we assume that pressure does not affect the relative configuration of charge but merely the size of the spherical molecule, then

$$\frac{d\ln\mu_0^2}{d\ln\rho}\cong-\frac{2}{3}\frac{K_m}{K_L}, \quad (14)$$

where K_m is the compressibility of the molecule and K_L is the compressibility of the bulk liquid. At most the ratio K_m/K_L can be unity and so we would expect for spherical molecules that $|d\ln\mu_0^2/d\ln\rho|<\frac{2}{3}$. For liquids with large ϵ, this is not far from being true in most cases. Equation (14) also suggests why $|d\ln\mu_0^2/d\ln\rho|$ invariably decreases with increasing temperature. The ratio K_m/K_L decreases as the free volume increases.

Thus, in a qualitative way at least, the behavior of the dielectric constant of polar liquids with high ϵ under pressure may be understood. The behavior of liquids with intermediate dielectric constant ($\epsilon\sim 5$) does not appear explicable in terms of the foregoing remarks alone. Either the assumption of spherical molecules is

[10] J. A. Pople, Proc. Roy. Soc. (London) **A205**, 163 (1951).

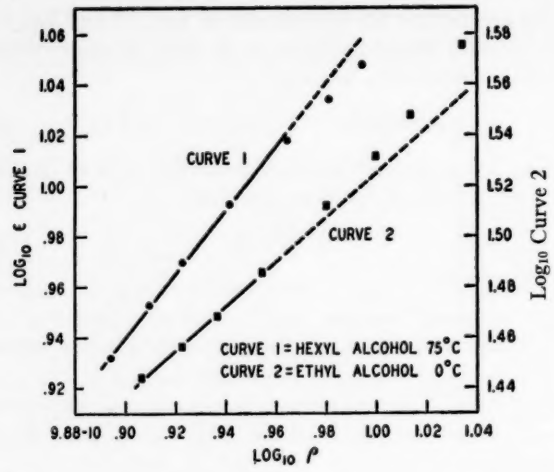

FIG. 1. Typical curves illustrating dependence of dielectric constant on density and showing how deviation from linearity may be either positive or negative.

bad in these cases, or $z\langle\cos\gamma\rangle$ is varying rapidly, or again the charge distribution is changing radically with pressure. An elucidation of these phenomena must be postponed until we have more adequate knowledge of the liquid state.

Before concluding this brief analysis, we digress somewhat to remark on the effect of the dipole-dipole interaction on the binding energy and compressibility of highly associated liquids. While it is dubious that the treatment of such liquids in terms of simple dipoles alone is adequate, nevertheless even in this approximation it is not permissible to neglect terms involving $d\ \ln\mu\cdot\bar{\mu}/d\ \ln\rho$ without making appreciable error.

This point may be illustrated as follows: In the case of water. Writing for the energy (following Stockmayer)[11]

$$E=\frac{zN}{2}\left[-\frac{2\mu^2\langle\cos\gamma\rangle Nf}{V}-\frac{bN^2f^2}{V^2}+\frac{C}{V^4}\right], \tag{15}$$

where b and C are constants and f is the packing factor defined above, we obtain by straightforward thermodynamics

$$p=-zN\left[\frac{\mu^2\langle\cos\gamma\rangle}{V^2}Nf\left(1+\frac{\partial\ \ln\mu^2}{\partial\ \ln\rho}\right)+\frac{N^2f^2b}{V^3}+\frac{2C}{V^5}\right]+T\frac{\partial p}{\partial T}\Big)_V. \tag{16}$$

[11] W. H. Stockmayer, J. Chem. Phys. 9, 398 (1941).

For equilibrium $p=0$, so

$$E=-\frac{zN^2\mu^2\langle\cos\gamma\rangle f}{V}\left[1-\frac{1}{4}\left(1+\frac{\partial\ \ln\mu^2}{\partial\ \ln\rho}\right)\right]-\frac{zN^3f^2b}{V^2}-\frac{VT}{4}\frac{\partial p}{\partial T}\Big)_V. \tag{17}$$

By a second differentiation we obtain an expression for the bulk modulus

$$B=\frac{fzN^2\mu^2\langle\cos\gamma\rangle}{V^2}\left(3+2\frac{\partial\ \ln\mu^2}{\partial\ \ln\rho}\right)+\frac{2zN^3f^2b}{V^3}-5T\frac{\partial p}{\partial T}\Big)_V+T\frac{\partial B}{\partial T}\Big)_P. \tag{18}$$

We may make numerical estimates of E and B by using the following data. From x-ray diffraction studies the nearest neighbor distance for water is known to be 2.92°A. Combining this value with the molar volume of 18 cc, we calculate f to be 1.20. By use of a value of 1.54×10^{-24} cm^2 for the polarizability and Oster and Kirkwood's value of 1.70 for $z\langle\cos\gamma\rangle$, we then find for $\mu\cdot\bar{\mu}$ a value of 15.3×10^{-6}. For the quantity b we have used the value 7.0×10^{-59} estimated by Stockmayer[11] (albeit using a repulsive force of a higher power). For $\partial p/\partial T)_V$ and $\partial B/\partial T)_P$, we have used experimental values. We may write

$$E=E_1+E_2+E_3,$$

where E_1, E_2, and E_3 correspond to the three terms in Eq. 17. Then we calculate $E_1=-3.64$ kcal/mole, $E_2=-1.84$ kcal/mole, and $E_3=-1.51$ kcal/mole, corresponding to a binding energy of 7.0 kcal/mole. The heat of vaporization of water at 20°C is 10.3 kcal/mole, so our estimate is about 30 percent low. If we had ignored the term $\partial\ \ln\mu^2/\partial\ \ln\rho$, our estimate would have been somewhat higher, namely, 9.2 kcal/mole. Thus, it is evident that terms of this type decrease the binding energy appreciably. The agreement between experiment and theory is to be considered satisfactory in view of the neglect of other than nearest neighbor interactions, the assumption of a simple dipole model, and the rather questionable value of b.

For the bulk modulus B we find at 20°C the value 2.14×10^{10} dynes/cm^2. The corresponding experimental value is 2.37×10^{10} dynes/cm^2. In view of the discrepancy between the observed and calculated value of E this agreement must be considered fortuitous, but the calculation reveals the role of dipole interactions in reducing the compressibilities of highly associated liquids below the usual values for nonpolar substances.

Modifications of the Absorption Spectra of Anions Induced by Complex Formation*

LEONARD I. KATZIN†
Chemistry Division, Argonne National Laboratory, Chicago, Illinois
(Received February 1, 1952)

The absorption of thiocyanate, chloride, bromide, and iodide ions are markedly altered on complexing with nickelous or cobaltous ions in isopropyl alcohol solution, new peaks appearing at longer wavelengths. In the case of iodide ion, the absorption spectra of the complexes with nickelous ion, cobaltous ion, and iodine (the "tri-iodide" complex) are practically distinguishable only by their extinction coefficients. A characteristic feature of the modified iodide spectrum is the pair of peaks, found at shorter wavelengths in the spectra of the free iodide ion, and in other forms. The cobaltous complexes with bromide and chloride ions show analogous splittings, but the absorption of the trihalide ions show single peaks which agree in wavelength with the longer-wavelength peak of the cobalt-complexed ion. The nickelous complexes absorb at shorter wavelengths.

WHEN a colored cation forms a complex with an anion, the absorption spectrum is usually altered, and this altered spectrum is often referred to as the absorption spectrum of the complex. In many cases this absorption is clearly a modification of the absorption spectrum of the hydrated cation, suggesting that other portions of the spectrum may be similarly related to the anion absorption.

With the exception of some such as chromate and permanganate, which have a transition metal as the central atom which is itself colored in the cationic form, inorganic anions are generally colorless and do not absorb even in the near ultraviolet. Nitrate ion, with a small absorption peak at about 300 millimicrons, and a portion of an intense absorption visible to the Beckman spectrophotometer at wavelengths below this, constitutes one of the exceptions. Study of the absorption of this group when it is coordinated to cations[1] has shown that changes are induced, which are most marked when the metallic component is a transition element with an incomplete *d* subshell.

Another polyatomic anion which possesses multiple bonds, and might be expected to show an absorption spectrum above 220 millimicrons, is thiocyanate, which possesses the additional property of being a good complexing agent. The absorption of this anion is only partially visible above 220 millimicrons, but its spectrum is strongly modified by both cobaltous and nickelous perchlorates so that new peaks appear above 220 millimicrons. An unexpected and interesting finding is that there apparently also occurs sufficient alteration of the absorption of the monatomic halide anions (chloride, bromide, and iodide) in cobaltous and nickelous ion complexes to give characteristic spectra within the reach of the Beckman spectrophotometer.

EXPERIMENTAL

Cobalt perchlorate hexahydrate was prepared from the carbonate and perchloric acid, and recrystallized twice. Other salts used were the commercial chemically pure salts. Since potassium thiocyanate was insufficiently soluble in organic solvents for our purposes, equivalent portions of lithium chloride and potassium thiocyanate were metathesized in the presence of the organic solvent (usually isopropyl alcohol) to yield a solution of lithium thiocyanate and a residue of insoluble potassium chloride. The water content of the solvents was checked by analysis with Karl Fischer reagent. No difficulties were found in observing to wavelengths of 215 millimicrons with tertiary butyl alcohol, but only the Merck isopropyl alcohol, of the several brands tested, was sufficiently free of absorbing impurities.

Solutions for spectrophotometric observation were made by mixing measured aliquots of stock solutions of cobaltous perchlorate or nickelous perchlorate in the organic solvent with aliquots of solutions of the halide or thiocyanate salts of lithium (tetrabutylammonium, in case of the iodide). The mixtures were made to volume in a flask, and observed in 1-cm quartz cells with the Beckman model DU quartz spectrophotometer, using a hydrogen light source. Pure solvent was used as the "blank" in all cases.

RESULTS

Both cobaltous and nickelous perchlorates are essentially transparent, in alcohol solution, in the region 210–350 millimicrons. Contributions from possible peaks below 220 mμ do not exceed extinction coefficients of 1 or 2 at 220 mμ. Lithium thiocyanate in the alcohols has an absorption with a maximum somewhere below 210 millimicrons, and an extinction coefficient which falls rapidly from about 3750 at 210 millimicrons and 2450 at 220 millimicrons to 100 at about 245 millimicrons. On mixing with the metal perchlorate, the absorption below 250 millimicrons becomes altered, and above this wavelength, a new absorption is found. The details of the spectrum depend on the cation and the ratio of thiocyanate to cation.

In the case of cobalt and the thiocyanate, the new peak is well resolved (Fig. 1), and has its maximum at 295 millimicrons for one, 305 millimicrons for two, and

* Presented in part at the Symposium on Molecular Structure and Spectroscopy, Ohio State University, Columbus, Ohio, June 11–15, 1951.

† With the technical assistance of Miss Elizabeth Gebert.

[1] L. I. Katzin, J. Chem. Phys. **18**, 789 (1950).

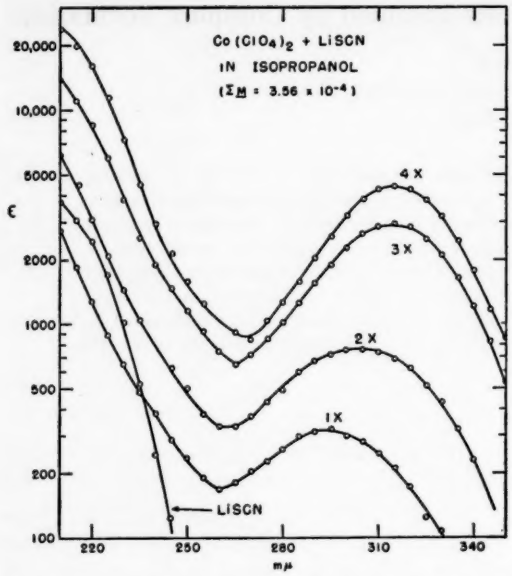

FIG. 1. Absorption of solutions with variable ratios of LiSCN to $Co(ClO_4)_2$ in isopropyl alcohol. Total molality, 3.56×10^{-4}. Formal extinctions based on cobalt concentration ($\epsilon=D\div M_{Co}$).

315 millimicrons for three or more equivalents of thiocyanate per cobalt atom. It is known from studies of the absorption in the visible region[2] that this system shows complexes with three, two, and probably one thiocyanate per cobalt; a tetrathiocyanate is not readily formed in the alcohol medium, although it does form in acetone. A "continuous variations" study[3,4] in the ultraviolet indicates the same complexes are contributing to the altered absorption. It therefore seems justifiable for the purposes of this paper to consider that

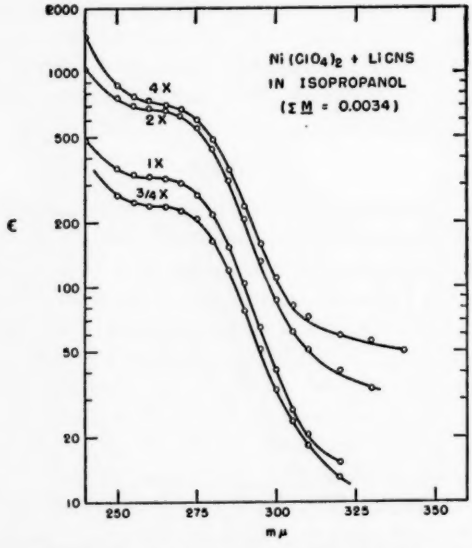

FIG. 2. Absorption of solutions with variable ratios of LiCNS to $Ni(ClO_4)_2$ in isopropyl alcohol. Total molality, 3.4×10^{-3}. Formal extinctions based on nickel concentration.

[2] L. I. Katzin and E. Gebert, J. Am. Chem. Soc. **72**, 5659 (1950).
[3] P. Job, Ann. chim. [10] **9**, 113 (1928).
[4] L. I. Katzin and E. Gebert, J. Am. Chem. Soc. **72**, 4455 (1950).

the spectra for the several reagent ratios listed approximate the spectra (in shape, if not in extinction coefficient) of the pure complexes. With this crude assumption, and the assumption of complete association of the lower complexes, one obtains minimum extinction coefficients per thiocyanate of about 330 at 295 millimicrons for the monothiocyanate complex, about 380 at 305 millimicrons for the dithiocyanate, and perhaps 1270 at 315 millimicrons for the trithiocyanate complex, assuming complete formation at a ratio of four thiocyanates per cobalt.

The new peak produced on mixing thiocyanate and nickel is less well resolved (Fig. 2), and any wavelength shift on adding higher concentrations of thiocyanate is less well defined. There is a fairly clearly demarcated difference between the absorption of the solutions containing up to one equivalent of thiocyanate per nickel,

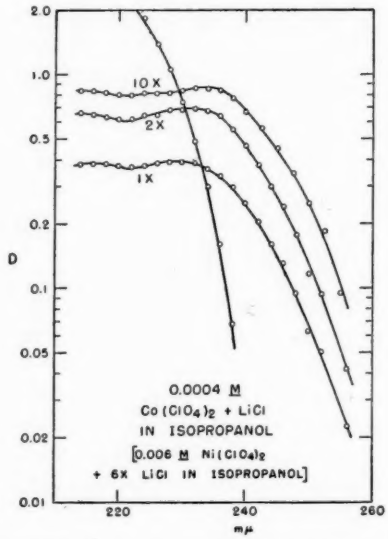

FIG. 3. Absorption of solutions with variable ratios of LiCl to $4\times10^{-4}M$ $Co(ClO_4)_2$ in isopropyl alcohol. Single curve, six equivalents of LiCl with $6\times10^{-3}M$ $Ni(ClO_4)_2$ in isopropyl alcohol.

and those containing approximately two or more equivalents, which may be attributed to complexes containing one and two thiocyanates per nickel, respectively. Continuous variations investigation bears this out and indicates that under the experimental conditions little if any higher complexes are formed. At 260 millimicrons, the minimum extinction coefficient calculated from either of the two lower curves is about 320 per thiocyanate for the first complex, and from the upper curves, 350–370 per thiocyanate for the dithiocyanate complex.

Lithium chloride in the alcohols is nonabsorbing so far as it can be followed into the ultraviolet. On mixing with cobalt or nickel perchlorate, an intense absorption arises whose peak falls in the region near 230 millimicrons (Fig. 3). With one equivalent of chloride per cobalt, the peak of the broad absorption falls at about 228 millimicrons, and with the addition of more

chloride it shifts towards 232 millimicrons. A shallow minimum at about 222 millimicrons leads to another broad peak somewhere in the vicinity of 215 millimicrons or below. With a solution of cobaltous chloride in tertiary butyl alcohol, the long wavelength peak comes at about 232 millimicrons, and the minimum at 222 millimicrons, in agreement with the more absorbing isopropyl alcohol solution. To further verify that the low wavelength peak is not an instrumental artifact[5] measurements were made with the tertiary butyl alcohol solution and a path length of 1 mm (to diminish the solvent absorption) and comparable results were obtained. The results with the salt mixtures indicate the presence of two complexes; this agrees with findings from the spectra in the visible region[6] and with a check by the method of continuous variations. The extinction per chloride of the longer wavelength peak is 1000 at 228 millimicrons for the monochloro complex, and perhaps 1100 at 232 mμ for the dichloro complex, judged from the curve with ten equivalents of chloride per cobalt.

Mixtures of nickel perchlorate and lithium chloride also show an absorption in the region 220–240 millimicrons (Fig. 3) but the peak falls somewhere below 220 millimicrons, and the system has not been studied in detail.

The tail of the absorption peak of lithium bromide is visible as an absorption with a coefficient of about 1.7 at 224 millimicrons, about one-third this value at 226 millimicrons, and essentially nothing at higher wavelengths. A mixture of lithium bromide and cobaltous perchlorate in isopropyl alcohol gives a decided absorption to above 300 millimicrons (Fig. 4) and evidence for two complexes. There is evidence for at least three absorption peaks for the dibromo complex—at about 266 millimicrons, 242 millimicrons, and at some wavelength below 220 millimicrons. The extinction coefficients for the bromide in the two complexes are about the same, and judged from the curve for the dibromo complex in excess bromide are 700 at 266 millimicrons and 800 at 242 millimicrons.

With nickel, there again appears a modified absorption of the bromide (Fig. 5) but at somewhat shorter wavelengths than for the cobalt bromide complex. The continuous variations method shows the major contribution to be from a monobrom complex in the wavelength region of the peak (227–228 millimicrons), and evidence for a weak dibrom complex can be seen. Since the wavelength shifts are again small, and it is not certain how much the dibromo complex may contribute even at two equivalents of lithium bromide per nickel perchlorate, one may say the extinction coefficient of the bromide in the monobrom complex is 1000–1300. The second peak indicated at nine equivalents of bromide may be due largely to the excess lithium bromide, since from the cobalt bromide results

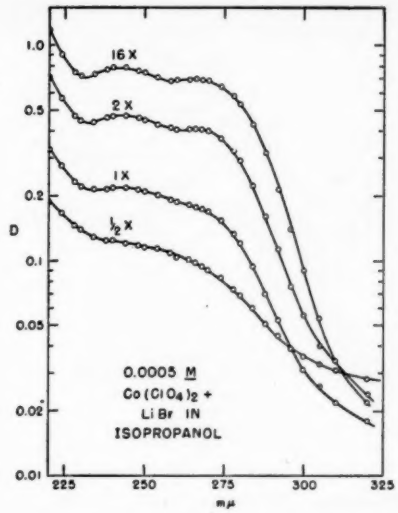

FIG. 4. Absorption of solutions with variable ratios of LiBr to $5\times10^{-4}M$ $Co(ClO_4)_2$ in isopropyl alcohol.

one would expect the second peak of the nickel-complexed bromide to appear at somewhat shorter wavelengths.

Iodide has an absorption which is very intense below 240 millimicrons, and drops precipitously to about 1 percent of the value at about 270 millimicrons. In the presence of cobaltous or nickelous perchlorate in isopropanol, the absorption maximum becomes shifted slightly to shorter wavelengths, and there appear a pair of broad absorption peaks in the vicinity of 295 and 360 millimicrons, respectively. Curves for various stoichiometric ratios of iodide and metal are shown in Figs. 6 and 7. It will be noted that the wavelengths of these peaks shift from 290 and 350 millimicrons for the lowest iodide-cobalt ratios to 295 and 355–360 millimicrons for the higher ones, and from about 295

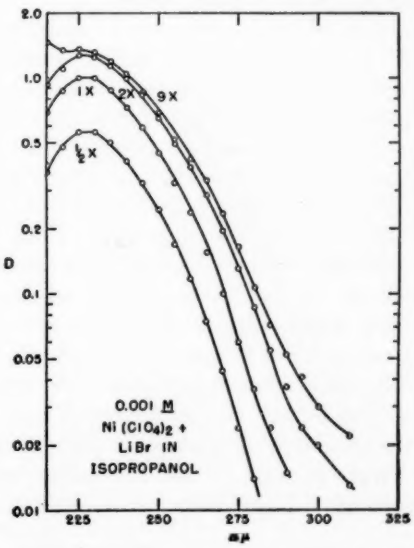

FIG. 5. Absorption of solutions with variable ratios of LiBr to $0.001M$ $Ni(ClO_4)_2$ in isopropyl alcohol.

[5] Saidel, Goldfarb, and Kalt, Science **113**, 683 (1951).
[6] L. I. Katzin and E. Gebert, J. Am. Chem. Soc. **72**, 5464 (1950).

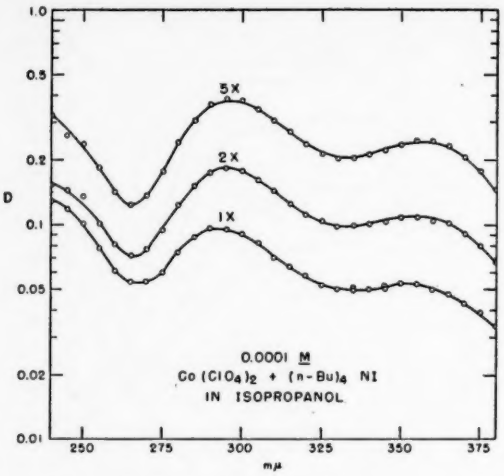

FIG. 6. Absorption of solutions with variable ratios of tetrabutylammonium iodide to $0.0001M$ $Co(ClO_4)_2$ in isopropyl alcohol.

and 360 millimicrons for the low iodide-nickel ratios to values some 2.5 millimicrons lower at the higher ratios. The same type of difference in wavelength shift can be discerned with the bromide and thiocyanate spectra, and seems to be a characteristic difference between the associations with nickelous and cobaltous ions. Both the absorptions characteristic of nickelous ion and of cobaltous ion in the visible region show the usual modifications ascribable to spectral alterations of the metal ion. In addition, a new band appears with nickel, centering at about 510 millimicrons (in acetone there are indications of another very small peak at about 580 millimicrons) which is not clearly ascribable to either the iodide or the nickel. This peak, coming at the usual transmission maximum of green nickel solutions results in a dark reddish-brown color of the iodide-nickel solutions, and presumably accounts for the black color reported for solid nickel iodide.

The spectra of the iodide-metal complexes assume particular interest on considering that although potassium iodide in alcoholic solution has essentially no absorption in the wavelength region under consideration, concentrated aqueous solutions of potassium iodide show variable amounts of absorption in this region which can be shown to be related to air oxidation of the iodide to iodine (e.g., reference 7). That is to say, the 290 and 350–360 millimicron bands are the result of tri-iodide ion, I_3^-, as can be seen by adding iodine to aqueous KI. The bands in the iodide-metal complex spectrum are apparently due to an electronic transition of the iodide ion which is matched in the iodide complex with elemental iodine. It may be noted that the spectrum of the tri-iodide complex is not independent of the system. Thus, in aqueous KI the longer wavelength peak comes at 352 millimicrons[8] as it does also with iodine solutions in isopropanol. If one dissolves tetrabutylammonium iodide or sodium iodide in alcohol (isopropanol, or better, tertiary butyl alcohol, in which reduction of iodine is extremely slow, and negligible), the tri-iodide formed on addition of excess iodine has the peak shifted to 360 millimicrons. The intensity of the 360 mμ peak in the tertiary butanol seems to be identical with that of the extinctions calculated[8,9] for aqueous KI solutions, but there are other variations, such as the increased resolution of the 290 millimicron peak from the absorption with peak at 220 millimicrons or below, for the sodium iodide case.

Rather analogous relations are found between the spectra in water solution of bromine and Br_3^-, and chlorine and Cl_3^- (Figs. 8 and 9). The solution of the element in water shows two or more peaks, the longest wavelength peak (analogous to the 450 millimicron peak of I_2) being less intense by a factor of 2 (bromine) to almost 4 (chlorine). When the element is dissolved in salt solution, to give the trihalide ion, the wavelength of the longest wavelength peak is shifted slightly, and its intensity relative to the shorter wavelength neighbor is considerably reduced. One gets somewhat similar spectra on dissolving iodine in chloride or bromide solutions, with a peak at about 247 millimicrons for the addition to chloride, and a broad peak centering at 260 millimicrons for the bromide solution. It seems most likely that these spectral alterations represent addition of I_2 to the halide anion, forming I_2X^-. Oxidation of chloride to give Cl_3^-, for example, seems ruled out by the difference in wavelength from the addition of Cl_2 to chloride.

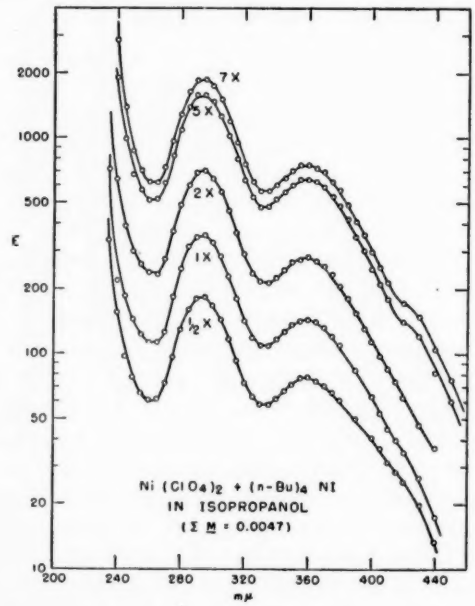

FIG. 7. Absorption of solutions with variable ratios of tetrabutylammonium iodide to $4.7\times10^{-3}M$ $Ni(ClO_4)_2$ in isopropyl alcohol.

[7] W. R. Brode, J. Am. Chem. Soc. **48**, 1877 (1926).

[8] J. J. Custer and S. Natelson, Anal. Chem. **21**, 1005 (1949), recalculated.

[9] A. D. Awtrey and R. E. Connick, J. Am. Chem. Soc. **73**, 1842 (1951).

There are large differences between the trichloride and tribromide spectra and those of the simple anions complexed to cobalt, in contradistinction to the situation with the iodine system. Tribromide, for example, shows no clearly resolved peak at 240 millimicrons such as is shown by the cobalt bromide complex, although the 265 millimicron peaks correspond well. The nickel complexes, as stated above, show wavelengths different from those with cobalt. The trichloride peak at about 227 millimicrons agrees approximately with the cobalt chloride peak wavelength, but shows a single peak instead of the double peak characteristic of the cobaltous complex.

Discussion

Taking the findings with the halogens and the trihalide ions into account, it seems certain that the spectral modifications found on mixing isopropanol solutions of cobaltous or nickelous perchlorate with solutions of lithium or tetrabutylammonium halides or thiocyanates are to be attributed to modifications of the absorption of the anionic portion of the complex, in the same manner that the spectral alterations in the visible region are to be ascribed to the metallic constituents of the complexes. Taken together with the nitrate case reported earlier,[1] and the influence of the metallic constituent on the alterations found for that case, the details of the alteration for a given partner, metal or anion, are a function of the electronic configuration characteristic of the second party to the complex.

The characteristic shift of the anion absorption to longer wavelengths in the complex indicates that the energy difference between the ground state and excited state is less than in the free anion. With special reference to the halides, the following points should also be encompassed in any theoretical explanation. The complexes of iodide with nickelous ions and cobaltous ions,

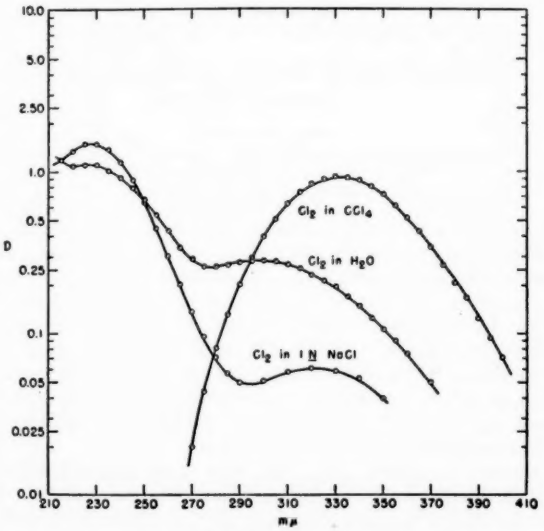

FIG. 8. Spectra of chlorine in various media. Concentrations not equal.

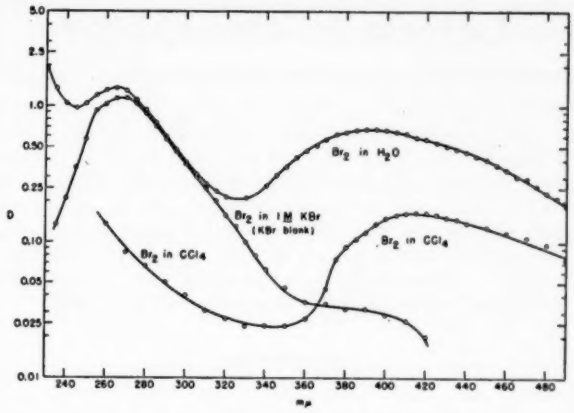

FIG. 9. Spectra of bromine in various media. Concentrations not equal.

and with I_2, show essentially the same absorption spectrum except for the differences in extinction coefficient. The relative heights and the separation of the pair of peaks (about 6400 cm^{-1} for the cobaltous complex) are characteristic of the spectra of the free iodide ion[10] and of the ion in various molecular combinations,[11] and are customarily related to the split ground-states of the iodine atom.[10,11] In the case of the three corresponding bromide complexes, all show different spectra, with the cobaltous complex showing again a bipeaked absorption (separation, about 3730 cm^{-1}), but the other complexes apparently show single peaks. The complex with Br_2 shows a peak wavelength close to the 265 millimicrons of the longer-wavelength cobalt complex peak, while the peak of the nickel complex absorption comes at much shorter wavelength. The three chloride complexes show relations like those of the bromides, the cobalt complex showing a rather large separation of peaks (about 2000 cm^{-1}) and the single peak of the Cl_3^- complex coming at about the wavelength of the longer wavelength peak.

Another question which theory will have to answer is that of the extinction coefficient differences in the otherwise almost indistinguishable iodide complex spectra. In terms of a distinction between "electron transfer bands" and "electron excitation bands" with a dividing line[11] at values of 10^4 for the extinction, the I_3^- bands with an extinction of 26,500 even at 360 millimicrons would fall into the former category, whereas the nickel and cobalt complexes, with extinctions of about 155 and 1200 in the same region would be classified as "electron excitation bands."

Another point of interest is that revealed in the difference of the spectra of I_3^- and the other trihalides. Why does only the former show the characteristic peak splitting associated with the halogen atom ground-state splitting, and why, in contrast, does the cobaltous complex always evoke it?

[10] J. Franck and G. Scheibe, Z. physik. Chem. **A139**, 22 (1928).
[11] E. Rabinowitch, Revs. Modern Phys. **14**, 112 (1942).

Letters to the Editor

THIS section will accept reports of new work, provided these are terse and contain few figures, and especially few half-tone cuts. The Editorial Board will not hold itself responsible for opinions expressed by the correspondents. Contributions to this section should not exceed 600 words in length and must reach the office of the Editor not later than the 15th of the second month preceding that of the issue in which the Letter is to appear. No proof will be sent to the authors. A publication charge of $10.00 per Letter is made which, when honored, will entitle the Institution to 100 free reprints.

Complexes of Iodine with an Ether and an Alcohol*

JOE S. HAM†
Department of Physics, The University of Chicago, Chicago 37, Illinois
(Received April 22, 1952)

HISTORICALLY, the solutions of iodine in oxygenated solvents have received much attention in the study of molecular interaction in solution.[1] In view of the recent interest in solutions containing halogen complexes,[2] it was thought that a thorough spectrophotometric study of several examples of the complexes of iodine with oxygenated solvents would prove useful.

Frequently, oxygenated solvents react chemically with iodine to form, among other things, I_3^-. Small traces of this ion can obscure the entire ultraviolet region (the molar extinction coefficient ϵ of I_3^- at its 3530A peak is 26,400, and at its 2875A peak is 40,000).[3] Iodine in diethyl ether and in *t*-butyl alcohol[4] produces inappreciable amounts of I_3^-.

A study was made of the absorption spectra of solutions of iodine in mixtures of *t*-butyl alcohol and *n*-heptane, and in mixtures of ether and *n*-heptane, from 2100A to 6200A. The equilibrium constants K of the 1:1 complexes formed in these solutions were determined using a method similar to that described by Landauer and McConnell[5] at numerous wavelengths in the visible and ultraviolet regions. The values obtained at 21.5±0.5°C are $K=4.9$ for the ether-iodine complex and $K=6.0$ for the alcohol-iodine complex (K in mole-fraction units). The values are independent of wavelength to within the experimental error and are the same for both the visible and ultraviolet peaks. These values may be compared with $K=12.6$ for the dioxane-iodine complex in carbon tetrachloride solution at 17°C measured from the visible absorption spectrum.[6]

Figures 1 and 2 show the spectra of free iodine and of the 1:1 complexes, in heptane solution. One notices that, while there is little change in shape or intensity of the complex in the visible over that of free iodine, a new transition appears in the ultraviolet analogous to the 2900A band of the benzene-iodine complex. The peak of the band for the ether-iodine complex is at 2500A, with $\epsilon\sim6000$; for the alcohol-iodine complex it is near 2330A with an $\epsilon\sim9000$, but part of the intensity may belong to another transition whose peak lies somewhat further in the ultraviolet.

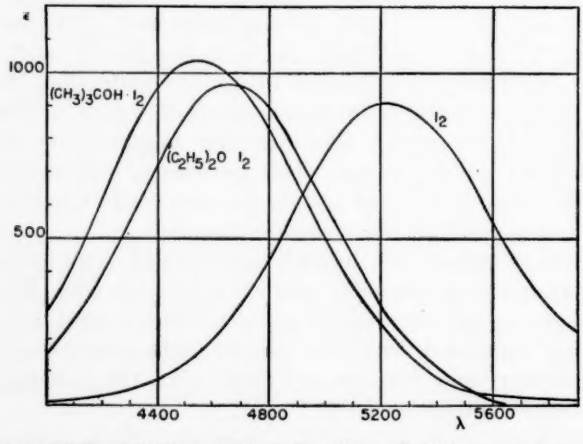

FIG. 1. Molar extinction coefficients for iodine, ether-iodine complex, and alcohol-iodine complex in *n*-heptane in the visible region.

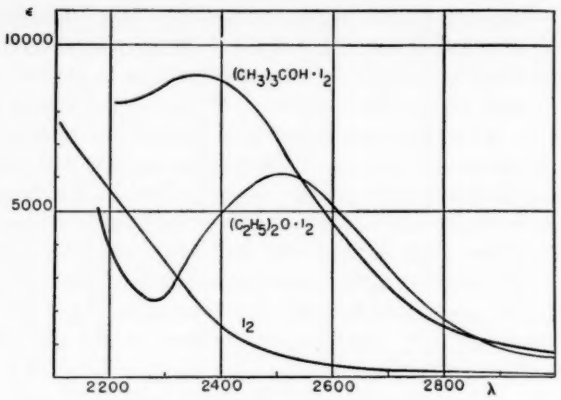

FIG. 2. Molar extinction coefficients for iodine, ether-iodine complex, and alcohol-iodine complex in *n*-heptane in the ultraviolet region.

Mulliken[4] has attributed strong transitions in the ultraviolet like those just described, which cannot be clearly correlated with transitions of either component molecule in the complex, to "intermolecular charge-transfer" transitions.

One notices that the ether-iodine complex absorbs less than free iodine near 2200A,[7] which suggests that the 1880A peak of iodine has been shifted, like the visible absorption, toward shorter wavelengths.

* Assisted, as to equipment, by the ONR under Task Order IX of Contract N6ori-20 with The University of Chicago.
† AEC Predoctoral Fellow, 1951–52.
[1] A review of earlier work is given by J. Kleinberg and A. W. Davidson, Chem. Rev. **42**, 601 (1948).
[2] R. S. Mulliken, J. Am. Chem. Soc. **74**, 811 (1952), gives references to recent work.
[3] A. D. Awtrey and R. E. Connick, J. Am. Chem. Soc. **73**, 1842 (1951).
[4] L. I. Katzin (private communication; to be published shortly).
[5] J. Landauer and H. McConnell, J. Am. Chem. Soc. **74**, 1221 (1952).
[6] Ketelaar, van de Stolpe, and Gersmann, Rec. trav. chim. Pays-Bas **70**, 499 (1951).
[7] A similar effect has been observed for the benzene-iodine complex: Ham, Platt, and McConnell, J. Chem. Phys. **19**, 1301 (1951).

Pure Quadrupole Spectra: Alphiatic Chlorine Compounds*

RALPH LIVINGSTON
Chemistry Division, Oak Ridge National Laboratory, Oak Ridge, Tennessee
(Received April 25, 1952)

MEASUREMENTS on substituted methanes[1] have been extended to include some of the chloroethanes and related compounds. These new data are summarized in Table I. As before, the magnitude of the nuclear quadrupole coupling is taken as twice the observed frequency, using the average frequency in case of multiple lines presumed to originate from nonequivalent Cl positions in the crystal lattice. Couplings are computed at 20°K at which temperature the effects of lattice vibrations are small. All these substances presumably form molecular crystals where the intermolecular forces are weak.

Figure 1 is a comparison among some of the couplings of Table I and the couplings for the chloromethanes.[1] In every case the magnitude of the coupling decreases in the molecule formed by replacing H in the chloromethane by one or more CH_3 groups. The qualitative explanation proposed for the coupling change in

TABLE I. Observed frequencies and quadrupole couplings for Cl^{35}.

Compound	Observed frequency, Mc 77°K	Observed frequency, Mc 20°K	$\lvert eqQ \rvert_{Av}$ Mc 20°K
CH_3CCl_3	38.052 37.829	38.249 38.052	76.30
CH_3CHCl_2	35.412	35.609	71.22
CH_3CH_2Cl		33.080 32.891	65.97
$(CH_3)_2CHCl$		32.069	64.14
$(CH_3)_3CCl$	31.065	31.195	62.39
CCl_3CCl_3	40.761 40.714 40.685 40.551	40.885 40.823 40.798 40.652	81.58
CCl_3CHCl_2	39.862 39.836 39.758 38.759 38.711	39.988 39.954 39.923 38.888 38.852	79.91[a] 77.74[a]
CH_2ClCH_2Cl	34.361	34.442	68.88
$CH_3CH_2CH_2Cl$	32.968	33.195	66.39
$C_2H_5(CH_3)_2CCl$		30.961	61.92
$CH_2ClCHClCH_2Cl$		35.026 34.838 34.677	69.69[b]
CH_2FCl		33.799	67.60

[a] Separate couplings are computed for each group of frequencies since they appear to represent different types of chlorine atoms in the molecule.
[b] A single coupling is computed since the frequencies are too close together to make specific assignments to the different chlorine atoms in the molecule.

the chloromethanes[1] was based on an increase in ionic character in the carbon chlorine bond when Cl was replaced by electropositive H. The extension of this argument leads to the concepts that in these molecules CH_3 acts as a strongly electropositive group and the ionic character in the carbon chlorine bond decreases in the order $(CH_3)_3CCl$, $(CH_3)_2CHCl$, CH_3CH_2Cl, etc. These concepts are consistent with other chemical observations.

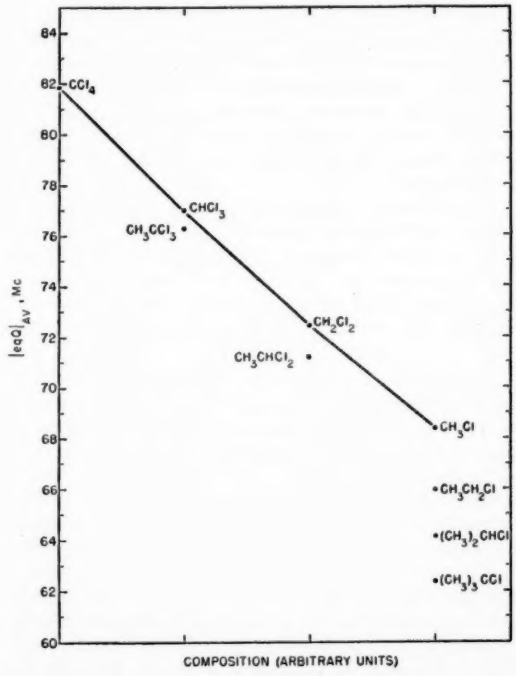

FIG. 1. Cl^{35} quadrupole couplings in alkyl chlorides at 20°K.

For example, the ease with which alkyl chlorides enter metathesis reactions is in the direction of decreasing coupling (increasing ionic character).

The comparisons made on the "methyl substituted chloromethanes" of Fig. 1 may be extended to the other chloroethanes. Replacing H in $CHCl_3$ by CCl_3 increases the coupling by 4.6 Mc while replacing an H in CH_2Cl_2 by CCl_3 gives a 5.3-Mc increase. In the latter case the lower coupling of the two computed for CCl_3CHCl_2 in Table I is assigned to the $CHCl_2$ half of the molecule. In both cases the CCl_3 group gives a large coupling increase quite comparable to the effect of a Cl substitution. Similar comparisons show the $CHCl_2$ group to have a noticeably smaller effect than CCl_3 while the CH_2Cl group has very little effect.

Two of the compounds in Table I are higher homologs of compounds discussed above. The coupling in $CH_3CH_2CH_2Cl$ is 0.6 percent higher than in CH_3CH_2Cl while the value in $C_2H_5(CH_3)_2CCl$ is 0.8 percent lower than in $(CH_3)_3CCl$. These small differences are of the same order as the separations of lines seen in crystals with nonequivalent Cl lattice positions and hence the coupling changes could be largely due to the effects of the environment of the molecule in the crystal lattice. The coupling for CH_2FCl completes the set of one carbon "Freons" previously published.[1] Its value is consistent with the interpretation already given.

* This work was performed for the AEC.
[1] R. Livingston, J. Chem. Phys. **19**, 1434 (1951).

Heat of Formation of Phenyl Radical and the Related Bond Dissociation Energies

M. SZWARC AND D. WILLIAMS
Chemistry Department, University of Manchester, Manchester, England
(Received April 18, 1952)

THE pyrolysis of bromo-benzene has been investigated with the intention of determining the dissociation energy of the Ph—Br bond. Determination of D(Ph—Br) enables us to calculate the heat of formation of the phenyl radical and subsequently to compute the related bond dissociation energies.

We found that bromo-benzene decomposes unimolecularly into phenyl radicals and bromine atoms:

$$Ph.Br \rightarrow Ph\cdot + Br,$$

and, using toluene as a carrier gas, we removed these fragments, producing hydrogen-bromide, benzene, and benzyl radicals. The

TABLE I.

T°C	$P_{Ph.Br}$ mm Hg	P_{total} mm Hg	Time sec	% decomp	k sec^{-1}
757	1.16	15.0	0.631	1.86	0.0292
762	1.00	13.7	0.648	1.98	0.0306
764	1.24	14.0	0.666	1.87	0.0281
764	1.10	15.2	0.638	2.32	0.0365
768	1.06	13.8	0.660	2.63	0.0399
770	0.56	13.75	0.665	2.31	0.0347
792	0.25	17.25	0.596	4.58	0.0786
792	0.27	15.0	0.588	4.71	0.0815
797	0.72	14.25	0.643	5.74	0.0923
798	0.40	10.0	0.713	6.23	0.0896
799	0.38	10.5	0.750	7.13	0.0975
799	0.25	17.65	0.604	5.33	0.0960
801	0.66	14.0	0.632	5.98	0.0976
805	0.31	14.0	0.657	7.20	0.114
806	0.39	14.0	0.656	7.70	0.123
809	0.096	13.5	0.633	8.44	0.139
811	0.37	14.5	0.676	8.96	0.139
817	0.36	14.0	0.649	9.73	0.162
818	0.39	14.5	0.670	9.66	0.1515
828	0.12	13.5	0.654	14.76	0.243
830	0.27	14.0	0.643	13.3	0.222
844	0.20	15.5	0.651	18.9	0.322
847	0.22	14.0	0.548	22.6	0.467
848	0.21	11.0	0.262	10.3	0.414
849	0.18	15.3	0.650	25.7	0.457
851	0.20	11.2	0.266	13.05	0.525
859	0.30	14.5	0.558	31.1	0.668
870	0.33	11.0	0.258	15.8	0.668

principle of this method, and also the details of the experimental technique, are described elsewhere.[1,2]

The pyrolysis of bromo-benzene has been studied in the temperature range 757–870°C. The rate of the initial decomposition was measured by the rate of formation of hydrogen-bromide. It was found that the rate of decomposition is not affected by the variation of the partial pressure of toluene, indicating that neither toluene, nor its decomposition products, influence the rate of the initial dissociation of bromo-benzene. This is fortunate, since the considerable strength of the Ph−Br bond forced us to work at relatively high temperatures at which the decomposition of toluene is appreciable. However, measuring the rate of the reaction by the rate of formation of HBr, we could easily discriminate between the decomposition of Ph.Br and the decomposition of toluene.

The experimental results are summarized in Table I. The plot of the unimolecular rate constant *versus* $1/T$ is shown in Fig. 1. The activation energy has been estimated, using the least square method, at 70.9 kcal/mole, corresponding to the frequency factor of 2.10^{13} sec^{-1}. Making the usual assumptions, we identify this activation energy with the Ph−Br bond dissociation energy, and thus

$$D(\text{Ph}-\text{Br}) = 70.9 \text{ kcal/mole}.$$

The heat of formation of gaseous bromo-benzene was estimated tentatively by Hartley, Pritchard, and Skinner[3] at 23.2 kcal/mole. On the other hand, Carson[4] combined the work of Skinner[3] with his data on the heat of combustion of mercury-diphenyl, and derived

$$\Delta H_f(\text{Ph.Br})_{gas} = 25.4 \text{ kcal/mole}.$$

Use the latter value and the equation,

$$D(\text{Ph}-\text{Br}) = \Delta H_f(\text{Ph}\cdot) + \Delta H_f(\text{Br}) - \Delta H_f(\text{Ph.Br}),$$

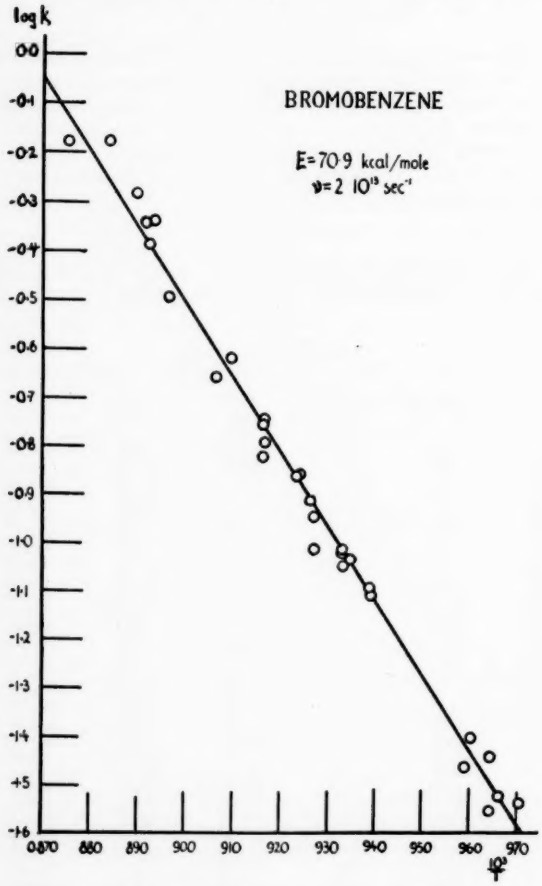

FIG. 1. Plot of the unimolecular rate constant *versus* $1/T$.

to arrive at

$$\Delta H_f(\text{Ph}\cdot) = 69.6 \text{ kcal/mole}.$$

We accept this value of the heat of formation of the phenyl radical and derive the following values for the various Ph−X bond dissociation energies:

$$D(\text{Ph}-\text{H}) = 101.8 \text{ kcal/mole}$$
$$D(\text{Ph}-\text{Cl}) = 85.6 \text{ kcal/mole}$$
$$D(\text{Ph}-\text{I}) = \sim 57 \text{ kcal/mole}^*$$
$$D(\text{Ph}-\text{OH}) = \sim 105 \text{ kcal/mole}$$
$$D(\text{Ph}-\text{CH}_3) = 88.6 \text{ kcal/mole}$$
$$D(\text{Ph}-\text{CH}_2.\text{Ph}) = 69.4 \text{ kcal/mole}$$
$$D(\text{Ph}-\text{CO.Ph}) = 74.6 \text{ kcal/mole}$$
$$D(\text{Ph}-\text{CO}\cdot) = \sim 27.5 \text{ kcal/mole}.^\dagger$$

Two factors contribute to the experimental errors involved in determining these dissociation energies: the experimental error of our direct determination of $D(\text{Ph}-\text{Br})$, which we estimate at about 1.5 kcal/mole, and the errors inherent in the thermochemical determinations of heats of formation of Ph.Br and Ph.X. The latter errors might be as large as 2 kcal/mole (see original papers).

A detailed report of this work will be published later.

* $D(\text{Ph}-\text{I})$ was determined by Butler and Polanyi [Trans. Faraday Soc **39**, 19 (1943)] at 54 kcal/mole. Their work was repeated by Szwarc [Chem. Revs. **47**, 75 (1950)], who derived for $D(\text{Ph}-\text{I})$ a value of about 57 kcal/mole in agreement with the present work.

† This value is derived from $\Delta H_f(C_6H_5.CO\cdot) = 15.6$ kcal/mole determined by Ladacki, Leigh, and Szwarc [J. Chem. Phys. (to be published)].

[1] M. Szwarc, Proc. Roy. Soc. (London) **A207**, 5 (1951).
[2] Szwarc, Ghosh, and Sehon, J. Chem. Phys. **18**, 1142 (1950).
[3] Hartley, Pritchard, and Skinner, Trans. Faraday Soc. **47**, 254 (1951).
[4] Carson, Carson, and Wilmhurst, Nature (to be published).

The Effect of Oxygen on a Radioreduction Reaction*

NORMAN TODD AND S. L. WHITCHER
Atomic Energy Project, School of Medicine, University of California, Los Angeles, California

(Received April 18, 1952)

THE influence of dissolved oxygen on the course of radiation induced chemical reactions in aqueous solution has played an important part in the development of the present theory of radiation chemistry. Its effect has been clearly demonstrated for the formation of hydrogen peroxide in irradiated water[1] and for certain oxidation reactions, notably that of ferrous sulfate.[2] However, the rather numerous reactions for which radiation causes reduction of the solute have not received much consideration from this point of view.

In air-free solution, the hydrogen atoms which are formed in the primary radiochemical process[3] react partly with the solute but many of them disappear by recombination; while in the presence of dissolved air the solute may encounter further competition for these radicals from the oxygen due to the reaction:

$$\text{H} + \text{O}_2 = \text{HO}_2.$$

Hence the addition of oxygen to a solution which is undergoing irradiation causes a part of the available H atoms to be replaced by HO_2 radicals. The latter may react in a variety of ways with the solute or its reduction products as well as with the other radicals in the solution.

As a result of the replacement reaction deaeration could, under certain conditions, lead either to an increase in the amount of radioreduction or to the formation of a reaction product in an oxidation state lower than that produced in oxygenated solution. Experimental realization of these effects seemed possible in solutions containing the iodate ion since it occupies a somewhat intermediate position with respect to redox potential.

0.0005 N solutions of potassium iodate in specially purified water have been irradiated in 150 ml spherical cells with un-

TABLE I.

		H_2O_2 formed	I_2 formed	IO_3^- reduction
*p*H 1	Air saturated	100	24	70
	Air free	125	22	50
*p*H 7	Air saturated	85	3	35
	Air free	15	1	64
*p*H 12.7	Air saturated	18	0	160
	Air free	8	0	220

filtered 250 KVP x-rays at various values of the *p*H and in the presence and absence of dissolved air. At each *p*H the removal of air produced significant changes in the pattern of radiation effects.

In sulfuric acid at *p*H 1, the iodate was reduced with the formation of free iodine and hydrogen peroxide in the solution. Deaeration altered the relative amounts to some extent but the most interesting effect appeared post-irradiation. In the air-saturated solution an after-reaction set in immediately with the regeneration of the iodate and the disappearance of the iodine and most of the peroxide. The reaction was complete in about one hour. With air-free solutions, on the other hand, the concentrations remained unaltered for somewhat over twenty hours when a change began which led to the same result as the first reaction. It therefore appears that HO_2 radical can form an intermediate reduction product which eliminates the induction period in the iodine-peroxide reaction.

In neutral and alkaline solutions there was little or no iodine formed and no after reaction, but the amount of iodate reduction was increased by 25 to 80 percent following the removal of air. Some representative data for the amounts of chemical change in microequivalents per liter are given in the accompanying table for a dose of 160,000 roentgens. Under the conditions of the experiments this dose corresponds to an energy absorption of approximately 6×10^{21} ev per liter of solution.

The iodate was determined iodometrically while the peroxide analyses were made in two ways: first by the method of Clark and Coe[4] and second by colorimetric analysis using titanium sulfate reagent.[5] The free iodine was determined by extraction of the solutions with carbon tetrachloride.

Further investigation is in progress in an attempt to determine the mechanism of the post irradiation reactions.

* This article is based on work performed under Contract No. AT-04-1-GEN-12 between the AEC and the University of California at Los Angeles.

[1] Bonet-Maury and Lefort, Nature **162**, 381 (1948).
[2] H. Fricke and E. J. Hart, J. Chem. Phys. **3**, 60 (1935).
[3] Weiss, Nature **153**, 748 (1944).
[4] G. H. Clark and W. S. Coe, J. Chem. Phys. **5**, 97 (1937).
[5] Bonet-Maury, C. R. Acad. Sci. **218**, 117 (1944).

Size and Shape of Polyelectrolyte Molecules in Solution

TERRELL L. HILL
Naval Medical Research Institute, Bethesda, Maryland
(Received April 21, 1952)

THE methods used in another connection[1-3] can be extended to the present problem. Flory and Fox[4,5] have discussed the case of zero charge. Hermans and Overbeeck[3] and Kimball *et al.*[6] considered a spherical shape without polymer-solvent interactions.[2,4] In the approximate theory outlined here (a detailed account with examples will be published later), the equilibrium shape and size is determined as the geometry (α_x, α_y, α_z below) with lowest free energy. The stable shape at zero charge is spherical but with high enough charge (and low enough ionic strength) nonspherical shapes must be considered, since the resulting decrease in electrostatic free energy (roughly dependent on the increase in surface "area" of the molecule at constant "volume"—see below) may more than offset the increase in configurational entropy of the chain.

The free energy $A-A_0$ of the single polyelectrolyte molecule relative to a reference state is the sum of ΔA_1, ΔA_2, and ΔA_3 (below). In the random flight configuration the density of segments around the center of gravity is taken as Gaussian.[4,7] If this most probable Gaussian distribution ($\alpha_x=\alpha_y=\alpha_z=1$) is distorted to another Gaussian distribution with α_x, α_y, α_z (α_x=expansion factor of x-component density distribution, etc.), then the method used and result obtained by Wall[8] in another problem both apply here without Flory's additional assumption.[4] We therefore write for the configurational term

$$\Delta A_1=-kT[\tfrac{3}{2}-\tfrac{1}{2}(\alpha_x^2+\alpha_y^2+\alpha_z^2)+\ln\alpha_x\alpha_y\alpha_z]. \tag{1}$$

For large extensions, a non-Gaussian distribution should be used.

Following Flory[4] but using our previous notation,[1] the free energy of mixing the polymer molecule with solvent is

$$\Delta A_2=B'V_0(V-V_0)/V+[(V-V_0)kT/v_0\beta]\ln[(V-V_0)/V]$$
$$V_0=Zv_0\beta, \tag{2}$$

where B' is a van Laar "heat" of mixing constant, βv_0 is the volume of a statistical segment, v_0 is the volume of a solvent molecule, and Z is the number of statistical segments (length l). $V(\alpha_x, \alpha_y, \alpha_z)$ is the "equivalent volume"[4] of the polymer molecule using a *uniform* density of segments. For example, for an ellipsoid, $V=4\pi R_xR_yR_z/3$, where we may use[4] $R_x=\alpha_x lZ^{\frac{1}{2}}/2$, etc. Alternative but somewhat less realistic geometries are an elliptical cylinder and a rectangular parallelopiped. Actually, Flory and Fox[5] have shown that the use of an "equivalent volume" to replace the Gaussian distribution can be avoided in the present connection.

Suppose there are n charges ϵ distributed uniformly along the molecular chain, and that the "solvent" is a solution of electrolyte. The charge density distribution has the same form as the polymer segment density distribution (it has been shown in the spherical case[3] that replacing a Gaussian charge distribution by a uniform one introduces no appreciable error). If the Poisson-Boltzmann (PB) equation is linearized and the n charges are considered point charges, the potential ψ at any point is given by the integral of the familiar $[\epsilon\exp(-\kappa r)]/Dr$ over the charge distribution, where r is the distance of an arbitrary charge ϵ from the point. With the potential available, $\Delta A_3(\alpha_x, \alpha_y, \alpha_z)$ is calculated as the work of charging all of the n charges simultaneously (constant geometry), in the presence of electrolyte.[1] If the nonlinearized PB equation is used, no exact solution is in general available, but Kimball[6] has discussed an approximate solution (see also Hill[1] and below).

Using an equivalent volume, a good approximation (linear or nonlinear PB) when κR_x, κR_y, and κR_z are not less than three or four is to assume that ψ changes near the surface in the same way that it does near an infinite plane surface. For example, in the linear PB case, one finds

$$\Delta A_3=(2\pi n^2\epsilon^2/D\kappa^2V)-(\pi n^2\epsilon^2\mathcal{A}/D\kappa^3V^2), \tag{3}$$

where $\mathcal{A}(\alpha_x, \alpha_y, \alpha_z)$ is the surface area. An approximation of wider applicability for the cylinder and parallelopiped is to use the exact ψ along a given direction neglecting edge or end effects. For example, for a circular cylinder of radius R_x and height $2R_z$, in the linear PB approximation, $\mathcal{A}$ in Eq. (3) is replaced by

$$4\kappa VI_1(\kappa R_x)K_1(\kappa R_x)+2\pi R_x^2[1-\exp(-2\kappa R_z)], \tag{4}$$

where I_1 and K_1 are Bessel functions.

For shapes constrained to a sphere as an illustration, and with $\alpha\geqslant1$, using Eqs. (1), (2), and (3) one finds from an expansion of $\partial A/\partial\alpha=0$

$$\alpha^5-\alpha^3=\left[q\left(1-\frac{2}{\kappa R_0\alpha}\right)+\frac{Z}{2}(1-K)\right]\left(\frac{6\beta v_0}{\pi l^3}\right)\frac{1}{Z^{\frac{1}{2}}} \tag{5}$$
$$q=2\pi n^2\epsilon^2/D\kappa^2kTV_0,\quad K=2B'v_0\beta/kT,\quad R_0=lZ^{\frac{1}{2}}/2.$$

This is in essential agreement with Flory[4] for $q=0$. Compare also Hill's[1] Eq. (57) with $t=0$.

Other possible extensions of the theory include dissociable charges (adsorption of ions), charges of different sign,[1] and an original unperturbed shape of the polymer molecule nonspherical owing to cross-linking.[1]

[1] T. L. Hill, J. Chem. Phys. (to be published); Trans. Faraday Soc. (to be published).
[2] P. J. Flory and J. Rehner, J. Chem. Phys. **11**, 521 (1943).
[3] J. J. Hermans and J. Th. G. Overbeeck, Rec. trav. chim. **67**, 761 (1948).
[4] P. J. Flory, J. Chem. Phys. **17**, 303 (1949).
[5] P. J. Flory and T. G. Fox, Jr., J. Am. Chem. Soc. **73**, 1904 (1951).
[6] Kimball, Cutler, and Samelson, J. Phys. Chem. **56**, 57 (1952).
[7] P. Debye, J. Chem. Phys. **14**, 636 (1946).
[8] F. T. Wall, J. Chem. Phys. **10**, 132 (1942); **11**, 527 (1943).

A Model for Epitaxy in Metal-Rock Salt Pairs*

OLIVE G. ENGEL
National Bureau of Standards, Washington 25, D. C.
(Received April 23, 1952)

THE importance of developing a working model for epitaxy in the deposition of metal films from the vapor phase derives from the need of predicting metal-substrate pairs and their epitaxial temperatures for the production of single crystal films. In searching for a basis on which such predictions can be made, a model for epitaxy of metal-rock salt pairs has been developed. A true ionization process on the surface has been advanced and correlation between the known epitaxial temperatures for six metals and the ionization potentials of their common valence states has been found.

The process is considered to consist of two steps,

$$M-ne\rightarrow M^{n+} \quad (1)$$

$$nS+ne\rightarrow nF, \quad (2)$$

where M is the metal in question, S is a vacant anion site on the surface which serves as an electron trap, and F is a color center. The ionization potential of the adsorbed deposit metal is reduced because of the dielectric constant of the substrate. Energy terms due to polarization and to the presence of an additional ion on the substrate surface have been included in considering the energy change involved in the ionization process for silver and palladium for which the epitaxial temperatures on rock salt are known. Calculations show the process is energetically feasible.

In terms of this model, epitaxial deposits must consist of the three layers: substrate salt/deposit-metal salt/deposit-metal, of which the deposit-metal salt layer is a monolayer. Misfit must be considered between the salt lattices and between the lattices of the deposit-metal salt and the deposit-metal, rather than simply the misfit between the lattices of the substrate salt and deposit-metal.

Brück's rule,[1] which states that the distance sum between deposit-metal atoms and the substrate chloride ions must be minimized in an elementary cell, has been extended. For the cleavage face of rock salt, the distances between deposit-metal ions and chloride ions in the substrate surface, which determine the bonding energy, must be as small as possible; distances between deposit-metal ions and sodium ions in the substrate surface, which determine the antibonding energy, must be as large as possible. The distance sums must be considered not simply in an elementary cell, but over the area which is enclosed by points of fit between the salt lattices. The observed orientation is considered to be the configuration of lowest energy at the temperature in question. The densest lattice plane of the deposit-metal, which affords maximum electrovalent bonding to the substrate, is the low temperature orientation which is observed first.

Experimentally observed orientations of silver on the (100), (110), and (111) faces of rock salt, which are hard to explain in terms of best fit, are the orientations to be expected in terms of this model. The difference in the orientation of face-centered and body-centered cubic metals on the cleavage face of rock salt which was observed by Brück is also explained. Epitaxial temperatures predicted by this model for lead, antimony, and platinum have been semi-quantitatively verified both in this laboratory and elsewhere.

A detailed paper will appear later.

* Work sponsored by the ONR.
[1] L. Brück, Ann. Physik **418**, 233 (1936).

The Relationship between Dissociation Energies and Interaction Constants in the Potential Function, for Polyatomic Molecules

P. TORKINGTON
British Rayon Research Association, Urmston, England
(Received April 24, 1952)

WE write as the general anharmonic potential function suited to considerations of dissociation

$$V=\sum_i \sum_j D_{ij}[1-\exp(-a_i\Delta_i)][1-\exp(-a_j\Delta_j)], \quad (1)$$

this being derived from the Morse function for diatomic molecules. a_i is the Morse constant for the ith bond, Δ_i the ith valence stretching coordinate, and the D_{ij} are components of the dissociation energy of the molecule; some of the D_{ij} may be zero for $i\neq j$, and all of the D_{ii} are nonzero and positive. Bending coordinates are ignored.

An approximation to quartic terms for Eq. (1) is the following:

$$V=\sum_i \sum_j a_i a_j D_{ij}\Delta_i\Delta_j(1-\tfrac{1}{2}a_i\Delta_i)(1-\tfrac{1}{2}a_j\Delta_j) \quad (2)$$

giving negative cubic and positive quartic terms, which is satisfactory. Comparing with the usual valence-force potential function,

$$V=\tfrac{1}{2}\sum\sum d_{ij}\Delta_i\Delta_j \quad (3)$$

for the harmonic oscillator approximation. We have

$$d_{ij}=2a_ia_jD_{ij} \quad (4a)$$

$$d_{ii}=2a_i^2D_{ii}. \quad (4b)$$

From (4b),

$$a_i=(d_{ii}/2D_{ii})^{\frac{1}{2}}, \quad (5)$$

and hence from (4a),

$$D_{ij}=[(D_{ii}D_{jj})/(d_{ii}d_{jj})]^{\frac{1}{2}}d_{ij}. \quad (6)$$

Now the complete dissociation energy of the molecule, i.e., its heat of formation from atomic species, is

$$D=\sum\sum D_{ij}, \quad (7)$$

which is therefore immediately related to the signs of the interaction constants d_{ij}; a negative interaction constant should be associated in some way with a relative lowering of the heat of formation.

A more usable conclusion results from considering the component of the potential function involving one linkage only. Thus for linkage k

$$V_k=\{D_{kk}[1-\exp(-a_k\Delta_k)]+2\sum_j{}' D_{kj}[1-\exp(-a_j\Delta_j)]\}\times[1-\exp(-a_k\Delta_k)]. \quad (8)$$

Then the energy of dissociation of this linkage in the molecule can be expressed as

$$D_k=D_{kk}+2\sum_j{}' D_{kj}[1-\exp(-a_j\bar{\Delta}_j)], \quad (9)$$

where the quantities $\bar{\Delta}_j$ represent the maximum displacements of the coordinates Δ_j in the mode of vibration describable as k-stretching. D_k is only identical with D_{kk} if either all the re-

maining coordinates remain at zero or if all the cross-terms of the dissociation energy matrix (D_{ij}) are zero. Equation (9) can be written

$$D_k = D_{kk} + 2 \sum_j{}' \alpha_j D_{kj}. \tag{10}$$

Assuming the $\bar{\Delta}_j$'s positive, the α_j's will also be positive. Hence if D_{kk} is taken as the "pure" dissociation energy, then the observed value D_k will be greater or less than D_{kk} according as $\Sigma' \alpha_j D_{kj}$ is positive or negative. The D_{ij} can be expressed in terms of the d_{ij} by Eq. (6), giving an immediate relation between the dissociation energy of a bond and interaction constants involving it with other stretching coordinates in the potential function. Often, one interaction may be of over-riding importance; for a single interaction

$$\begin{aligned} D_k &= D_{kk} + 2\alpha_j D_{kj} \\ &= D_{kk} + 2[(D_{kk}D_{jj})/(d_{kk}d_{jj})]^{\frac{1}{2}} d_{kj}, \end{aligned} \tag{11}$$

where α_j is assumed of order unity (the treatment is of course only approximate). It may be noted that a relative strengthening of a linkage in a given molecule should be associated with a positive stretching-stretching interaction constant; there is some evidence for this. (See, for example, Duchesne, reference 1.)

[1] J. Duchesne, Acad. Roy. Belg. Classe sci. **26**, 1–44 (1952).

The Possibility of a Theoretical Calculation of the Critical Temperature

JOHAN VAN DRANEN
Laboratory for Analytical Chemistry, University of Amsterdam, Amsterdam, Netherlands
(Received April 21, 1952)

IN order to calculate theoretically the critical temperature of a substance we accept the following hypothesis.

The critical point of a substance arises from the fact that at the critical temperature (T_c) the average kinetic energy (K_c) is equal to the average (negative) potential energy (U_c).

From this hypothesis we obtain the relation

$$3/2RT_c = -U_c \quad \text{or} \quad T_c = -2/3RU_c.$$

It is difficult to calculate exactly the value of U_c; therefore we try to make some rather crude estimates for the case of the inert gases.

According to London[1] for nonpolar atoms and molecules U is proportional to $\alpha^2 I/r^6$; r^3 is of course proportional to V_c. Using these formulas we see that the quotient $Q = V_c^2 T_c/\alpha^2 I$ must be a constant. It will be noted that Q is reasonably constant, except of course for helium. (Helium is "blown up" by its quantum-mechanical zero point energy.)

It is possible to deduce from the Lennard-Jones potential for the crystal energy E that the attractive potential energy, when a state of equilibrium has been reached, is equal to twice the repulsive (Born) energy; viz., $E = -A/r^6 + B/r^{12}$ and $(dE/dr)_{eq} = 0$ gives for the state of equilibrium

$$E_{eq} = -(A/r_{eq}^6)(1-\tfrac{1}{2}) \quad \text{or} \quad U_{eq} = 2E_{eq}.$$

(E_{eq} is equal to the sublimation energy.)

The critical volume V_c is about three times the volume of the solid V_0. One obtains for U_c: $U_c = (V_0/V_c)^2 U_{eq}$. (At the critical temperature the repulsive energy is about one percent of the total potential energy and can therefore be neglected.)

For T_c we get $T_c = -2/3R(V_0/V_c)^2 U_{eq}$ or substituting the values for V_0/V_c, R and U_{eq}: $T_c = (2/27)E_{eq}$. This relation was already known empirically.[1] The results are given in Table I.

In principle it is possible to deduce $U_c = -A/r^6 - B/r^8 \cdots$ from the known values for polarizibilities, ionization energies, and diamagnetic susceptibilities using the formulas of London or Slater and Kirkwood. From the mere existence of a number of formulas for the attractive energy the conclusion can be drawn that there remains a considerable degree of uncertainty in the calculated value of U.

TABLE I.[a]

	T_c(exp) °K	T_c(calc) °K	V_c(exp) cm³/mol	Q arbr. un.	$-E$ cal/mol	$-U_c$ cal/mol	r cryst. A	r calc A
2 He	5.2	...	57.8	17.4	...	...	1.79	1.66
10 Ne	44.4	43.7	41.7	26.4	590	131	1.60	1.48
18 A	150.7	150.3	75.3	24.3	2030	451	1.91	1.81
36 Kr	209.4	207.3	92.1	25.7	2800	622	1.97	1.93
54 Xe	289.7	289.0	113.8	25.6	3900[b]	867	2.18	2.08
86 Rn	377.6	...	145[c]	(25.6)	(5100)[d]	(1134)[d]	...	2.26

[a] The numerical values have been mainly taken from reference 1 and N. V. Sidgwick, *The Chemical Elements and Their Compounds* (Clarendon Press, Oxford, 1950).
[b] Less accurate value.
[c] Calculated using 25.6 for Q.
[d] Calculated using T_c(exp).

By making a number of more or less arbitrary assumptions (coordination number, distances, powers of r included) it is possible to obtain the right, however, not a scientific, result. The virial theorem gives the relation $Z = 3PV - 2K$; Z is the virial of the intermolecular forces. In classical statistics $K = (3/2)RT$. For Z Lorentz[2] and Boltzmann[3] have obtained the expression $Z = 3U + 8K(V_a/V)$. V_a is the total volume of the atoms (molecules). If a is the radius of the atom, $V_a = 4/3\pi Na^3$. At the critical point $K_c = -U_c$; therefore we may write $P_c V_c = RT_c[(4V_a/V_c) - \frac{1}{2}]$ or $P_c = -(2/3)(U_c/V_c)[(4V_a/V_c) - \frac{1}{2}]$. From a given value of V_c it is therefore possible to deduce theoretically T_c as well as P_c. We use this relation to compute a value for the radii of the atoms of the inert gases, taking the average value 0.292 for the critical coefficient $P_c V_c/RT_c$. Taking into account the fact that the radius of an atom is not a well-defined quantity the agreement between the computed value (eight column) and the value from x-ray analysis (seventh column) is satisfactory. This agreement is, however, not a good proof of the hypothesis, for the radius is very insensitive for changes in the value of the critical coefficient.

[1] F. London, Z. phys. Chem. **B11**, 222 (1931).
[2] H. A. Lorentz, Wied. Ann. **12**, 127, 660 (1881).
[3] L. Boltzmann, *Gastheorie* (1898), p. 149.

On the Validity of Anomalous Population Temperatures in Flames*

S. S. PENNER
Guggenheim Jet Propulsion Center, California Institute of Technology, Pasadena, California
(Received May 1, 1952)

IT should be obvious to anyone reading our recent papers objectively that our "principal thesis" was (a) to examine the origin of the basic relations involved in the customary procedure for the determination of population temperatures in flames, with emphasis on the effect of spectral line shape on the final equations,[1] and (b) to present experimental data on low pressure combustion flames[2] which support the earlier experimental findings of Gaydon and Wolfhard.[3] We noted that the usual equations hold only if $(P_\nu)_{max} X \ll 1$, and pointed out some time ago[4] that this condition is equivalent to the absence of self-absorption. Furthermore, contrary to Shuler's interpretation of our remarks,[5] use of the best available intensity data, namely, the data obtained by Oldenberg and Rieke,[6] led us to the conclusion that the condition $(P_\nu)_{max} X \ll 1$ is apparently not satisfied in representative low pressure combustion flames. We therefore arrived at the conclusion that anomalous population temperatures reported for low pressure combustion flames[3] may be the result of misinterpretation of experimental data.

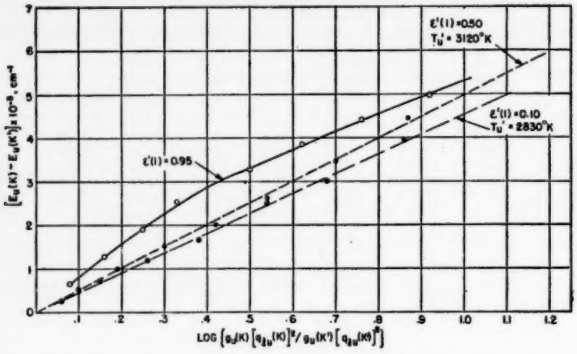

FIG. 1. Plot of $[E_u(K)-E_u(K')]$ *vs* $\log\{g_u(K)\,[q_{1u}(K)]^2/g_u(K')\,[q_{1u}(K')]^2\}$ for lines with equal total intensities at 3000°K as a function of $\epsilon'(1)$ for the P_1-branch, (0, 0)-band, $^2\Sigma\rightarrow{}^2\Pi$ transitions of OH.

Since we have done no experimental work on flames burning at atmospheric pressure, no reference was made to the attempts to correct for self-absorption in flames of this type. However, since Shuler[5] has furnished us with a résumé of what he considers to be important with regard to the study of flames burning at atmospheric pressure, it may be desirable if we indicate our position with regard to this work. First of all, we wish to call attention to the many important contributions made by Dieke and his collaborators to the development of valid techniques for the determination of population temperatures.[7] This work appears to have been done competently and with care. To the best of our knowledge, Dieke has not emphasized the occurrence of "anomalous" temperatures. We have not attempted investigations of flames burning at atmospheric pressure (1) because we were fortunate in having at our disposal the very excellent low pressure flame apparatus constructed by Gilbert,[2] and (2) because we did not feel in a position to carry out an unambiguous analysis of data obtained by examination of very narrow reaction zones, particularly if the field of view contains strong temperature gradients.

A straightforward quantitative study has been carried out recently[8] on the effect of self-absorption in an isothermal system at 3000°K on the observable experimental data by using the quantity

$$\epsilon'(1)=1-\exp(-P_{\max}X)$$

for the first line of the P_1-branch, (0,0)-band, $^2\Sigma\rightarrow{}^2\Pi$ transitions of OH, as a variable parameter. These detailed calculations lead to the conclusions enumerated below.

(1) Apparent population temperatures between 3000 and 19,000°K are obtained in conventional plots from the lines with $9\leqslant K\leqslant 18$ as $\epsilon'(1)$ is varied from 0.1 to 0.99.

(2) Self-absorption must occur in absorption experiments for an isothermal system whenever it occurs in emission experiments since the spectral emissivities and absorptivities are identical. Nevertheless, it appears to be possible to correlate the results of absorption experiments by conventional plots even under conditions in which self-absorption is not negligible. However, the temperatures calculated[9] from the slopes are not reliable.[8]

(3) As is implied by the work of Cowan and Dieke,[7] the isointensity method of Shuler[10] is not always a valid procedure, since the effects of self-absorption do not necessarily cancel in first order. This last statement is amplified by the curves shown in Fig. 1, which were constructed according to Shuler's method.[10] Reference to Fig. 1 shows that the temperatures calculated from the slopes differ slightly from the known temperature of 3000°K for small values of $\epsilon'(1)$ and that the curves become nonlinear for large values of $\epsilon'(1)$. The absolute intensity estimates obtained by Oldenberg and Rieke[6] are consistent with $0.3\leqslant\epsilon'(1)\leqslant 0.99$ for representative flames at 3000°K.

On the basis of our present knowledge of his work and the results of our calculations, we do not feel that we can accept Shuler's "anomalous" vibrational temperatures[11] as valid experimental evidence without (1) convincing proof that all necessary corrections for temperature gradients in the field of view have been applied, preferably by use of the methods of Cowan and Dieke,[7] and (2) a quantitative demonstration, using the absolute intensity estimates of Oldenberg and Rieke,[6] that the effects of self-absorption do not produce significant distortion of the experimental data.

* Supported by the ONR under Contract Nonr-220(03), NR 015 210.

[1] S. S. Penner, J. Chem. Phys. **20**, 507 (1952). It should be noted that, in general, peak intensity ratios are obtained if the instrumental slit width is small compared to the line width, whereas total intensity ratios are measured when the instrumental slit width is large compared to the line width.

[2] Penner, Gilbert, and Weber, J. Chem. Phys. **20**, 522 (1952); M. Gilbert, Jet Propulsion Laboratory Report No. 4–54, August, 1949.

[3] A. G. Gaydon and H. G. Wolfhard, Proc. Roy. Soc. (London) **194A**, 169 (1948), and later publications.

[4] S. S. Penner, Technical Report No. 2, Contract Nonr-220(03), NR 015 210, November 1951; Technical Report No. 4, February, 1952.

[5] K. E. Shuler, J. Chem. Phys. (to be published).

[6] O. Oldenberg and F. F. Rieke, J. Chem. Phys. **6**, 439 (1938); R. J. Dwyer and O. Oldenberg, J. Chem. Phys. **12**, 351 (1944). The numerical values of maximum absorption coefficients listed in Table II of reference 1 must be used in conjunction with optical densities X which represent the population of molecules in the lower energy level involved in a given energy transition.

[7] R. D. Cowan and G. H. Dieke, Revs. Modern Phys. **20**, 418 (1948); G. H. Dieke and H. M. Crosswhite, Bumblebee Report No. 87, November, 1948.

[8] S. S. Penner, Technical Report No. 5, April, 1952 (to be published).

[9] H. P. Broida, J. Chem. Phys. **19**, 1385 (1951).

[10] K. E. Shuler, J. Chem. Phys. **18**, 1466 (1950).

[11] H. P. Broida and K. E. Shuler, J. Chem. Phys. **20**, 168 (1952).

On the Validity of Spectroscopic Temperature Determinations in Flames

KURT E. SHULER
Applied Physics Laboratory, The Johns Hopkins University, Silver Spring, Maryland*
(Received April 17, 1952)

IT is the purpose of this note to call attention to the fact that some of the points raised recently by Penner[1] have been discussed in the literature several times previously. The conclusions reached by Penner as to the validity of some of the reported results of spectroscopic studies of flames should be considered in that context.

It is the principal thesis of Penner's papers[1] that the relations usually employed in the determination of "population temperatures" in flames from emission spectra are valid only if $(P_\nu)_{\max}X\ll 1$, i.e., if the product of the maximum value of the spectral absorption coefficient and the optical density of the emitter is much less than unity. This condition is equivalent to the requirement that the self-absorption of a given chemical species must be very small in order for accurate quantitative intensity measurements of emission lines to be feasible. This point has been discussed already by Cowan and Dieke[2] and Dieke and Crosswhite,[3] and the workers in the field of kinetic spectroscopy of flames are cognizant of the necessity of taking account of this self-absorption in the interpretation of their results.

For example, Dieke and Crosswhite[4] have shown that the "anomalous" intensity distributions of OH observed in some atmospheric pressure flames are principally due to self-absorption; when the appropriate intensity corrections are made on the basis of direct absorption measurements, the intensity distributions quite often become "normal" and lead to reasonable rotational flame temperatures. Broida[5] has used direct absorption measurements to correct for self-absorption in his OH emission study. The anomalous intensity distributions observed by him, after these corrections were made, thus cannot be attributed to an erroneous interpretation of experimental data due to lack of self-absorption corrections. The author[6] has used a modification of the iso-intensity method of Dieke and Crosswhite[3] in the analysis of his data on OH radicals. With this method, as has been pointed out repeatedly,[3,6] it is possible to avoid the complication introduced by

self-absorption by using only weak lines of equal intensity. The results obtained from these iso-intensity studies should thus lead to valid population temperatures.

Penner's suggestion that the commonly accepted f value for OH[7] may be erroneous—and presumably so by orders of magnitude—would not appear to have a basis in fact. The experiments on which Penner bases his suggestion, i.e., the determination of rotational intensity distributions from absorption measurements, are not comparable in accuracy with the much more precise and detailed measurements of Oldenberg[7] which led to the determination of the f value. Furthermore, the use of Oldenberg's f value in conjunction with iso-intensity measurements for the rotational (emission) temperature of OH leads to reasonable equilibrium results for the oxy-hydrogen flame[8] so that no internal inconsistency between the accepted f value for OH ($f^{nm}=1.26\cdot10^{-3}$) and rotational intensity distribution measurements is evident.

* This work was supported by the Bureau of Ordnance under contract NOrd-7386.

[1] S. S. Penner, J. Chem. Phys. **20**, 507, 522 (1952).
[2] R. D. Cowan and G. H. Dieke, Revs. Modern Phys. **20**, 418 (1948).
[3] G. H. Dieke and H. M. Crosswhite, "The Ultraviolet Bands of OH, Fundamental Data," Bumblebee Series Report No. 87, November, 1948, The Johns Hopkins University.
[4] G. H. Dieke and H. M. Crosswhite, Quarterly Reports, JHB-3, Problem A, Contract NOrd 8036, Johns Hopkins University; see particularly the reports for October, 1950 and January, 1951.
[5] H. P. Broida, J. Chem. Phys. **19**, 1385 (1951).
[6] (a) K. E. Shuler, J. Chem. Phys. **18**, 1466 (1950); (b) H. P. Broida and K. E. Shuler, J. Chem. Phys. **20**, 168 (1952).
[7] O. Oldenberg and F. F. Rieke, J. Chem. Phys. **6**, 439 (1938); R. J. Dwyer and O. Oldenberg, J. Chem. Phys. **12**, 351 (1944).
[8] K. E. Shuler, J. Chem. Phys. **19**, 888 (1951); see also reference 6(b).

On the Electronic Spectra of *o*-Dichlorobenzene in the Solid State

S. C. Sirkar and H. N. Swamy
Indian Association for the Cultivation of Science, Calcutta, India
(Received May 19, 1952)

THE ultraviolet absorption spectra of many substituted benzene compounds have been studied by several previous workers, and some of the results have been reviewed by Sponer and Teller[1] and also by Sponer.[2] Investigations on the influence of change of state on the electronic spectra of these compounds are, however, very few. In a series of investigations undertaken to study such an influence the ultraviolet absorption spectrum of orthodichlorobenzene in the solid state at −180°C has been found to show some interesting features which are not found in the absorption spectra of either *meta*- or *para*-dichlorobenzene in the solid state. Microphotometric traces of the absorption spectra of *ortho*-dichlorobenzene in the liquid state at 30°C and in the solid state at −180°C are reproduced as curves I and II, respectively, in Fig. 1. The spectra were photographed with a technique described previously.[3]

Figure 1 shows that in the liquid state at 30°C o-$C_6H_4Cl_2$ yields only three broad bands and the fine structure observed in the case of the vapor[4] is absent. In the solid state at −180°C the substance produces four intense bands, each of the first three of which is accompanied by two fainter bands on its two sides. The fainter band on the longer wavelength side of the first principal band at 35,587 cm^{-1} cannot be due to a $v\rightarrow0$ transition, because the distance between these two bands is about 352 cm^{-1}, and at −180°C the number of molecules present in the excited state of this mode of vibration is negligible. It is to be concluded, therefore, that the electronic energy level is split up into three components in the case of the substance in the solid state at −180°C. The assignment of the bands made under this assumption is given in Table I.

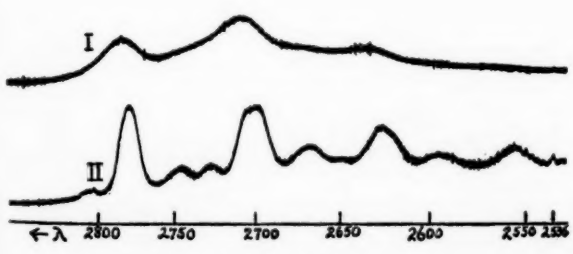

FIG. 1.

TABLE I. Absorption bands of *o*-dichlorobenzene, ν in cm^{-1}.

Liquid at 30°C		Solid at −180°C	
35,848		35,587(M)	C_0
(VS, broad)	ν_0	35,939(VS)	A_0
		36,399(M)	B_0
36,876		36,636(M)	C_1
(VS, broad)	ν_0+1028	36,983(VS)	A_1 (A_0+1044)
		37,450(M)	B_1
37,910		37,690(VW)	C_2
(M)	$\nu_0+2\times1031$	38,036(S)	A_2
		38,494(M)	B_2
		39,081(S)	A_3

The new companions of the absorption bands are much feebler than the main bands. A similar phenomenon, however, has been observed also in the case of benzene in the solid state at −259°C by Kronenberger.[5] As pointed out by Sponer and Teller,[6] the new bands marked I_0, I_1, etc., are observed in this case, and the 0,0 band which is forbidden in the vapor state appears strongly in the case of the solid at −259°C due to the interaction of neighboring molecules. It may be pointed out in this connection that such splitting of the electronic energy level and destruction of the symmetry of the electronic configuration in the benzene ring cannot be due to ordinary van der Waals forces in the lattice, and that the appearance of strong new Raman lines in the low frequency region with the solidification of these substances may be intimately connected with the changes in the electronic spectra of these substances mentioned above. All these phenomena may be due to formation of virtual bonds between neighboring molecules in the lattice. Such a hypothesis is corroborated by the facts observed earlier[7] that even in the case of solid benzene the new Raman lines become sharper and shift away from the Rayleigh line as the temperature of the solid is lowered. The changes in the electronic spectra observed in the case of benzene and *ortho*-dichlorobenzene and other similar compounds probably furnish additional evidence in support of the hypothesis that virtual bond is formed between neighboring molecules when these substances are solidified. Details will be published elsewhere.

[1] H. Sponer and E. Teller, Revs. Modern Phys. **13**, 75 (1941).
[2] H. Sponer, Revs. Modern Phys. **14**, 224 (1942).
[3] H. N. Swamy, Indian J. Phys. **25**, 262 (1951).
[4] See reference 2, p. 229.
[5] A. Kronenberger, Z. Physik **63**, 497 (1930).
[6] See reference 1, p. 117.
[7] S. C. Sirkar and A. K. Ray, Indian J. Phys. **24**, 189 (1950).

Paramagnetic Resonance of Manganese Activated Zinc Orthosilicates

E. G. Spencer, M. A. Garstens, C. C. Klick, and J. H. Schulman
Naval Research Laboratory, Washington, D. C.
(Received May 15, 1952)

PARAMAGNETIC resonance line widths of manganese activators in a zinc orthosilicate lattice have been measured as a function of manganese concentration. Further measurements were made to determine the effects of the addition of beryllium to form $(Zn, Be)_2SiO_4$:Mn. This system was chosen for study because of the interest shown in it in the discussion of sources of emissions in phosphors.

According to the coordination hypothesis of luminescence emission advanced by Linwood and Weyl[1] and elaborated by

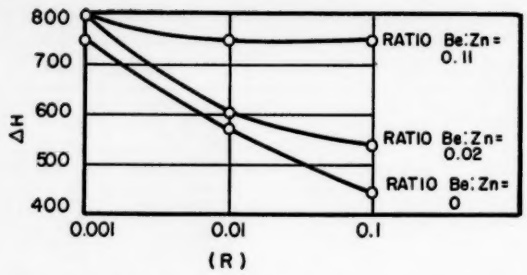

FIG. 1. Ratio R of Mn to (Zn+Be) *vs* line widths, in gauss, in $(Zn, Be)_2SiO_4$:Mn.

Schulman[2] to apply to certain phosphors, the emission spectrum of the manganese is mainly dependent upon the nature of the anion in the first coordination sphere of the manganese and the number and symmetry of this coordination group. A more recent hypothesis advanced by Kroger[3] relates the spectral changes in divalent-manganese activated phosphors to a change in the relative number of Mn^{+2} ion clusters of different size or configuration, produced by changes in manganese concentration or by alteration of the constituents of the host crystal. The "cluster" hypothesis as opposed to the coordination theory assumes that the effect of beryllium in $(Zn, Be)_2SiO_4$:Mn phosphors is to cause increased clustering of the manganese ions.

Figure 1 shows measured values of the line widths as a function of the concentration ratio R of Mn to (Zn+Be).

Calculation of the dipole-dipole interaction[4] assuming random distribution of the manganese ions in the lattice gives 600 gauss for the width at the highest concentration and 5 gauss at the lowest. The width of the observed line at low concentrations can be explained by assuming that the manganese ions cluster together more strongly than is indicated by random clustering. The decreasing width of the observed line with increasing concentration is then explained by assuming that the manganese ions cluster close enough together to allow narrowing of the line by exchange forces. It appears that, if these assumptions are correct, exchange forces must contribute to this narrowing even at the low concentrations.

Static susceptibility measurements[5] of exchange demagnetization in other phosphors also indicate clustering at the high concentrations such as to give rise to exchange effects among the manganese ions. Both these measurements and our own should not be considered as absolute values. In our measurements the variation in line width amounted to as much as 10 percent for samples of identical chemical content but fired and treated in different ways.

The addition of beryllium to the Zn_2SiO_4:Mn system causes a widening of the line. It may then be concluded that beryllium causes the manganese ions to spread out in such a way as to weaken the exchange forces and thus does not cause additional clustering of the manganese ions. Experimentally the effect of beryllium addition is opposite to the effect of increased manganese concentration, which is not in accord with predictions from Kroger's theory.

The measurements were made at 24,000 mc and about 8500 gauss, using the general techniques of Cummerow and Halliday,[6] except that a hybrid wave-guide "T" bridge was used. In addition, a 30-cps coherent detector scheme was used which is similar to that used in nuclear magnetic resonance.[7]

We would like to thank Mrs. Esther W. Claffy for preparing and making chemical analyses of the samples used.

[1] S. H. Linwood and W. A. Weyl, J. Opt. Soc. Am. **32**, 443 (1942).
[2] J. H. Schulman, J. Appl. Phys. **17**, 902 (1947); *Preparation and Characteristics of Solid Luminescent Materials, Cornell Symposium* (John Wiley & Sons, Inc., New York, 1948), p. 406.
[3] F. A. Kroger, *Some Aspects of the Luminescence of Solids* (Elsevier Publishing Company, Inc., Houston, Texas, 1948), p. 190.
[4] J. H. Van Vleck, Phys. Rev. **74**, 1168 (1948).
[5] Corliss, DeLabarre, and Elliot, J. Chem. Phys. **18**, 1256 (1950).
[6] Cummerow, Halliday, and Moore, Phys. Rev. **72**, 1233 (1947).
[7] Bloembergen, Purcell, and Pound, Phys. Rev. **73**, 679 (1948).

The Infrared Emission Spectra of OH, CO, and CO_2 from 3 μ to 5.5 μ

EARLE K. PLYLER AND JOSEPH J. BALL
National Bureau of Standards, Washington 25, D. C.
(Received May 14, 1952)

IT has been shown by Plyler and Humphreys[1] that the emission spectrum of oxy-acetylene flames has a considerable amount of structure in the region from 3 to 3.8μ. This structure was only partially resolved, but the close correspondence of the wave numbers of several of the maxima to values calculated for OH gave a strong indication that the spectrum in this region was produced by OH.

The spectrum in the 3.0 to 3.8μ region has been recently studied on a grating spectrometer, and many components of the P branch of the OH fundamental band have been observed, including lines of the 1→0 and the 2→1 transitions.

The good resolution for this spectrum has been obtained by the use of a 7500 line-per-inch grating, which has a ruled area of 4½ inches by 7½ inches. A PbTe cell has been used as a detector; and its sensitivity was such that lines separated by 0.3 cm^{-1} were resolved at 2800 cm^{-1}.

The rotational lines of the OH spectrum from P_{10} through P_{20} in the 1→0 band and from P_7 through P_{17} in the 2→1 band have been identified. A part of the band which extends from 2750 to 3000 cm^{-1} is shown in Fig. 1. On the figure is given the identification of the lines of the spectrum.

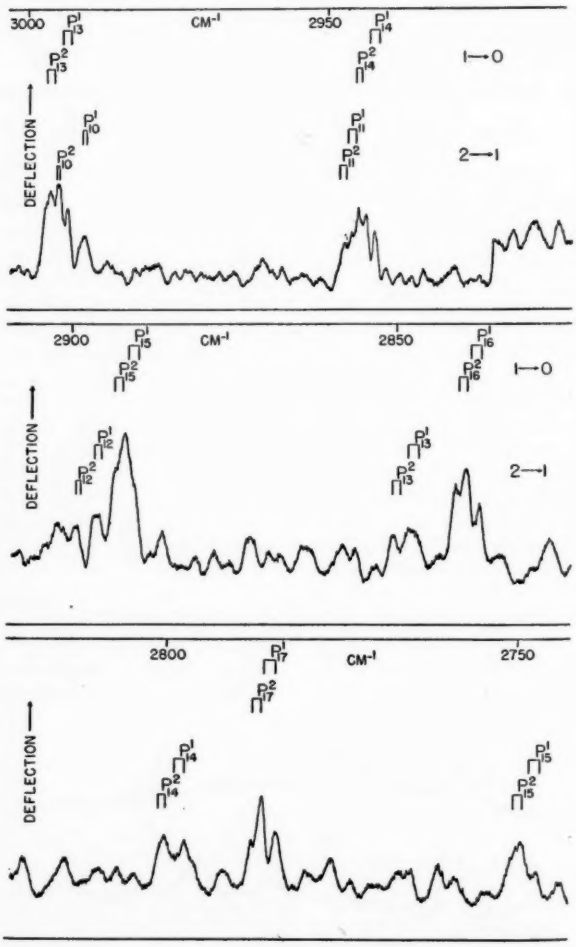

FIG. 1. The emission spectrum of OH from 2750 to 3000 cm^{-1}. Several of the components of the 1→0 and the 2→1 bands of the OH are marked on the figure.

The oxygen-methane flame was also used to observe the emission of CO and CO_2 in the region from 4.1 to 5.5μ. In Fig. 2, the band heads of CO_2 for 001→000 and 01^11→01^10 transitions are prominent. In between these two band heads are many closely spaced lines, which are a part of the R branch of the 001→000 band. At wavelengths greater than the 01^11→01^10 head the CO_2 absorption in the atmosphere becomes very intense on account of the 4-meter path of the spectrometer and precludes the observation of band heads of other transitions of the molecule which would occur in this region. At the center of the CO_2 absorption, 4.25μ, the deflections increase and some of the absorption lines can be identified. The observed spectrum from the center of the CO_2 band to about 2100 cm^{-1} is complicated. This region includes the absorption and emission bands of $C^{12}O_2$ and $C^{13}O_2$ and the R branches of the CO bands for the transitions 1→0, 2→1, and 3→2. This part of the spectrum has been omitted from the figure. Starting at 2090 cm^{-1} and extending to 1850 cm^{-1}, the P branches of the CO bands stand out clearly. The lines from P_{14} through P_{28} of the 1→0 band, from P_8 through P_{23} of the 2→0 band, and from P_1 through P_{17} of the 3→2 band are shown in Fig. 2. The P_{54} line, at about 1852 cm^{-1}, of the 1→0 band has been definitely identified. At longer wavelengths, the H_2O lines seriously overlap the CO spectrum, and the identification of lines with high J values is uncertain.

The observed values of the CO lines correspond closely to the calculated values obtained from the CO constants which have previously been determined.[2] Further precise measurements of the CO spectrum in emission and in absorption will show whether the present values of the CO molecular constants will need any modification.

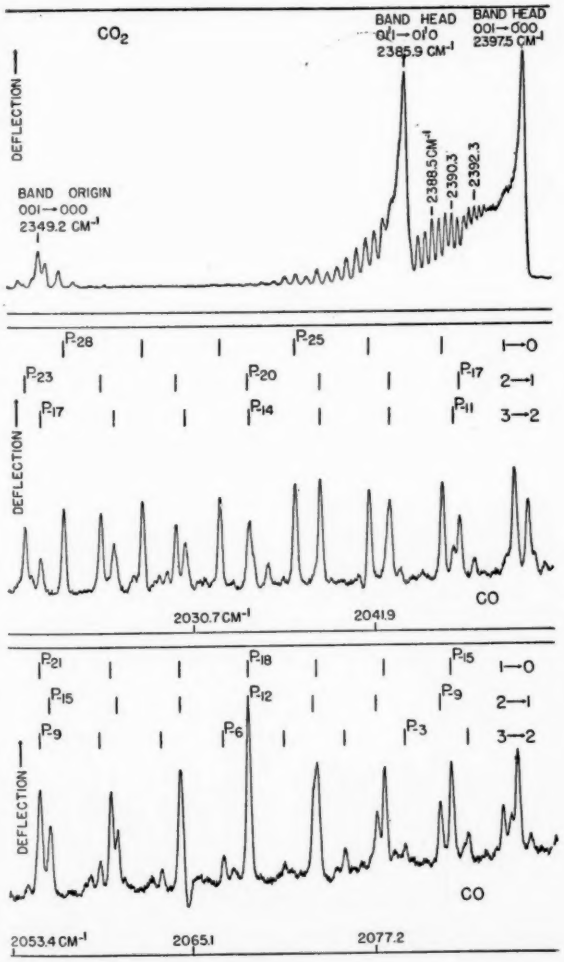

FIG. 2. The upper part of the figure represents two band heads of CO_2. The two lower parts show a number of the rotational lines of the P branches of 1→0, 2→1, and 3→2 bands of CO.

[1] Earle K. Plyler and Curtis J. Humphreys, J. Research Natl. Bur. Standards **40**, 449 (1948).
[2] Plyler, Benedict, and Silverman, J. Chem. Phys. **20**, 175 (1952).

The Entropy of Fluorine*

GEORGE M. MURPHY AND E. RUBIN
Chemistry Laboratories of Washington Square College, New York University, New York, New York
(Received May 12, 1952)

THE standard entropy of fluorine gas has been calculated by Murphy and Vance,[1] who obtained the result $S^0(298.16) = 48.484$ eu per mole, with the most reliable molecular data available. Essentially the same value has also been obtained by Garner and Yost,[2] by Kelley,[3] and by Brewer.[4] All of these investigators appear to have overlooked the fact that experimental heat capacities have been measured by Kanda[5] from 15°K to the boiling point of liquid fluorine. However, Cady and Burger[6] have pointed out that the entropy of fluorine from the heat capacity data is 2.46 eu per mole lower than that calculated by the statistical method. An unexplained discrepancy between the two methods of calculating entropies as large as this is unusual, and we have thought it important to re-examine the original data.

The details of our results follow:

Standard entropy of fluorine gas at 298.16°K	
0–15°K from Debye equation ($\theta = 101.1$)	0.467
15–55.20°K (melting point) by graphical integration	5.834
Fusion, 372 cal per mole/55.20°	6.739
55.20–85.11°K (boiling point) by graphical integration	4.778
Vaporization, 1560.3 cal per mole/85.11°	18.333
Correction for gas imperfection, Berthelot equation $p_c = 55$ atmos., $T_c = 144$°K	0.147
85.11–298.16°K from molecular data	8.864
Total from experimental heat capacities	45.162 eu per mole
0–298.16°K from molecular data for the ideal gas by statistical calculations	48.484 eu per mole
Unexplained discrepancy	3.322 eu per mole

The experimental values of C_p at the three lowest temperatures were converted to C_v by the empirical equation of Nernst and Lindemann.[7] The average value of θ calculated from these results was then used to obtain the entropy change between 0 and 15°K. The melting point and heat of fusion come from Kanda's own measurements. The boiling point and heat of vaporization are averages of data from Kanda,[5] Claussen,[8] and Cady and Hildebrand.[9] The entropy of the gas was obtained by the usual statistical method with the molecular constants used by Murphy and Vance.[2] Our calculations are in good agreement with those of Kanda except for the liquid, where he found $\Delta S = 5.46$ eu per mole. We believe our result of 4.778 to be correct for we have plotted both C_p against log$T$ and C_p/T against T, have evaluated the area of these curves by counting squares and with a polar planimeter, and all of these procedures have been done by each of us independently. Moreover, the heat capacity of the liquid from the melting point to the boiling point can be reproduced by the equation $C_p = a + bT + cT^2$ with $a = 9.912$, $b = 1.777 \times 10^{-2}$, $c = -2.776 \times 10^{-5}$, the maximum difference between calculated and observed heat capacity over the entire liquid range being ± 0.005 cal per mole. When integrated, this equation also gives a value of ΔS which agrees with our graphical result to ± 0.003.

The measured heat capacity of the solid between 15°K and about 45°K can also be reproduced by an empirical equation like that used for the liquid, with $a = -2.099$, $b = 0.2209$, $c = -1.599 \times 10^{-4}$, and a maximum deviation between observed and calculated points of ± 0.03 cal per mole. Above 45°K, a smooth curve can only be drawn through the experimental points on a C_p

against T plot, if a point of inflection is permitted. The measured data around this temperature are at 43.10, 47.95, 52.98, and 53.98°K, and the shape of the curve in this temperature range suggests that a transition in the solid phase might occur. It could have been missed by Kanda because of the wide spacing of his measurements. If it existed, a more normal looking heat capacity curve would then result and if the heat of transition were of the order of 150 cal per mole, the entropy of transition would be about three entropy units per mole which would account for the discrepancy which now appears to exist. An experimental test of this assumption should be relatively easy. It seems unlikely that the heat capacity data alone are in error by a large enough amount to account for the disagreement. The only molecular quantity of importance in the statistical calculation is the internuclear distance since the vibrational entropy is negligible. The inter nuclear distance depends on an electron diffraction measurement, and any error in it could not possibly account for three entropy units.

* This work supported by the AEC under Contract No. AT(30-1)-1256.

[1] G. M. Murphy and J. E. Vance, J. Chem. Phys. **7**, 806 (1939); **18**, 1514 (1950).
[2] C. S. Garner and D. M. Yost, J. Am. Chem. Soc. **59**, 2738 (1937).
[3] K. K. Kelley, U. S. Bureau Mines Bull. 434 (1941).
[4] L. Brewer, *The Chemistry and Metallurgy of Miscellaneous Materials, Thermodynamics*, National Nuclear Energy Series, Vol. IV-19B (McGraw-Hill Book Company, Inc., New York, 1950), edited by L. L. Quill.
[5] E. Kanda, Bull. Chem. Soc. Japan **12**, 511 (1937).
[6] G. H. Cady and L. L. Burger, *Fluorine Chemistry* (Academic Press, Inc., New York, 1951), edited by J. H. Simons, Vol. 1.
[7] W. Nernst and F. A. Lindemann, Z. Elektrochem. **17**, 817 (1911).
[8] W. H. Claussen, J. Am. Chem. Soc. **56**, 614 (1934).
[9] G. H. Cady and J. H. Hildebrand, J. Am. Chem. Soc. **52**, 2839 (1930).

Erratum: Hindered Intermolecular Rotation in the Solid State: Thermal and Dielectric Phenomena in Long-Chain Compounds

[J. Chem. Phys. **20**, 541 (1952)]

J. D. HOFFMAN
General Electric Company, Research Laboratory, Schenectady, New York

THE paragraph containing Eq. (25) should read as follows:

"By subtracting the heat changes in $C_{22}H_{45}Br$ observed on cooling ($\Delta h_{\text{freezing}}$, $c_p\Delta T$, Δh_T) from those observed on warming ($c_p\Delta T$, Δh_{fusion}) after standing 48 hours below T_t, it was found that the enthalpy change of the vertical-tilted transformation* was approximately

$$\Delta H_{\text{vertical}\rightarrow\text{tilted}} \cong 1.0 \text{ kcal/mole.} \quad (25)$$

The tilted form of $C_{22}H_{45}Br$ is more stable, has a higher melting point, and no rotational transition." The asterisk in the above still pertains to the long footnote concerning nomenclature of transformations and transitions.

It should be expressly noted that the last sentence in the paragraph and reference 25 have been removed as it is not certain that Professor Garner's work refers to the type of phase change discussed.

Infrared Spectrum of Some Complex Fluorides

A. DE LATTRE
Centre d'analyse spectrale moleculaire, Université de Liége, Liége, Belgium

(Received May 5, 1952)

IN a previous letter (J. Chem. Phys. **19**, 1610 (1951)) we reported on the infrared spectra of some complex fluorides. The experimental results have been confirmed and extended, and x-ray spectrograms of the Al compounds taken to ascertain their nature. Hydrated and anhydrous Al fluorides were found to have a band analogous to that found in cryolites. Brosset's $KAlF_4$ was also studied and also gave the same band.

Hydrated ferric fluoride showed the same broad and diffuse absorption as fluoferriates.

Fluosilicates of K, Cu, Zn, and Ni, show two bands at 488±6 and 735±6 cm^{-1}, irrespective of the nature of the cation and the degree of hydration, at least for the range of compounds studied.

In KBF_4 a new band has been found at 523 cm^{-1} which agrees rather well with Lecomte's prediction[1] 545, made by calculation from a combination band of shorter wavelength.

Further theoretical work showed that Wilson's formulas[2] are false, which ruins the derivation of force constants made in our previous letter. To get correct expressions, just write the (simple valence-deformation) potential in the form

$$2V = k_1 \Sigma \Delta R_{oi}^2 + 2A \Sigma \Delta R_{ij}^2 + k_\alpha \Sigma \Gamma_{ij}^2,$$

where $R_{oi} = X-Y$ distance, R_{ij} = vicinal $Y-Y$ distance, $\Gamma_{ij} = YXY$ angle, and put $B=0$ in the formulas given by Heath and Linnett[3] for the F_{1u} frequencies of XY_6 molecules of o_h symmetry (use the "*SVFF*" formulas).

Incidentally, these formulas contain a small error if a full Urey-Bradley potential is used. In the F_{1u} expressions at least, B should in our opinion be replaced everywhere by $B/\sqrt{2}$.

Our best thanks are due to Professor D'Or, under whose leadership and guidance this work was done.

[1] Lecomte, Bull. Soc. Chim. France **V 14**, 1057 (1947).
[2] Quoted by Yost *et al.*, J. Chem. Phys. **2**, 313 (1934).
[3] Heath and Linnett, Trans. Faraday Soc. **45**, 266 (1949).

Capillary Condensation in Contact Zones between Nonporous Particles of a Powder

IZUMI HIGUTI AND HIROSHI UTSUGI
Chemical Institute, Faculty of Science, Tohoku University, Sendai, Japan

(Received May 19, 1952)

WE have obtained adsorption isotherms for ethyl alcohol at 0°C, as illustrated in Fig. 1, on nonporous anatase powder, the radius of the particles of which was estimated to be

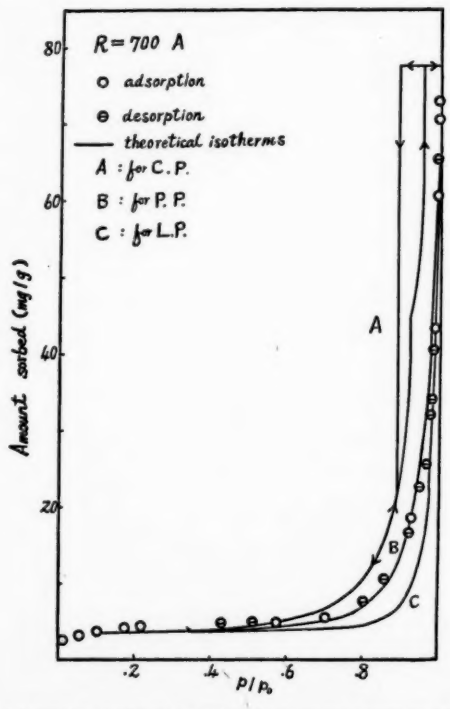

FIG. 1. Adsorption isotherm for ethanol on anatase together with curves showing calculated capillary condensation for closest packing (C.P.), planar close packing (P.P.), and linear packing (L.P.).

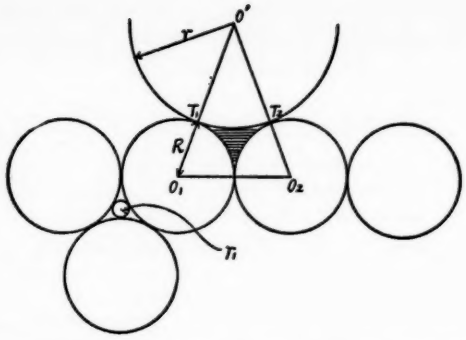

FIG. 2. Contact zones (shaded) of spherical particles O_1 and O_2 of radius R.

0.05μ by means of electron microscope photographs. The surface area, 10.6 m^2/g, determined from the *BET* plot in the range of relative pressure $x<0.05$ is essentially in agreement with that obtained from the particle size, 15.6 m^2/g. We adopted $R=0.07\mu$ as the radius of the particles in order to match the more reliable *BET* area. The steep slope of the curve near $x=1$ may be attributed to capillary condensation in the contact zones of particles. In order to explore this idea, the volume $V(r)$ in the contact zones has been calculated geometrically as a function of radius (r) of meniscus formed, as shown in Fig. 2. The particles are assumed, as a first approximation, to be spherical and of equal radius R. The $V(r)-r$ relation depends strongly on the type of packing. Therefore, we made calculations for three representative types: closest packing (C.P.), planar close packing (P.P.), and linear packing (L.P.). For C.P. and P.P., the volume $V(r)$ may conveniently be expressed in two terms, V_1 and V_2. V_1 is the space within the contacting sphere O', obtained by partially rolling O' around the line O_1-O_2, and V_2 is essentially the space enclosed by the sphere O' and the powder particles. Formulas follow which give the volume $V(r)$ in cm^3 per unit true volume of powder particles, independent of their sizes, as a function of $y=r/R$.

(1) *For linear packing.*—

$$V(y)=V_l(y)=\tfrac{3}{2}y^2\{1-[(\pi/2)-\theta][y(y+2)]^{\frac{1}{2}}\};\ \theta=\arccos(1+y)^{-1}.$$

(2) *For planar close packing.*—

(a) If $y\leqslant y_1=0.15470$, $V(y)=3V_l(y)$. Note that r_1 is the radius of the small circle shown in Fig. 2, contacting the cross section of three particles.

(b) If $y>y_1$, $V(y)=V_1(y)+V_2(y)$;

$$V_1=(9/\pi)\Theta y^2\{1-[(\pi/2)-\theta][y(y+2)]^{\frac{1}{2}}\};$$

$$V_2=(9/2\pi)\left\{\tfrac{1}{3}[3y(y+2)-1]^{\frac{1}{2}}+2\Theta+(\pi/3)y^3-(y^3+1)\arccos\left(\frac{1-(y+1)^2}{2y(y+2)}\right)\right\};$$

$$\Theta=(\pi/2)-\arcsin(1-\tfrac{1}{3}\tan^{-2}\theta)^{\frac{1}{2}}.$$

(3) *For closest packing.*—

(a) If $y\leqslant y_1$, $V(y)=6V_l(y)$.

(b) If $y_1<y\leqslant y_2=0.22475$, $V(y)=2V_1+4V_2$.

(c) If $y_2<y\leqslant y_3=0.4142$

$$V(y)=\tfrac{1}{2}V_1+4V_2-(9/\pi)\{1-[(\pi/2)-\theta][y(y+2)]^{\frac{1}{2}}\}\Theta_3+[2y_2^3+4V_2(y=y_2)];$$

$$\Theta_c=\Theta(y=y_c)=0.61555;$$

$$[2y_2^3+4V_2(y=y_2)]=0.0992\ cm^3/cm^3.$$

Note that $r_2(=y_2R)$ and $r_3(=y_3R)$ are the radii of spherical holes, which inevitably exist in closest packing, contacting, respectively, 4 and 6 particles.

The formula for the vapor pressure depression of the condensed sorbate in the contact zones may be subject to some uncertainty. If we adopt the Thomson equation, $x=\exp(-2\gamma v/rkT)$, for the sake of simplicity as well as appropriate *à posteriori* reasons, we can easily obtain the theoretical isotherm due to capillary condensation for any given sorption system, on the basis of the $V(y)-y$ relation mentioned above. In Fig. 1 are represented such theoretical isotherms for the present system. The capillary condensation is added on to a monolayer of the sorbate, which is complete at low pressure. Experimental points, denoted by ○ or ⊖, lie essentially on the theoretical curve for planar close packing. The agreement supports the idea of capillary condensation in the contact zones of particles even though they are nonporous. Similar results were reported by Holmes and Emmett[1] in the adsorption of nitrogen on two samples of glass spheres whose radii are 3.5 and 1.5–2.5μ. They also concluded that the adsorption near saturation was due to capillary condensation. Our calculation confirms their conclusion, exhibiting good agreement in the region higher than $x\doteq 0.99$, as shown in Fig. 3.

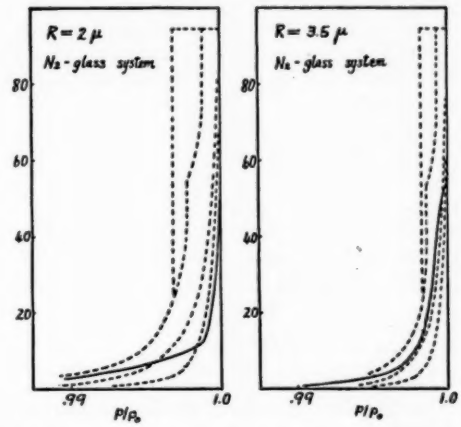

FIG. 3. Adsorption isotherms for N_2 on glass spheres. Solid lines, experimental data (see reference 1); dotted lines, theoretical isotherms for closest packing, planar close packing, and linear packing, respectively.

In view of these satisfactory results, we might conclude that if particle sizes are reduced sufficiently, nonporous particles can give rise to a marked capillary condensation in their contact zones. If this is valid, we may say that the multilayer adsorption does not occur at least for the anatose-ethyl alcohol system. Details will be published elsewhere.

In conclusion, the authors wish to express their sincere thanks to Professor F. Ishikawa for his helpful advice and encouragement. We are also indebted to Professor P. H. Emmett for helpful criticism of this note.

[1] J. Holmes and P. H. Emmett, J. Phys. Colloid Chem. **51**, 1262 (1947).

The Crystallography of Nickel Kieselguhr*

RAYMOND B. ROOF, JR.
Mineralogical Laboratory, University of Michigan, Ann Arbor, Michigan
(Received May 12, 1952)

AN x-ray investigation was made of a nickel kieselguhr substance used as a catalyst in organic hydrogenation reactions. Nickel kieselguhr is a diatomaceous earth upon, and in which, nickel has been chemically deposited. The investigation shows Ni and NiO are present and that there is no significant change in lattice parameter in either of these substances. NiO is present in sufficient amounts to give powder lines of appreciable intensity.

This analysis is different from that of de Lange and Visser's (1946) work on nickel catalysts deposited on kieselguhr.[1] They state that the normal lattice of metallic Ni does not occur in materials prepared in this way, and the reduced active catalyst is a result of the attack of hydrogen on a nickel hydrosilicate.

Certain crystal planes are common to both the face-centered cubic Ni and to the ideal hexagonal close-packed Ni, so that their interplanar spacings check exactly (for example, face-centered cubic 111 and the hexagonal close-packed 0002). The additional cubic Ni powder lines and the powder lines of NiO have interplanar spacings which approximate those of the hexagonal close-packed structure.[2] Accordingly, on a poor quality powder film of a mixture of Ni and NiO, especially one taken with a short x-ray wavelength which would cause a crowding together of the lines, the composite pattern might have been mistakenly indexed as belonging to a hexagonal close-packed structure. It thus appears to the writer that the much debated form of hexagonal close-packed nickel might be the result of a wrong interpretation of what are actually lines belonging to Ni and NiO.

The size of the Ni and NiO particles are of colloidal dimensions and result in definite line broadening on the film. The particle sizes were determined by methods outlined in James.[3] Owing to the interchangeability of indices in the cubic system it is impossible to give definite values for the length of a particular axis or the thickness of the particle in a given direction. However, it is possible to determine an average volume and thus the linear dimension of the particles. The linear dimension of the particles was found to be of the order of magnitude of 330A and 160A for the Ni and NiO particles, respectively. The linear dimension is by definition the cube root of the volume.

* This work supported in part by the ONR.
[1] J. J. de Lange and G. H. Visser, Ingenieur (Utrecht) **58**, No. 26, 24 (1946).
[2] H. S. Rawdon and H. C. Vacher, Metal Progress, 40 (1941).
[3] R. W. James, *The Optical Principles of the Diffraction of X-Rays* (G. Bell and Sons, Ltd., London, 1948).

On the Bromination of Neopentane

SIDNEY W. BENSON AND HERMAN GRAFF
Department of Chemistry, University of Southern California, Los Angeles 7, California
(Received April 14, 1952)

IN recent work on the bromination of neopentane,[1,2] the rate-determining step in the chain

$$\mathrm{Br}+\mathrm{NpH}\rightarrow\mathrm{Np}+\mathrm{HBr} \qquad (2)$$

is assigned a frequency factor of 9.34×10^{16} cc mole^{-1} sec^{-1} and an activation energy of 18.1 kcal at 197.4°C. Both values are inconsistent with values obtained from the bromination of H_2, CH_4, and C_2H_6 shown in Table I.

The steric factor derived from the above frequency factor is 473, an impossible value for a single, bimolecular step reaction. All other work on such radical reactions have shown steric factors considerably less than unity.[3] Since neopentane bromination is faster than that of H_2 or CH_4 and the chain breaking efficiency is greater for the former, the chain must be faster and thus the activation energy of reaction 2 must be smaller than 18.1 kcal.

TABLE I. Br+XH→HBr+X.

X	Range studied °C: Photochemical	Range studied °C: Thermal	ΔH_f^0 kcal/mole	E_a kcal/mole	A cc mole^{-1} sec^{-1}
H[a,b,e]	433–499	470–575	16.7	17.5	1.14×10^{12}
CH_3[e]	423–503	570	12.3	17.8	1.48×10^{12}
C_2H_5[d]	308–363	···	8.3	13+	···
Np[f]	371–470	470	$-1.6+H_f^0$(Np)	18.1	9.34×10^{16}

[a] M. Bodenstein and S. C. Lind, Z. physik. Chem. **57**, 168 (1906).
[b] M. Bodenstein and H. Lutkemeyer, Z. physik. Chem. **114**, 208 (1924).
[e] G. B. Kistiakowsky and E. R. Van Artsdalen, J. Chem. Phys. **12**, 469 (1944).
[d] H. C. Anderson and E. R. Van Artsdalen, J. Chem. Phys. **12**, 469 (1944).
[e] See reference 1.
[f] See reference 2. ΔH_f^0 based on N.B.S. tables except for H_f^0 of CH_3 and C_2H_5 which were taken from Swarc, Chem. Revs. **47**, 75 (1950).

A possible explanation of the above anomaly lies in the rather interesting reaction of the neopentyl radical

$$\mathrm{Np}\rightarrow\text{isobutene}+\mathrm{CH_3}, \qquad (4)$$

followed by

$$\mathrm{CH_3}+\mathrm{NpH}\rightarrow\mathrm{CH_4}+\mathrm{Np} \qquad (5)$$
$$\mathrm{CH_3}+\mathrm{Br_2}\rightarrow\mathrm{CH_3Br}+\mathrm{Br} \qquad (6)$$
$$\text{isobutene}+\mathrm{Br}\rightarrow\text{Br-isobutyl} \qquad (7)$$
$$\text{Br-isobutyl}+\mathrm{Br_2}\rightarrow\text{di Br-isobutane}+\mathrm{Br}. \qquad (8)$$

Reaction 4 is expected to have an activation energy of about 23 kcal[4] and assuming the usual unimolecular frequency factor of 10^{13} sec^{-1} will compete with other reactions of the Np radical.

When reactions 4 to 8 are included in the scheme postulated by the original workers[1,2] a new rate expression is obtained from which an activation energy for reaction 2 can be estimated of about 12 ± 2 kcal. This still leads to a steric factor of near unity which although probably too high is at least within the limits of experimental error and uncertainty in the chain mechanism.[5]

[1] E. I. Hormats and E. R. Van Artsdalen, J. Chem. Phys. **19**, 778 (1951).
[2] F. E. Schweitzer and E. R. Van Artsdalen, J. Chem. Phys. **19**, 1028 (1951).
[3] E. W. R. Steacie and M. Swarc, J. Chem. Phys. **19**, 1309 (1951).
[4] S. Bywater and E. W. R. Steacie, J. Chem. Phys. **19**, 319 (1951). They give a value of 23 kcal for the scission of C_3H_7 into $CH_3+C_2H_4$.
[5] It is to be noted that no analyses were made of the products of the reaction by the original authors.

Chemical Reactions near Equilibrium

W. R. GILKERSON,* M. M. JONES,† AND G. A. GALLUP*
University of Kansas, Lawrence, Kansas
(Received May 1, 1952)

IN seeming contradiction to usual deductions from thermodynamics, it has been shown by De Donder[1] on the basis of his affinity function, by Prigogine[2] on the basis of the Chapman-Enskog model, and by Manes, Hofer, and Weller[3] using purely mathematical methods, that the rate of a chemical reaction close to equilibrium is directly proportional to the free energy difference between reactants and products. This relation may be shown to be a consequence of the theory of absolute reaction rates, also.

If one has the generalized reaction

$$A+B+\cdots\rightleftharpoons M+N+\cdots,$$

$$\Delta F_f^{\ddagger}=\Delta F_f^{\ddagger 0}+RT\ln Q_f^{\ddagger}=\Delta F_f^{\ddagger 0}+RT\ln\frac{a^{\ddagger}}{a_A a_B\cdots}$$

$$\Delta F_r^{\ddagger}=\Delta F_r^{\ddagger 0}+RT\ln Q_r^{\ddagger}=\Delta F_r^{\ddagger 0}+RT\ln\frac{a^{\ddagger}}{a_M a_N\cdots},$$

where $\Delta F_f^{\ddagger}$ is the free energy of activation of the forward reaction at any concentration, $\Delta F_r^{\ddagger}$ is the free energy of activation of the reverse reaction at any concentration, $\Delta F_f^{\ddagger 0}$ is the standard free energy of activation of the forward reaction, and $\Delta F_r^{\ddagger 0}$ is the standard free energy of activation for the reverse reaction. a_i is the activity of the ith component and $a^{\ddagger}$ is the activity of the activated complex.

We may now write the expressions for the rate constants of the forward and reverse reactions as

$$k_f=\kappa_f\frac{kT}{h}\exp\left(-\frac{\Delta F_f^{\ddagger 0}}{RT}\right); \qquad k_r=\kappa_r\frac{kT}{h}\exp\left(-\frac{\Delta F_r^{\ddagger 0}}{RT}\right);$$

$$=\kappa_f\frac{kT}{h}Q_f^{\ddagger}\exp\left(-\frac{\Delta F_f^{\ddagger}}{RT}\right); \qquad =\kappa_r\frac{kT}{h}Q_r^{\ddagger}\exp\left(-\frac{\Delta F_r^{\ddagger}}{RT}\right).$$

The expression for the rate of this reaction becomes

$$\frac{da_A}{dt}=\frac{da_B}{dt}=\cdots=-\frac{da_M}{dt}=-\frac{da_N}{dt}=\cdots$$

$$=k_f a_A a_B\cdots-k_r a_M a_N\cdots.$$

If we assume that $\kappa_f=\kappa_r$

$$\frac{da_A}{dt}=\kappa\frac{kT}{h}a^{\ddagger}\left[\exp\left(-\frac{\Delta F_f^{\ddagger}}{RT}\right)-\exp\left(-\frac{\Delta F_r^{\ddagger}}{RT}\right)\right]$$

$$=\kappa\frac{kT}{h}a^{\ddagger}\sum_{n=0}^{\infty}\frac{1}{n!}\left[\left(-\frac{\Delta F_f^{\ddagger}}{RT}\right)^n-\left(-\frac{\Delta F_r^{\ddagger}}{RT}\right)^n\right].$$

If the reaction is close enough to equilibrium, $\Delta F_f^{\ddagger}/RT\ll 1$, $\Delta F_r^{\ddagger}/RT\ll 1$, and

$$\frac{da_A}{dt}\cong\kappa\frac{kT}{h}\frac{a^{\ddagger}}{RT}(\Delta F_r^{\ddagger}-\Delta F_f^{\ddagger})$$

$$\cong\frac{\kappa a^{\ddagger}}{hN}\Delta F,$$

where $\Delta F=\Delta F_r^{\ddagger}-\Delta F_f^{\ddagger}$ and N is Avogadro's number. This approximation also becomes better as the temperature becomes higher.

Near equilibrium, $a^{\ddagger}$ will be approximately constant and the rate becomes directly proportional to the free energy change.

It is to be noted that this development indicates such behavior only in the limit. Some experimental results in the literature support this contention. This development also indicates that attempts to apply this treatment to the kinetics of reactions not very close to equilibrium will not be successful.

The most useful form of the absolute reaction rate theory involves the Gibbs free energy. However, as Manes *et al.*, show, the mathematical analysis can be carried out for any thermodynamic state function. So long as the conditions on the reaction are appropriate, any state function may be used in the absolute reaction rate theory to obtain results analogous to those of Manes.

* AEC Predoctoral Fellow.
† du Pont Fellow.
[1] Th. De Donder, *L'affinite* (Gauthier-Villars, Paris, France, 1927).
[2] I. Prigogine, *Etude thermodynamique des phenomenes irreversibles* (Desoer, Leige, Belgium, 1947).
[3] Manes, Hofer, and Weller, J. Chem. Phys. **18**, 1355 (1950).

The Infrared Spectra of CF_3Br and CF_3I

S. R. Polo* and M. Kent Wilson
Mallinckrodt Chemical Laboratories, Harvard University, Cambridge, Massachusetts
(Received April 24, 1952)

A THOROUGH investigation of the infrared spectra of CF_3Br and CF_3I has recently been published by Plyler and Acquista.[1] Since their interpretation of the spectrum is not in complete agreement with our conclusions from a similar investigation, it seems of interest to mention briefly the results of our study of the spectra of these molecules.

The CF_3I was prepared from CF_3COOAg and iodine[2,3] while the CF_3Br was obtained through the courtesy of the Minnesota Mining and Manufacturing Company. The spectra were obtained with three spectrographs: a Perkin-Elmer Model 12C equipped with CaF_2, NaCl, and KBr prisms, a modified Perkin-Elmer Model 12B with a KRS-5 prism,[4] and a Baird Associates double-beam spectrograph equipped with NaCl optics.

The frequencies, species, and probable assignment of the fundamental vibrations are given in Table I. The values of the two lowest frequencies for each molecule were deduced from combination and overtone bands, all of which are listed in Table II. On the whole, there is acceptable agreement with the data of Plyler and Acquista. Our estimated values for ν_3 of 350 cm^{-1} for CF_3Br and 290 cm^{-1} for CF_3I are in good agreement with the observed values of 348 and 284 cm^{-1}.

The main discrepancy occurs in the position of the, as yet unobserved, bending frequency, ν_6. Plyler and Acquista locate ν_6 at 180 cm^{-1} for CF_3Br and 163 cm^{-1} for CF_3I on the basis of Stepanov's[5] calculated value of 180 cm^{-1} for CF_3Br and because of the possibility of explaining several bands as combinations of these frequencies in each molecule with observed fundamentals. To us such low values for ν_6 seem extremely unlikely when it is noted that the lowest fundamentals of $CFCl_2Br$ and CCl_3Br are located at 203 cm^{-1} and 187 cm^{-1}, respectively. The apparently satisfactory interpretation of several combination bands with such low values for ν_6 may be attributed to the fact that the difference between these and the values we consider to be correct is about the same as that between ν_4 and ν_1 for both molecules.

There are several bands reported by Plyler and Acquista which we did not observe. These bands are at 470, 689, and 830 cm^{-1} in CF_3Br and 711, 1114, and 1246 cm^{-1} in CF_3I. A possible interpretation of the 470 cm^{-1} band in CF_3Br may be $\nu_2-\nu_6=469$ cm^{-1}. In an impure sample of CF_3I we observed a band at about 1250 cm^{-1} which did not appear in a pure sample. There seems to be no obvious explanation for the other bands which we did not observe.

TABLE I. Frequencies of the fundamental vibrations of CF_3Br and CF_3I.

Assignment	Type	ν(cm^{-1}) CF_3Br	CF_3I
ν_6	E	(297)	(265)
ν_3	A_1	(350)	(290)
ν_5	E	548	540
ν_2	A_1	764	746
ν_1	A_1	1087	1076
ν_4	E	1206	1183

TABLE II. Observed overtones and combination bands of CF_3Br and CF_3I.

CF_3Br Obs.	CF_3Br Calc.	Assignment	CF_3I Obs.	CF_3I Calc.
		$\nu_2-\nu_3$	457	456
649	647	$\nu_3+\nu_6$	~563	555
700	700	$2\nu_3$	~575	580
733	737	$\nu_1-\nu_3$	782	786
848	845	$\nu_5+\nu_6$	813	805
910	909	$\nu_4-\nu_6$	920	918
		impurity?	949	
1120	1114	$\nu_2+\nu_3$	1027	1036
		?	1173	
1304	1312	$\nu_2+\nu_5$	1273	1286
1470	1464	$\nu_2+2\nu_3$		1326
			1336	
1381	1384	$\nu_1+\nu_6$		1341
1429	1437	$\nu_1+\nu_3$	1359	1366
1503	1503	$\nu_4+\nu_6$	1444	1448
1625	1635	$\nu_1+\nu_5$	1609	1616
1755	1754	$\nu_4+\nu_5$	1722	1723
1843	1851	$\nu_1+\nu_2$	1816	1822
1863	1862	$\nu_2+2\nu_5$	?	1826
1882	1878	$2\nu_2+\nu_3$	1775	1782
1962	1970	$\nu_4+\nu_2$	1921	1929
2160	2174	$2\nu_1$	2142	2152
2177	2183	$\nu_1+2\nu_5$	?	2156
2198	2201	$\nu_1+\nu_2+\nu_3$	2100	2112
2281	2293	$\nu_4+\nu_1$	2250	2259
2315	2320	$\nu_4+\nu_2+\nu_3$	2202	2219
2399	2412	$2\nu_4$	2354	2366
	2524	$2\nu_1+\nu_3$		2442
2510			2459	
	2518	$\nu_4+\nu_2+\nu_5$		2469
2830	2841	$\nu_4+\nu_1+\nu_3$	2776	2799
	2940	$2\nu_1+\nu_2$		2898
2935			2890	
	2960	$2\nu_4+\nu_5$		2906
~3360	3380	$\nu_4+2\nu_1$	~3315	3335
~3475	3499	$2\nu_4+\nu_1$	~3420	3442
~3590	3618	$3\nu_4$	~3350	3549

* Research Fellow of the Spanish National Council for Scientific Research.
[1] E. K. Plyler and N. Acquista, J. Research Natl. Bur. Standards **48**, 92 (1952).
[2] A. L. Henne and W. G. Finnegan, J. Am. Chem. Soc. **72**, 3806 (1950).
[3] R. N. Hazeldine, J. Chem. Soc. 584 (1951).
[4] The authors wish to thank Professor Richard C. Lord for the use of this instrument.
[5] B. I. Stepanov, Compt. rend. acad. sci. U.R.S.S. **45**, 56 (1944).

The Raman Spectra of Ethoxychlorosilanes

HIROMU MURATA
The Osaka Municipal Technical Research Institute, Osaka, Japan
(Received April 22, 1952)

THE Raman spectra of tetramethoxysilane and tetraethoxysilane for the determination of the four fundamental frequencies attributable to the SiO_4 group have been reported by several investigators.[1] I have already measured the Raman spectra of methoxychlorosilanes[2] and I shall now report on that of ethoxychlorosilanes. The samples were prepared as follows: Tetrachlorosilane was added slowly to vigorously stirred anhydrous ethanol, and after careful fractional distillation, they gave the following boiling point: $C_2H_5OSiCl_3$, 102°; $(C_2H_5O)_2SiCl_2$, 134°; $(C_2H_5O)_3SiCl$, 153°. The results for these compounds together with the data available for the two compounds $SiCl_4$ and $Si(OC_2H_5)_4$ are given in Table I. From the results obtained for methylchlorosilanes,[3] ethylchlorosilanes,[4] and methoxychlorosilanes,[2] assuming ethoxy groups as one particle, I have tentatively assigned the observed lines as shown in Table I, where *A* denotes totally symmetric, *B* antisymmetric, *E* twofold degenerate, and *F* threefold degenerate vibrations of the tetrahedral molecule, respectively.

[1] B. T. Thosar and R. N. Bapat, Z. Physik **109**, 472 (1938).
[2] H. Murata, J. Chem. Phys. **20**, 347 (1952).
[3] Shimanouchi, Tsuchiya, and Mikawa, J. Chem. Phys. **18**, 1306 (1950).
[4] Murata, Okawara, and Watase, J. Chem. Phys. **18**, 1308 (1950).

TABLE I. Raman spectra of ethoxychlorosilanes (cm^{-1}).

Modes of vibrations	$SiCl_4$	$C_2H_5OSiCl_3$	$(C_2H_5O)_2SiCl_2$	$(C_2H_5O)_3SiCl$	$(C_2H_5O)_4Si$
δ(Si−Cl)	E 150	E 171(8*s*)(*ek*)	A_1 ···		
			A_2 ···	E ···	E ···
δ(Si−OC_2H_5)	F_2 221	A_1 215(4*s*)(*ek*)	A_1 240(3*b*)(*e*)	A_1 290(2*b*)(*e*)	F_2 ···
		E 249(2*s*)(*ek*)	B_1 295(2*b*)(*ek*)	E ···	
			B_2 ···		
δ(C−C)		294(2*s*)(*ek*)	···	···	···
δ(O−C)		364(4*s*)(*e*)	399(2*b*)(*ek*)	435(2*b*)(*ek*)	···
ν(Si−Cl)	A 424	A_1 475(10*s*)(*ek*)	A_1 490(6*s*)(*ek*)	A_1 520(4*s*)(*ek*)	A_1 652
	F_2 608	E 603(3*b*)(*ek*)	B 598(2*s*)(*ek*)	A_1 695(3*b*)(*ek*)	F_2 782
ν(Si−OC_2H_5)		A_1 775(4*s*)(*ek*)	A_1 744(2*b*)(*ek*)	E 799(1*b*)(*ek*)	
			B 813(1*b*)(*e*)		
ν(C−C)		951(2*s*)(*ek*)	950(2*s*)(*ek*)	950(3*s*)(*ek*)	938
		995(2*s*)(*ek*)	992(2*s*)(*ek*)	997(3*s*)(*ek*)	
ν(O−C)		1092(3*s*)(*ek*)	1091(3*s*)(*ek*)	1090(3*s*)(*ek*)	1085
δ(C−H)		1294(3*s*)(*ek*)	1295(2*s*)(*ek*)	1291(2*s*)(*ek*)	1285
		1322(1*s*)(*ek*)	1325(1*s*)(*k*)	1324(2*s*)(*k*)	
		1347(2*s*)(*ek*)	1346(2*s*)(*e*)	1346(2*s*)(*e*)	
		1395(2*s*)(*ek*)	1391(2*s*)(*ek*)	1390(2*s*)(*ek*)	
		1446(3*s*)(*ek*)	1445(3*s*)(*ek*)	1445(3*s*)(*ek*)	1443
ν(C−H)					2776
			2866(4*s*)(*ek*)	2868(4*s*)(*ek*)	
		2899(3*s*)(*ek*)		2899(2*s*)(*ek*)	2883
		2936(9*s*)(*ek*)	2935(7*s*)(*ek*)	2935(6*s*)(*ek*)	
		2980(8*s*)(*ek*)	2980(6*s*)(*ek*)	2980(5*s*)(*ek*)	2995